

A Thesis Submitted for the Degree of PhD at the University of Warwick

Permanent WRAP URL:

<http://wrap.warwick.ac.uk/87354>

Copyright and reuse:

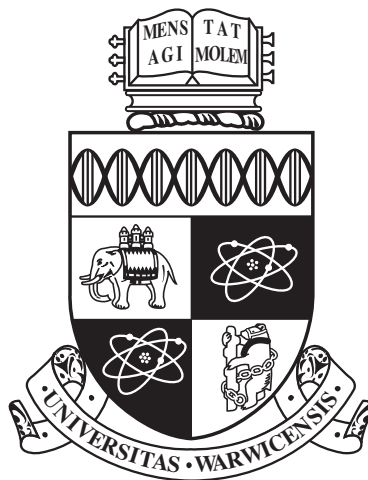
This thesis is made available online and is protected by original copyright.

Please scroll down to view the document itself.

Please refer to the repository record for this item for information to help you to cite it.

Our policy information is available from the repository home page.

For more information, please contact the WRAP Team at: wrap@warwick.ac.uk



**The Effect of Diet on *Plasmodium falciparum*
Development Revealed by NMR Metabolomics and
Image Analysis.**

by

Eva Caamaño Gutiérrez

Thesis

Submitted to the University of Warwick

for the degree of

Doctor of Philosophy

Systems Biology

October 2016

THE UNIVERSITY OF
WARWICK

Contents

List of Tables	v
List of Figures	vii
Acknowledgments	x
Declarations	xii
Abstract	xiii
Abbreviations	xv
Chapter 1 Introduction	1
1.1 The burden of malaria in the world	1
1.1.1 The disease	2
1.1.2 Control strategies of malaria	3
1.1.3 Malaria eradication strategies would benefit from implemen- tation of nutritional factors in their design	6
1.2 <i>Plasmodium</i>	8
1.2.1 Brief summary of <i>Plasmodium falciparum</i> life cycle and intra- erythrocytic stages	8
1.3 <i>P. falciparum</i> metabolism	13
1.3.1 Central Carbon Metabolism	14
1.3.2 Amino acid metabolism	25
1.3.3 Nucleotide biosynthesis	26
1.3.4 Apicoplast metabolism	27
1.3.5 ROS	28
1.4 Metabolites, not only biochemical intermediates	28
1.5 Metabolomics as an emerging field	29
1.5.1 Mass Spectrometry	32

1.5.2	Fourier Transformed Nuclear Magnetic Resonance Spectroscopy	34
1.5.3	Advantages and shortcomings of MS and NMR	36
1.5.4	Metabolomics of the malaria parasite	37
1.6	Aims and Objectives	39
Chapter 2 General Materials and Methods		41
2.1	Cryopreservation and parasite retrieval	41
2.1.1	Parasite retrieval	41
2.1.2	Cryopreservation	41
2.2	Maintenance of <i>Plasmodium falciparum in vitro</i>	42
2.2.1	Standard culture media	42
2.2.2	Red blood cells	43
2.2.3	Culture conditions	43
2.3	Synchronisation of cultures	44
2.4	Culture media. Design and preparation	45
2.4.1	Preparation and storage of stocks	45
2.4.2	Mixture and storage	45
2.5	Metabolite extraction	48
2.6	The effect of glutamine on glycolytic flux	50
2.6.1	Ringer's solution	50
2.6.2	Experimental procedure	50
2.7	NMR Analysis	51
2.7.1	Sample preparation for analysis in the NMR	51
2.7.2	NMR set-up and parameters	51
2.7.3	Metabolite identification	51
2.7.4	Preparation of standards for the creation of calibration curves	51
2.7.5	NMR Data analysis	52
2.8	Imaging sample preparation and analysis	54
2.8.1	High content Imaging.	54
2.8.2	Bright field microscopy	55
2.9	Life-cycle time course experiment	57
2.10	Statistical analyses	57
2.10.1	Statistical hypothesis tests	57
2.10.2	Principal Component Analysis (PCA)	58
2.10.3	Propagation of error	59
2.10.4	Analysis of covariance (ANCOVA)	59

Chapter 3	A tailored method to identify and quantify metabolites of <i>Plasmodium falciparum</i> in cell and media samples using Nuclear Magnetic Resonance (NMR)	60
3.1	Introduction: <i>P. falciparum</i> intra-erythrocyte meta-bolic network revealed by metabolomics	60
3.2	Experimental	63
3.3	Results and discussion	64
3.3.1	Adequate signal detection on undisturbed parasites	64
3.3.2	Metabolite identification	74
3.3.3	Creation of calibration curves for metabolite quantification	81
3.3.4	Validation and pipeline assembly	89
3.3.5	Pilot study: Glycolysis and glutaminolysis are drivers of the biomass production, a trophozoite study	91
3.4	Conclusions	99
Chapter 4	Comparative metabolomics of early and late developmental stages of intra-erythrocytic <i>Plasmodium falciparum</i>	101
4.1	Introduction: Paucity of metabolic studies involving early intra-erythrocytic stages of <i>P. falciparum</i>	101
4.2	Experimental	103
4.3	Results and Discussion	103
4.3.1	Intracellular metabolite fingerprint showed unique and distinguishable features between RBCs and iRBCs at the different asexual stages ring and trophozoite	103
4.3.2	Extracellular metabolite fingerprint showed unique and distinguishable features between RBCs and iRBCs at the different ring and trophozoite asexual stages	111
4.4	Conclusions	119
Chapter 5	Morphological and initial metabolic characterisation of <i>Plasmodium falciparum</i> in physiological (blood-like) medium	121
5.1	Introduction: <i>Plasmodium in vitro</i> culturing conditions	121
5.2	Experimental	123
5.2.1	Media preparation	123
5.2.2	Image analysis	123
5.2.3	Metabolomics experiment	123
5.3	Results and discussion	124

5.3.1	A qualitative and quantitative analysis on the effects of physiological media on <i>P. falciparum</i> trophozoites	124
5.3.2	Uninfected RBCs and iRBCs present distinguishable metabolic profiles when in blood-like medium	131
5.4	Conclusions	135
Chapter 6 Developmental and metabolic consequences of nutrient availability in intra-erythrocytic stages of <i>Plasmodium falciparum</i>		136
6.1	Introduction: The role of metabolites beyond pathways intermediates	136
6.2	Experimental	140
6.2.1	NMR metabolomics	140
6.2.2	Imaging	141
6.3	Results and discussion	141
6.3.1	Characterisation of parasite growth phenotypes in response to nutrient availability using HCl	141
6.3.2	Bright field microscopy reveals the effect of nutrient availability in cycle length and progeny numbers	147
6.3.3	NMR metabolomics shows how nutrient availability alters consumption and excretion of metabolites	154
6.4	Conclusion	173
Chapter 7 General conclusions		175
Bibliography		179
Appendix A NMR metabolomics datasets		218
Appendix B Publication		254
Appendix C Curriculum Vitae		261

List of Tables

1.1	<i>Plasmodium</i> -specific databases.	14
1.2	A comparison between mammal and parasitic glycolytic enzymes . .	16
1.3	MS and NMR pros and cons	37
2.1	Concentrations of RPMI culture media.	46
2.2	Stock solutions details.	47
2.3	Concentrations of glucose and glutamine.	50
2.4	Image analysis validation statistics	57
2.5	Propagation of error formula calculation	59
3.1	NMR acquisition parameters (on 600 MHz spectrometer)	64
3.2	Identified metabolites, their position in spectrum and signal selected for quantification.	79
3.3	Coefficients of the linear model fitted for quantification	86
3.4	Coefficient discrepancy and error associated of carbons used for quan- tification	88
3.5	Concentration comparison measured vs theoretical	91
4.1	Consumption/Excretion concentrations (in mM) of the main drivers of glycolysis. Average of three samples.	117
4.2	Picomoles consumed and excreted per cell of the main drivers of gly- colysis.	117
5.1	Mann-Whitney-Wilcoxon test results	130
6.1	TMRE area linear model parameters	147
6.2	Number of merozoites per schizont. Mann-Whitney-Wilcoxon test results.	153
6.3	Area comparison. Mann-Whitney-Wilcoxon test results.	155

6.4	ANCOVA significance values for the comparison of fitted linear model slopes.	169
A.1	Chapter 3- Cellular extracts concentrations (mM)	218
A.2	Chapter 3- Supernatant concentrations (mM)	222
A.3	Chapter 4- Cellular extracts concentrations (mM)	223
A.4	Chapter 4- Supernatant concentrations (mM)	225
A.6	Chapter 5- Media concentrations (mM)	227
A.7	Chapter 6- Media concentrations (mM)	228
A.5	Cellular extracts fold change with respect to RBC comparison.	253

List of Figures

1.1	Estimated malaria cases and deaths 2000-2015	2
1.2	Classification of countries by stage of malaria eradication	2
1.3	The world map of undernourishment 2014-2015.	7
1.4	<i>P. falciparum</i> life cycle with special emphasis on intra-erythrocytic stages.	10
1.5	Mid-trophozoite stage of <i>P. falciparum</i>	13
1.6	TCA and electron transport chain representation of <i>P. falciparum</i> .	20
1.7	Similarities between cancer cells and <i>P. falciparum</i>	22
1.8	Representative diagram of the system presented in Newsholme <i>et al.</i>	24
1.9	Newsholme <i>et al.</i> model simulation.	25
1.10	Giemsa stained <i>P. falciparum</i>	26
1.11	Metabolomics work-flow.	32
1.12	Diagram of a simple mass spectrometer	33
1.13	Basic arrangement of an NMR spectrometer	35
1.14	Objectives	40
2.1	Metabolite extraction method.	49
2.2	Sample analysis and concentration calculations diagram	53
2.3	Media samples analysis pipeline	54
2.4	Bright field analysis validation	56
3.1	1D ^{13}C Spectra of Trophozoite suspension after 2h incubation in Ringers containing 11 mM $1\text{-}^{13}\text{C}$ -Glucose.	66
3.2	1D ^1H NOESY Spectra of Trophozoite suspension after 2h incubation in Ringers containing 11 mM $1\text{-}^{13}\text{C}$ -Glucose	68
3.3	1D ^{13}C Spectra of enriched mature trophozoite-iRBC sample after 2h incubation in Ringers containing 11 mM $1\text{-}^{13}\text{C}$ -Glucose	69
3.4	1D ^{13}C Spectra of mature 15%-parasitaemia trophozoite-iRBC sample after 2h incubation in Ringers containing 11 mM $1\text{-}^{13}\text{C}$ -Glucose .	71

3.5	2D ^1H - ^{13}C HSQC Spectra of cellular extract from mature trophozoite-iRBCs after 2h incubation in Ringers containing 11 mM 1- ^{13}C -Glucose	72
3.6	^1H - ^{13}C HSQC Spectra of cellular extracts from mature trophozoite-iRBCs in different glucose types	74
3.7	^1H - ^{13}C HSQC Spectra of cellular extract from mature trophozoite-iRBCs	77
3.8	^1H - ^{13}C HSQC Spectra of media after incubation with mature trophozoite-iRBCs	78
3.9	Calibration curves chosen for quantification (I)	83
3.9	Calibration curves chosen for quantification (II)	84
3.9	Calibration curves chosen for quantification (III)	85
3.10	RPMI measured concentrations	90
3.11	Experimental conditions tested in glucose-glutamine experiment . .	92
3.12	Concentrations of metabolite extracts (glucose-glutamine experiment)	94
3.13	Percentages of artificially introduced ^{13}C after incubation with U- ^{13}C -D-glucose	96
3.14	Representation of carbon magnetisation pathways of glucose.	97
3.15	Percentages of artificially introduced ^{13}C before and after incubation with 1- ^{13}C -D-glucose	98
4.1	PCA score plots of intracellular concentrations	105
4.2	PCA loading plot of cellular extracts.	106
4.3	Concentrations of cellular samples.	108
4.4	Heatmaps fold change with respect to RBCs	110
4.5	PCA media samples	112
4.6	Concentrations in media before and after incubation with cells . . .	114
4.7	Consumption/Excretion of metabolites per parasite per hour	118
5.1	Bright field imaging of parasites growing in RPMI based media	126
5.2	Bright field imaging of parasites growing in different media 124h after exposure	128
5.3	Bright field imaging quantitative analysis of parasites growing in different media	129
5.4	PCA scatterplot of metabolite concentrations in blood-like medium .	132
5.5	Concentrations of metabolites found in Blood-like media	134
6.1	TMRE stained <i>P. falciparum</i> trophozoite infected erythrocytes	142
6.2	Examples of rejected fields	143

6.3	<i>P. falciparum</i> 3D7 area stained by Hoechst (a) and TMRE (b) . . .	146
6.4	Bright field microscopy images of selected time points	150
6.5	<i>P. falciparum</i> 3D7 parasites after 119 h incubation (74 h post sampling)	151
6.6	Number of merozoites in schizonts in second generation parasites . .	152
6.7	Area of second generation parasites	154
6.8	Principal Component Analysis Score plots from spectra bucket tables	156
6.9	Principal Component Analysis results from means of metabolite concentration in media	157
6.10	Percentage of amino acid abundance in <i>H. sapiens</i> haemoglobin . . .	158
6.11	Concentration changes over time in complete culture medium containing <i>P. falciparum</i> infected RBCs	161
6.12	Concentration changes over time in blood-like and low glucose blood-like media containing <i>P. falciparum</i>	163
6.13	Absolute change over time in all media containing <i>P. falciparum</i> infected RBCs	165
6.14	Illustration of the linear models fitted	167
6.15	Slopes of the linear models	168
6.16	Percentage of excreted products with respect to glucose and glutamine consumed	172

Acknowledgments

In chronological order, I would firstly like to thank my parents Jose and Laly, my sister Ana and my grandmother and godmother (2 in 1) Alla, that even though did not understand some of my decisions they loved me, supported and encouraged me to arrive to where I am now. I would like to thank them for putting my interests first when health family problems started and for secretly hoping I would come back every time I did (and probably some others more). Special thanks to my dad that had never any doubt I would achieve whatever I was committed to, he gave me the strength to become a better me every day.

I would also like to make a special mention to my grandfather Ezequiel Manuel Guillermo Caamaño Sendón, who left us recently. He taught me that every day you have to make an effort, earn your bread in one way or another. He also keeps my scepticism and lost faith in not such absolute states and for whom I wish, I dream, is back with his love.

I would like to thank all those inspiring teachers I had in Leon who never put limits to where their students could arrive. To my school friends Patri, Angel, Diego and Adri for your good wishes and constant friendship. In this path to adulthood I have met incredible people and of them I must mention specially, David Garcia Valcarce who is a first class scientist and a first class (with honours) person and my team; with whom I spent the best times I can remember during both University and Masters years.

To the people that believed in me and gave me the opportunity of my life that started in Leon with Paqui and Vences, followed by my time as research assistant in Warwick with Jose Gutierrez-Marcos and Lili and finally to the ones that gave me

the real opportunity that changed my life Jim Beynon and Vicky Buchanan. Thank you for selecting me for the Systems Biology program at the University of Warwick.

It has been in the last 5 years at Warwick where I have made for life friendships such as Nikita and Lucienne who deserves a special huge thank you for her help with my English issues, for choosing me to be her collaborator and for the daily whatsapps and science debates that make us both better scientists. Last but not least the person with whom I share every aspect of life, my partner, my life-mate and my pillar during this last 4 years, Arturas Grauslys. He has made me a better person, a better scientist and gave me so much that I do not have words to express.

Finally I would like to thank the people without whom this work would not have been possible. The Parasitology Department at LSTM, specially Giancarlo Biagini for giving me the opportunity to work in his lab and Ghaith, Grazia, Ricky and Lisa (RIP) for their final proofreading effort and their friendship and encouragement. To the NMR centre people, especially Marie Phelan for her incredible support setting up the metabolomics experiments and Rudi Grosman for his help setting up my ssh-ing remotely to the NMR centre. To Arturas Grauslys once more for being the other half of the team that made possible to do all the time-course experiments we did. I would like to thank Fidel Madrazo for his ideas towards image analysis and Alejandro Peña and Maria Getino for putting us in contact. I would also like to mention Matt Gibson because thanks to his support I could find a compatible job that allowed me to finish my thesis while still doing very cool research.

During the past 5 years I have overcome many difficulties and pass hard times, but over all things I have learned, which gives me an incredible satisfaction. Thank you for reading.

Declarations

The work contained in this thesis is my own, with exception of where acknowledged below, and completely original. I confirm that this thesis has not been submitted for another degree at another University.

The proliferating hypothesis presented in the Introduction was published as: Salcedo-Sora JE, **Caamano-Gutierrez E**, Ward SA, Biagini GA. The proliferating cell hypothesis: a metabolic framework for Plasmodium growth and development. Trends Parasitol 2014;30:1705. Paper attached in Appendix B.

NMR spectroscopy parameter set up and experiment choices used in Chapters 3 to 6 were provided by Dr. Marie Phelan, Shared Research Facility Manager of the NMR Centre at the University of Liverpool.

Samples of the 54 h experiment presented in Chapter 6 were collected with the assistance of Arturas Grauslys.

Abstract

The development of axenic *in vitro* growth models of the human malaria parasite *Plasmodium falciparum*, has been pivotal in accelerating knowledge of this very important human pathogen. Despite the importance of this pathogen, there have been very few studies relating to the metabolism of the parasite. Furthermore, much of the preceding studies have been undertaken using culture conditions that do not accurately represent the physiological environment of the human host. There is a need to address whether different nutrient environments would trigger a parasite response at the systems level promoting a metabolic rewiring that would have an effect in progeny generation or life cycle progression. Because of its robustness, reproducibility and suitability for footprinting studies, NMR spectroscopy was chosen as the analytic technique for the study. One of the disadvantages of NMR is limited availability of software for identification and quantification of metabolites. This was taken as an opportunity to develop a pipeline using free, open-source programming framework.

This tool was used to find unique and discriminatory metabolic profiles for both uninfected and *P. falciparum* infected red blood cells at various life-cycle stages using cell extracts and extracellular material. With the aim of studying parasite development in physiological conditions a culture medium mimicking human blood conditions was developed and tested on *P. falciparum* infected RBCs finding both phenotypic and metabolic differences.

Further studies consisted of the development of tightly synchronised parasite cultures that were followed during 54 h using NMR-based metabolomics to assess

consumption and excretion of metabolites in media, and high content imaging and bright field microscopy to assess parasite size and progeny. The measurements were taken under three different nutritional conditions: usual *in vitro*, physiological-like and hypoglycaemic. In usual culturing conditions *P. falciparum* 3D7 life cycle lasted around 45 h. During the early stages there was moderate consumption of glucose and glutamine and excretion of lactate, alanine and glycerol. During the mature trophozoite stages and schizonts, glucose uptake dramatically increased with a consequent augmentation of the lactate, alanine and glycerol production. These were excreted but their function was not clear. It was observed that these “wasteful” products were proportionally lower in the early developmental stages than in the later ones, suggesting a higher demand of raw materials (glucose) for biomass production during the early stages. During the late trophozoite stage the most abundant amino acids in the haemoglobin chain (leucine, valine and glycine) were excreted, a likely consequence of the need for space to finish maturation. Myoinositol, which is essential for creation of membranes was also avidly consumed.

When comparing these findings with parasites growing in more physiological conditions there was a noticeable delay in the life cycle of at least 9 h. Consequently haemoglobin digestive products were excreted later in the time course. A decrease in the progeny resulting from schizonts containing significantly fewer merozoites was also observed. Parasites growing in physiological conditions but challenged with lower glucose availability also presented a further delay of the life-cycle and a decreased number of merozoites with respect to usual laboratory conditions. Haemoglobin degradation products were also excreted later in the life cycle and at lower rates compared to the parasites grown in complete media.

These results suggest that there are significant differences between *in vivo* and *in vitro* life-cycles of *P. falciparum*. Such effects as the reduction in growth rates and elongation of the life cycle, if not accounted for, could severely compromise the *in vivo* results of *in vitro* drug killing rates assays.

Abbreviations

1D	One dimensional
2D	Two dimensional
ACT	Artemisinin-based Combination Therapy
Ald	Aldolase
AT	Artemisinin
ATP	Adenosin triphosphate
BCKDH	Branch chain ketoacid dehydrogenase
BL	Blood-like medium
BL parasites	<i>P. falciparum</i> 3D7 growing in blood-like medium
CG	Cycloguanil
CM	Complete medium (no serum)
CM parasites	<i>P. falciparum</i> 3D7 growing in complete medium
CoA	Coenzyme A
CQ	Chloroquine
DHAP	Dihydroxyacetone phosphate
DNA	Deoxyribonucleic acid
EC	Enzyme commission number
EIF2 α	Eukaryote initiation factor two alpha
ER	Endoplasmic reticulum
ETC	Electron transport chain
FA	Fusidic acid
FADH ₂	Flavin adenine dinucleotide
FAO	Food and agriculture organization of the United Nations

FH	Fumarate hydratase
G3PDH	Glyceraldehyde 3 phosphate dehydrogenase
GC	Gas chromatography
GPI	Glucose phosphate isomerase
GSH	Glutathion reduced
HCI	High content imaging
HIF	Hypoxia inducing factor
HMDB	Human metabolome database
IC ₅₀	Half maximal inhibitory concentration
iRBC	Infected red blood cell
IUPAC	International union of pure and applied chemists
K _m	Michaelis constant
LacDH	Lactate dehydrogenase
LC	Liquid chromatography
LG	Low glucose blood-like medium
LG parasites	<i>P. falciparum</i> 3D7 growing in low glucose blood-like medium
MCT	Monocarboxylate transporter
MQO	Malate-quinone reductase
MS	Mass spectrometry
NAD	Nicotinamide adenine dinucleotide
NCBI	National Centre for Biotechnology Information
NMR	Nuclear magnetic resonance
NPP	New Permeation Pathways
P	<i>Plasmodium</i>
pABA	para-aminobenzoic acid
PC	Principal component
PCA	Principal component analysis
PDH	Pyruvate dehydrogenase
PEP	Phosphoenolpyruvate
PEPCK	Phosphoenolpyruvate carboxykinase

PFK	Phosphofructokinase
PfHT	<i>Plasmodium falciparum</i> hexose transporter
PG	Proguanil
PGK	Phosphoglycerate kinase
PI	Phosphatidyl inositol
PK	Pyruvate kinase
PRPP	5-phospho-D-ribose- α -1-pyrophosphate
PSAC	<i>Plasmodium</i> surface anion channel
QCDs	Quinoline containing drugs
RBC	Red blood cell
ring	Young trophozoite
RNA	Ribonucleic acid
ROS	Reactive oxygen species
RPMI	Roswell Park Memorial Institute medium
RT	Room Temperature
SEM	Standard error of the mean
SOD	Superoxide dismutase
TCA	Tricarboxylic acid cycle
TMRE	Tetramethyl rhodamine ethyl ester
TNF	Tumor necrosis factor
TOR	Target of rapamycin
TPI	Triose phosphate isomerase
troph	Mature trophozoite
TSP	Trimethylsilyl propionic acid
V_{max}	maximum velocity
VEGF	Vascular endothelial growth factor
vs	Versus
WHO	World Health Organisation

Chapter 1

Introduction

1.1 The burden of malaria in the world

Malaria is a prominent disease with an extremely high burden worldwide. In 2015 alone it caused over 200 million cases (see Figure 1.1) and this is a figure from a year in which 37% reduction of its incidence was reported [1]. Malaria is a vector-borne infectious disease, whose pathology and symptoms are caused by a protozoan parasite of the genus *Plasmodium*. *Plasmodium* spp. are transmitted to humans by the bite of the specific arthropod vector, the female *Anopheles* mosquitoes. *Anopheles* habitat is distributed across the world [2], but currently malaria incidence affects the warmest areas of the planet including Africa, Central and South America and South-East Asia (malaria distribution across the world shown in Figure 1.2). However, in the past malaria outbreaks have occurred in colder climates as for example Canada in 1820s [3] and in Mediterranean countries [4] but improvements in the health systems, control programmes and general infrastructure, have allowed the elimination of the *Plasmodium* parasite from more developed countries. Although climate change and other environmental factors are increasing the risk of malaria outbreaks in countries where elimination was established [5] and resistance emergence is a major problem, it has been historically proven that by applying the correct control measures and providing access to good health conditions, eradication is possible. Further examples are the elimination of the disease on islands such as the Falkland Islands, Mauritius, Taiwan and rapidly developing tropical regions such as Hong Kong [6]. Thus this is a very challenging matter for the poorest countries in which access to medication and control resources are very limited. Programmes such as the Roll Back Malaria partnership, the Grand Challenges supported by the Bill and Melinda Gates Foundation or the recent creation of Ross Fund are helping

to pave the way towards the reality of malaria eradication.

WHO region	Estimated number of malaria cases (000's)				Change	Estimated number of malaria deaths				Change
	2000	2005	2010	2015	2000-2015	2000	2005	2010	2015	2000-2015
African	214 000	217 000	209 000	188 000	-12%	764 000	670 000	499 000	395 000	-48%
Americas	2 500	1 800	1 100	660	-74%	1 600	1 200	1 100	500	-69%
Eastern Mediterranean	9 100	8 600	4 000	3 900	-57%	15 000	15 000	7 000	6 800	-51%
European*	36	5.6	0.2	0	-100%	0	0	0	0	
South-East Asia	33 000	34 000	28 000	20 000	-39%	51 000	48 000	44 000	32 000	-37%
Western Pacific	3 700	2 300	1 700	1 500	-59%	8 100	4 200	3 500	3 200	-60%
World	262 000	264 000	243 000	214 000	-18%	839 000	738 000	554 000	438 000	-48%
Lower bound	205 000	203 000	190 000	149 000		653 000	522 000	362 000	236 000	
Upper bound	316 000	313 000	285 000	303 000		1 099 000	961 000	741 000	635 000	

* There were no recorded deaths among indigenous cases in WHO European Region for the years shown.
Source: WHO estimates

Figure 1.1: **Estimated malaria cases and deaths 2000-2015.** World Health Organisation (WHO) [1].

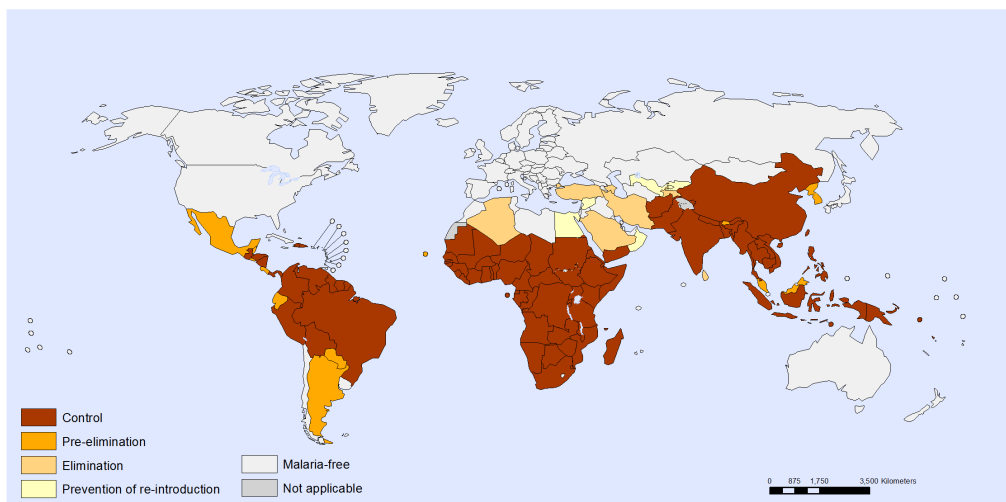


Figure 1.2: **Classification of countries by stage of malaria eradication (December 2013).** WHO [1].

1.1.1 The disease

Malaria symptoms usually manifest 8-25 days post-infection, as consequence of the release of parasites into the blood stream. Malaria disease can be classified in

uncomplicated or severe. Uncomplicated malaria symptoms are flu-like (unspecific) including headaches, fever, chills and body aches, which makes diagnosis difficult [7]. The most typical symptom is the cyclical occurrence of shivers and high fever every 36 to 72 h depending on the *Plasmodium* species. Severe malaria results when infections are complicated by abnormalities in patient's blood and metabolism such as severe anaemia, hypoglycaemia and lactic acidosis. Other specific signs include the presence of haemoglobin in the urine and retinal damage [8]. More severe symptoms of the disease involve organ failure. The most severe case presents when cerebral malaria is developed (only caused by *P. falciparum*). Cerebral malaria includes neurological symptoms that range from abnormal posturing to seizures or coma [7] and in all cases prompt diagnosis and treatment are paramount to avoid fatal outcomes. Consequences of the disease are not limited to the obvious health burden but also the socio-economic factors that it involves, not only in health care expenses but also in labour and productivity decrease with the consequential effect in family economy.

1.1.2 Control strategies of malaria

Methods to control and ultimately eradicate malaria can be classified as prevention or treatment.

1.1.2.1 Prevention

Prevention of malaria can be classified as vector control, vaccine development or preventive chemotherapy. Vector control tools include insecticide-treated mosquito nets [9] and indoor residual spraying [10]. These measures have been proven very effective in reducing malaria prevalence in highly populated areas. However insecticide resistance is a serious threat and existing methods of vector control need to be improved to achieve malaria elimination targets [11]. Disease prevention has also been tried by vaccine development but due to the high antigen variability of the parasite and the different life stages, no vaccine with over 70% protective effect has been achieved [12, 13]. Antimalarial drugs have applications beyond curing patients and they are used in prevention, especially in high risk groups such as pregnant women and children.

1.1.2.2 Treatment

Medication reduces mortality and diminishes transmission. The most widely spread antimalarial drugs can be classified into five main categories, according to both their

structure and biological activity [14]. Even though resistance has developed to all of them [15, 16], they are the most common way of fighting the disease. These drugs target mostly the specialised organelles of the parasite, generally in the erythrocyte stage. Their modes of action can be classified into the following groups:

1. **Quinoline-containing drugs (QCDs)**

Since their introduction in the 1940s, these drugs have been essential in the treatment of malaria. QCDs are a broad group of drugs that include quinines, 4-aminoquinolines, 8-aminoquinolines and quinolinemethanols [17]. Nowadays, these drugs are classified in two types: type-1 which are weak bases and hydrophilic and type-2 that are even weaker bases and lipid soluble at neutral pH [18]. Their core structure is a central solid aromatic nitrogen ring whose properties would vary depending on the functional groups added to the main quinoline molecule. Some examples of these antimalarial drugs are chloroquine, quinine and mefloquine. QCDs act primarily on haem disposal in the food vacuole of the parasite. Under normal conditions, haemoglobin is degraded and haem, which is cytotoxic, is generated and detoxified by the formation of an inert crystal called hemozoin [14] (see Section 1.3). The QCDs form complexes with haem in order to prevent its conversion to an inner element and therefore keeping its cytotoxic character. Resistance is conferred by multiple gene mutations and different mechanisms have been described, from a reduced accumulation of drug in the cell to an alteration in the transport processes [19]. Even though all QCDs are thought to act in a similar way, their effects on the feeding process are slightly different. For example, type-1 drugs (chloroquine, amodiaquine and piperazine) cause an accumulation of undigested haemoglobin which suggests an inhibition of haemoglobin digestion. However type-2 drugs (quinine and mefloquine) do not show an accumulation of haemoglobin, indicating an inhibition of the ingestion of host haemoglobin [20].

2. **Antifolates drugs and combinations**

The malaria parasite can synthesise and salvage folate precursors, whilst mammals have no *de novo* synthesis and rely on dietary sources, meaning that disturbing this pathway would definitely have a negative impact on the parasite. Antifolates are classified in two classes: type-1 that mimic p-aminobenzoic acid (pABA), competing for the active site of dihydropteroate synthase (EC 2.5.1.15) and type-2 that inhibit dihydrofolate reductase (EC 1.5.1.3). Both inhibit the folate pathway which results in decreased pyrimidine synthesis,

hence, reduced DNA [18].

3. **Hydroxynaphthaquinones: Atovaquone**

Atovaquone (ATQ) is used for treatment and prevention of malaria, usually in combination with the antifolate proguanil (PG). The mitochondrial electron transport chain is critical for parasite survival and ATQ acts principally on mitochondrial functions, specifically inhibiting the cytochrome *bc*₁ complex by kidnapping ubiquinone and consequently collapsing the mitochondrial membrane potential [21]. It also acts on the dihydroorotate dehydrogenase (EC 1.3.3.1), which catalyses the reaction from dihydroorotate to orotate, bridging pyrimidine biosynthesis and the mitochondrial electron transport system [22]. The half maximal inhibitory concentration (IC₅₀) of ATQ and PG are reduced when used together. Even though PG inhibits the dihydrofolate reductase (EC 1.5.1.3), the effect of both drugs in the pyrimidine biosynthesis seems to not explain the synergistic effect [23] so it has been suggested that PG affects a mitochondrial function that becomes essential when ATQ inhibits the electron transport chain [21].

4. **Endoperoxide compounds: Artemisinin group**

The endoperoxides are active throughout all the phases of the asexual intra-erythrocytic cycle and also work on young gametocytes. Artemisinin and derivatives have a trioxide ring with endoperoxide bridge (C-O-O-C), which differs in its nitrogen content from most antimalarial drugs and this gives them several advantages over others such as their speed of action or little cross resistance with other drugs. However, they have short elimination half-lives which results in inability to eliminate all parasites during the treatment, resulting in recrudescence infections [24]. The current hypothesis of their mode of action relies on the formation of C-centred radicals by a reductive cleavage of the peroxide by ferroheme ferrous-protoporphyrin IX (Fe(II)PPIX). These radicals would alkylate biomolecules creating general damage and leading to the death of the parasite. There are further hypotheses that indicate a role in the haem crystallisation process which would result in general damage or other potential mechanisms that consider artemisinin as a source of hydroperoxide that causes the death of the parasite. Resistance to artemisinin has been reported since 2009 [25], and it has been suggested to be multigenic and share similarities with the quinoline family [26]. It has also been indicated from transcriptomic studies that this resistance may be associated with the increased capacity of protein synthesis in the schizont stage because it counteracts the

protein damage caused by the oxidative stress and/or protein alkylation effect of this drug [27].

5. Antibiotics

All plastids arose by endosymbiosis of a primitive prokaryotic cell. Following this primary endosymbiosis, some other plastids are thought to have been laterally transferred to other organisms and *Plasmodium* is one of them [28]. Thus, *Plasmodium* apicoplast and mitochondrion present certain susceptibility to several antibiotics. A good representative of this drug type is fusidic acid. It slows down bacterial translation and blocks peptidyl tRNA in the ribosomal P site [29]. The effect of fusidic acid is immediate and even though ribosomes continue working, they do it very slowly [30].

Resistance poses a problem for malaria control. For *P. falciparum* the use of two or more drugs with different modes of action in combination is the recommended treatment to provide an adequate cure rate and also delay development of resistance. The most widely used, and recommended by the WHO, is artemisinin-based combination therapy (ACT) in which the quick acting artemisinin (or one of its derivatives) is administered with a drug from a different class such as mefloquine, amodiaquine, piperaquine or lumefantrine [31, 32]. Chloroquine is still the first line of treatment for *P. vivax* [33] and *P. ovale*, while primaquine is used to treat the liver stages of *P. vivax* [34]. Resistance emergence is an increasing concern due to the limited recent antimalarial drug developments [35]. In the last decade, numerous novel antimalarial inhibitors and targets have been, and currently are, evaluated to provide alternatives for treating drug-resistant malaria parasites. Some of the targets being evaluated are chromatin-modifying enzymes, parasitic metabolic pathways (e.g. the coenzyme A pathway), parasite transporters and mitochondrial enzymes [36]. The most successful up-to-date new compounds have been the spiroindolones, a new class of fast-acting schizont-targeting drugs that present activity against drug-resistant *Plasmodium* through targeting protein synthesis in the malaria parasite [37]. Efforts to keep researching for compounds and alternatives to control drug resistance emergence are still crucial in the path towards malaria eradication.

1.1.3 Malaria eradication strategies would benefit from implementation of nutritional factors in their design

Mosquito population control and drug treatment and prevention are not enough to completely eradicate the disease. Socio-economic changes also need to be implemented, facilitating the access to health care and increasing surveillance for the

disease. An improvement in other health areas such as sanitation and nutrition will also aid the control and eradication of the disease. For example, children with severe malnutrition are not only more vulnerable to disease but also do not present the usual symptoms of malaria, thus obstructing diagnosis and treatment [38]. The relationship between poverty and disease can be illustrated by looking at the world map of undernourishment (see Figure 1.3), which widely overlaps with the regions where malaria is endemic.

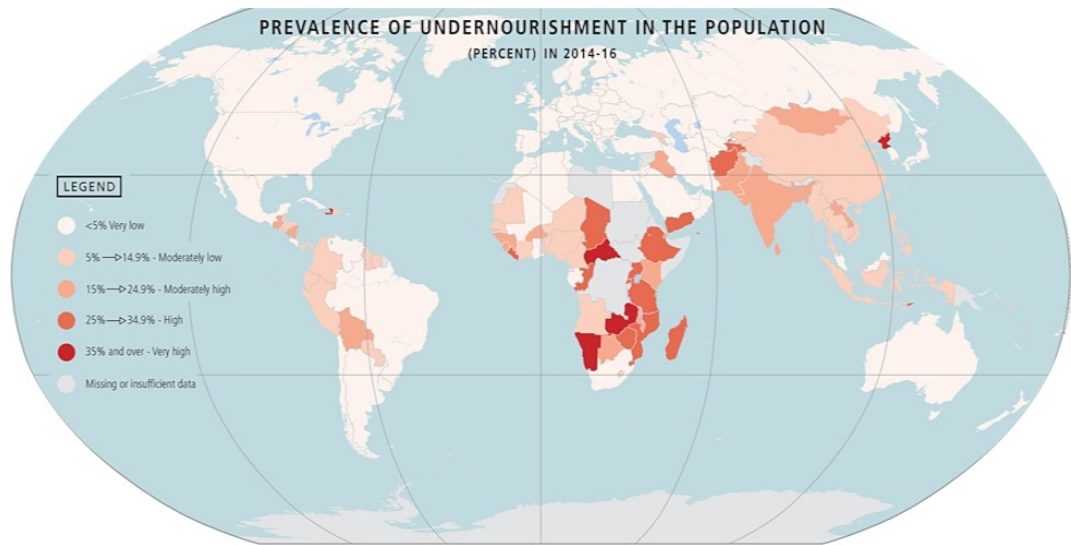


Figure 1.3: **The world map of undernourishment 2014-2015.** Source: Food and Agriculture Organisation of the United Nations (FAO).

Nutritional deficiencies are linked with increased susceptibility to infectious diseases [39]. In the same way that nutritional excesses have been linked with genetic mutation and disease proliferation [40], nutritional deficiencies often exhibit complex interactions with infectious diseases. For example the micronutrient zinc, when low in plasma has been related to increased mortality from malaria [41]. Zinc deficiency affects immune responses and exacerbates malaria for which the immune response relies on macrophage killing of infected cells [42]. Moreover, studies have shown a protective effect of zinc supplementation during malaria infection. Supplementation of zinc to the diet of mice during *P. berghei* infection resulted in decreased oxidative stress markers [43]. Overall *Plasmodium* as a parasite is affected by its host's health and better strategies for malaria control need to implement nutritional factors in their design.

1.2 *Plasmodium*

The genus *Plasmodium* comprises over 200 species that infect a wide range of hosts from humans to bats, squirrels, marsupials, rodents or birds. In fact, much of our knowledge of pathogenesis depends on studies in non-human species such as the rodent parasites *P. berghei* and *P. yoelii* and *in vitro* cultures. There are five species of malaria parasites that affect humans namely; *P. falciparum*, *P. vivax*, *P. malariae*, *P. ovale* and *P. knowlesi*. *P. vivax* and *P. ovale* present dormant forms during their life cycle called hypnozoites that can cause relapsing infections. However, the most severe manifestations of the disease are caused by *P. falciparum*, thus patients suffering from malaria are classified into uncomplicated or severe malaria. Different species present susceptibility to different drugs, thus correct identification is paramount for successful treatment. *P. falciparum* [44] and to a much lesser extent *P. vivax* [45] are the main causes of disease and death from malaria. Due to its importance in disease and robust culturing methods available, *P. falciparum* is the species of interest in this thesis.

1.2.1 Brief summary of *Plasmodium falciparum* life cycle and intra-erythrocytic stages

P. falciparum life cycle involves stages in humans and mosquitoes [46]. The infection is initiated when sporozoites are injected with the saliva of a feeding mosquito. Sporozoites are then carried by the circulatory system to the liver where they invade hepatocytes. The intracellular parasite undergoes asexual replication within the hepatocyte, which culminates in the production of merozoites that are released into the bloodstream. The merozoites invade erythrocytes and undergo an enlargement period in their life cycle as trophozoites (which in their early stages are referred to as ring form due to their morphology). Trophozoites have an active metabolism that includes the proteolysis of host haemoglobin (this is further reviewed in Section 1.3). This stage ends with multiple rounds of nuclear division (schizont stages) resulting in a final burst of merozoites, which will start the cycle again (see Figure 1.4) lasting, in total, around 48 hours [47, 46]. The blood stage of the infection is responsible for much of the disease pathology, with the typical fever episodes occurring coincidentally with the erythrocyte burst [48]. A variable percentage of parasites (typically 1%, but can be more, depending on selective pressure [49]) do not carry on with the asexual cycle and instead they differentiate into sexual forms known as macro and microgametocytes. Gametocytogenesis is modulated by environmental factors [50] with the percentage of gametocytes produced increased

under stress conditions. Ingestion into the mosquito also induces gametocytogenesis and breaking away from the host erythrocyte. These gametes join together into a zygote, which is the only diploid stage, and meiosis occurs within it. During this process, *Plasmodium* shows recombination between genes determining characters such as enzymes, antigens, drug resistance and virulence [51]. The zygote develops into a motile ookinete, which penetrates the gut epithelial cells of the mosquito and matures into an oocyst [52]. Multiple rounds of asexual replication will result in the production of sporozoites, which are released into the mosquito hemocele and migrate to the salivary glands, thus completing the life cycle [47, 46, 52]. The life stage that has been studied in this project is the intra-erythrocytic one; thus further sections expand upon processes related to this stage.

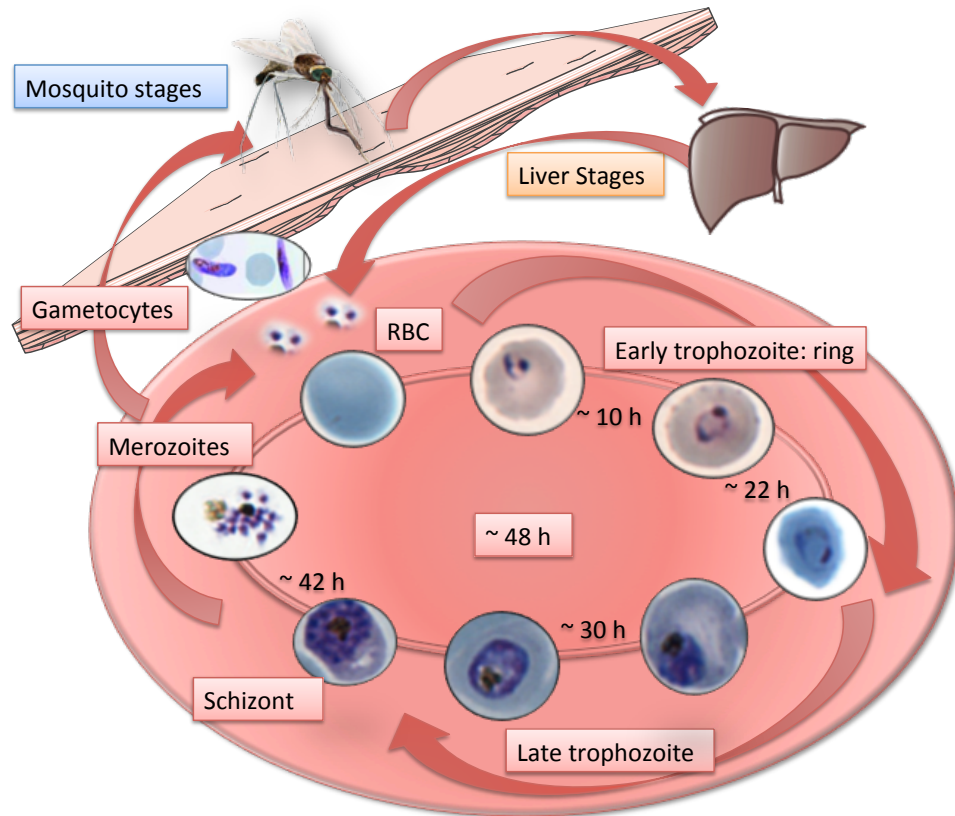


Figure 1.4: *P. falciparum* life cycle with special emphasis on intra-erythrocytic stages. After a mosquito meal, sporozoites are released into the blood stream. There they travel to the liver where they colonise hepatocytes and reproduce releasing a large number of merozoites into the blood stream. Each successful merozoite colonises an erythrocyte and in a period of approximately 48 h will develop into an assortment of forms with different appearances and metabolic profiles (rings and trophozoites) until nuclear division starts being evident in a syncytium form called schizont. Schizonts will burst releasing into the blood stream between 8-32 merozoites to carry on the asexual life cycle. A proportion of new invading merozoites will differentiate into single male or female gametocytes.

1.2.1.1 Red blood cell (RBC) invasion and immune evasion strategies

All merozoites of the *Plasmodium* species must undergo apical reorientation and engage with binding receptors on the RBC to induce invagination of the erythrocyte bilayer, resulting in engulfment of the parasite [53]. Receptors that mediate this step are one of the limiting factors for most of the *Plasmodium* species, that can only invade cells with specific types of these receptors. However *P. falciparum* has redundant invasion pathways, some of which rely on interactions with glycoproteins containing sialic acid residues but others do not [54, 55]. This gives this species the most versatility, allowing it to have a high rate of RBC invasion success.

Once the parasite has invaded the RBC a full remodelling of the membrane and the metabolism of the erythrocyte converts the RBC to a carcass to fulfil the needs of the parasite. Some of these modifications involve the transport to the host of virulent proteins. The best characterised is *P. falciparum* erythrocyte membrane protein 1 (PfEMP1) which is involved in placental and cerebral malaria [56], its capability to adhere to endothelial cells is another important feature exclusive to *P.falciparum*. Only gametocytes and late trophozoites are able to undergo this adhesion step and this allows them to evade the immune system. They are sequestered in various organs including the brain and placenta; these are the most dangerous forms of the disease. Parasites in the placenta can cause premature delivery, low birth weight and increased mortality in both newborn and mother [57]. Accumulation in the brain is related to cerebral malaria, the most aggressive form of the disease.

1.2.1.2 Trophozoite stage: ring and trophozoite

The trophozoite stage comprises of a series of structural modifications, size enlargement and drastic shape remodelling that allows a more efficient invasion and colonisation of the host red blood cell. The merozoite is highly specialised to find, attach and colonise a RBC, utilising a core complement of organelles found in most eukaryotic cells. These include: a nucleus, endoplasmic reticulum (ER), a mitochondrion and Golgi apparatus and others not that common including a non-photosynthesising plastid (apicoplast) and some other apical organelles typical from apicomplexan protozoa and mostly involved in invasion [58]. After invasion, the parasites rapidly flattens into a ring, thus giving its name to the early trophozoite stages [59]. During this early trophozoite stage the centre of the parasite is thin and contains few structures, which are spread towards the edge of the parasite. Nuclear shape varies from sausage-like to a disk and this is what gives the ring appearance when look-

ing at Giemsa-stained slides. From this stage the parasite starts to establish an exomembrane system in the host cell cytoplasm to communicate with the extracellular environment [60]. The parasite starts feeding from the surrounding RBC through the cytostome [61]; this forms a tube to connect with the host cell. A second feeding mechanism is also observed consisting of small vesicles formed from either the cytostomal tube or the food vacuole [62]. Haemoglobin starts being digested, the globular part is used as amino acid source but the haem derivative is toxic and thus is converted into the inert haemozoin crystals that accumulate within the pigment vacuole [63].

Afterwards, there is an increase in the number of ribosomes, ER enlarges and Golgi shows more complexity, all signs of very active protein synthesis and trafficking. Mitochondrion and apicoplast, which are attached to each other, increase in size and the apicoplast contacts the food vacuole, which indicates some metabolic interaction [64]. After which, the surface of the trophozoite enlarges and membranous structures can be observed in the host cell. These are the Maurer's clefts, which have not been completely functionally characterised but they are thought to be involved in a parasite's unique secretory compartment used to route parasite proteins across the host erythrocyte towards the extracellular membrane where they play a role in nutrient uptake and immune evasion [65]. After feeding is established, the parasite exports various proteins into the RBC cytoplasm and surface. These proteins are classified into two types depending on whether they contain a motif called Parasite Export Element (PEXEL) [66, 67]; those without it are transmembrane proteins. Maurer's clefts play a crucial role in the storage and transport of these proteins [68]. Finally, at around 12 h after invasion, the RBC membrane undergoes changes causing increased permeability to a wide range of low molecular weight compounds such as isoleucine in a range of changes called NPP (new permeation pathways) [69, 70]. By mid-trophozoite stage an almost autonomous parasite has proliferated considerably and increased in size and complexity with a very much enlarged rough ER. Further changes occur associated with the RBC membrane that allow the parasite to adhere to endothelial cells. An illustrated representation of a mature trophozoite can be observed in Figure 1.5 , adapted from [64].

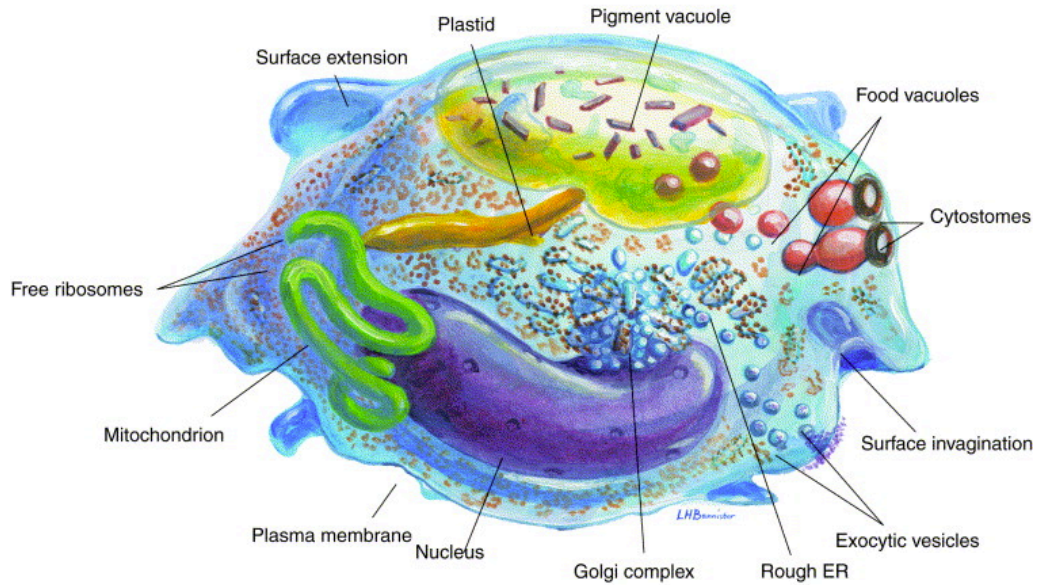


Figure 1.5: **Mid-trophozoite stage of *P. falciparum*.** This figure represents the parasite only (without the RBC). Note the pigment vacuole is where the haemozoin is stored and it is equivalent to inclusion bodies in bacteria Source: [64].

1.2.1.3 Schizonts

Schizont stages are defined by nuclear division. During this last stage, DNA replication, which started in the trophozoite stage must be completed by undergoing several rounds of mitosis to create progenies ranging from 8 to 32 cells. Nuclear division is accompanied by rough ER and ribosomal proliferation and later by the multiplication of mitochondria and apicoplast [64]. All these components are needed to assemble fully viable merozoites that would have everything necessary to invade a red blood cell and proliferate in the same manner.

1.3 *P. falciparum* metabolism

The information concerning the malaria parasite metabolic make-up, connectivity and regulation has been collated in different databases (see in Table 1.1). This information has been used to create different mathematical models [71, 72]. A summary of key metabolic pathway databases for *Plasmodium* is given in Table 1.1.

Table 1.1: *Plasmodium*-specific databases.

Name	Description	Reference
PlasmoDB	Functional genomic database for <i>Plasmodium spp.</i> that provides a resource for data analysis and visualization on a gene-by-gene or genome-wide scale with recent implementation of pathway and metabolite search.	[73]
Malaria Parasite Metabolic Pathways (MPMP)	This website contains over 120 maps that include not only classical biochemical pathways, but also biological processes dealing with replication, transcription and translation, cell-cell interactions, protein trafficking and transport among others.	[74, 75]
PlasmoCyc	Database that integrates pathway information with information about the complete genome of <i>P. falciparum</i> 3D7, using its annotated genomic sequence. In addition to the annotations provided in the genome database, this contains 956 additional annotations to hypothetical proteins found by the GeneQuiz annotation system. 216 chokepoint enzymes (those that uniquely degrade a specific substrate or produce a specific product) were identified.	[76]

1.3.1 Central Carbon Metabolism

The classic textbook scheme of central carbon metabolism includes glycolysis, the pentose phosphate pathway and the tricarboxylic acid (TCA) cycle. Typically each molecule of glucose would be broken down into intermediate sugars during glycolysis. These would then feed processes such as the pentose phosphate pathway and build nucleic acid intermediates. Pyruvate, the product of glycolysis is decarboxylated into acetyl coenzyme A (acetyl-CoA) and enters the TCA cycle. TCA intermediates provide metabolic precursors for amino acid synthesis and NADH and FADH₂, which are processed in the electron transport chain, generating up to 38 ATP molecules for glucose molecule. However, the intra-erythrocytic asexual stages of the malaria parasite do not follow the canonical central carbon metabolism and catabolism in the Krebs cycle is highly impaired. The parasite actively ferments glucose as a primary source of energy instead of obtaining it from the TCA cycle. It increases the utilisation of glucose to between 50 and 100 times the rate of uninfected host red cells [77] and up to 85% of that metabolised glucose is converted to lactate. This

process provides 2 ATP molecules, much less than the possible 38 by TCA cycle. Further insights into this metabolic rewiring are discussed in Section 1.3.1.3.

1.3.1.1 Glycolysis

Glycolysis is a tightly regulated pathway with steps catalysed by the enzymes hexokinase (HK, EC. 2.7.1.1), phosphofructokinase (PFK, EC. 2.7.1.11) and pyruvate kinase (PK, EC. 2.7.1.40) of which the second is the most important. The parasite generates its own glycolytic enzymes [78, 79] and reduces competition by inhibiting glucose consumption by uninfected erythrocytes [80]. Glucose uptake is significantly higher in infected erythrocytes and so are the activities of most of enzymes with a role in the parasite's glycolysis, especially HK, aldolase (EC. 4.1.2.13), enolase (EC. 4.2.1.11) and PK [78]. The most notable differences between the *Plasmodium* glycolytic enzymes and mammal's are summarised in Table 1.2. These modifications allow for a more efficient glucose entry into the parasite and promote a higher glycolytic flux with the subsequent production of glycolytic intermediates that feed other pathways involved in biomass production but with the final product pyruvate fermented into lactate. Other peculiarities of glycolytic products include the production and excretion of glycerol [81] and alanine. Further discussion follows in Section 1.3.1.3 and Figure 1.7.

Table 1.2: A comparison between mammal and parasitic glycolytic enzymes

Enzyme	Enzyme and gene identities	Differences mammal vs parasite	Refs
HEXOSE TRANS-PORTER	PF3D7_0204700	PFHT1 is a saturable sodium independent and stereospecific transporter. Maximum mRNA levels for this transporter are found in the early ring stage and lowest in gametocytes. It is localised to the parasite plasma membrane and not present in the host's membrane. PFHT1 differs from GLUT-1 (the main hexose transporter in erythrocytes) in that it has a higher affinity for glucose and it can also transport fructose. Whilst the latter of these properties is observed in other mammalian hexose transporters such as GLUT-2 and GLUT-5, it is not combined with an affinity for glucose.	[82, 83]
HEXOKINASE (HK)	EC 2.7.1.1; PF3D7_0624000	The total HK activity is increased 25-fold over that of non infected erythrocytes. The parasite's HK has a lower affinity for glucose than the mammalian enzyme (K_m parasite = $431\mu\text{M}$ vs K_m RBC = $98\mu\text{M}$). However the K_m for ATP and the V_{max} for both glucose and ATP are similar. This modification allows the production of more Glucose-6P that can enter the pentose phosphate pathway where NADPH is generated in reaction coupled with glutathion reduction.	[84]
GLUCOSE PHOSPHATE ISOMERASE (GPI)	EC 5.3.1.9; PF3D7_1015900, PF3D7_1436000	GPI activity in iRBCs is 4-9 fold higher than in RBCs. It is shown that the increase is of parasitic origin and that the expression of GPI parallels parasite maturation and reaches a maximum during the trophozoite/schizont stage.	[85]

Enzyme	Enzyme and gene identities	Differences mammal vs parasite	Refs
PHOSPHOFRUCTO-KINASE (PFK)	EC 2.7.1.11; PF3D7_0915400, PF3D7_1128300	PFK is typically inhibited by ATP accumulation. In the malaria parasite this inhibition is two orders of magnitude less than in the erythrocyte. Parasite PFK presents high homology to the plant-like pyrophosphate (PPI)-dependent that, despite not showing PPI dependency (only ATP), is insensitive to fructose biphosphate regulation, opposite to that of the human enzyme.	[86, 87, 88]
ALDOLASE (Ald)	EC 4.1.2.13; PF3D7_1444800	Studies using recombinant <i>P. falciparum</i> aldolase have reported specific changes in the kinetics of the enzyme as well as a differential spatial configuration. In mammalian tissues, the glycolytic pathway involves the cytoskeleton as a matrix to keep PFK, Ald and G3PDH in an optimal sterical position. These three enzymes bind to the band 3 protein in RBC or to actin in muscle cells. <i>P. falciparum</i> aldolase is believed to bind actin II.	[89, 90]
TRIOSE P ISOMERASE (TPI)	EC 5.3.1.1; PF3D7_1439900, PF3D7_0318800	Human and <i>Plasmodium</i> enzymes share 42% of amino acid sequence identity. There are several changes in certain amino acids. Particularly, a mutation in the S96 for F96 might provide the enzyme the capacity of binding to the cytoskeletal erythrocyte band 3 protein.	[91, 92]
GLYCERALDEHYDE 3P DEHYDROGENASE (G3PDH)	EC 1.2.1.12; PF3D7_1462800	Dipeptide insertion (-KG-) in the S-loop of the enzyme together with other amino acid substitutions alters the chemical environment and might be responsible for the selective inhibition of the enzyme by ferriprotophyrin IX.	[93]

Enzyme	Enzyme and gene identities	Differences mammal vs parasite	Refs
PHOSPHOGLYCERATE KINASE (PGK)	EC 2.7.2.3; PF3D7_0922500, PF3D7_1308500	A study in recombinant <i>P. falciparum</i> PG showed near to 1.5 fold increased affinity towards ATP and 2 fold higher affinity for 3-phosphoglycerate when compared to the human enzyme.	[94, 95]
ENOLASE	EC 4.2.1.11; PF3D7_1015900	Studies in recombinant <i>P. falciparum</i> enolase showed that the substrate affinity is similar to the mammalian enzyme. However it differs in inhibition levels of Mg^{2+} and the inability of K^+ to significantly activate it. <i>P. falciparum</i> enolase localises to the cytosol, nucleus, cell membrane and cytoskeletal elements, suggesting multiple non-glycolytic functions for this protein	[96, 97]
PYRUVATE KINASE (PK)	EC 2.7.1.40; PF3D7_0626800, PF3D7_1037100	PK of <i>P. falciparum</i> is not affected by fructose-1,6 biphosphate, which is a general activating factor of PK for most species. Similar to rabbit PK, it shows susceptibility to inactivation by 1mM pyridoxal-5-phosphate but to a lesser extent. PK from <i>P. falciparum</i> is markedly inhibited by ATP and citrate. This is similar to human isoform M2 which is associated with proliferating cells.	[98, 99]
LACTATE DH (LacDH)	EC 1.1.1.27; PF3D7_1324900, PF3D7_1014000, PF3D7_1325200	<i>Plasmodium's</i> LacDH, as opposed to human LacDH, exhibits only weak inhibition by pyruvate or by the pyruvate/NAD+ complex. Its active site has an insertion of five amino acids in the active site loop, which creates an enlarged volume in the substrate binding site. There is also a displacement of the NADH cofactor binding site when compared to its position in the mammalian enzyme.	[100, 101]

1.3.1.2 TCA cycle and electron transport chain

The glycolytic product pyruvate does not follow canonical metabolism into acetyl-CoA into the mitochondrion to enter the Krebs cycle. Pyruvate is mostly fermented into lactic acid, which is excreted [102]. There is a small flux of pyruvate that is converted into acetyl-CoA and that follows metabolism in the Krebs cycle [103]. This is a recent finding after a polemic against the nature of the Krebs cycle in *Plasmodium* resulted in the retraction of a publication in *Nature* which described the *Plasmodium* Krebs cycle as being bifurcated [104]. The Krebs cycle has always been a questionable element in the biochemistry of the parasite. During the asexual stages there is almost no flux into it; however, this is reversed during the asexual stages where a programmed remodeling of central carbon metabolism is observed [103], which might be related to parasite survival in the mosquito vector. The pyruvate dehydrogenase (PDH) is localised in the apicoplast and as such cannot contribute to the mitochondrial acetyl-CoA and its consequent incorporation in the Krebs cycle. However, a branch chain ketoacid dehydrogenase (BCKDH, EC 1.2.4.4), with PDH activity contributes to acetyl-CoA entering the Krebs cycle [105]. Nevertheless the rate of acetyl-CoA production is much slower than the rate pyruvate is produced from glycolysis [105], which is translated to high lactate production by the parasite.

Despite the low contribution of acetyl-CoA, the TCA is driven by glutaminolysis [103, 106, 105]. Glutamine is actively taken up by the parasite, converted into glutamate and incorporated in the TCA via α -ketoglutarate. This is linked to an active transport of oxaloacetate into the cytoplasm where it is converted into phosphoenolpyruvate (PEP) by the phosphoenolpyruvate carboxykinase (PEPCK, EC 4.1.1.49). It has been thought that glutaminolysis has a role in maintenance of ubiquinone levels for pyrimidine biosynthesis (essential for the dihydroorotate dehydrogenase (EC 1.3.5.2) step converting dihydroorotate into orotate, see Figure 1.6). However, with exception of the enzymes with multiple functions such as MQO (malate-quinone reductase, EC 1.1.5.4) and FH (fumarate hydratase, EC 4.2.1.2), the TCA cycle and glutaminolysis are not essential for asexual stages *in vitro* [107].

Atypical mitochondrial function does not relate solely to the TCA. As shown in Figure 1.6, the electron transport chain (ETC) of *P. falciparum* is also atypical with low oxygen consumption and very low synthesis of ATP [108]. Other peculiarities involve the absence of typical transmembrane Complex I. Instead, the type II NADH:quinone oxidoreductase (PFNDH2) is not involved in proton pumping but enables oxidation of NADH, which presents advantages such as a reduction of mitochondrial superoxide generation and potential DNA damage [108]. Another important role is played by the glycerol-3P dehydrogenase, which is linked to the

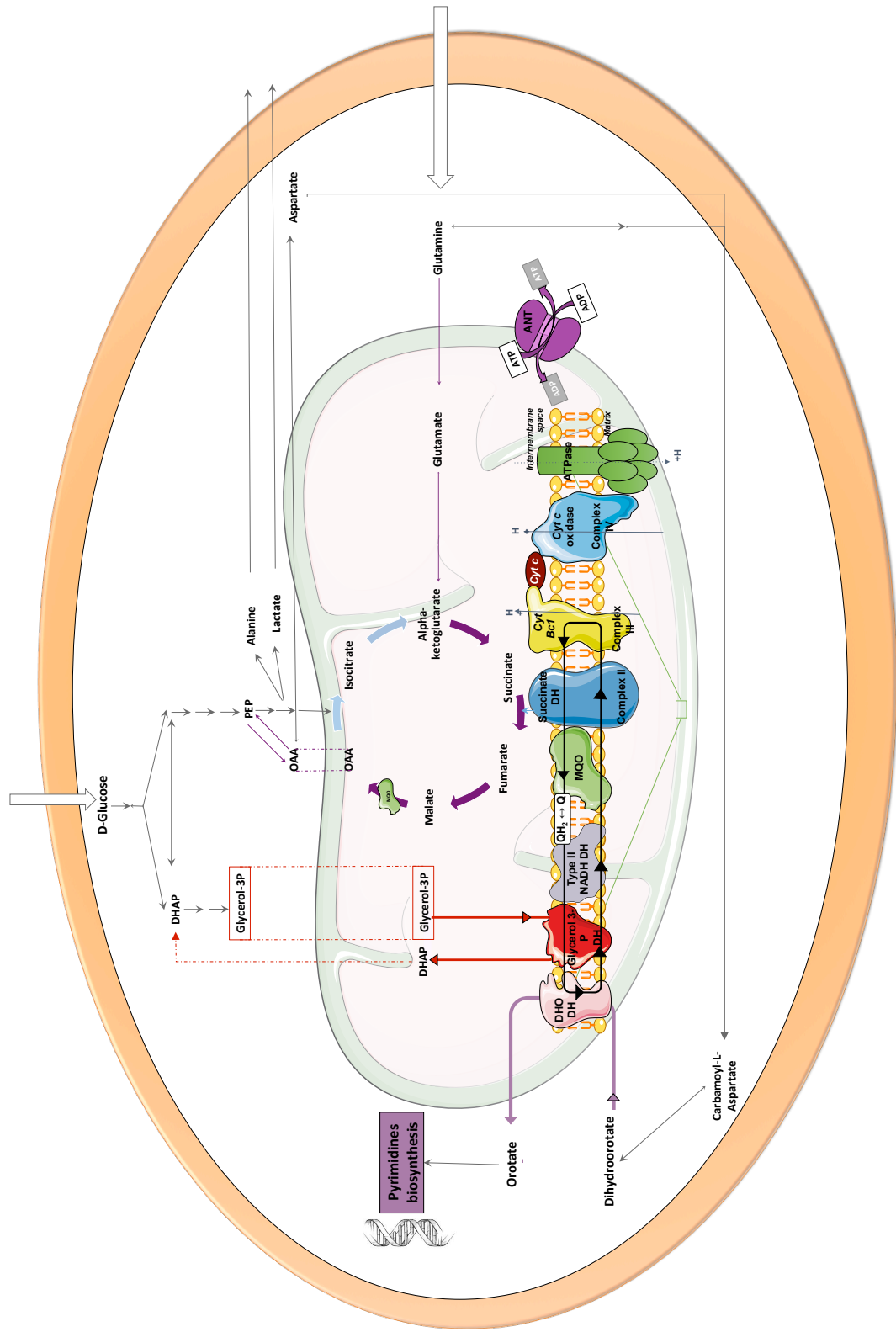


Figure 1.6: **TCA and electron transport chain representation of *P. falciparum*.** ETC consists of 5 dehydrogenase enzymes that provide electrons to the downstream complexes III and IV. These are dihydroorotate dehydrogenase (DHODH), glycerol-3P dehydrogenase, Type II NADH DH, malate-quinone oxidoreductase (MQO) and succinate dehydrogenase (complex II). Complex III and IV are cytochrome bc1 (cyt bc1) and cytochrome c oxidase respectively, Ubiquinone coenzyme Q functions as electron carriers (Q-QH₂).

glycerol shuttle and converts glycerol-3P into dihydroacetone phosphate (DHAP) that is returned to the cytosol where it can be reincorporated into glycolysis or used for other purposes such as lipid formation or glycerol production and excretion. Finally it is also worth mentioning the presence in the ETC of dihydroorotate dehydrogenase which converts dihydroorotate in orotate, both precursors for DNA synthesis. Complex V, ATP synthase, makes a minimal contribution to ATP synthesis but it is essential for parasite survival [109].

1.3.1.3 High proliferating cells; the role of a high lactic fermentation in cancer and malaria.

P. falciparum presents a very active glycolytic flux that finishes with high levels of lactic fermentation (and other products such as glycerol and alanine) and a subsequent low flux into the mitochondrion and a reduction of ATP formed. This is particularly striking when compared to the sexual stages where the parasite follows the typical catabolism pathway, maximising ATP production [103]. An evolutionary reason for this particular metabolic rewiring might be linked to other highly proliferating cells such as yeast and cancer cells. *P. falciparum* seeks to produce up to 32 merozoites every 48 h and even though trading 38 ATPs for 2 might seem not economical, when crunching the numbers an energetic advantage can be clearly accounted for [110, 111]. Glycolytic intermediates are used as precursors for biomass production. For example glucose-6P feeds the pentose phosphate pathway that via 5'-phosphoribosyl α -pyrophosphate (PRPP) synthesises nucleotides. Glyceraldehyde-3P is a precursor for lipid biosynthesis [112] and isoprenoid biosynthesis [113]. The DHAP formed by the glycerol-3P DH in the mitochondrion can be converted into the latter to further feed these anaplerotic pathways. PEP, which is actively formed via glycolysis and glutaminolysis, feeds the shikimate pathway, essential for folate biosynthesis via p-amino benzoic acid (pABA) [114] (see Figure 1.7). This has been recently reviewed and compared with the well described modern concept of the Warburg effect [115, 110, 116] in cancer cells [111].

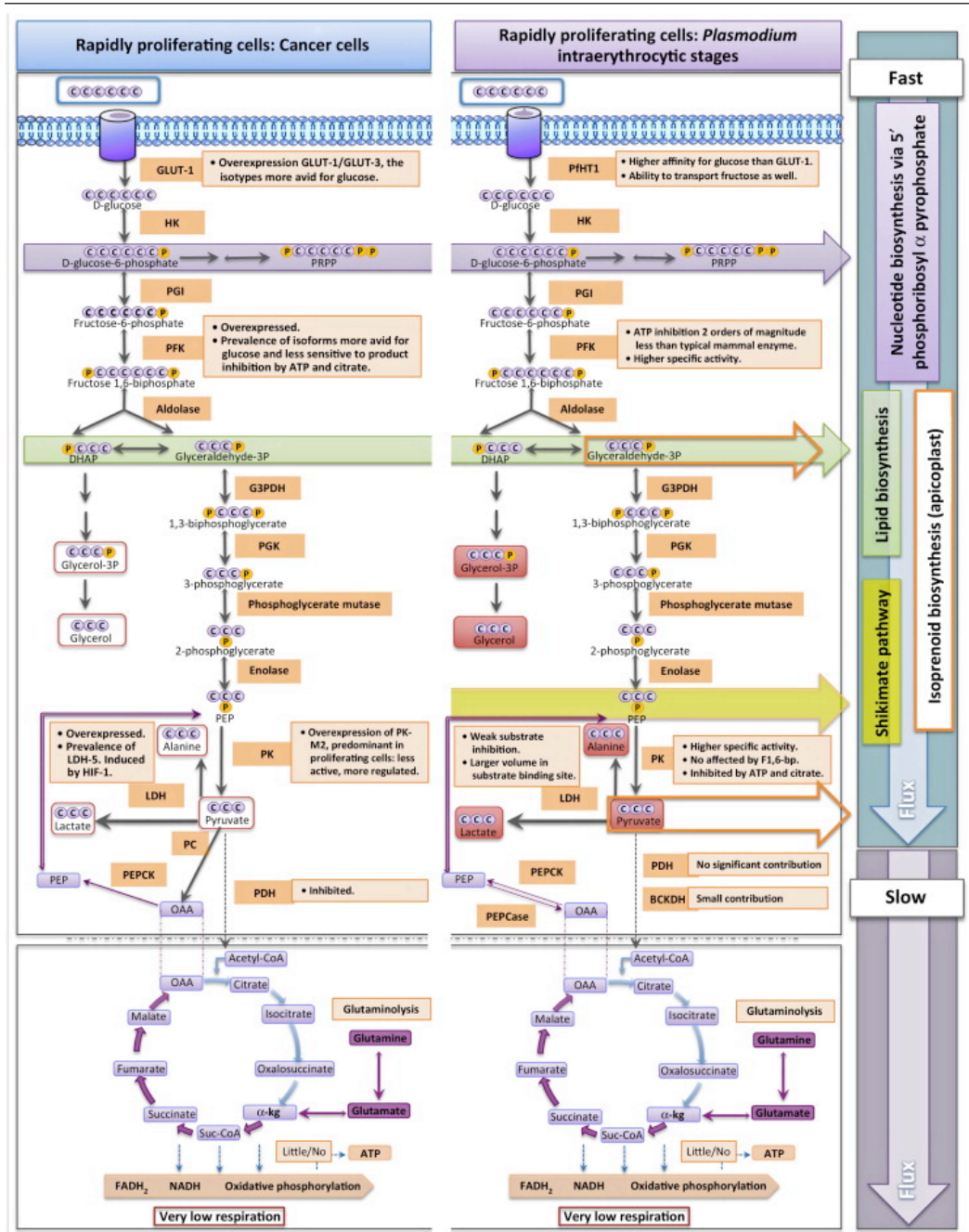


Figure 1.7: **Similarities between cancer cells and *P. falciparum*.** Principal end products of glucose consumption (shown in red boxes) are similar in both cancer cells and asexual intraerythrocytic malaria parasites. A high glycolytic flux maintains rate-limiting glycolytic intermediates to support nucleotide (via glucose-6-P to PRPP) and lipid biosynthesis (via DHAP to glycerol-3P). Anapleurotic glutaminolysis follows past part of the TCA cycle through α -ketoglutarate. Subsequent conversion to PEP by PEPCK, allows for further synthesis of biosynthetic intermediates (e.g. via shikimate pathway and isoprenoid biosynthesis) [111].

The preference for fermentative glycolysis even under aerobic conditions (Warburg effect) has the obvious consequence of high production of lactic acid, which is excreted as a waste product. The consistent use of this metabolic rewiring together with high rates of glutaminolysis by highly proliferating cells has generated different hypotheses for its role. To the above-mentioned role in rapid proliferation via production of biosynthetic precursors, there is a complementary theory presented by Newsholme *et al.* [117]. Defining sensitivity as the quantitative relationship between the change of concentration of a regulator and its consequent change in enzyme activity; the authors suggested that high fluxes are required for high sensitivity of the pathways involved in creation of biomass to specific regulators i.e. to permit high rates of proliferation when required. Simplifying the glycolytic flux to the system presented in Figure 1.8, if the flux towards one branch is in great excess (lactate, represented as J_b vs DNA production represented as J_a), then the sensitivity of the low-flux pathway to regulators will be elevated. This can be proved by calculating the intrinsic sensitivity of the production of biomass (J_a) by E2 to the regulator X as a function of the intrinsic sensitivities of the different enzymes to the presence of substrate and to the presence of regulator (see Equation 1.1). When plotting the net sensitivity of J_a to X versus the flux to waste (J_b), sensitivity increases when J_b is greater (simulation of Equation 1.1 presented in Figure 1.9). Thus, it is proposed that high rates of glycolysis and glutaminolysis not only supply precursors for biomass production but also provide an effective proliferation control system. This hypothesis has been further supported in other publications studying cancer cell metabolism. It has been observed that glucose and glutamine consumption still greatly exceeds the catabolic and anabolic needs of cancer cells thus supporting the hypothesis towards a control role in this metabolic reprogramming [118, 119, 120, 121].

In addition, recent studies of cancer cells have shown how lactate is an important signalling molecule, triggering the stabilisation of hypoxia inducible factor 1α (HIF- 1α) [122], which triggers the expression of vascular endothelial growth factor (VEGF) [123], resulting in angiogenesis. It has also been suggested that regions of high lactate and subsequent low pH modulate the activity of the local immune response, helping to create immune tolerance [124]. The role of lactate has also been proposed as an energy reservoir in cases of severe decreases in glucose availability. In tumors containing aerobic and hypoxic regions, aerobic cancer cells take up lactate via monocarboxylate transporter 1 (MCT1) and utilise it for oxidative phosphorylation, allowing the hypoxic cells to keep utilising glucose. MCT1 knock-outs cannot use lactic acid and thus, in glucose deprivation conditions, only the cells with access

to the sugar can survive [125, 126]. The potential role that lactate might play in malaria has not been investigated.

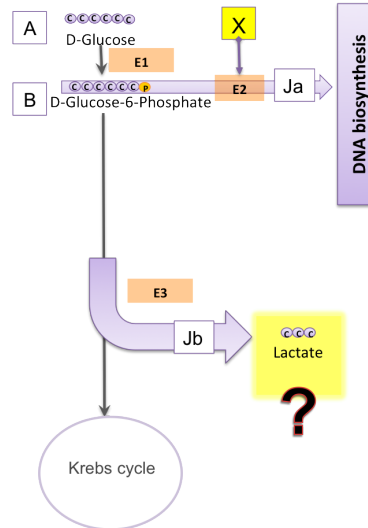


Figure 1.8: **Representative diagram of the system presented in [117].** A new role for the high flux towards lactate (J_b) is proposed by which when the right regulator is detected (X), some of the J_b flux can be redirected towards biomass production (J_a) in a more efficient manner than otherwise. This is supported by Equation 1.1, which simulation is shown in Figure 1.9.

$$S_X^{J_a} = \frac{S_i^{E_2} \times S_i^{E_3} \times J_b}{S_i^{E_3} \times J_b + S_i^{E_2} \times J_a} \quad (1.1)$$

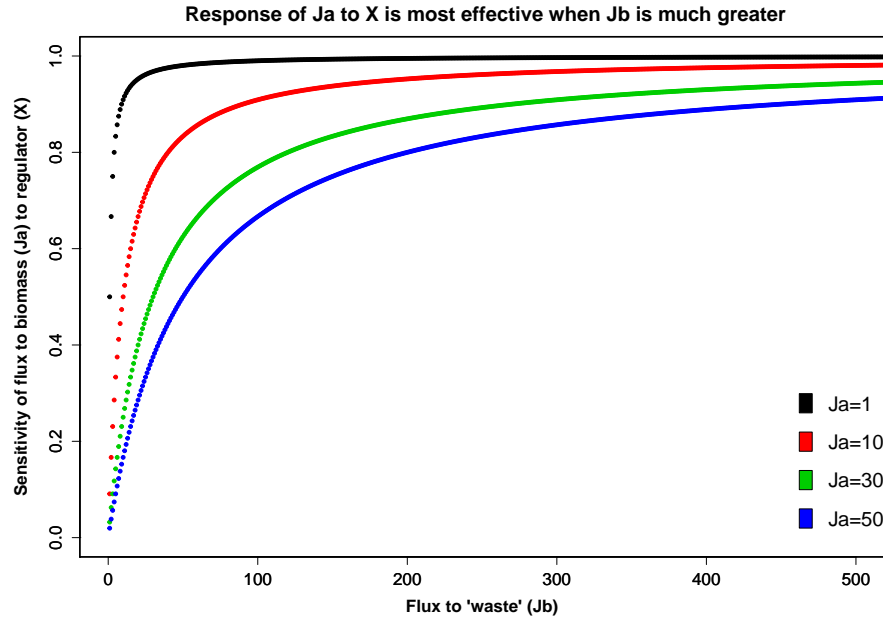


Figure 1.9: **Newsholme *et al.* model simulation.** As the flux to waste/lactate increases (x-axis, J_b), the sensitivity of a regulator (y-axis, S_{XJ_a}) to trigger the biomass production (J_a , legend) increases. Simulation was built from Equation 1.1 by keeping all terms constant to 1 but J_a, J_b and $S_X^{J_a}$.

1.3.2 Amino acid metabolism

Plasmodium, among other eukaryotes, has lost the ability to synthesise nine of the 20 amino acids which are phenylalanine (Phe), tryptophan (Trp), isoleucine (Ile), leucine (Leu), valine (Val), lysine (Lys), histidine (His), threonine (Thr) and methionine (Met). *P. falciparum* has retained the ability to synthesise only seven amino acids namely alanine (Ala), aspartate (Asp), asparagine (Asn), glutamate (Glu), glutamine (Gln), glycine (Gly) and proline (Pro) [127]. Despite lacking the means to produce 13 amino acids, intra-erythrocytic *P. falciparum* can grow in medium containing only three of these amino acids namely cysteine (Cys), Met and Ile. Regardless of the existence of biosynthetic pathways to form them, in order to sustain minimum continuous growth, glutamine, glutamate and proline also need to be supplied exogenously [128]. The reason why no other amino acids need to be supplemented in medium despite the absence of biosynthetic pathways is the capability of the malaria parasite to ingest the host's haemoglobin and use the globular part to salvage amino acids. Haemoglobin degradation takes place in the food vacuole and it is mediated by over ten proteases [129]. This process releases haem, which is not used or recycled [130], instead it is transformed into pigmented crystals called

hemozoin [131]. These can be observed using electron microscopy but their agglomeration can be appreciated already in bright field microscopy (see Figure 1.10). The hemozoin formation process is still not completely understood but it is a highly interesting area given its relevance in aminoquinolines mode of action and resistance emergence [132]. Catalytic enzymes and contributing lipids have recently been characterised [133, 134, 135] and associated to the formation of a complex comprising many of those proteases identified and a haem detoxification protein [136].

Haemoglobin is the most abundant protein in erythrocytes and between 25-80% is consumed from the early trophozoite (ring) stage [62]. Amino acids derived from the globin are incorporated into proteins [137] and also used for energy metabolism [131]. Even though *P. falciparum* has redundant pathways for amino acid supplies [138] haemoglobin degradation is essential for parasite survival even in rich medium conditions, but parasites growing in medium lacking most amino acids are most sensitive to haemoglobin proteolysis blockers [139]. The necessity of this process even in rich culture conditions points towards additional roles, some of which might be involved in reduction of the osmotic pressure within the host erythrocyte to prevent its premature lysis [140]. Of all the amino acids salvaged, only 16% are incorporated into proteins, the rest are excreted into the medium [141]. This is believed to provide space to the subsequently growing parasite.

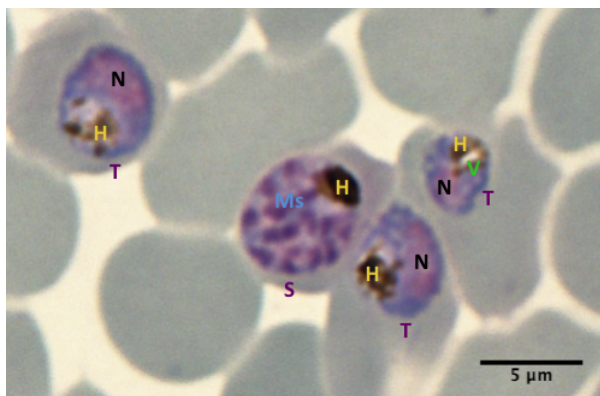


Figure 1.10: **Giemsa stained *P. falciparum* infected erythrocytes in mature trophozoite (T) and schizont (S) stages.** Structures seen include nuclei (N), hemozoin pigment (H) and food vacuole (V). In the schizont stage merozoites (Ms) can be counted.

1.3.3 Nucleotide biosynthesis

Plasmodium spp. lack a *de novo* purine salvage pathway and they rely on exogenous sources [142, 143]. Purine nucleosides are transported across the parasite plasma

membrane by the NT1 transporter [144]. Hypoxanthine is the preferred precursor for purine biosynthesis, routinely supplied in *in vitro* cultures and taken up *in vivo* from the erythrocyte purine pool [143]. Adenosine can also be used prior conversion to hypoxanthine through the enzymes adenosine deaminase (ADA, EC 3.5.4.4) and purine nucleoside phosphorylase (PNP, EC 2.4.2.1). Once taken up, hypoxanthine is converted to inosine monophosphate (IMP) by hypoxanthine-guanine-xanthine phosphoribosyltransferases (EC 2.4.2.8 and EC 2.4.2.22) that serves as precursor for the other purine nucleotides. These enzymes are highly expressed in *Plasmodium* [145, 146].

On the contrary, the parasite is capable of pyrimidine *de novo* biosynthesis from aspartate and carbamoyl phosphate, similar to other eukaryotes. The latter is formed from bicarbonate and glutamine. As mentioned in Section 1.3.1.2, one of the enzymes of this pathway, essential for the parasite's development, is localised in the mitochondrion (dihydroorotate dehydrogenase EC 1.3.5.2) and depends on ubiquinone to fulfil its function [147]. Pyrimidine synthesis also requires folates which also rely on pABA (para-aminobenzoic acid, made in the apicoplast through the shikimate pathway) and which the parasite can also synthesise *de novo*. These are another drug targets exploited to treat malaria, with drugs such as pyrimethamine that target the dihydrofolate reductase, however resistant phenotypes are widely spread [148, 149].

1.3.4 Apicoplast metabolism

The apicoplast is a non-photosynthetic plastid that harbours several plant-like metabolic pathways such as isoprenoid biosynthesis, part of the haem synthesis pathway and a type II fatty acid synthesis (FASII) [150, 151]. Despite the high rates of haemoglobin consumption, *Plasmodium* cannot use the human haem and synthesises its own. Haem biosynthesis is initiated in the mitochondrion from glycine and succinyl-CoA [152] and finished in the apicoplast [153].

FAS II is dispensable in blood-stage parasite but crucial in liver and mosquito stages of *P. falciparum* [154, 155]. Initially the parasite was thought to rely completely in the host for fatty acid production [156, 157] and in fact parasites can scavenge, modify and incorporate exogenously supplied fatty acids [158, 141]. The discovery of FASII has led to identification of compounds with antimalarial activity [159, 160] and it has been proposed as vaccine candidate [154]. FASII is responsible for synthesis of lipoic acid [161] and incorporation of fatty acids into precursors for membrane lipid synthesis [153].

The only indispensable apicoplast function during the intraerythrocytic stages

of *P. falciparum* is isoprenoid biosynthesis [162]. Isoprenoids functions range from prosthetic enzyme groups to forming the basis of ubiquinones and dolichols. The isoprenoid pathway in the parasite is similar to plants which is different to the classical acetate/mevalonate in mammals mainly in its starting compounds which are pyruvate and glyceraldehyde 3 phosphate [163], both produced during glycolysis.

1.3.5 ROS

Plasmodium induces high oxidant stress within the host erythrocyte mostly due to haemoglobin degradation which produces haem and numerous reactive oxygen species (ROS) such as H_2O_2 . The parasite deals with ROS with the host's superoxide dismutase (SOD) and catalase [164] and also produces high quantities of reduced glutathione (GSH). GSH at millimolar concentrations plays a pivotal role in antioxidant defence. GSH serves as electron donor for the reduction of peroxides, being reduced to glutathione disulphide (GSSG) which cycles back into GSH by converting NADPH into NADP. The latter is reduced back to NADPH through the pentose phosphate pathway [165].

1.4 Metabolites, not only biochemical intermediates

Metabolites are not just intermediates and products of the metabolism. They have regulatory power on their own. In every cell replication there are checkpoints that allow the cell to progress to the next step of replication, or not. These checkpoints take into account cellular status and environmental signals. Among those are specific metabolites which function as nutrients such as vitamins A and D, iron, folic acid or glucose [166]. For example, folic acid deficiency not only results in cell cycle inhibition, but also has a role in DNA methylation in humans [167].

In organisms such as the malaria parasite with a very complex life cycle in very diverse hosts, tightly controlled mechanisms for survival under changing environments are key for success and epigenetic mechanisms are crucial for *Plasmodium* adaptation. They regulate numerous processes including nutrient uptake [168]. *Plasmodium* infected erythrocytes present an increased permeability to many solutes [169], which is essential for nutrient uptake and waste excretion. This is thought to be mediated by *Plasmodium* surface anion channel (PSAC) [170] which is associated with a genetic locus containing two paralogous genes *clag3.1* and *clag3.2* (PF3D7_0302500 and PF3D7_0302200) [171] which expression is mutually exclusive [172, 173] by default. However under strong selective pressure, parasites can activate more than one *clag3* [174]. *Clag3* silencing is associated with a repressive histone

mark (methylation site, typical epigenetic mechanism) thus providing a link between epigenetic signals as responses to the environment. Furthermore it has been shown that parasites are able to adapt to environmental stress such as the drug blasticin and reduce expression of PSAC to impair drug uptake via epigenetic mechanisms [175, 176]. Thus, nutrient environment can trigger epigenetic signals that would promote metabolic rewiring with consequent adaptation to new environments.

The study of the effect of nutrient deprivation has not been possible in a high-throughput manner until the recent emergence of metabolomics. By applying controlled changes to growing parasites, effects on metabolism rewiring can be detected and bound to specific processes. Challenges are not merely technological but also encountered throughout biological experimentation. The development of continuous cultures of the malaria parasite *in vitro* was a challenging process that once achieved has been conserved almost unchanged for over 40 years since its conception [177]. However in the usual *in vitro* conditions parasites grow in abundance with over double the glucose concentration available than in human, three times the glutamine and over one order of magnitude higher vitamins amongst others [178]. Growing the parasites in such rich media, where most of the experiments and biological insights are made is equivalent to the design human trials on obese cohorts. They are part of the population but they are not a representative group of most of it. For the malaria parasite this is even more emphasized given that its media is its host and unfortunately malaria is most widely spread amongst the poorest where malnutrition and disease are most interlinked. There is a need therefore, to adapt laboratory methods to more physiological conditions in order to improve our experimentation models but also to gain insight on what adaptation mechanisms parasites undertake and how those might influence drug effectiveness and dosage.

1.5 Metabolomics as an emerging field

The recent development of the omics methodologies have allowed to collect large datasets used to predict global behaviours of a system based on the interactions found [179, 180, 181]. Omics take into account all constituents of a system using both *in vitro* and *in silico* methods. Numerous omics fields have emerged and developed including genomics, proteomics and metabolomics. The aim of these fields is to tackle challenging problems whilst looking at entire systems at any level of organisation. This approach differs from the reductionist one commonly used in biology and allows the discovery of emerging properties.

Historically, the first omics to be developed was genomics [180]. Genomics

expanded in to transcriptomics, which in turn led to the development of proteomics and finally metabolomics and other omics such as epigenomics or fluxomics. The metabolome determines phenotype and is affected by changes in gene expression, mutation in the genome or misregulation of proteins. These factors might have small effects on metabolic fluxes but a large effect on metabolite concentration. Metabolomics seems an ideal level at which to analyse a change in the system as it considers changes at all levels and ultimately represents compounds that determine phenotype. However, metabolomics as an emerging field is relatively unexplored, especially if compared to genomics or transcriptomics. Metabolomics studies provide quantitative and qualitative information, which describes broadly the biochemical status of an organism under certain conditions. The conditions in which a system is studied can result in large variation in measurements [179, 182]. A variety of environmental conditions, drugs and stress conditions can all be tested. These perturbations provoke changes in the systems that can be identified although they might not be based in a genotypic change. Furthermore, metabolite profiling can elucidate links and relations that occur primarily through regulation at the metabolic level [179, 183, 180, 181]. Metabolomics is starting its golden era; projects such as the human metabolome database [184], created in 2007, determine the foundations to study different human disease in this level of organization. Metabolomics is also emerging in the field of plants in order to gain more understanding of gene function and elucidate the evolutionary divergence between ecotypes [183]. Metabolomics also has a great impact on biotechnology helping in breeding tastier cultivars and improvements of food processing procedures [185], assessing the quality of processed green tea [186] and distinguishing among olive oils produced in different districts [187].

Metabolic models have proven to be useful to study the metabolome and its internal and external relationships [180, 188]. A metabolic model is a representation of the network of biochemical reactions and transmembrane transporters that the cell uses to produce energy to grow and reproduce. Detailed pathway modelling can only be achieved using quantitative information derived from precise kinetic data [189], which techniques such as mass spectrometry (MS) and nuclear magnetic resonance (NMR) can provide. Metabolic modelling can also be used to generate further hypotheses which can be experimentally tested to shed light upon cellular behaviour, thus iteratively producing refined models and insight into the system studied [190]. These models range from global views of cellular systems or more detailed ones with narrower scope [191] and ultimately, they not only increase the biological understanding of complex systems but also, allow the creation of novel

biotechnology with well defined targets for drugs.

To be a useful tool, metabolite profiling must be fast, consistent, sensitive and suitable for mechanisation, as well as covering a significant number of metabolites [183]. Metabolome measurement is, however, a multi-step process, laborious and time-consuming. A brief and general diagram of the metabolomics work-flow is shown in Figure 1.11. Briefly, first biological samples need to be obtained, in the case of cells they need to be cultured and grown to amounts on which metabolites can be quantified which varies depending on the technique of choice. Opposite to genomic studies, cell handling can be a source of artificial variation and might introduce artefacts in the study [192], thus careful and robust methods need to be in practice. Secondly, the metabolism must be quenched usually following a time-course experiment in which different treatments are applied to the cells. For absolute metabolite quantitation, it is important to add isotopic internal standards in this step, so that the standards experience equal chances for degradative and absorptive losses as the endogenous compounds [193, 194]. Samples need to be kept at low temperatures to avoid degradation before and during the extraction process. Different techniques and instruments can be used for signal detection, but only two provide both qualitative and quantitative data: mass spectrometry (in concrete terms, liquid chromatography tandem mass spectrometry (LC-MS/MS), gas chromatography mass spectrometry (GC-MS)), and Nuclear Magnetic Resonance (NMR) [195, 196, 197]. The data obtained should be normalized and processed before further analyses. These can range from multivariate statistics to pure comparison of metabolite levels between conditions tested.

Metabolomics methodologies can be classified into targeted and untargeted. Whilst targeted approaches measure a defined group of characterised and biochemically annotated metabolites, untargeted performs a holistic analysis of all the measurable metabolites regardless on whether they are known or not. The latter presents the opportunity of discovery of new metabolites, inherent to the sample analysed however it also presents the challenge of novel metabolite identification and biochemical assignment, which is not trivial. To tackle this task a combination of statistical methods for prediction of metabolites and assignment of chemical groups [198] coupled with *in silico* predictions powered by the information collated in databases such as the Human Metabolome Database [184] or the Madison Metabolomics Consortium Database [199] and analyses in both NMR and MS of the unknown sample are needed.

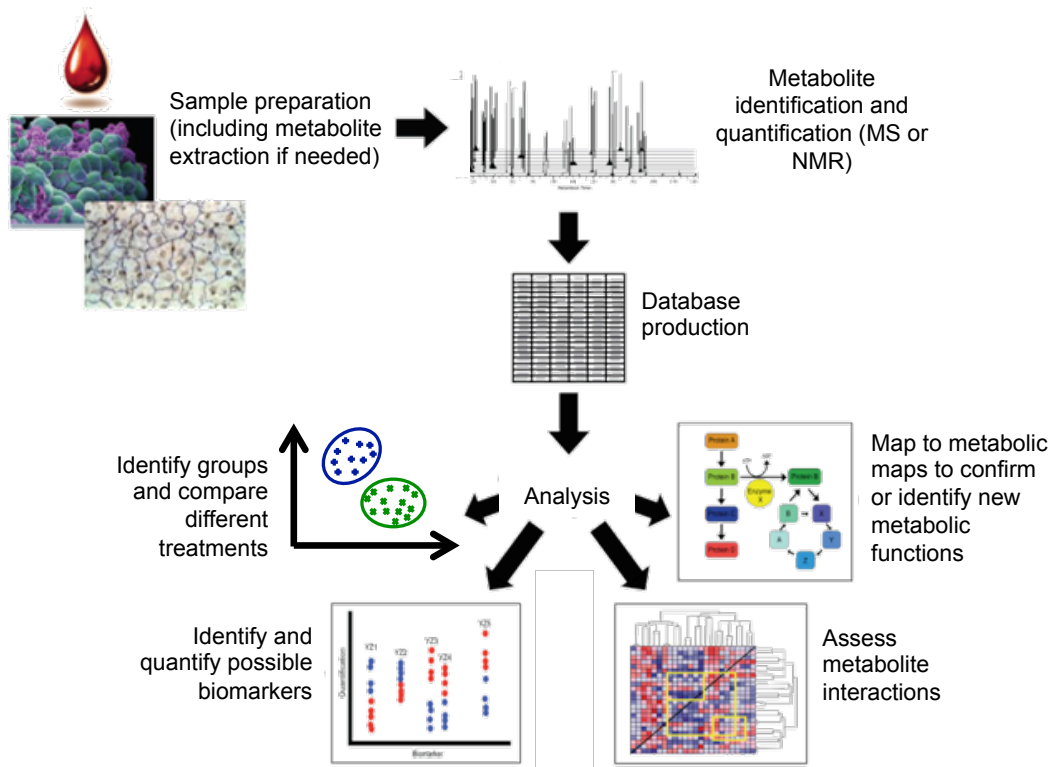


Figure 1.11: **Metabolomics work-flow.** Biological samples are processed and in the case of cellular and tissue samples metabolites are extracted prior to analyses by NMR or MS. Data are scaled and normalised and statistical analyses can be performed with different aims.

1.5.1 Mass Spectrometry

1.5.1.1 Principle

Mass-spectrometry (MS) is the study of molecular structure by measuring mass-to-charge ratios (m/z) of ionised molecules in a magnetic field in vacuum conditions to avoid influence from molecules in the air. In a magnetic field, ions can be deflected and under the same magnetic strength their deflection depends on their mass. By measuring the deflection the mass can be inferred. The standard steps in a mass spectrometer are ionisation (to ensure the molecules can be deflected), acceleration (to ensure all ions have the same kinetic energy), deflection (by the magnetic field) and detection. Thus a basic mass spectrometer consists of an ion source (to convert molecules into ions), a mass analyser and a detector (see diagram in Figure 1.12). The most common mass analysers are time of flight (TOF) and orbitrap [200]. Detection can be improved by using tandem MS, which is a mass spectrometer able

of several rounds of MS, allowing further fragmentation and very accurate mass determination [201].

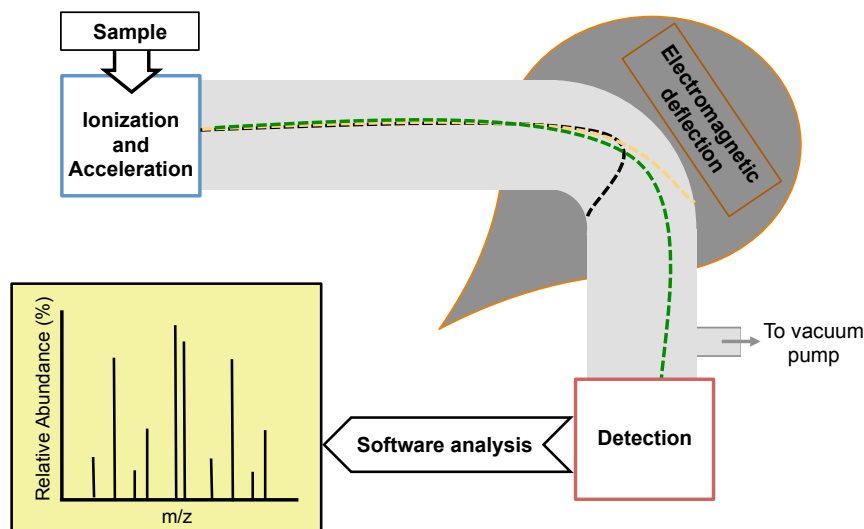


Figure 1.12: **Diagram of a simple mass spectrometer** A sample is injected into the spectrometer and the molecules are ionized and accelerated. The ions are then separated by their mass and charge via electromagnetic deflection and ions properly aligned are detected. Note that the entire system is in vacuum.

1.5.1.2 MS approaches in metabolomics

One of the limitations of MS is that only ionised molecules can be measured. In complex samples such as metabolite extracts, variable ionization and ion suppression effects may impair exact quantification. To compensate these limitations further techniques have been applied.

LC-MS Prior to MS, a step of high-performance LC (HPLC) is implemented [201]. During HPLC the sample is passed through a column by liquid (typically a mixture of water and organic solvents such as methanol) at high pressure. This step allows the sample to be eluted in different fractions depending on the sample interaction with the column matrix (thus different columns would interact different with metabolites and favour extractions of different kinds i.e. hydrophilic or hydrophobic metabolites).

GC-MS Prior to MS, the sample is vaporised and the volatile molecules are pushed through a column by an inert gas at high temperature (usually helium). Once in the column the molecules interact with the column coating. This coating

can be varied to favour detection of specific metabolites. The major limitation of this technique is that the metabolites to analyse need to be volatile (or derivatised to be volatile) and fairly stable at high temperatures [202].

Others Even though the current gold standard techniques for MS are LC and GC, others are being developed and quickly integrated in analyses pipelines. Some examples are ultrahigh-performance LC (UHPLC) [203] or Capillary Electrophoresis MS (CE MS). In CE-MS, charged analytes from a given sample are separated in a capillary by electric charge and then their electrophoretic mobility allowing for separation by charge and mass [204]. The field is rapidly advancing and even though the review of the different techniques falls outside the scope of this project, it is worthwhile mentioning the recent development of Rapid evaporative ionization MS (REIMS), which coupled with an endoscopic polypectomy snare allows real time *in vivo* metabolomics studies of living tissue [205].

1.5.2 Fourier Transformed Nuclear Magnetic Resonance Spectroscopy

1.5.2.1 Principle

NMR spectroscopy exploits the magnetic properties of some nuclei and their interactions when immersed in a strong external magnetic field to study molecular structure [206]. Some nuclei (such as ^1H , ^{13}C , ^{15}N , ^{31}P) possess a spin value which enables them to produce a nuclear magnetic moment. In their natural state, these nuclei are found oriented in random directions and when in a strong external magnetic field, they can either align with the field (lower energy) or against it (higher energy). By pulsing different electromagnetic waves these nuclei can flip from the more stable alignment (low energy) to the less stable (higher energy), a phenomenon known as resonance condition. This also causes the synchronisation of the magnetisation vectors, consequently inducing a signal in the detector. As the nuclei lose the absorbed energy the signal slowly decays and the system returns to its original state. The recorded diminishing signal is referred as a Free Induction Decay (FID). Upon Fourier transformation it registers as the typical NMR peaks. The resonant frequency and intensity of the signal are proportional to the strength of the magnetic field of the spectrometer, for example in a 14.1 Tesla magnetic field, protons resonate at 600 MHz. A simple diagram of NMR spectrometer arrangement is shown in Figure 1.13. Each atom experiences not only the magnetisation of the external magnetic field but also the magnetic field of neighbour atoms. The position of each peak in the spectrum represents its chemical shift in respect to the exter-

nal magnetic field and it is measured in part per million (ppm). This definition is independent of the external magnetic field strength and consequently data taken at different spectrometers can be compared.

^1H NMR spectra have a small chemical shift (0-15 ppm) which results in major overlap when analysing complex samples such as metabolite extracts. To overcome this problem two dimensional experiments are applied, either homonuclear (H-H) or heteronuclear that in case of metabolomics very often consists of heteronuclear single-quantum correlation spectroscopy (HSQC, H-C) experiments that analyse all carbons bound to hydrogen in the sample. The limitation of studying solely carbon lies in the low abundance of the ^{13}C isotope (only 1.1%). However, molecules enriched in ^{13}C can be used not only to boost the signal but also to trace their break down in the metabolism of the organism of study.

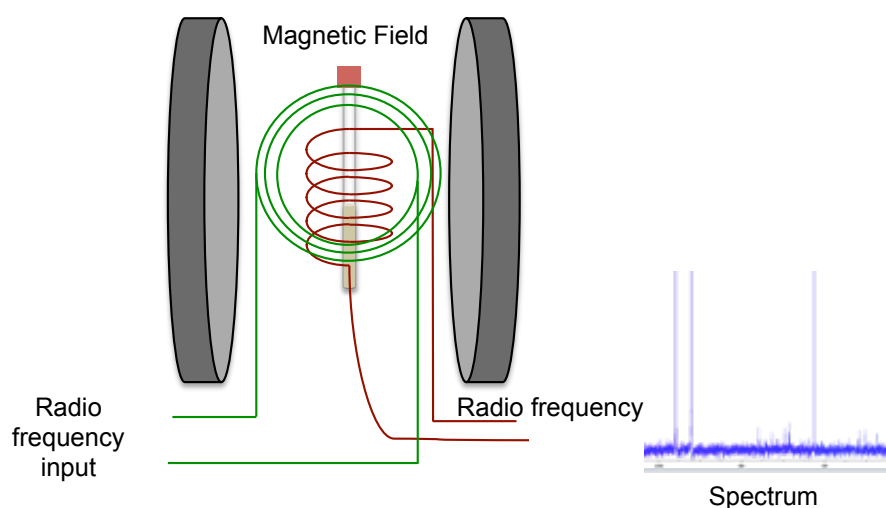


Figure 1.13: **Basic arrangement of an NMR spectrometer** The sample is placed in the magnetic field where it is excited via pulses of the radio frequency input. The relaxation signal is registered in the output circuit and used to generate the signal that is Fourier transformed into the spectrum.

1.5.2.2 NMR approaches used in metabolomics

Even though NMR is a reasonably established analytical technique (discovered in 1944 by Isidor Isaac Rabi and experimentally developed in the 50s by F. Bloch and E. Purcell), its use in metabolomics is recent. The first real application of NMR to the analysis of biofluids was done in the early 80s [207, 208] but it was not until some NMR technical improvements in the 90s such as the introduction of cryo-probes to boost sensitivity that made NMR spectroscopy a counterpart to

MS in metabolomics studies [209]. The incorporation of robotics in NMR analyses has allowed for establishment of high-throughput assays that can analyse up to 100 samples a day and monitor between 20 and 70 compounds [210, 211].

1.5.3 Advantages and shortcomings of MS and NMR

MS is a universal detector of ionised compounds with very high resolution and sensitivity (reaching fmol). Its sensitivity is the main reason of its frequent adoption, thus many analysis methods have been developed along with specialised software and databases. Robust methods have been published for the detection of up to 200 metabolites [212] that have been exploited for the analysis on many different organisms. However, MS is limited to the analysis of ionizable molecules, requires a very time consuming sample preparation and if a targeted approach is used, numerous standards need to be prepared with each run of experimentation, increasing vastly the data acquisition time. NMR spectroscopy makes it possible to perform structural analysis of many metabolites in crude extracts, cells suspensions, intact tissues or whole organisms [213]. However nowadays sensitivity is still one of the major issues of this technique with only highly abundant metabolites being detected (ranges from micromolar to millimolar). Nevertheless NMR spectroscopy has numerous advantages, amongst them: it does not need time-consuming sample preparation steps, it is quantitative [214], non-destructive (which provides extra analysis options for the same sample) and very robust with high reproducibility between experiments and between laboratories. Because of the later, NMR standards can be run in independent runs and do not need to be repeated while they are prepared and acquired in the same conditions than the experimental samples. NMR can also differentiate between molecules with the same mass but different conformation. This is crucial to analyse sugars. NMR can for example differentiate between α and β glucose and between glucose, galactose and mannose that even though have same masses, they all have slightly different structural conformations and very different roles in metabolism. These make NMR spectroscopy best suited for untargeted profiling of metabolites. An overview of the main advantages and disadvantages of both analytical techniques is shown in Table 1.3.

Table 1.3: MS and NMR pros and cons

Technique	Advantages	Disadvantages
MS	<ul style="list-style-type: none"> - High sensitivity and specificity - Many analysis resources available 	<ul style="list-style-type: none"> - Chemical modification needed - Destructive to sample
NMR	<ul style="list-style-type: none"> - Non destructive - Low per-experiment cost - No need for derivatization & Not selective - Robust and reproducible 	<ul style="list-style-type: none"> - Less sensitive - Signal overlap - Limited resources for analysis

1.5.4 Metabolomics of the malaria parasite

Even though the field of *Plasmodium* metabolomics is still in its infancy, it has already shown its incredible potential. As presented in Section 1.3, the conundrum of the Krebs cycle and mitochondrial function of the different life stages of the malaria parasite has been elucidated thanks to metabolomics studies [103, 106, 105, 107]. Metabolomics studies have also been used to trace glucose metabolism in infected erythrocytes and discover novel metabolites such as glycerol [81] which is not excreted as a wasteful product in humans. Metabolic steps unpredicted by genomic studies have also been discovered by metabolomics such as the conversion of arginine to ornithine by parasite arginase [195] linked to the clinical hypoargininemia observed in patients. Other novel pathways have also been unveiled such as carotenoid biosynthesis [215] or parasite-specific lipid biosynthesis [158]. Further studies have also linked some parasite specific fatty acids to parasite-mediated host immune modulation [216], emphasising the power that metabolites have as molecular signals.

Extensive metabolite profiles of the malaria parasite have been published [217, 218, 219, 195] and comparative studies between resistant and susceptible strains have proved effective to discriminate between them [217]. Other studies have involved perturbation of the parasite's enzymes to study the effect of polyamine depletion as an anti-malarial strategy by inhibiting the S-adenosylmethionine decarboxylase and ornithine decarboxylase [220]. Metabolic profiling has also been used to further explore the mode of action of drugs. A battery of drugs with known and unknown modes of action were used to profile their effects and more insight was gained in the mode of action of some. For example the novel compound Torin 2 was

found to inhibit haemoglobin metabolism. The endoperoxide dihydroartemisinin was found to disrupt haemoglobin catabolism and pyrimidine biosynthesis which results in an increased glucose flux towards malate production [221]. Other studies have been done to link metabolic responses with multidrug resistance. For example *P. falciparum* multidrug resistance-associated protein 1 has been related to the export of folate from parasite to erythrocyte [222].

Numerous studies have been done to better understand the metabolism of the parasite and its response to drugs. Most of them are studies of only the intracellular metabolome with very brief mention to the analysis of extracellular medium. This is a completely non-invasive approach with far less sources of variation in its processing that consists of measuring the extracellular metabolites (consumed and excreted) of a given culture i.e. its footprint. Studying the parasite footprint can provide very useful information. For example by analysing the uptake of 2-¹³C Glucose by infected and uninfected red blood cells, it was observed that infected cells down regulate the glucose utilisation of uninfected ones [223]. Discovery of glycerol production by the parasite was done by looking at cellular suspensions containing the extracellular media [81]. Identification of acetate excretion by gametocytes has also been shown by analysis of the footprint [103]. Footprinting has also served to study metabolic alterations in mice infected with *P. berghei* in different tissues [224] and sex dimorphism have been observed during early stages of infection when females showed greater alterations in urine metabolites and males in serum. Metabolite profiles of serum samples from patients with different malaria severity have also served to classify them into disease categories, proving its potential for diagnostics [225]. Not only parasites, but also their hosts have been studied by metabolomic approaches and used to identify possible metabolic targets in future drug development [226]

However, many questions are still left to be answered regarding the *Plasmodium* footprint that might aid the understanding of the metabolic mechanisms by which the parasite reacts to the environment. It has been shown that the parasite can react to changes in oxygen availability by elongating their life cycle [227] but no footprinting nor fingerprinting studies have been done to understand what are the metabolic responses associated with it. Further understanding of the methods to slow its life cycle are paramount to further comprehend some of the processes related to drug resistance. *Plasmodium* early asexual stages can respond to artemisinins by arresting metabolic processes such as protein synthesis and glycolysis (entering in what is known as dormancy). This response is responsible for the increased tolerance against artemisinins [228, 229]. Dormancy capabilities are highly linked with resis-

tant phenotypes This metabolic arrest differs from the changes observed in apoptotic parasites [230]. Thus footprinting monitoring may aid on the characterisation on resistant strains.

After it was shown that the parasite can delay its life cycle responding to environmental conditions such as hyperoxia [227] or some nutritional impairments such as asparagine synthesis [231] or isoleucine deprivation [232] the main question left unanswered is, whether and how the parasite adapts its metabolism and life cycle to different environments and whether this adaptation results in different rates of replication, drug susceptibility and transmissibility. *In vitro* studies remain the gold standard not only in malaria metabolomics but also as first line on the drug discovery pipeline. However as mentioned in Section 1.4, culture media and healthy host's nutritional conditions are vastly different [178] and there is a need to study what is the impact on growing the parasite in such rich conditions with respect to experimental outputs and assess whether metabolic adaptation plays a role in parasite survival on hosts under different nutritional challenges.

1.6 Aims and Objectives

In light of the knowledge gap on the nature of environmental adaptation of the malaria parasite, there is a need to address whether different nutrient environments would trigger a response on the parasite at the systems level promoting a metabolic rewiring that would have an effect in progeny generation or life cycle progression. Most studies on nutritional requirements of *Plasmodium* were done in the 80s and focus solely on viability reports [128, 233, 234] while more recent studies have mainly focused on the effect of deprivation of one amino acid by either not supplementing it in the media [232] or disrupting the machinery for its use [231]. The overarching aim of this thesis was to characterise major metabolic parasite features during intra-erythrocytic growth and development in multiple environments. This aim was addressed through the following specific objectives, also summarised in Figure 1.14.

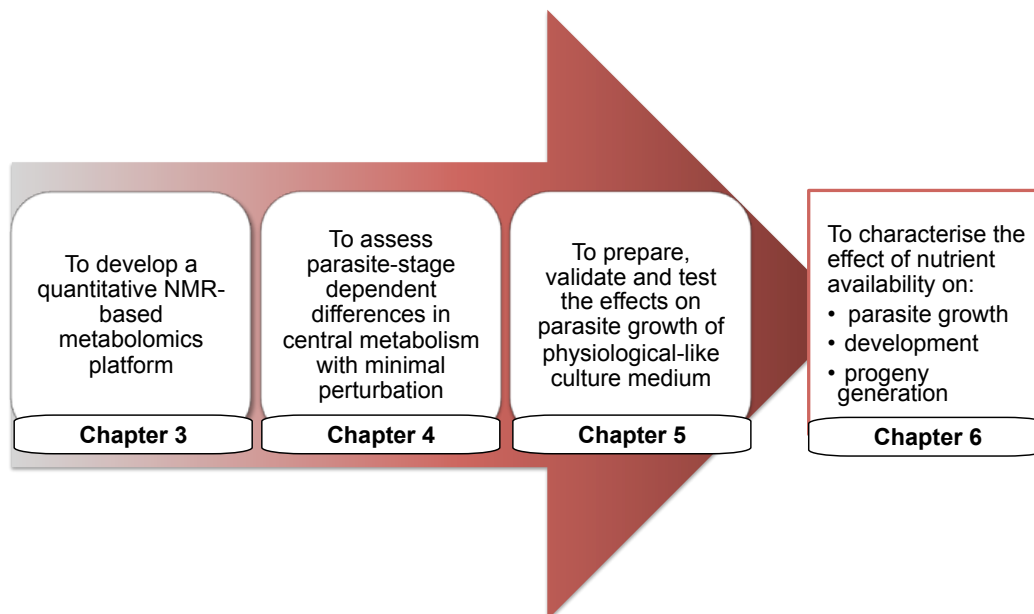


Figure 1.14: **Objectives.**

- To develop a quantitative NMR-based metabolomics platform for the assessment of intracellular and excreted parasite metabolites (Chapter 3).
- To assess parasite-stage dependent differences in central metabolism in normal *in vitro* conditions to ensure life cycle monitoring with minimal perturbation of the natural host-parasite environment (Chapter 4).
- To prepare, validate and test the effects on parasite growth of RPMI-based culture medium mimicking physiological conditions (Chapter 5).
- To characterise the effect of nutrient availability on parasite growth and development and the relationship between parasite metabolism, growth and progeny, as determined by bright field microscopy, high-content imaging and NMR metabolomics (Chapter 6).

Chapter 2

General Materials and Methods

All the procedures involving the culture of *Plasmodium falciparum* were performed in a CAT 3 lab inside a class II microbiology safety cabinet (NU-S434-500E, NuiAIRE) using aseptic technique. 70% ethanol was used when opening and closing the fume hood as well as when introducing material inside it. All the solutions have been filter sterilised using a 0.22 μm membrane filter unless stated otherwise.

2.1 Cryopreservation and parasite retrieval

2.1.1 Parasite retrieval

All cultures of *Plasmodium falciparum* strain 3D7 were stored in liquid nitrogen. A vial was removed from cold storage and thawed at 37 °C for approximately 2 minutes. Then a volume of 12% NaCl, equal to 0.1X the volume of the vial, was added drop by drop while gently shaking the tube, which was then left standing for 5 min. Next, 10 volumes of 1.6% NaCl were added in the same way and the tube was immediately centrifuged at 500 *g* and 20 °C for 5 min. The supernatant was discarded and 10 volumes of complete culture media were added as previously described for the NaCl solutions. This was centrifuged as above and the supernatant was discarded leaving the pellet ready to be cultured in a 25 mL flask following routine culturing techniques described in Section 2.2.

2.1.2 Cryopreservation

2.1.2.1 Cryopreservation solution

Cryopreservation solution was prepared as follows; 4.2% (w/v) sorbitol was dissolved in 0.95% (w/v) NaCl solution (prepared in distilled water). To this 35% (v/v)

glycerol was added before sterilisation by filtration and storage at 4 °C until use.

2.1.2.2 Cryopreservation procedure.

Parasite cultures at a parasitaemia greater than 5% and highly synchronous at ring stage were transferred to 50 mL tubes and centrifuged at 500 *g* for 5 min at RT. The supernatant was discarded and an equal volume of cryopreservation solution (Section 2.1.2.1) was added to the pellet. This suspension was left to equilibrate for 5 min at RT. Finally aliquots of 1000 μ L were transferred to cryotubes that were transferred to permanent storage in a liquid nitrogen tank where they are kept in the gas phase of the element.

2.2 Maintenance of *Plasmodium falciparum* in vitro

2.2.1 Standard culture media

P. falciparum was cultured in RPMI-1640 R8758 (Sigma Aldrich) supplemented with 0.04 mM hypoxanthine (section 2.2.1.1) and 0.25% Albumax I (section 2.2.1.2). In order to avoid contamination 0.02 $mg\ mL^{-1}$ of gentamicin was added. Medium was buffered to pH 7.4 with 25 mM of the phosphate buffer HEPES (section 2.2.1.3). Then the medium was filtered and stored at RT until use for a maximum of one week. (Storage at room temperature allows identification of possible contamination in the media.)

2.2.1.1 Hypoxanthine

A 4 mM stock solution was prepared by dissolving hypoxanthine powder in a 0.1 mM NaOH solution. The solution was filtered-sterilised and kept at 4 °C for a maximum of 3 months.

2.2.1.2 Albumax I

A solution of 5% (w/v) Albumax I (Gibco CAS 11020-039) was prepared, filtered and stored at 4 °C for a maximum period of 6 months.

2.2.1.3 HEPES

HEPES (4-(2-hydroxyethyl)-1-piperazineethanesulfonic acid, Amresco CAS 7365-45-9) buffer was prepared as a 1M stock in distilled water, pH 7.4 and sterile filtered. HEPES was stored at 4 °C for a maximum of 6 months.

2.2.1.4 Gentamicin

Gentamicin was acquired from Sigma-Aldrich in sterile vials at 50 mg mL^{-1} and kept at $4 \text{ }^\circ\text{C}$.

2.2.2 Red blood cells

Fresh human blood type O+ in citrate-phosphate-dextrose bags was received every fortnight from the North West Regional Blood Transfusion Service in the UK. This blood had been tested for common pathogens such as HIV (Human Immunodeficiency virus) and HBV (Hepatitis B Virus). The blood was kept in the bags at $4 \text{ }^\circ\text{C}$ until it was aliquoted into 50 mL falcons. Aliquots of 25 mL were washed in 45 mL of RPMI 1640 R8758 before centrifuging at 1800 g for 5 min. Supernatants were discarded and the washing step was repeated twice more. The washed pellet was kept at $4 \text{ }^\circ\text{C}$ for a maximum of one week.

2.2.3 Culture conditions

Pellets obtained after retrieval (as explained in section 2.1.1) were cultured in 75 mL culture flasks at 2% haematocrit. Media was changed a minimum of once a day and parasitaemia was kept under 12% in order to reduce stress for nutrients and host competition (see section 2.2.3.1 for further details) [235]. However, it should be noted that higher parasitaemias were needed for metabolomics experiments. These flasks were gassed (as described in section 2.2.3.2) and kept in an incubator at $37 \text{ }^\circ\text{C}$.

2.2.3.1 Daily monitoring: thin blood smears

Culture flasks were removed from the incubator with care in order to avoid disturbance of the monolayer created in the bottom of the flasks. A monolayer aliquot of approximate $10 \text{ }\mu\text{L}$ was removed using a Pasteur pipette in order to prepare a smear on a glass microscope slide. This was fixed with absolute methanol and placed in 10% Giemsa solution for 10 min to stain. The slide was then washed in running water and dried using a hair dryer. The slide was then visualised under a $100\times$ lens of a microscope using immersion oil. Parasitaemia was estimated by dividing the number of infected red blood cells (iRBC) between the total number of cells, counting a minimum of 500 cells per slide. This resolution also allows the monitoring of the life stage of the parasite.

Parasitaemia was calculated daily to assess a suitable dilution for the parasites in culture. Typically, healthy asynchronous cultures increase their population

twice every day. Well-synchronised cultures increase their parasitaemia $4\times$ every cycle (which is 48 h for *P. falciparum*).

2.2.3.2 Culture gas phase

The environment for optimal growth of the malaria parasite must contain a lowered oxygen and raised carbon dioxide level [236]. Consequently, prior to incubation, each flask was gassed with a combination of 3% oxygen, 4% carbon dioxide and 93% nitrogen obtained from a tank supplied by British Oxygen Special Gases. The gas was administered through a length of pre-sterilised silicon rubber tube with a 0.22 μm pore size filter attached to a single used sterile filter pipette. Each flask was gassed for approximately 1 minute based on 75 cm^2 culture flask or 30 s for 25 cm^2 flasks.

2.3 Synchronisation of cultures

Within the human body, *P. falciparum* displays synchrony in its life stages, but in culture it tends to be asynchronous thus producing a mixed population consisting on a number of life-stages [177]. In order to identify stage-specific susceptibilities to different treatments a synchronous culture is required. The method used involved double round of synchronisation by sorbitol, which promotes late trophozoite lysis by modifying its osmolarity [237]. By exposing the parasites to a solution of the sugar, high enrichment of the early ring stages was achieved. The method consisted of incubating the cell pellet of a culture in 5 volumes of a pre-warmed 5% sorbitol solution for 25 min in a water bath at 37 °C and mixing gently every 5 min. After incubation the tube was centrifuged at 500 *g* for 5 min and the supernatant was discarded, followed by two further washes with 20 volumes of complete medium. Finally the cells were reintroduced into culture for 48 h prior experimentation to allow the cultures to recover.

The sorbitol synchronisation results in a population of parasites synchronous with life stages within 10 to 18 h of each other [238]. This window is sufficient for routine culturing but for metabolomics experiments more accuracy was needed. In order to achieve high synchrony, the above protocol was repeated 42 h after the first synchronisation, resulting in a reduction of the synchronisation window to less than 8 h.

2.4 Culture media. Design and preparation

One of the aims of this project was to determine the effect of the nutrient availability in the life cycle of *P. falciparum*. Five variations of RPMI culture media were used in these experiments: commercial RPMI (R8758, Sigma), RPMI prepared in-house, blood-like RPMI (which is RPMI media formulation at physiological conditions) and a modification of the latter with 2/5 standard glucose content. Values for the physiological conditions used in the preparation of blood-like RPMI were obtained from LeRoux *et al.* (2009) [178] and completed by the information found in the Human Metabolome Database (HMDB) [184]. Within the HMDB, several conditions were reported as intervals and in this case the upper bound was always selected for the production of blood-like RPMI (Table 2.1. Osmolarity of the final mixture was calculated and salts were adjusted to keep it within physiological range (280-295 mOsm/Kg).

2.4.1 Preparation and storage of stocks

Each component for the different media were prepared in 50 mL aliquots, sterile filtered and stored at $-80\text{ }^{\circ}\text{C}$ until use (see Table 2.2). Each aliquot was thawed for use and stored at $4\text{ }^{\circ}\text{C}$ for a maximum of a week. Asparagine, glutamine, and sodium bicarbonate were added immediately prior to use (due to their instability in solution).

2.4.2 Mixture and storage

The media were prepared as in Table 2.2, pH adjusted to 7.4 and filter-sterilised. Media was stored at $4\text{ }^{\circ}\text{C}$ for a maximum of 6 months. Aliquots without glucose were also prepared in order to perform the experiments with labelled glucose, in which case, this was added immediately prior to the experiment. Immediately prior to the experiment, albumax, HEPES and gentamicin were added in the same proportion stated in section 2.2.1. Hypoxanthine is added as 0.04 mM in the in-house produced RPMI and as 0.004 mM in the blood-like media, consistent with the value reported in the HMDB.

Table 2.1: Concentrations of RPMI culture media.

Compounds	RPMI (mM)	Blood-like RPMI (mM)
Inorganic Salts		
Calcium Nitrate 4H ₂ O	0.423	2.380
Magnesium Sulfate	0.406	0.830
Potassium Chloride	5.365	4.150
Sodium Bicarbonate	23.807	25.713
Sodium Chloride	116.507	110.891
Sodium Phosphate Dibasic (anhydrous)	5.635	0.380
Amino Acids		
L-Arginine	1.148	0.110
L-Asparagine (anhydrous)	0.378	0.043
L-Aspartic Acid	0.150	0.021
L-Cystine 2HCl	0.271	0.110
L-Glutamic Acid	0.136	0.047
L-Glutamine	2.053	0.600
Glycine	0.133	0.240
L-Histidine	0.072	0.085
Hydroxy-L-Proline	0.177	0.016
L-Isoleucine	0.381	0.071
L-Leucine	0.381	0.170
L-Lysine HCl	0.219	0.250
L-Methionine	0.101	0.028
L-Phenylalanine	0.091	0.078
L-Proline	0.174	0.190
L-Serine	0.285	0.140
L-Threonine	0.168	0.180
L-Tryptophan	0.024	0.046
L-Tyrosine 2Na 2H ₂ O	0.159	0.084
L-Valine	0.171	0.230
Vitamins		
D-Biotin	0.001	0.000
Choline Chloride	0.021	0.008
Folic Acid	0.002	0.000
myo-Inositol	0.194	0.030
Niacinamide	0.008	0.000
p-Aminobenzoic Acid	0.007	0.015
D-Pantothenic Acid (hemicalcium)	0.001	0.004
Pyridoxine HCl	0.005	0.000
Riboflavin	0.001	0.001
Thiamine HCl	0.003	0.000
Vitamin B12	0.000	0.000
Other		
D-Glucose	11.101	5.000
Glutathione (reduced)	0.003	0.037
Phenol Red Na	0.015	0.015

Table 2.2: Stock solutions details.

Compounds	Stock solution (mM)	CAS	Company
Inorganic Salts			
Calcium Nitrate 4H ₂ O	423.460	13477-34-4	Sigma-Aldrich
Magnesium Sulfate	405.729	10034-99-8	Analar
Potassium Chloride	1341.202	7447-40-7	Fluka
Sodium Bicarbonate		144-59-8	Sigma-Aldrich
Sodium Chloride	4928.131	7647-14-5	Sigma-Aldrich
Sodium Phosphate Dibasic (anhydrous)	433.925	7558-79-4	Analar
Amino Acids			
L-Arginine	399.541	74-79-3	Sigma-Aldrich
L-Asparagine (anhydrous)		70-47-3	Fluka
L-Aspartic Acid	26.520	56-84-8	Sigma-Aldrich
L-Cystine 2HCl	83.229	56-89-3	Sigma-Aldrich
L-Glutamic Acid	46.979	56-86-0	Sigma-Aldrich
L-Glutamine		56-85-9	Sigma-Aldrich
Glycine	133.209	56-40-6	Sigma-Aldrich
L-Histidine	71.565	04/02/7048	Sigma-Aldrich
Hydroxy-L-Proline	176.788	51-35-4	Sigma-Aldrich
L-Isoleucine	251.220	73-32-5	Sigma-Aldrich
L-Leucine	148.171	61-90-5	Sigma-Aldrich
L-Lysine HCl	219.058	657-27-2	Sigma-Aldrich
L-Methionine	100.536	63-68-3	Sigma-Aldrich
L-Phenylalanine	90.799	63-91-2	Sigma-Aldrich
L-Proline	173.717	147-85-3	Sigma-Aldrich
L-Serine	285.470	56-45-1	Fluka
L-Threonine	167.926	72-19-5	Sigma-Aldrich
L-Tryptophan	24.486	73-22-3	Sigma-Aldrich
L-Tyrosine 2Na 2H ₂ O	160.000	60-18-4	Sigma-Aldrich
L-Valine	170.721	72-18-4	Fluka
Vitamins			
D-Biotin	0.819	58-85-5	Sigma-Aldrich
Choline Chloride	21.490	67-48-1	Sigma-Aldrich
Folic Acid	2.266	59-30-3	Sigma-Aldrich
myo-Inositol	194.229	87-89-8	Sigma-Aldrich
Niacinamide	8.190	98-90-0	Sigma-Aldrich
p-Aminobenzoic Acid	7.294	150-13-0	Sigma-Aldrich
D-Pantothenic Acid (hemicalcium)	0.514	137-08-06	Sigma-Aldrich
Pyridoxine HCl	4.768	58-56-0	Sigma-Aldrich
Riboflavin	0.531	83-88-5	Sigma-Aldrich
Thiamine HCl	3.324	67-03-8	Sigma-Aldrich
Vitamin B12	0.004	68-19-9	Sigma-Aldrich
Other			
D-Glucose		50-99-7	Sigma-Aldrich
Glutathione (reduced)	3.186	70-18-8	Sigma-Aldrich
Phenol Red Na		143-74-8	Sigma-Aldrich

2.5 Metabolite extraction

An extraction method based on Olszewski *et al.* and Beckonet *et al.* [239, 240] was implemented as follows. Extraction solution must be at least 4 times the volume of the sample. Due to the need to process more than 400 μL of complete sample, multiple aliquots were used of the same culture. These were then pooled post-extraction into 15 mL Falcon tubes. For each 400 μL sample, 1 to 3 Eppendorfs of 2 mL capacity were labelled. Also a 15 mL tube per complete sample and an 2 mL eppendorf for media sample. The three eppendorfs, namely 1, 2a, and 2b were chilled on dry ice. Tube one contained a volume equal to 4 times the cells of the extraction solution, of a 20:20:10 mixture of acetonitrile (CAS 75-05-8, Sigma-Aldrich, HPLC pure solvent), methanol (CAS 67-56-1, Sigma-Aldrich, HPLC pure solvent), and water (CAS 7732-18-5, Sigma-Aldrich, HPLC pure) respectively. Tube 1 also contained the internal standard TSP (3-(Trimethylsilyl)propionic-2,2,3,3-d4 acid, CAS 24493-21-8, Sigma-Aldrich) at 2.5 mM.

The extraction process is shown in Figure 2.1. After incubation, a sample of supernatant equivalent to the volume of cells taken was collected in the media tube and a sample of at least 1.4×10^9 cells was taken and washed twice in ice cold $1 \times$ PBS (Phosphate Buffered Saline). Aliquots of 400 μL per sample were taken and rapidly deposited in tube 1, vortexed vigorously and left on dry ice. When all the samples were collected they were vortexed again and kept on dry ice for 15 min, vortexing every 5 min.

After this step there were two modalities of the method that will be further discussed in Chapter 3 but briefly:

- a)* **Single extraction.** The samples were centrifuged at 16000 g for 10 min at 4 $^{\circ}\text{C}$. The supernatant was then transferred to the 15 mL tube where all of the aliquots of tube 1 from the same cell sample were pooled together. Then the samples were stored at -80 $^{\circ}\text{C}$ until the next step.
- b)* **Double extraction.** The samples were centrifuged at 500 g for 5 min at 4 $^{\circ}\text{C}$. The supernatant was then transferred to tube 2a and stored on dry ice. The pellet was resuspended with 1 mL of pre-chilled extraction solution, vortexed and sonicated on ice for 15 min. The samples were immediately centrifuged at 16000 g for 5 min at 4 $^{\circ}\text{C}$. The supernatant was transferred to tube 2b and the pellet discarded. Both tube 2a and 2b were centrifuged at 16000 g for 10 min at 4 $^{\circ}\text{C}$. Finally all the supernatants of the same cell sample were pooled in a Falcon that was stored at -80 $^{\circ}\text{C}$ until further experimentation.

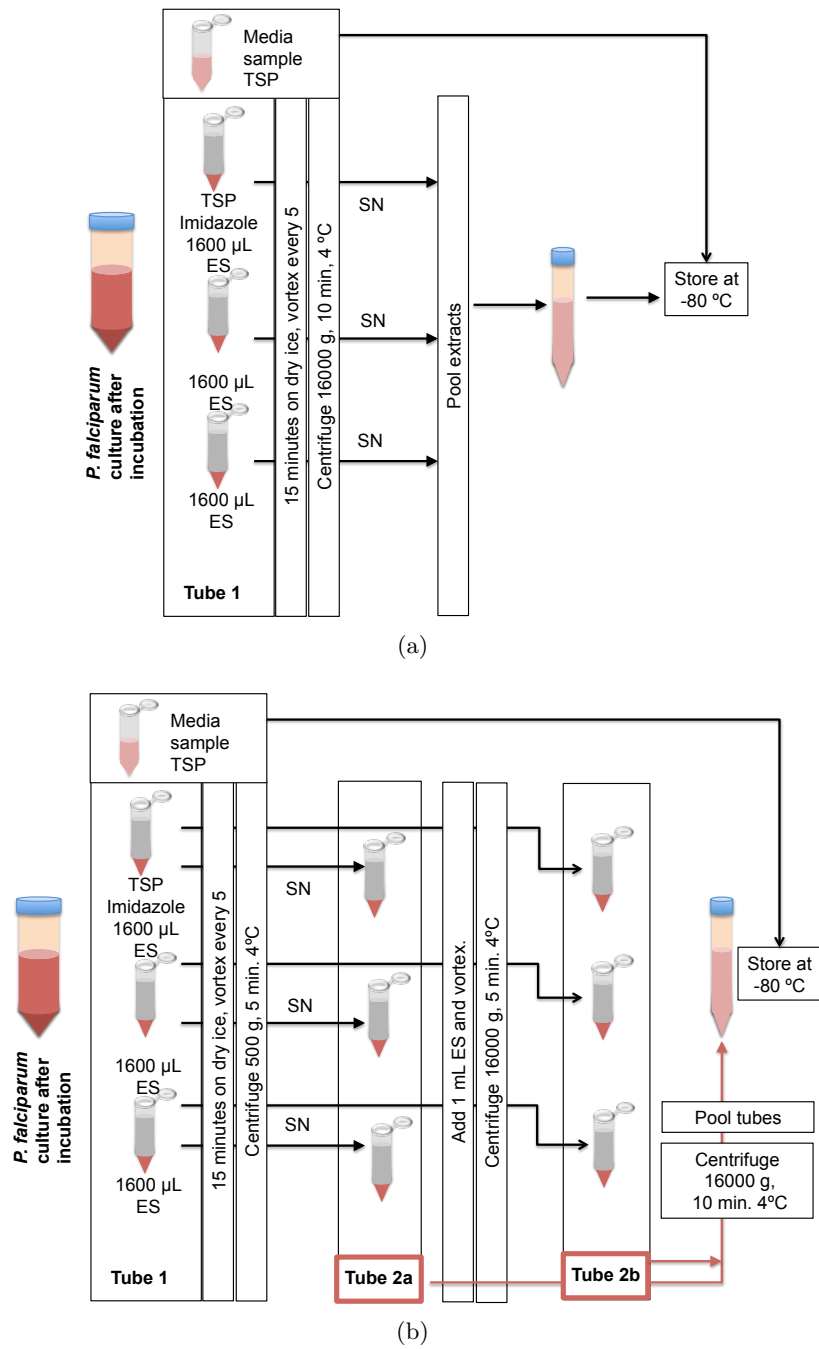


Figure 2.1: **Metabolite extraction.** (a) **Single.** (b) **Double.** ES stands for extraction solution. The internal standards were added in one of the tubes with the extraction solution. This figure shows the main differences between metabolite extraction procedures.

2.6 The effect of glutamine on glycolytic flux

2.6.1 Ringer's solution

Ringer's solution was prepared in distilled water adding 106 mM NaCl (CAS 7647-14-15, Sigma-Aldrich), 24 mM NaHCO₃ (CAS 144-59-8, Sigma-Aldrich), 5.4 mM KCl (CAS 7447-40-7, Fluka), 1.2 mM CaCl₂ (CAS 10043-52-4, Sigma-Aldrich), 1 mM Na₂HPO₄ (CAS 7558-79-4, Analar), and 0.8 mM MgCl₂ (CAS 7786-30-3, Sigma-Aldrich). Then it was adjusted to pH 7.4, filter-sterilised and stored at 4 °C.

2.6.2 Experimental procedure

900 μ L of highly synchronous *P. falciparum* cultures at 10.4% parasitaemia were incubated for 2 h in 10 mL of pre-warmed Ringer's solution containing different levels of glucose and glutamine, which were shown in Table 2.3. For each condition two solutions were prepared, one with U-¹³C-glucose and other with unlabelled glucose and parasites were incubated in both. An RBC control was also incubated for each condition, using Ringer's solution containing labelled glucose. The incubation was performed in a 6-well plate (Nunc cell-culture treated multidishes, 6-well, round-bottomed, Thermo) deposited in a modular incubator chamber (PAT. NO. 532414, Billups-Rottenberg) containing a paper towel wet with distilled water in the bottom to maintain humidity levels. The chamber was gassed for two min as describe in section 2.2.3.2. After incubation, metabolites were extracted using the double extraction method described in section 2.5 *b*) and processed as described in Section 2.7.

Table 2.3: Concentrations of glucose and glutamine.

Conditions	Glucose [mM]	Glutamine [mM]
A	5	0
B	5	0.6
C	5	2
D	1	0
E	1	0.6
F	1	2

2.7 NMR Analysis

2.7.1 Sample preparation for analysis in the NMR

At least 24 h before the NMR analysis, both extracts and media samples were freeze-dried. The dried samples were stored at $-80\text{ }^{\circ}\text{C}$ or directly prepared for analysis. Samples were resuspended in $300\text{ }\mu\text{L}$ of NMR buffer (100 mM sodium phosphate buffer (Na_2HPO_4 , CAS 7558-79-4 and NaH_2PO_4 , CAS 7558-80-7), pH 7.4 in $^2\text{H}_2\text{O}$) and vortexed vigorously. Then they were centrifuged at 16000 g for 5 min. $280\text{ }\mu\text{L}$ of the supernatant was transferred to a 3 mm diameter NMR tube with a Pasteur pipette.

2.7.2 NMR set-up and parameters

1D ^1H and 2D ^1H - ^{13}C heteronuclear single-quantum correlation (HSQC) spectra of each sample were acquired using Topspin 3.1 on a Bruker Avance III 600 MHz spectrometer. NMR set up was performed daily by calibrating the temperature of the machine to $25\text{ }^{\circ}\text{C}$ using a methanol thermometer [241] and the tuning or shimming of the spectrometer followed by the optimisation of acquisition parameters O1 to optimise the suppression of the residual H_2O signal and DE to ensure baseline reproducibility. 2D HSQC were acquired in 4 transients, with 8192 directly acquired points and 1028 increments with sweep and offset optimised for aliphatic metabolites. Spectrum was then Fourier transformed with standardised shifted sine bell window function, zero-filled, and phased in TopSpin. A full list of parameters is provided in Appendix A.

2.7.3 Metabolite identification

Phased spectrum was introduced in CCPNmr software [242] for further analysis. Metabolites were identified by overlapping spectra of different hydrophilic metabolite standards with our query spectra. Initially an *in silico* collection of spectra provided by the metabolomics project [243] was used and then further expanded by importing spectra from the Madison Metabolomics Consortium Database [199]. The metabolite candidates identified by this method were then confirmed by running a reference sample of the specific metabolites in the same conditions as our spectra.

2.7.4 Preparation of standards for the creation of calibration curves

For all the metabolites identified, calibration curves were created. For each metabolite, solutions in $^2\text{H}_2\text{O}$ at 0.1, 0.2, 0.5, 1, 2, 5, and 10 mM were prepared. These

also contained the standards TSP and imidazole at 2.5 and 5 mM respectively. The samples were analysed in the spectrometer and HSQC spectra were acquired as detailed in Section 2.7.2. The spectra were entered into CCPNmr software to calculate heights and volumes of each peak. These were normalised by the TSP signal and plotted against concentration. A linear fit was obtained for each ^1H - ^{13}C one bond correlation peak. These will be further discussed in Chapter 3.

2.7.5 NMR Data analysis

2.7.5.1 Cell extracts

The values for the height and volume of all the peaks found in the spectra were extracted in a comma separated value (csv) file. Detailed information on the design of this analysis is provided in Chapter 3 but briefly, the pipeline of analysis for each sample dataset described below.

1. **Cleaning:** the file was formatted and redundant information removed.
2. **Normalisation:** the heights and volumes of the peaks were divided by the height and volume of TSP respectively.
3. **Nomenclature:** The peak reference codes were substituted by the corresponding IUPAC (International Union of Pure and Applied Chemistry) nomenclature for each carbon.
4. **Analysis:** Schematic representations in Figure 2.2. Data from differently labelled samples were processed separately. The natural abundance samples were used to calculate the concentration of the sample. Further processing allowed the estimation of intracellular concentrations. The heights and volumes of both natural abundance and labelled samples were used to calculate the labelled ratio per carbon or each metabolite found in the sample.

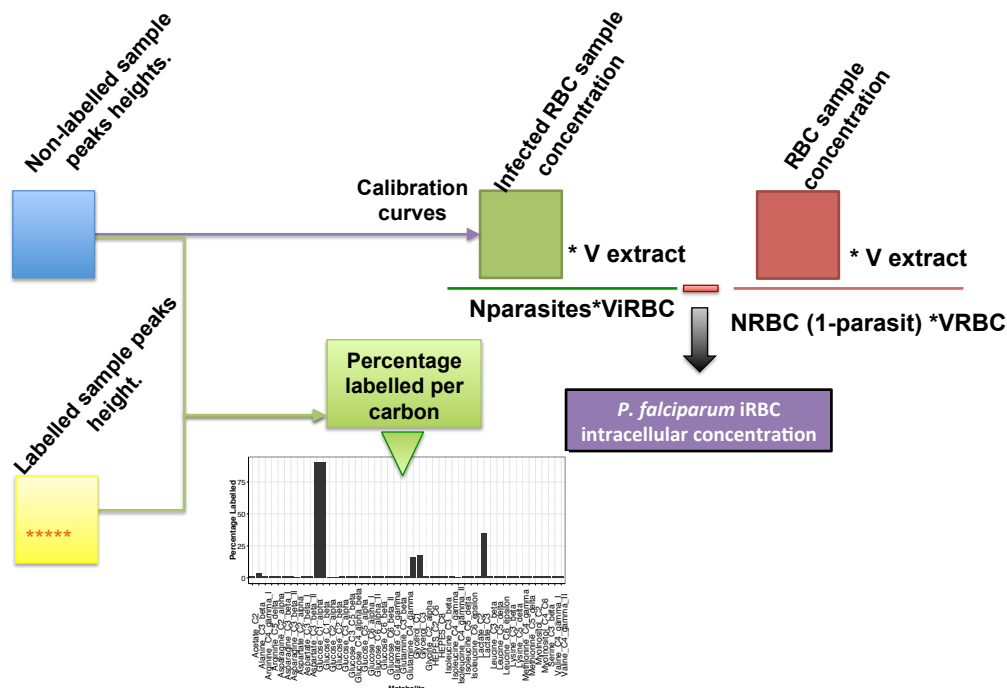


Figure 2.2: **Sample analysis and concentration calculations.** “V” stands for volume, “NRBC” stands for number of RBCs, “Nparasites” stands for number of parasites, “parasit” stands for parasitaemia and “Nat.Abund.” stands for natural abundance

5. **Calculation of concentrations:** By using the calibration curves, heights and volumes of peaks were translated into concentration values.
6. **Calculation of intracellular concentrations:** By having an homologous uninfected growth that is extracted and processed in the same manner as the infected one, intracellular concentrations can be estimated. The moles present in the non-infected RBC of the sample were subtracted from the mixed RBC + infected RBC sample. This was calculated by using the data from the RBC control sample scaled down by removing the percentage of infected RBC in the query sample.
7. **Plot concentrations**

2.7.5.2 Calculation of moles consumed or excreted: Media samples.

Media samples concentrations were calculated using the calibration curves. A correction factor to account for the difference between volume sampled and volume

in the NMR tube was implemented and concentrations used for further analysis. When estimation of consumption and excretion of moles per cell were required, further steps were implemented (see Figure 2.3).

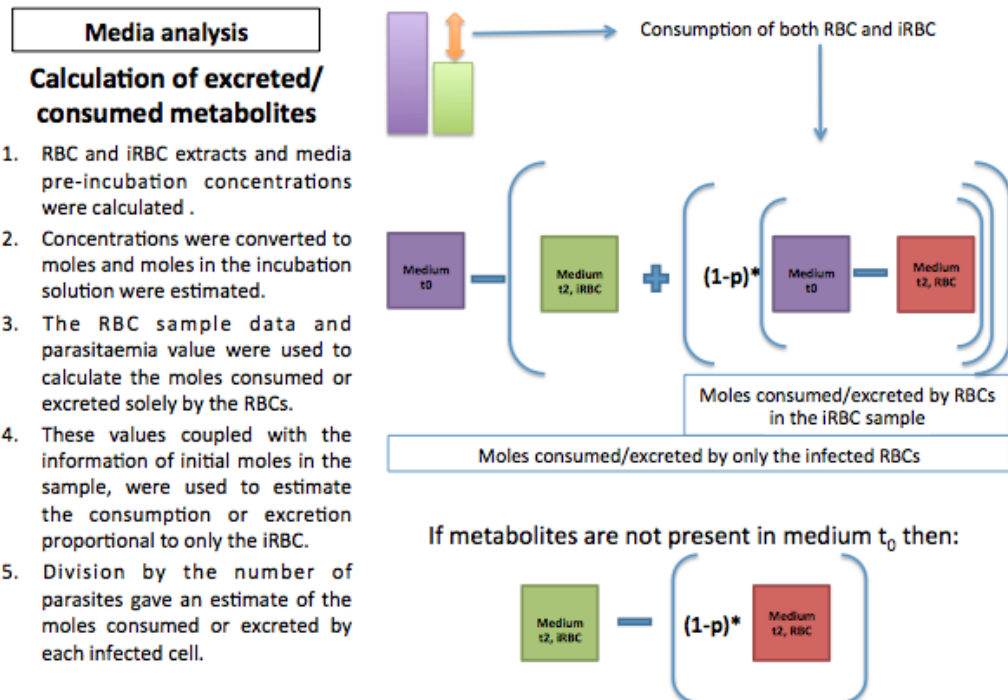


Figure 2.3: Media samples analysis pipeline

2.8 Imaging sample preparation and analysis

2.8.1 High content Imaging.

Tetramethylrhodamine ethyl ester perchlorate (TMRE, CAS 115532-52-0, Sigma Aldrich) and Hoechst 33342 (CAS 23491-52-3, Invitrogen) were diluted in culture media to a concentration of 200 nM and 2 $\mu\text{g}/\text{mL}$ respectively. Aliquots were prepared and frozen at the start of the experiment and were stored for no longer than a week. At each time point an aliquot was defrosted 30 min prior sampling and 50 μL and plated into the Cell Carrier-384 Black, optically clear bottom with lid (Perkin Elmer, product number 6007558). Cell suspensions at 0.02% haematocrit were prepared from each culture at each time point. 50 μL of each suspension was added to a well of the Cell Carrier, adjusting the final concentration of the dyes to 100 nM of TMRE and 1 $\mu\text{g}/\text{mL}$ of Hoechst 33342. The plate was incubated for 30 min prior to measurement at RT.

Plates were read in a PerkinElmer Operetta High Content Imaging System (Operetta) using the software Harmony. Images at 60X magnification from three channels were obtained *i.e.* Brightfield (exposure 400ms), Hoechst 33342 (exposure 50ms) and TMRE (exposure 500ms) of at least 56 fields per well. Excitation and transmission were 100%.

The data from the measurements was analysed in two phases. First Harmony was used to extract the data from the images. The parameters used to select the regions were (a) TMRE: find image with a threshold of 0.43 and object clustering allowed. Select a population with an area of $0.4 < x < 55 \mu\text{m}$, roundness > 0.4 and Intensity > 2000 . (b) Hoechst was selected with image region, threshold set to 0.73, allowing clustering and the selected population was cut by taking regions with an area of $0.5 < x < 50$, roundness > 0.4 and Intensity > 250 . Second the evaluation data was extracted and further cleaned using the statistical software R. The analysis pipeline will be discussed in Chapter 6 but briefly the data is further cleaned by removing fields with artifacts, then outliers are removed in two phases: first by further constriction of the area size and secondly by removing the top and bottom 10% quantiles. This is followed by the calculation of the mean and standard error and consecutive visualisation in plots and statistical analysis.

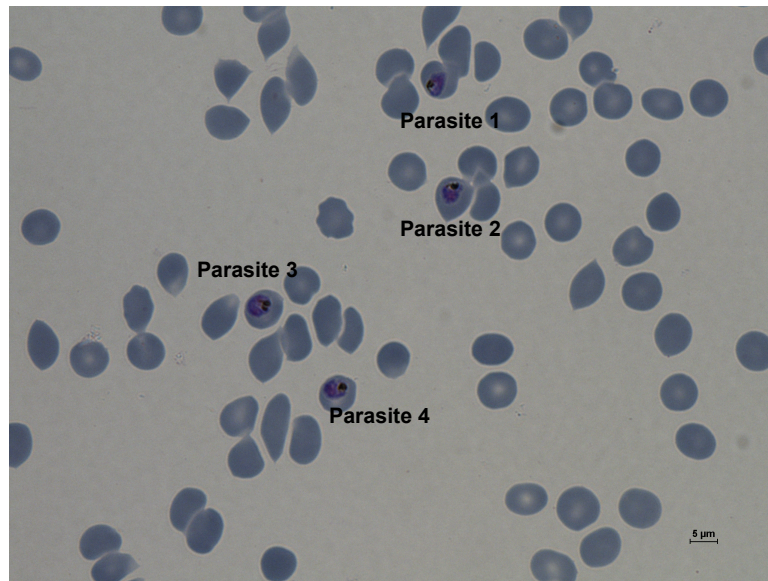
2.8.2 Bright field microscopy

Slides were prepared as explained in section 2.2. These were visualised in an Olympus bx-60 microscope and digitalised with the aid of a Nikon camera attached to it using the software NIS Elements v.3. These images were exported as tiff and further analysed with Fiji (Image J, version 2.0.0). Images were calibrated and converted to 8 bits followed by manually adjusting the threshold until regions of interest (ROI) were selected. The resulting image was made binary and converted to mask where ROIs were analysed obtaining measurement of area, intensity, circularity and solidity. Note that intensity is defined as $area \times mean \ gray \ value$, circularity is defined as $(4\pi \times area) / perimeter^2$ and solidity as $area / convex \ area$. Measurements of at least 30 parasites per treatment were obtained and used for statistical tests.

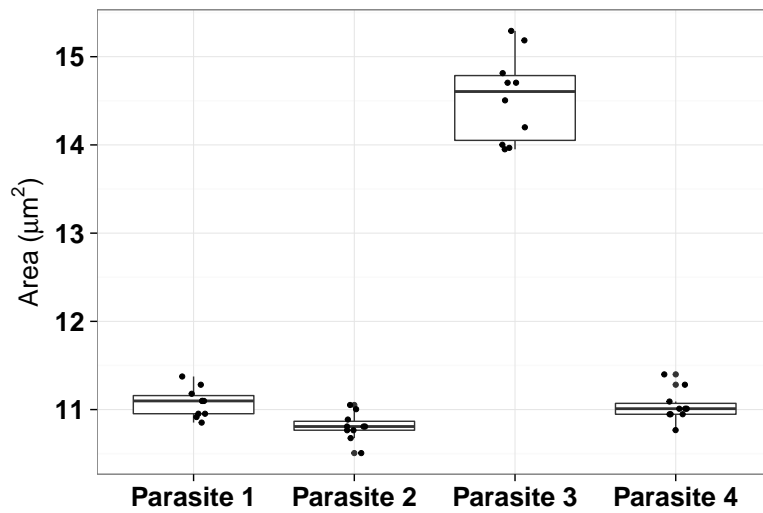
2.8.2.1 Bright field analysis validation

Image analysis procedure was validated by repeating the analysis on a representative image ten times (see Figure 2.4). The measurements of area were used to calculate the estimated coefficient of variation defined as the standard deviation divided by the mean of the sample. Results, presented in Table 2.4 did not exceed a 3.5% what

indicates good levels of repeatability.



(a)



(b)

Figure 2.4: **Bright field analysis validation** (a) Representative image used for validation. The four parasite areas were measured following the steps described in Section 2.8.2 ten times; (b) Box plots of the area measurements of the four parasites in the 10 iterations. Box plots represent median of the data (black line) contained into the first and third quantiles (box). Segments reach the maximum and minimum value excluding outliers.

Table 2.4: Image analysis validation statistics

	Mean	Standard Deviation	Coefficient of Variation
Parasite 1	11.0804	0.1665	0.015
Parasite 2	10.8083	0.1548	0.0143
Parasite 3	14.5324	0.4936	0.034
Parasite 4	11.041	0.1805	0.0163

2.9 Life-cycle time course experiment

P. falciparum 3D7 cultures were tightly synchronised (section 2.3) in two consecutive cycles. In the next consecutive cycle all the cultures were pooled together and 1.2 mL pellet aliquots at 3% parasitaemia were incubated in triplicate in different media: complete media, blood-like media and low glucose blood-like media (2 mM) (see section 2.4). These parasites were grown for 45 h changing media every 12h. After the incubation sampling was started, every 3 h an aliquot of 1.2 mL was taken from each flask. This aliquot was centrifuged at 13000g, 1 mL of the supernatant was collected in an sterile tube for NMR analysis, 5 μ L of the pellet were used to prepare a bright field microscopy preparation and 1.2-1.8 μ L were used to make a dilution for high content imaging as described above. Samples of media before incubation were also taken as well as samples after 3 h incubation with only RBCs in order to assess the background of the RBCs when analysing the metabolite samples. The sampling was planned to last until hour 48 post sampling start. However, after 48 h, those parasites growing in both blood-like and low glucose blood-like media were not fully developed. The experiment was prolonged until hour 54 when parasites growing in blood-like media showed some early life-stages forms. However low glucose blood like media were still in late development stages. The experiment was stopped but flasks of parasites in blood-like and low glucose blood like media were left in the incubator until hour 74 to confirm the presence of early life-stages parasites. All the samples were processed as described above and results are discussed in Chapter 6.

2.10 Statistical analyses

2.10.1 Statistical hypothesis tests

Univariate statistical tests for difference in means were used to determine if two sets of data were significantly different. This was determined from the p-value calculated in the test. The p-value is a measure of likelihood to obtain data with the difference in means as large or larger as one in the tested data under the null-hypothesis.

The null-hypothesis assumes that there is no difference between the datasets. An arbitrary significance level (usually $\alpha=0.05$) is used as a cut-off for rejecting the null-hypothesis. Confidence interval for the difference in means was also reported. A confidence interval is a range of numbers calculated to contain a statistic, in this case the difference in means 95% of the time. It gives a good measure of the uncertainty about the statistic.

Data variances were assumed to be unequal for robustness. Data normality was assessed by the Shapiro-Wilk test in order to select a suitable statistical test. Where data were confirmed to be normally distributed unpaired unequal variances t-tests (or Welch's tests) were applied. Where data were not normally distributed, the non-parametric Mann-Whitney-Wilcoxon rank-sum tests were used.

Calculated p-values were adjusted to account for the false discovery rate. This multiple testing correction is required in order to reduce false positive findings. Benjamini-Hochberg procedure was used for p-value adjustment. The formula used is the in-built "p.adjust" function in the statistical software R that given a vector 'v' of p-values, returns an adjusted vector by applying the formula $pBH = pn/i$ where p is the original p-value, n is the number of tests performed and i is the rank of the p-value calculated from ordering the 'v' vector of p values from smallest to largest and rank them from 1 to v. The hypotheses were rejected if adjusted p-values were lower than the significance level $\alpha=0.05$.

2.10.2 Principal Component Analysis (PCA)

PCA is a linear transformation of the data that converts a set of correlated variables into uncorrelated principal components. The principal components are constructed in such a manner that the first principal component accounts for the maximum variation in the original data, the second one - orthogonal to the first one - accounts for the maximum of the variance unexplained by the first, etc. This procedure results in a set of uncorrelated variables (principal components (PCs)) that are sorted by the variance they account for. In most datasets the first few principal components account for the majority of variance and the rest of the principal components can be discarded with minimal loss of information. This allows a reduction in the dimensionality of the original dataset for easier data visualisation and modeling.

PCA was used as an exploratory data analysis tool to unveil hidden structure of the data and was calculated on mean centred and scaled data. PCA scores plots of the first two or three PCs gave information of the relation between samples given that relative distances between points in such scores plots can be interpreted as similarities between samples. All plots reported in this thesis contained information

of the percentage of variance explained by each PC.

The proportions of each of the original variables in the principal components have been represented in loading plots which inform on the contribution of each variable to the distribution of points in the scores plots and thus their influence in either similarities or differences.

2.10.3 Propagation of error

Estimation of consumption/excretion of metabolites per cell were calculated performing arithmetic operations on the means of each variable. Each of those variables had associated an uncertainty (standard deviation) that upon combination in arithmetic operations increased in a non-linear manner. In order to estimate the error propagation the formulas in Table 2.5, derived from the Gaussian equation for normally-distributed errors, were used.

Table 2.5: Propagation of error formula calculation

Function	Standard Deviation
$f = aA$	$ a \sigma_A$
$f = aA + bB$	$\sqrt{a^2\sigma_A^2 + b^2\sigma_B^2 + 2ab\sigma_{AB}}$
$f = aA - bB$	$\sqrt{a^2\sigma_A^2 + b^2\sigma_B^2 - 2ab\sigma_{AB}}$
$f = AB$	$\sqrt{\left(\frac{\sigma_A}{A}\right)^2 + \left(\frac{\sigma_B}{B}\right)^2 + 2\frac{\sigma_{AB}}{AB}}$
$f = A/B$	$\sqrt{\left(\frac{\sigma_A}{A}\right)^2 + \left(\frac{\sigma_B}{B}\right)^2 - 2\frac{\sigma_{AB}}{AB}}$

2.10.4 Analysis of covariance (ANCOVA)

ANCOVA combines features of ANOVA (analysis of variance) and regression. It augments the ANOVA model with more additional quantitative variables (covariates), which are related to the response variable. ANCOVA was used as a way to assess the effect of the different nutrient concentrations in either growth or metabolite consumption and excretion. ANCOVA can be used to compare two or more regression lines by testing the effect of a factor (in this case the three media CM, BL and LG) on a dependent variable (parasite size/metabolite consumption/excretion) while controlling for the effect of a continuous co-variable (in this case time). ANCOVA allows us to find out if intercepts and slopes are different between factors.

Chapter 3

A tailored method to identify and quantify metabolites of *Plasmodium falciparum* in cell and media samples using Nuclear Magnetic Resonance (NMR)

3.1 Introduction: *P. falciparum* intra-erythrocyte metabolic network revealed by metabolomics

Understanding of the parasite's metabolism is paramount, not only because of its role in malaria pathogenesis but also because it is a target of antimalarial drugs [221] and for many of them the mode of action is not well characterised [244]. Attempts to unveil the metabolic network of the parasite has been investigated by *in vivo* biochemistry or indirectly by inference from genomic data and bioinformatic studies [71, 72]. The development of metabolomic technologies enabled the study at the systems level of the parasite and consequently the first metabolomic studies to understand *P. falciparum* blood stages metabolism were published. Shortly after the publication of Nuclear Magnetic Resonance (NMR) analyses of metabolic responses of mice infected with *Plasmodium berghei* using biofluids [218], two metabolic studies in cellular extracts *P. falciparum* were published in 2009 by independent groups.

Teng *et al.* [219] used ^1H NMR spectroscopy to analyse the metabolome of late trophozoite stages of *P. falciparum* that were isolated from the host red blood cell (RBC) by a treatment with saponin. Sample sizes of $1\text{--}4 \times 10^8$ cells (equivalent to $105 \mu\text{L}$ of cell pellet) were extracted using 4 different extraction solutions: perchloric acid, methanol/water, methanol/chloroform/water or methanol and they were compared. Around 40 metabolites were identified and quantified followed by estimation of intracellular concentrations. Partial least squares was used to compare the extraction methods. The authors concluded that perchloric acid was the most advantageous solution although results were broadly similar among extractions. However perchloric acid poses a problem for metabolomic studies by NMR spectroscopy. As an acidic solution, perchloric acid would vary the sample's pH, which can severely affect spectra acquisition. Thus a protocol that involved the use of an acid as extraction solution would require an obligatory step to adjust pH prior to NMR acquisition, increasing the complexity of the sample processing. Supernatants were also collected and used to assess metabolite loss during the separation of parasites and RBCs. Overall the work by Teng *et al.* set out the methodology and precedence for metabolomics by NMR spectroscopy of *P. falciparum*. Moreover, the same group has recently use this method to profile chloroquine sensitive and resistant strains of *P. falciparum* [217].

The Llinás group [195] used synchronised cultures of *P. falciparum* 3D7 to take samples at seven time points during its 48-hour blood stage, which were analysed using a liquid chromatography-tandem mass spectrometry (LC-MS/MS) method developed by Lu *et al.* [212]. Samples consisted of $50 \mu\text{L}$ (equivalent to 9.5×10^7 cells) of cell pellet of either infected (at 10% parasitaemia) or non-infected RBCs and the supernatants that were extracted as described in [239]. Overall 90 metabolites were detected and quantified over the time course. These span a wide range of metabolic pathways such as amino acids, nucleotides and central carbon metabolism intermediates. This study revealed a modulation of metabolite levels by the parasite (in contrast with the low metabolism of the RBC) with numerous metabolites varying in phase with intra-erythrocytic development, generally increasing concentration from ring stages to trophozoite stages and slightly decreasing towards the end of the incubation, coinciding with very mature schizonts and formation of merozoites. The authors considered noteworthy the high parasite consumption of arginine, consistent with the typical hypoargininemia observed in humans infected with malaria, which is associated with the cerebral pathogenesis of the disease.

Continuing with the quest to elucidate how central carbon metabolism of *P.*

falciparum works, the Llinás' group traced ^{13}C -labelled compounds and published a controversial paper in which they stated that the Krebs cycle was not only largely disconnected from glycolysis but also presented a branched structure, different from the canonical cyclical flux [104]. However this communication was retracted in 2013 [245]. Central carbon metabolism of the blood stages of *P. falciparum* was finally elucidated by MacRae *et al.* analysis ^{13}C -Glucose and ^{13}C -Glutamine flux through glycolysis and glutaminolysis using LC-MS/MS. This study confirmed that the parasite uses a canonical Krebs cycle, despite the flux from glycolysis being very low during the asexual stages and that most of the carbon skeletons of the Krebs cycle are instead provided by glutaminolysis [103]. The lack of pyruvate dehydrogenase (PDH) in the mitochondrion that could convert pyruvate in to acetyl-CoA influenced the hypothesis of a dysfunctional Krebs cycle. However a branched chain ketoacid dehydrogenase (BCKDH) was found to functionally replace mitochondrial PDH [106]. These studies were done in mature trophozoite and schizont stages of the asexual life cycle of the parasite. Aliquots equivalent to 10^8 cells were extracted with a chloroform:methanol (1:1) solution, yet another extraction solution, different from above-mentioned publications. Finally a study of the central carbon metabolism using knock-out (KO) parasites for the main enzymes involved in the Krebs cycle has been recently published by Llinás group confirming above-mentioned results and proving that none of the enzymes ablated were essential for asexual development of the parasite [107]. For this study the authors were not very explicit with the nature of the samples used (cell suspension vs washed cellular extracts) where they only reported the use of a methanolic metabolite extraction on 800 μL samples.

Metabolomic studies have unveiled the metabolic network of the asexual stages of *P. falciparum*. However the reason behind this metabolic rewiring is unclear. During the asexual stages, *P. falciparum* exhibits a very high glycolytic flux (with up to $100\times$ higher glucose intake than uninfected RBCs [223]) followed by a low flux into the Krebs cycle. During sexual stages, the Krebs cycle activity increases and parasites are more susceptible to mitochondrial inhibitors [103]. We have proposed that this metabolic rewiring, similar to the Warburg effect, which is well characterised in cancer cells [115], is a strategy to maximise biomass production by redirecting glycolytic intermediates into pathways that will lead to the construction of nucleic acids, lipids and other key metabolites to meet the high demand for biomass production [111]. The limited flux into Krebs cycle might be explained by a need to keep lactic fermentation ongoing as it might serve as a regulatory mechanism [117] (see Chapter 1, Section 1.3.1.3) or to reduce in general the otherwise high flux into the respiratory chain with the consequent ion leakage followed by the

production of reactive oxygen species (ROS) that would be harmful for the progeny.

All the above-mentioned studies were performed in conditions far from physiological. Some of these studies used RBC-free parasites. This process would be greatly stressful for the parasite and it is likely that it would trigger stress responses atypical from healthy parasites. All the experiments were done in laboratory conditions, with rich media that has in general much higher concentrations of the metabolites compared to typical human blood [178]. As described in Chapter 1, one of the knowledge gaps to address is whether nutritional availability has an effect upon parasite development. We aim here to further pursue the validity of the proposed hypotheses regarding the role played by high glycolytic fluxes followed by high lactic fermentation.

Because of the limitations of previous methods, in this Chapter we focus on the development of a robust metabolomics method to identify and quantify metabolites of intra-erythrocytic stages of *P. falciparum* in a NMR spectroscopy-based platform. The Chapter will detail the progression of the assay development including the following sections:

1. Adequate signal detection on undisturbed parasites.
 - (a) Assess the signal difference between cell suspension and individual media and cell extractions for similar samples.
 - (b) Use of iRBC samples without parasite enrichment methods in order to keep conditions as natural as possible.
 - (c) Optimise NMR signal strength in order to identify a relevant number of metabolites by using ^{13}C isotopic glucose and explore alternative NMR spectroscopy experiments.
2. Metabolite identification.
3. Metabolite quantification.
4. Validation and pipeline assembly
5. Pilot experiment to test the method.

3.2 Experimental

Specific sample extraction and preparation are described in each section of the Results and Discussion section below. Unless stated otherwise, all samples were freeze-dried and resuspended into 300 μL of deuterium oxide, of which 280 μL were pipetted in a 3 mm diameter NMR tube. All spectra were acquired in a 600.13 MHz Bruker spectrometer fitted with an inverse probe with z grad, ATM (bt02000) at 298K. Spectra were acquired with the parameters shown in Table 3.1 and processing steps

were carried out. All spectra were zero filled to 13 k data points with exponential line broadening of 0.3 Hz being applied before Fourier transformation. Baseline correction, phasing and referencing to the internal standard 3-(trimethylsilyl)-2,2',3,3'-tetradeuteropropionic acid (TSP) were done manually.

Table 3.1: NMR acquisition parameters (on 600 MHz spectrometer)

Pulse sequence	noesygppr1d	cpmgpr1d	zgpg	hsqctgps
Type experiment	Nuclear Overhauser Effect spectroscopy with gradient pulses, with presat 1D	Car-Purcell-Meiboom-Gill with presat	basic 1D ^{13}C with pulsed filled gradients	Heteronuclear single quantum coherence echo-antiecho with gradient pulses
Dimensions-Type	1D	1D	1D	2D
Nuclei	H	H	C	H-C
Number of Scans	(a) 32 (b) 4	128	(a) 256 (b) 4096	32
Number of datapoints (TD)	98304	73728	262144	1024
Acquisition time (s)	2.726	3.067	4.404	0.085
Spectral Width (ppm)	30.041	20.028	197.209	10.014
Offset (O1, Hz)	2826.4	2824.5	12072.22	2825
Dwell time (μs)	27.733	41.6	16.8	83.2
Echo time	NA	0.6 ms	NA	NA
Indirect dimension: number of points	NA	NA	NA	256
Indirect dimension: acquisition time	NA	NA	NA	0.0071
Indirect dimension: spectral width (ppm)	NA	NA	NA	120.044
Indirect dimension: offset (O2, Hz)	NA	NA	NA	7545.14

3.3 Results and discussion

3.3.1 Adequate signal detection on undisturbed parasites

The process described here involved the adaptation and improvement of a method used previously by our group [81]. The protocol involved the sampling of a cell suspension (cells and media) containing free parasites after incubation in Ringer's solution supplemented with 1- ^{13}C -Glucose. Samples were sonicated and centrifuged and supernatants were used for metabolomic analysis. This method was further refined in the group by including a step in which the cell suspension was added to an extraction solution consisting of a 2:2:1 acetonitrile-methanol-water solution and vigorously vortexed prior to sonication and centrifugation. The shortcomings that needed to be overcome from the previous method were:

1. The use of free-parasites to study the complete asexual life cycle was not

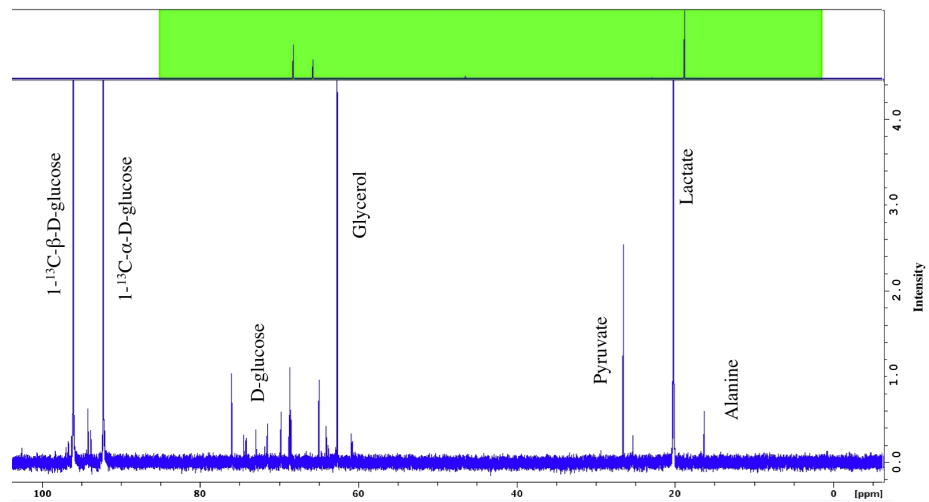
plausible. Firstly, only late trophozoites are susceptible to the methods to separate parasites from host cells. Secondly, and most importantly, to meet the aims of this study, it was required to grow the parasites in as close to physiological conditions as possible, which would never include their separation from the host. In fact, parasites released from the RBC are only able to survive for two to three hours [246].

2. Cell suspensions are ambiguous samples because discrimination between extra and intracellular metabolites cannot be achieved. Thus steps involving their separation and individual processing had to be implemented.
3. Cultures of *P. falciparum* are typically in no more than 10% parasitaemia. Tests to understand the effect of the RBCs background noise were done and the viability of using iRBC enrichment methods had to be assessed.

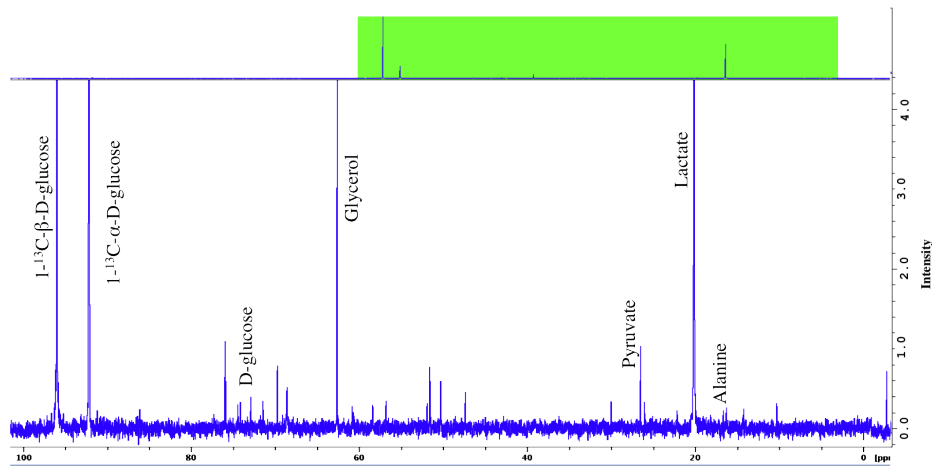
3.3.1.1 Replication of previous results using infected RBCs

The first step towards a method that could be used to meet our aims was to try to reproduce the results obtained by Lian *et al.* but using infected red blood cells (iRBCs) instead of free-parasites. This was the only variable changed from the method described in Lian *et al.*, and in order to achieve high parasitaemia levels an enrichment step using the VarioMacs magnetic separation [247] was introduced, prior incubation with Ringer's solution supplemented with 11 mM 1-¹³C-Glucose. This provided trophozoite pellets with 90% parasitaemia that were extracted and analysed as described in [81].

A qualitative comparison of the spectra of both experiments is shown in Figure 3.1. Results were similar, indicative of reproducibility between methods and the suitability of iRBCs for metabolomics analysis. In addition, in spite of subtle spectral changes, the resultant analysis presented no evidence of alteration by either choice (iRBC or free parasites). Given that iRBC conditions are more physiological and that the metabolism of the RBC has been extensively studied [248, 249], experimentation was continued on the malaria parasite inside its erythrocytic host.



(a)



(b)

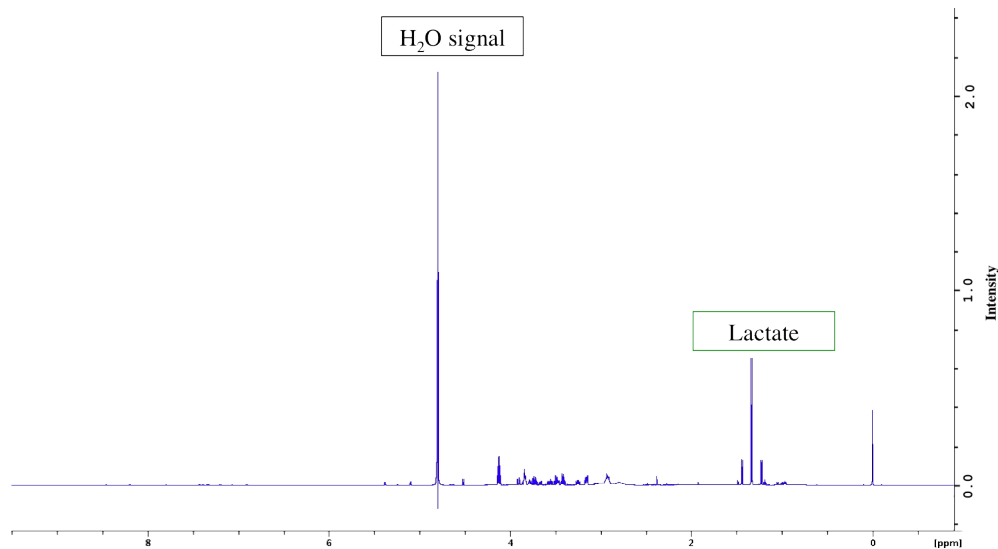
Figure 3.1: **1D ^{13}C Spectra of Trophozoite suspension after 2h incubation in Ringers containing 11 mM $1-^{13}\text{C}$ -Glucose.** (a) Spectrum from [81], (b) Spectrum of 90% parasitaemia iRBC cell suspension. The whole spectra shown above with the green box indicative of the area that is zoomed in the main figure.

3.3.1.2 Extraction step, separation of cells and supernatant and adjustment of parasitaemia

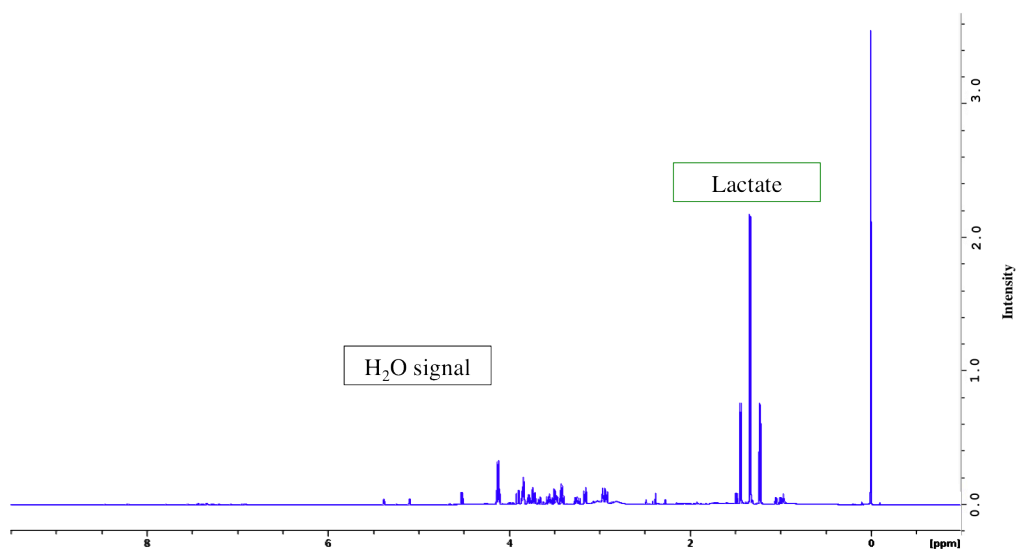
Following this, an extraction step which was in development within the laboratory by other group members was performed. This is explained in detail in Chapter 2, Section 2.5. The extraction method was based on work described by Olszewski *et al.* [239] but with two main modifications. The extraction solution used was

acetonitrile:methanol:water (at a ratio of 2:2:1 respectively, chosen for its improved capability to extract nucleotide triphosphates [250]) and the second extraction step was eliminated. A representation of this extraction can be seen in Chapter 2, Section *a*). Reasons for the step modifications were, amongst others, to reduce complexity and consequently increase robustness of sample preparation and reduce sample variance because when comparing acetonitrile:methanol:water to an only methanol based extraction solution, the sample variance was significantly smaller (personal communication with fellow PhD student A. Grauslys (MSc)).

P. falciparum in trophozoite stage were enriched by VarioMacs column [247], reaching a parasitaemia of around 90%. These parasites were incubated with Ringers containing 11 mM of 1-¹³C-Glucose during 2 hours while they were kept under usual culture conditions. Then 400 μ L of cell pellet (equivalent to 7.6×10^8 cells) were washed with ice cold 1 \times Phosphate Buffer Saline (PBS) and extracted as described in Chapter 2, Section 2.5 and Figure *a*). A sample of medium was also taken. Both were freeze dried and kept at -80°C until analysis, when they were resuspended in deuterium oxide and 1D ¹³C zgpg and ¹H NOESY spectra were acquired (as described in Table 3.1). When comparing 1D ¹H spectra of samples extracted with this method and without the extraction solution step, it is noticeable how the yield of metabolites has improved, as well as significantly reducing the water signal (see Figure 3.2). Signal to noise ratio was calculated for both samples by dividing the area under a signal area by the area under a noise area. Note that noise region was taken between -5 and -4 ppm and a signal region between 1.325 and 1.39 ppm. The spectrum from the extracted sample had 4 times better signal to noise ratio compared to samples that were not extracted (37652 and 9302 respectively).



(a)



(b)

Figure 3.2: **1D ^1H NOESY Spectra of Trophozoite suspension after 2h incubation in Ringers containing 11 mM $1\text{-}^{13}\text{C}$ -Glucose.** Both spectra were acquired with same parameters (NS=32 and RG=90.5), (a) Sample without extraction step (b) Sample with extraction step. Note how the water signal (black text) is almost minimal in (b) and the signal is higher (see for example lactate, green text box). TSP signal (0 ppm) is not representative of any difference as concentrations between spectra were different.

^{13}C spectra of both cell and supernatant fractions are shown in Figure 3.3. Spectrum of the supernatant was acquired with 256 scans while the same amount

of scans led to only noise in the cellular sample. The number of scans had to be increased to 4096 in order to detect some signal. Despite the huge increase in machine power (from approximately 30 min for 256 scans to almost 3 hours for 4k), the signal improvement was not sufficient. Thus, it must be assumed that the signal detected from previous experiments was mostly supernatant. It is interesting to notice that glycerol is then produced and excreted. Glycerol was not reported in the study of intracellular metabolites by Teng *et al.* [219], as the authors did not analyse the extracellular products of the parasite.

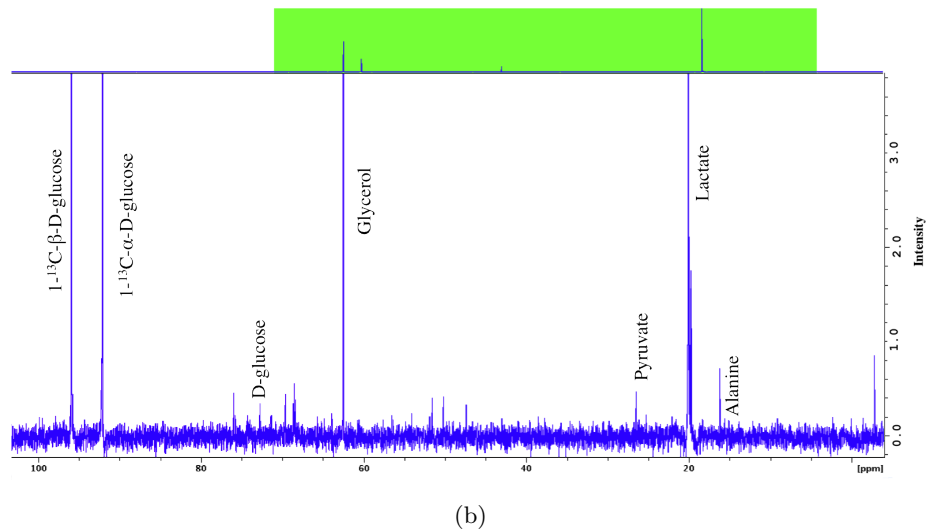
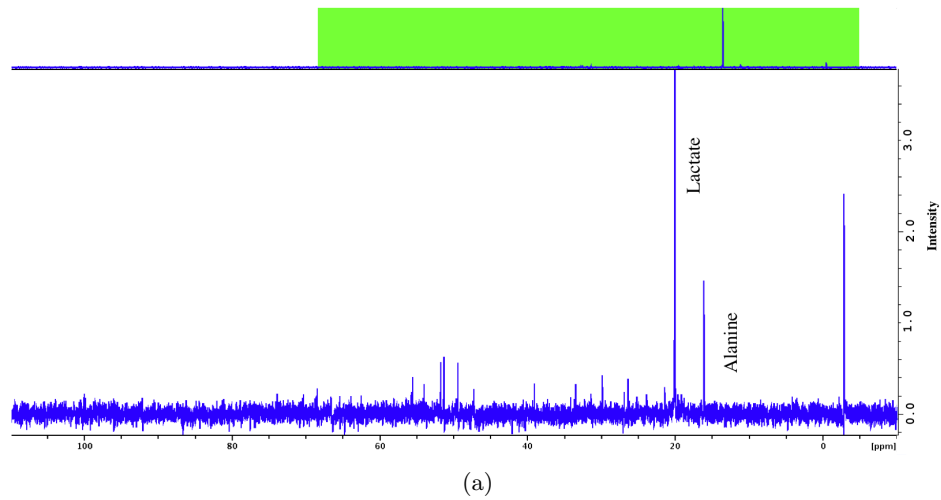
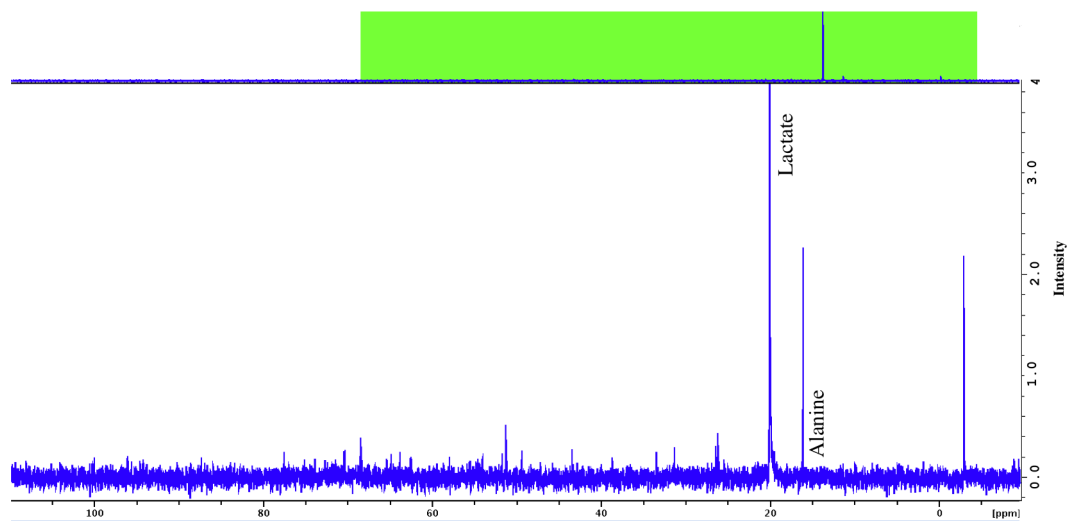
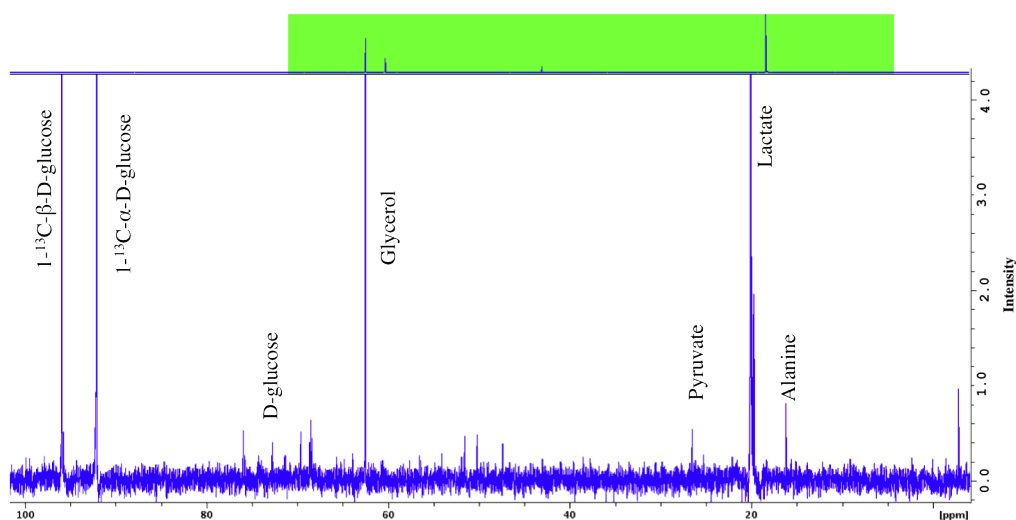


Figure 3.3: $1D$ ^{13}C Spectra of enriched mature trophozoite-iRBC sample after 2h incubation in Ringers containing 11 mM $1-^{13}C$ -Glucose (a) Cellular extracts (b) Supernatant.

Prior to tackling the low intra-cellular signal challenge, an additional test was performed. In order to do time-course experiments, the use of parasite-enrichment methods such as the VarioMacs column is not viable. These procedures increase the experimentation time by up to 6 h to achieve yields of a few hundred microlitres which are insufficient for multiple sampling. These methods also pose a problem because they target the mature trophozoite stage but the objectives of this project include the study of the whole life cycle and to do so in comparable conditions. Consequently, the next step was to assess the suitability of using a culture of *P. falciparum* in mature trophozoite stage at a high parasitaemia (15-17%, which is achievable in usual culture conditions) to repeat the steps described above. To compensate for the reduced parasitaemia, 600 μL of sample were used, which is the equivalent to (1.1×10^9) cells). By increasing the sample volume with respect to the previous experiment, in which samples had up to 90% parasitaemia, a number of parasites of the same order of magnitude was achieved. Results are shown in Figure 3.4. Supernatant signals were consistent with previous experiments. Cell signals were comparable, although there were some differences. Samples with enriched parasitaemia showed some higher peaks between 40 and 60 ppm and samples with normal-high parasitaemia showed some extra peaks between 60 and 80 ppm. The latter might be due to an increased RBC background signal but with the low cellular signal from either sample no conclusions could be drawn.



(a)



(b)

Figure 3.4: 1D ^{13}C Spectra of mature 15%-parasitaemia trophozoite-iRBC sample after 2h incubation in Ringers containing 11 mM $1\text{-}^{13}\text{C}$ -Glucose (a) Cellular extracts (b) Supernatant.

3.3.1.3 Optimising NMR signal strength by balancing cell numbers and including 2D ^1H - ^{13}C HSQC experiments

To improve the cellular signal, three steps were implemented: (a) a second extraction step including sonication was added, this is explained in detail in Chapter 2, Section *b*) and Figure 2.1, (b) cell volume per sample was increased, up to 800

μL (equivalent to 1.5×10^9 cells) and (c) use of 2D-HSQC NMR experiments. This provided correlation between an aliphatic carbon and its attached protons and it boosts the spectral resolution in multiple ways: (i) ^1H is more sensitive than ^{13}C due to its intrinsic physical magnetisation; (ii) cryoprobes are optimised for ^1H and (iii) decoupling of ^1H - ^{13}C , ^1H - ^1H and ^{13}C - ^{13}C .

A culture of *P. falciparum* iRBCs in mature trophozoite stage of approximately 15% parasitaemia was incubated for 2 h in Ringers buffer containing 11 mM $1\text{-}^{13}\text{C}$ -Glucose. After incubation a supernatant sample was taken and cells were washed twice with ice-cold $1 \times$ PBS. Cells were then extracted and analysed as described in Sections *b*) and 2.7 in Chapter 2. Signal of cells in the 1D ^{13}C experiments was comparable to previous attempts (data not shown), however the 2D HSQC vastly improved the signal obtained from the cells (see Figure 3.5).

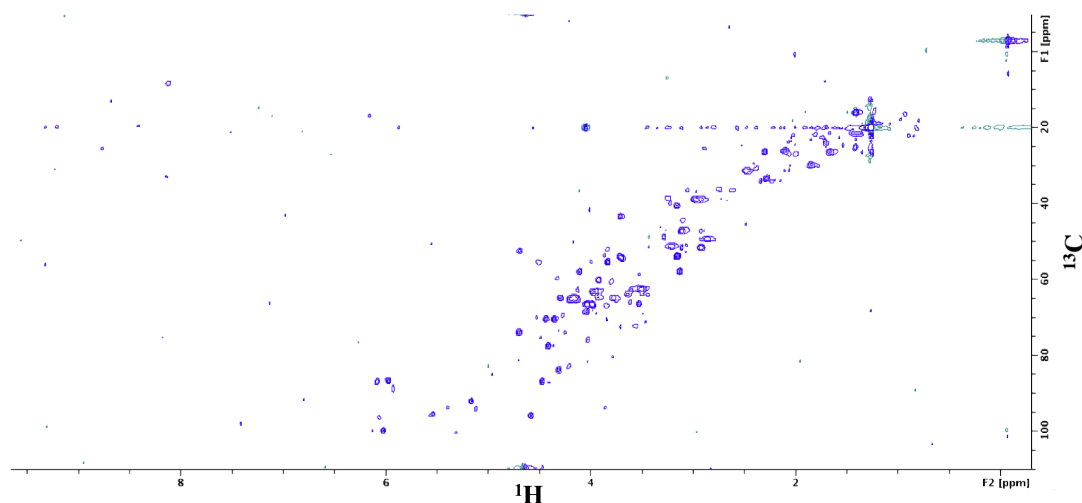


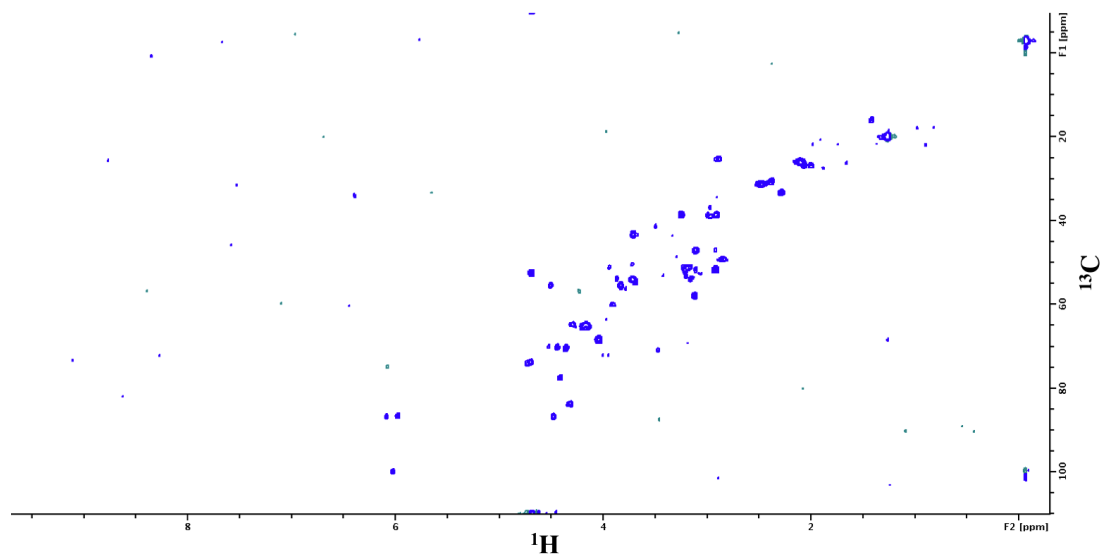
Figure 3.5: **2D ^1H - ^{13}C HSQC Spectra of cellular extract from mature trophozoite-iRBCs after 2h incubation in Ringers containing 11 mM $1\text{-}^{13}\text{C}$ -Glucose.** It can be observed how the signal has been improved vastly when compared to just 1D spectrum. Thus the number of metabolites that can be identified has increased.

3.3.1.4 Identification of signal from labelled and unlabelled samples

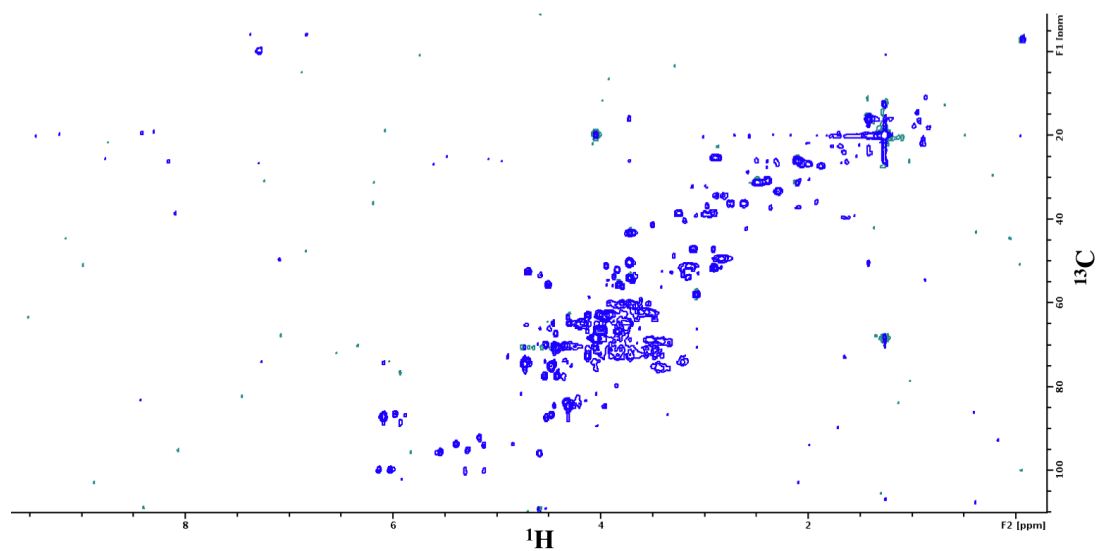
The use of labelled substrates has proven useful to boost the signal obtained from the samples [251]. Incubation with $\text{U-}^{13}\text{C}$ -D-glucose afforded maximum assignment of metabolites by boosting the signal from 1.1% when using natural abundance glucose, to 99%. My quantification strategy involved the creation of calibration curves from data of known concentrations. As it was not possible to purchase U-

^{13}C metabolites for the calculation of calibration curves calculation, only natural abundance metabolites were used thus only natural abundance samples were possibly quantified (see Section 3.3.3). Thus tests to check that signal from natural abundance samples was sufficient for quantification were also performed.

The experiment described in Section 3.3.1.3 was repeated changing solely the isotopic nature of glucose used. In one case D-glucose was used and in other U- ^{13}C -D-glucose. Results are shown in Figure 3.6. The signal from cells incubated without labelled glucose is much lower than that using labelled glucose, but it is still informative. Samples from cells incubated with U- ^{13}C -D-glucose presented very high and rich signal, superior to the one by 1- ^{13}C -D-glucose. For this reason, metabolite identification was done using the spectra from samples incubated with the fully labelled sugar.



(a)



(b)

Figure 3.6: ^1H - ^{13}C HSQC Spectra of cellular extracts from mature trophozoite-iRBCs after 2h incubation in Ringers containing 11 mM of (a) D-glucose and (b) U- ^{13}C -D-glucose

3.3.2 Metabolite identification

The most popular software for metabolite identification and quantification from NMR experiments is Chenomx NMR suite [252]. This platform contains a library

of 1D ^1H metabolite spectra that can be used for profiling by manually overlapping library spectra with the query spectrum. By using the reference standard TSP it also has the functionality of putative concentration prediction. Most of the publications of metabolomics of *P. falciparum* that used NMR not only for identification but also quantification have reported to use this software [253, 217, 219]. Others have identified metabolites and integrated the peaks as a measurement of quantity [254, 255, 256] and one group has used a model to predict quantities [257].

Other published resources for metabolite identification include numerous databases with spectra for consultation. Some of them can either be accessed online and also spectra can be downloaded in order to be used for overlapping with the query spectrum. These databases are the Human Metabolome Database (HMDB) [184], the Madison-Qindao Metabolomics Consortium Database (MQMCD) [199], the biological Magnetic Resonance Bank (BMRB) [258] and the Birmingham Metabolite Library (BML-NMR) [259].

Most of the software to analyse NMR metabolomics data rely on integrating the peaks and using the values for multivariate statistical analyses. Metabolite identification software are mostly commercial such as the mentioned Chenomx [252] and KnowItAll [260] or are based on commercial platforms such as the MATLAB packages Focus [261], MetaboQuant [262], MetaboID [263] and Dolphin [264]. There are some web-based programs such as MetaboHunter [265], MetaboAnalyst [266], COLMAR [267] or SpinAssign [268] and more interestingly some freely available options such as rNMR [269], Metabominer [270], Newton and Collaborative Computer Program for NMR (CCPN) Metabolomics [242, 243]. Free independent software for NMR metabolite quantification is limited to Batman [271]. Batman has a library of metabolites that it uses to fit the peaks from the query spectra which must be previously specified in the input file. This input file must be very complete and include metabolite identity, ppm positions, coupling pattern and constants and relative heights. In general all these cases use spectra that are either collected in predefined buffers/pH at specific field strengths or using imprecise models.

The aims of this project involved the use and when needed the creation of open-source software to identify and quantify metabolites in an automatic or semi-automatic manner to speed up the analysis of numerous samples. The freely available software CCPN metabolomics was chosen for metabolite identification. Others such as rNMR and Metabominer were tested but their functionality and user support was not comparable to that offered by CCPN, in particular for 2D ^1H - ^{13}C HSQC. Predictions from MetaboHunter were used to gather candidates when peaks were difficult to assign to a metabolite. Spectra from the MQMCD and

HMDB were also downloaded and imported into CCPN to aid in the metabolite identification. Finally, a battery of standards were also run in the same conditions as our samples in order to verify our assignments. Buffers and other parasite-specific metabolites were included in this *in-house* standard library. Details on the metabolites identified and which signals were used for further quantification are shown in Table 3.2. A representation of the metabolites identified in iRBC cellular and supernatant samples is shown in Figures 3.7 and 3.8 where signal complexity and both overlapping and clean peaks can be observed. Other metabolites were identified in the RBC-only samples such as 2-3 diphosphoglycerate but they were excluded from this study.

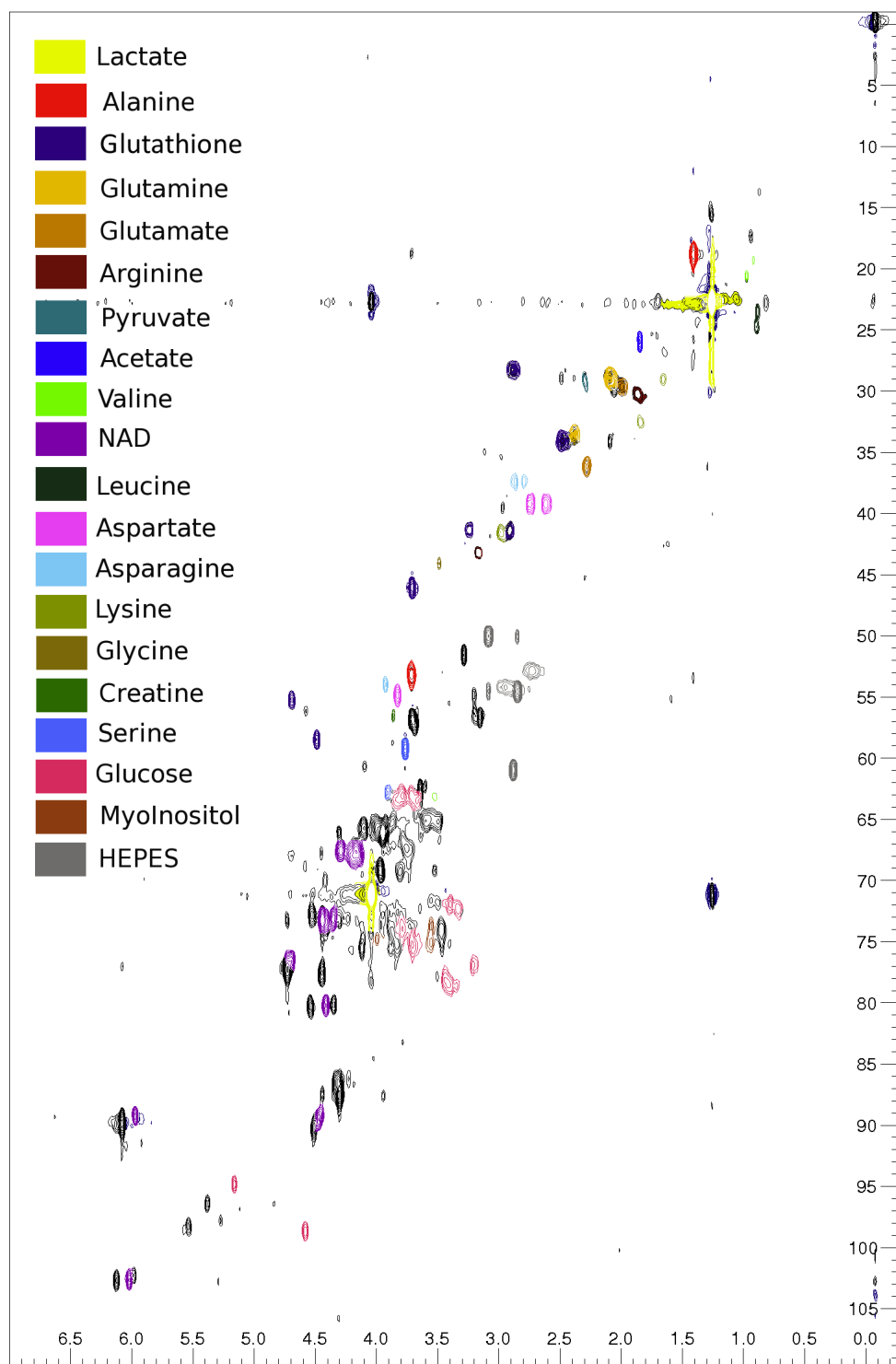


Figure 3.7: ^1H - ^{13}C HSQC Spectra of cellular extract from mature trophozoite-iRBCs after 2h incubation in culture media containing 11 mM of U- ^{13}C -Glucose.

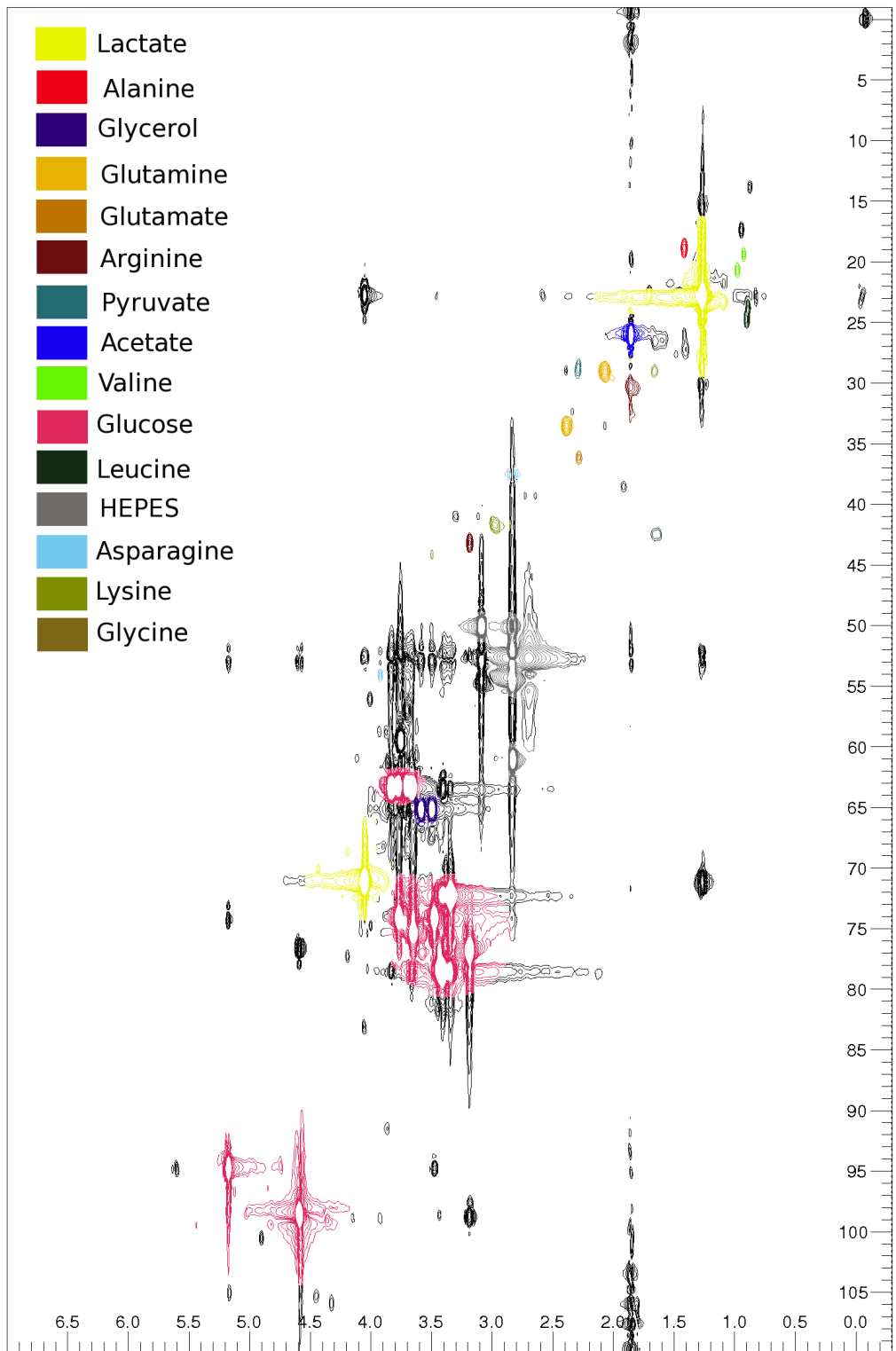


Figure 3.8: ^1H - ^{13}C HSQC Spectra of media containing 11 mM of $\text{U-}^{13}\text{C}$ -Glucose after 2h-incubation with mature trophozoite-iRBCs.

Table 3.2: Identified metabolites, their position in spectrum and signal selected for quantification.

Metabolite and KEGG identity	Carbon	H-ppm	C-ppm	For Quantification
Acetate (C00033)	C2	1.9	26.1	X
Alanine (C00041)	C2.alpha	3.8	53.6	X
	C3.beta	1.5	19	
Arginine (C00062)	C2.alpha	3.8	57.3	X
	C3.beta	1.9	30.5	
	C4.gamma.I	1.8	30.5	
	C4.gamma.II	1.9	30.5	
	C5.delta	3.2	43.3	
Asparagine (C00152)	C2.alpha	4	54.1	X
	C3.beta.I	2.9	37.4	
	C3.beta.II	2.8	37.4	
Aspartate (C00049)	C2.alpha	3.9	55	X
	C3.beta.I	2.8	39.5	
	C3.beta.II	2.7	39.3	
Creatine (C00300)	C2	3.9	56.4	X
	C4	3	39.5	
Glucose (C00031)	C1.alpha	5.2	94.9	X
	C1.beta	4.6	98.7	X
	C2.alpha	3.5	74.2	
	C2.beta	3.2	77	
	C3.alpha	3.7	75.6	
	C3.C5.beta	3.5	78.6	
	C4.alpha.beta	3.4	72.3	
	C5.alpha	3.8	74.1	
	C6.alpha.I	3.8	63.4	
	C6.alpha.II	3.7	63.4	
	C6.beta.I	3.9	63.5	
	C6.beta.II	3.7	63.4	
Glutamate (C00025)	C2.alpha	3.7	57.6	X
	C3.beta.I	2.1	29.8	
	C3.beta.II	2	29.8	
	C4.gamma	2.3	36.4	

Glutamine (C00064)	C2_alpha	3.8	57.2	X
	C3_beta	2.1	29.3	
	C4_gamma	2.4	33.9	
Glycerol (C00116)	C1	3.8	75	X
	C2	3.6	65.5	
	C3	3.6	65.4	
Glycine (C00037)	C2_alpha	3.5	44.3	X
GSH (C00051)	C10	3	28.3	X
	C6	4.6	58.6	
HEPES	C10	3.2	59.6	X
	C11	3.8	59	
	C2_C6	3.3	52.3	
	C3_C5	3.1	52.8	
	C7	3.2	48.4	
	C8	3.2	53	
Isoleucine (C00407)	C2_alpha	3.7	62.5	X
	C3_beta	2	38.7	
	C4_gamma	1.5	27	
	C4_gamma_II	1.4	27	
	C5_delta	0.9	13.9	
	C6_epsilon	1	17.4	
Lactate (C00186)	C2	4.1	71.1	X
	C3	1.3	22.9	
Leucine (C00123)	C2_alpha	3.7	56.2	X
	C3_beta	1.7	42.6	
	C4_gamma	1.7	26.8	
	C5_delta	1	24.8	
	C6_epsilon	0.9	23.6	
Lysine (C00047)	C2_alpha	3.7	57.5	X
	C3_beta	1.9	32.7	
	C4_gamma_I	1.5	24	
	C5_delta	1.7	29.2	
	C6_epsilon	3.02	42.1	
	C4_gamma_II	1.4	24	

Methionine (C00073)	C2_alpha	3.8	56.8	X
	C3_beta_I	2.2	32.7	
	C3_beta_II	2.1	32.7	
	C4_gamma	2.6	31.6	
	C5_delta	2.1	16.6	
MyoInositol (C00137)	C1_C3	3.5	74	X
	C2	4	75	
	C4_C6	3.6	75.1	
	C5	3.3	77.1	
NAD(P) (C0000(3/6))	C10	4.8	76.7	X
	C11	4.5	89.6	
	C13	4.5	80.3	
	C8	6.1	102.6	
Pyruvate (C00022)	C3	2.4	29.2	X
Serine (C00065)	C2_alpha	3.8	59.1	X
	C3_beta	4	63	
Valine (C00183)	C2_alpha	3.6	63.3	X
	C3_beta	2.3	31.9	
	C4_gamma_I	1.1	20.8	
	C4_gamma_II	1	19.4	

3.3.3 Creation of calibration curves for metabolite quantification

After metabolite identification, we proceeded to calculate calibration curves for each signal of each metabolite. First a test was done to identify the concentration limits for a few metabolites so an adequate range of concentrations was chosen. These were 0.1, 0.2, 0.5, 1, 2, 5 and 10 mM. Metabolites were separated into groups so their spectra would not overlap and mixtures of the mentioned concentrations were prepared in deuterium oxide with 2.5 mM of TSP as standard. 1D ^1H NOESY and 2D ^1H - ^{13}C HSQC spectra for each sample were acquired and processed as described in Section 3.3.1.

Spectra acquired in proprietary manufacturer format (Bruker, topspin) were inputted into CCPN after conversion to University of California San Francisco (UCSF) format. Metabolite signals were assigned to specific spin systems and resonances. Then the height and volume of each signal was calculated and text files were generated. The signal (height and volume individually) of each peak was nor-

malised by the signal of TSP and for each metabolite and signal the concentrations were plotted and used to fit a linear model with 0 intercept. The coefficients of each linear model and their R^2 values are reported in Table 3.3 and the ones used for quantification are shown in Figure 3.9. Height was chosen for quantification before volume because it is less likely to be affected by peak proximity/overlap. However all the functions for analysis were also implemented for volume and their outputs were used for validation. All these steps were implemented in a pipeline in R. Consequently the library of calibration curves can be increased automatically upon data collection. It is also worth noting that these data can be used for quantification of any sample of any biological extract, providing the same spectrum acquisition parameters and buffer conditions are used.

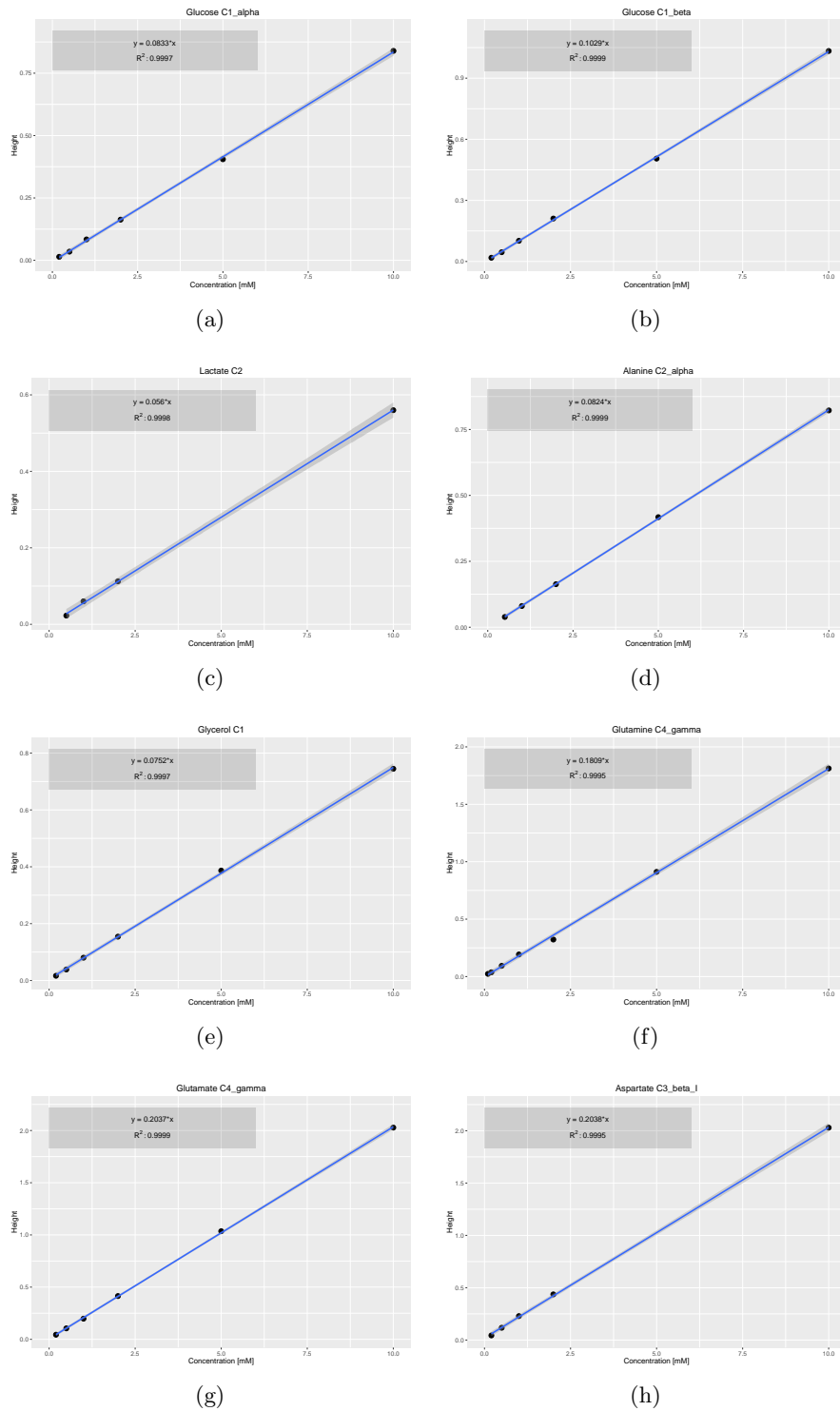
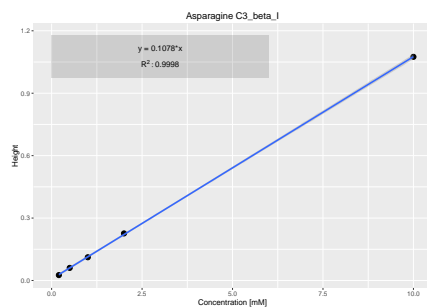
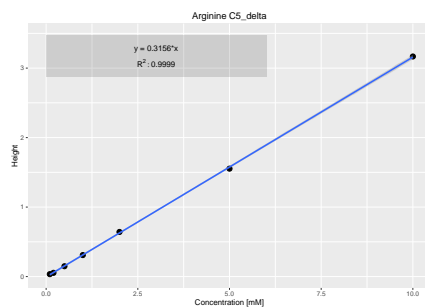


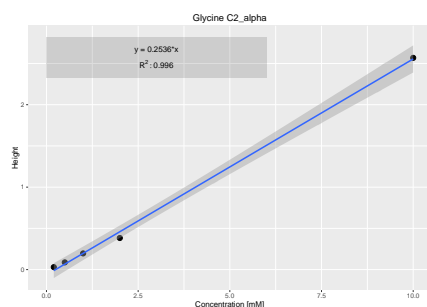
Figure 3.9: **Calibration curves chosen for quantification (I).** Concentration versus height. Best line fitted is represented in blue while grey area corresponds to the 95% confidence interval of the fit. In the top left corner it is shown the actual coefficient obtained and the goodness of fit represented by R^2 .



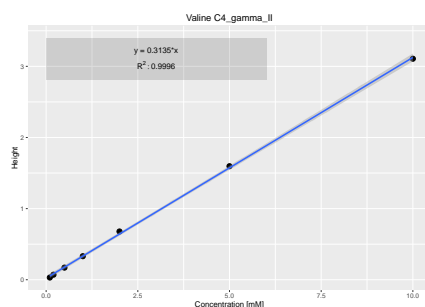
(i)



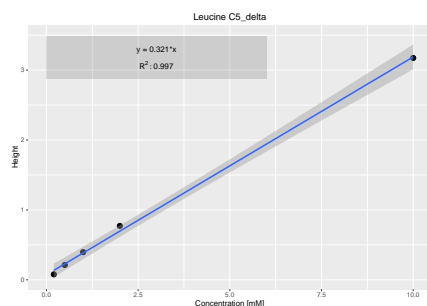
(j)



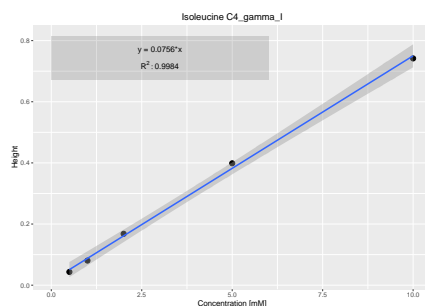
(k)



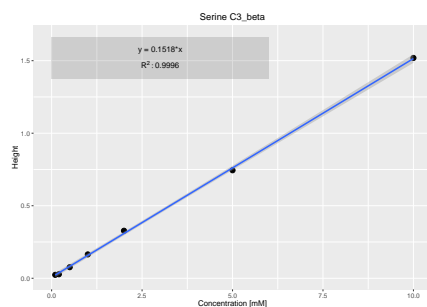
(l)



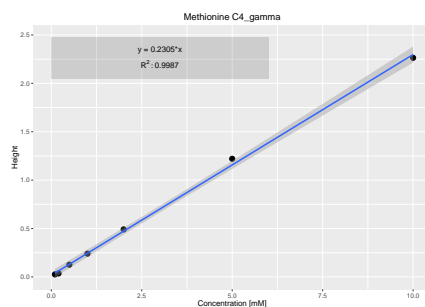
(m)



(n)



(o)



(p)

Figure 3.9: **Calibration curves chosen for quantification (II)**. Concentration versus height. Best line fitted is represented in blue while grey area corresponds to the 95% confidence interval of the fit. In the top left corner it is shown the actual coefficient obtained and the goodness of fit represented by R^2 .

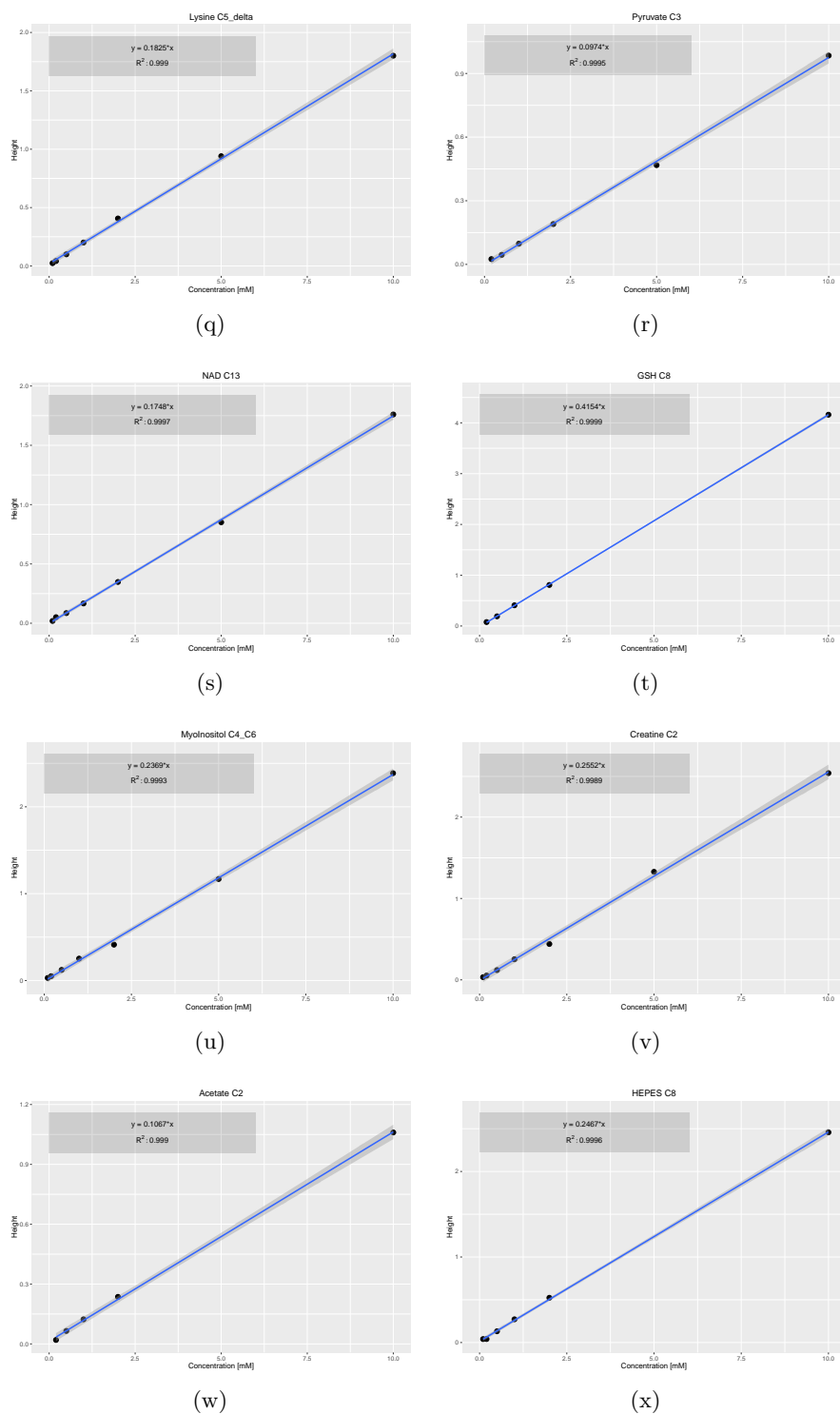


Figure 3.9: **Calibration curves chosen for quantification (III)**. Concentration versus height. Best line fitted is represented in blue while grey area corresponds to the 95% confidence interval of the fit. In the top left corner it is shown the actual coefficient obtained and the goodness of fit represented by R^2 .

Table 3.3: Coefficients of the linear model fitted for quantification

Carbons	Height	H-R ²	Volume	V-R ²
Acetate_C2	0.1067	0.999	0.1106	0.9993
Alanine_C2_alpha	0.0824	0.9999	0.0987	0.9999
Alanine_C3_beta	0.2522	0.9997	0.2843	0.9997
Arginine_C2_alpha	0.1875	0.9999	0.2084	0.9999
Arginine_C3_beta	0.1987	0.9979	0.2396	0.9987
Arginine_C4_gamma.I	0.0727	0.9995	0.0914	0.9995
Arginine_C4_gamma.II	0.068	0.9996	0.0852	0.9996
Arginine_C5_delta	0.3156	1	0.3532	0.9999
Asparagine_C2_alpha	0.1554	0.9994	0.1723	0.9995
Asparagine_C3_beta.I	0.1078	0.9998	0.1129	0.9989
Asparagine_C3_beta.II	0.0987	0.9994	0.1203	0.9998
Aspartate_C2_alpha	0.2905	0.9997	0.3254	0.9996
Aspartate_C3_beta.I	0.2038	0.9995	0.2176	0.9998
Aspartate_C3_beta.II	0.1767	0.9991	0.2174	0.9992
Creatine_C2	0.3872	0.9979	0.3829	0.999
Creatine_C4	0.2552	0.9989	0.2544	0.9993
Glucose_C1_alpha	0.0833	0.9997	0.0861	0.9997
Glucose_C1_beta	0.1029	0.9999	0.1158	0.9999
Glucose_C2_alpha	0.0616	0.9997	0.0741	0.9997
Glucose_C2_beta.I	0.096	0.9998	0.115	0.9998
Glucose_C3_alpha	0.0523	0.9995	0.0631	0.9994
Glucose_C3_C5_beta	0.1287	0.9997	0.1636	0.9998
Glucose_C4_alpha_beta	0.1281	0.9998	0.1578	0.9998
Glucose_C5_alpha	0.0628	0.9998	0.0751	0.9998
Glucose_C6_alpha.I	0.0593	0.9998	0.0672	0.9997
Glucose_C6_alpha.II	0.0538	0.9998	0.0628	0.9997
Glucose_C6_beta.I	0.0916	0.9998	0.1095	0.9997
Glucose_C6_beta.II	0.0891	0.9997	0.1132	0.9996
Glutamate_C2_alpha	0.1582	0.9994	0.1785	0.9996
Glutamate_C3_beta.I	0.0805	0.9993	0.102	0.9995
Glutamate_C3_beta.II	0.0833	0.9996	0.1053	0.9993
Glutamate_C4_gamma	0.2037	0.9999	0.2407	0.9999
Glutamine_C2_alpha	0.1623	0.9993	0.1787	0.9996
Glutamine_C3_beta	0.2068	0.9994	0.2426	0.9995

Carbons	Height	H-R ²	Volume	V-R ²
Glutamine_C4_gamma	0.1809	0.9996	0.214	0.9995
Glycerol_C1	0.1522	0.9998	0.1812	0.9995
Glycerol_C2	0.0752	0.9994	0.0861	0.9997
Glycerol_C3	0.1445	0.9987	0.1747	0.9991
Glycine_C2_alpha	0.2411	0.9832	0.2456	0.9829
GSH_C10	0.1507	0.9957	0.187	0.9956
GSH_C6	0.2077	0.9973	0.2317	0.9968
HEPES_C10	0.3273	0.9987	0.3727	0.999
HEPES_C11	0.3307	0.9992	0.3707	0.9992
HEPES_C2_C6	0.0473	0.9967	0.0481	0.9969
HEPES_C3_C5	0.0421	9994	0.0418	0.9993
HEPES_C7	0.283	0.9994	0.3469	0.9994
HEPES_C8	0.2467	0.9996	0.3008	0.9996
Isoleucine_C2_alpha	0.2262	0.9986	0.2317	0.9987
Isoleucine_C3_beta	0.1094	0.9982	0.1349	0.9984
Isoleucine_C4_gamma	0.0756	0.9984	0.0963	0.9983
Isoleucine_C4_gamma_II	0.0662	0.9977	0.0845	0.9978
Isoleucine_C5_delta	0.1754	0.9981	0.2043	0.998
Isoleucine_C6_epsilon	0.2757	0.9986	0.3011	0.9985
Lactate_C2	0.056	0.9998	0.0651	0.9999
Lactate_C3	0.2126	0.9995	0.2278	0.999
Leucine_C2_alpha	0.1587	0.9997	0.1786	0.9996
Leucine_C3_beta	0.0909	0.9954	0.1182	0.9965
Leucine_C4_gamma	0.0621	0.9994	0.0773	0.9991
Leucine_C5_delta	0.321	0.997	0.3424	0.9981
Leucine_C6_epsilon	0.3125	0.9991	0.3296	0.9861
Lysine_C2_alpha	0.2097	0.9994	0.231	0.9996
Lysine_C3_beta	0.2033	0.9986	0.247	0.9989
Lysine_C4_gamma	0.0759	0.9983	0.096	0.9984
Lysine_C5_delta	0.1825	0.999	0.2217	0.9992
Lysine_C6_epsilon	0.271	0.9996	0.325	0.9992
Methionine_C2_alpha	0.1727	0.9996	0.1936	0.9995
Methionine_C3_beta_I	0.0918	0.9995	0.115	0.9996
Methionine_C3_beta_II	0.09	0.9992	0.113	0.9991
Methionine_C4_gamma	0.2305	0.9987	0.271	0.9988
Methionine_C5_delta	0.1688	0.9994	0.1678	0.9994

Carbons	Height	H-R ²	Volume	V-R ²
MyoInositol_C1_C3	0.3066	0.9991	0.3632	0.9991
MyoInositol_C2	0.2655	0.9982	0.2665	0.999
MyoInositol_C4_C6	0.2369	0.9993	0.2803	0.9995
MyoInositol_C5	0.1379	0.9991	0.1617	0.9993
NAD_C10	0.1803	0.9999	0.2029	0.9998
NAD_C11	0.1772	0.9997	0.1873	0.9997
NAD_C12	0.1954	0.9997	0.215	0.9997
NAD_C13	0.1748	0.9997	0.1967	0.9998
NAD_C14	0.2003	0.9997	0.2216	0.9998
NAD_C15	0.1871	0.9998	0.2019	0.9997
NAD_C16_17	0.1188	0.9994	0.1485	0.9995
NAD_C18_19	0.1741	0.9998	0.2112	0.9999
NAD_C8	0.1034	0.9992	0.1133	0.9995
NAD_C9	0.1579	0.9999	0.1711	1
Pyruvate_C3	0.0974	0.9995	0.1	0.9994
Serine_C2_alpha	0.1518	0.9996	0.1616	0.9996
Serine_C3_beta	0.1424	0.9995	0.1756	0.9995
Valine_C2_alpha	0.1979	0.9991	0.2039	0.9993
Valine_C3_beta	0.0994	0.9994	0.1222	0.9995
Valine_C4_gamma_I	0.3188	0.9986	0.3465	0.9981
Valine_C4_gamma_II	0.3135	0.9997	0.3366	0.9996

Errata It should be noted that corrections of this work involved the removal of several outliers in the above-presented calibration curves, which are currently updated to their latest version. However all metabolite concentrations presented in this and other Chapters were calculated prior mentioned corrections and therefore they have an associated error. These are collated in Table 3.4.

Table 3.4: Coefficient discrepancy and error associated of carbons used for quantification

Carbon	Old Coefficient	New Coefficient	Error (%)
Acetate C2	0.1096	0.1106	0.9042
Aspartate C3 beta I	0.1886	0.2038	7.4583
Asparagine C3 beta I	0.1001	0.0887	-12.8523
Glycine C2 alpha	0.2411	0.2536	4.929
GSH C10	0.1506	0.1507	0.0664

Carbon	Old Coefficient	New Coefficient	Error (%)
Leucine C5 delta	0.3204	0.321	0.1869
HEPES C8	0.2512	0.2467	-1.8241

3.3.4 Validation and pipeline assembly

Identification of key metabolites and calibration curves calculations for their quantification was followed by validation. The aim of this step was to compare the theoretical concentrations of RPMI (as reported in the Sigma-Aldrich website and also collated in Chapter 2, Table 2.1) and calculated concentrations from actual media samples by using the equations presented above. For this purpose, three 1 mL samples of standard culture media (described in Chapter 2, Section 2.2.1), were taken and spectra were acquired and processed as in Section 3.3.3. Spectra were then converted into USCF format and imputed in CCPN software where peaks chosen for quantification were assigned an spin system and resonance and their heights and volumes calculated. These were exported as text files and imputed in R.

A pipeline to analyse these data was implemented in R. It consisted of (1) normalisation of the peak samples signal by TSP; (2) change labelling in CCPN of “spin systems” and “resonances” to the adequate carbon nomenclature shown in Table 3.2; (3) calculation of the concentration of each metabolite from height and volume values by using the linear regression coefficients calculated from standard curves in Section 3.3.3, Table 3.3; (4) adjust signal by the different volumes in original sample and deuterium oxide resuspension after the freeze drying step; (5) mean and standard error calculation between replicas and (6) plotting and data output. Steps for calculation of concentration per cell were also implemented.

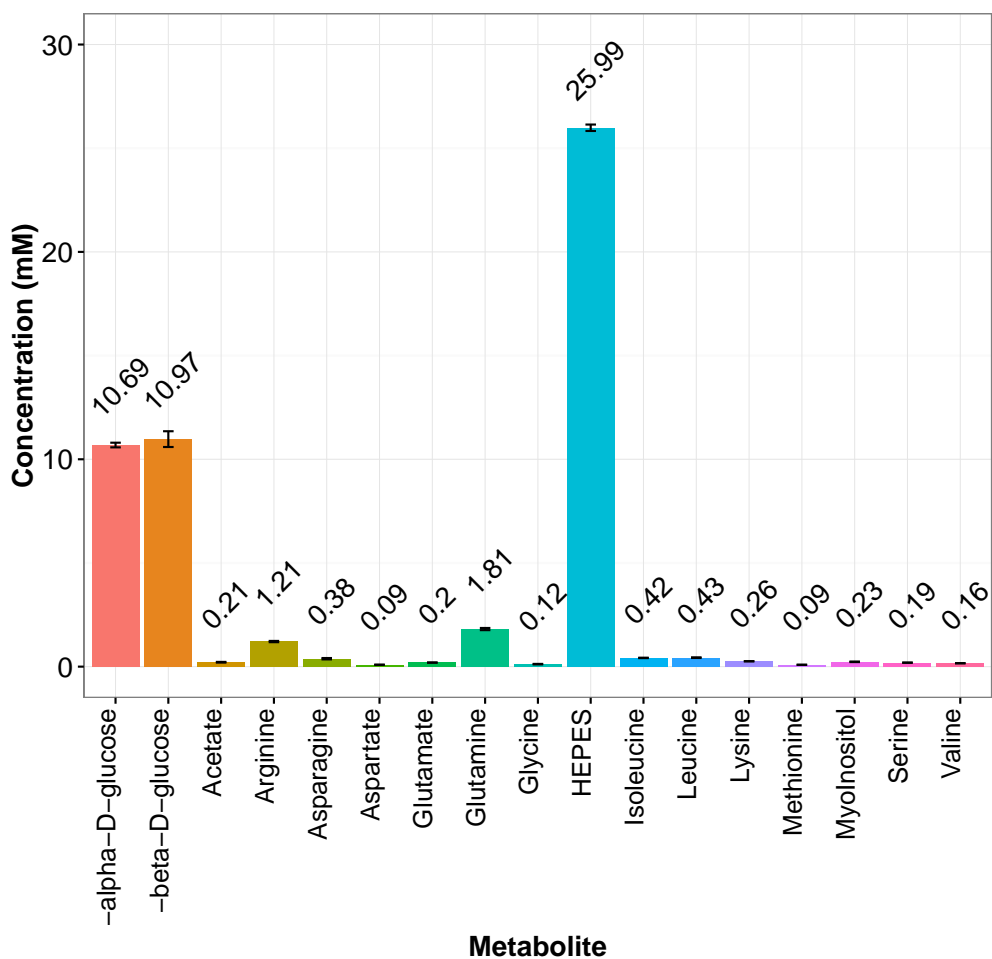


Figure 3.10: **RPMI measured concentrations.** Mean of 3 replicas represented with the standard deviation of the mean.

Results are shown in Figure 3.10 and a comparison of these with the theoretical values is shown in Table 3.5. Errors were calculated as the percentage of the difference between theoretical and empirical concentration divided by the theoretical. NMR can detect metabolites in samples that range from micromolar to millimolar concentrations. The most sensitive NMR spectra is 1D ^1H but it has the poorest resolution. Thus the sensitivity of experiments such as 2D ^1H - ^{13}C HSQC is improved with respect to carbon but reduced with respect to hydrogen. It is easier to resolve the spectrum but naturally small concentrations present larger error on quantification than large concentrations. For example glucose and HEPES, which are in the millimolar range, present less than 5% error, whilst aspartate, in the micromolar range, presents an almost 30% error. Despite this limitation, with this

method absolute quantification of metabolites was possible which did not rely on software predictions nor has to be fold changed to reduce variance such as the data presented by Olszewski *et al.* [195].

Table 3.5: Concentration comparison measured vs theoretical

Metabolite	Theoretical (mM)	Experimental (mM)	Error (%)
-alpha-D-glucose	11	10.69	2.82
-beta-D-glucose	11	10.97	0.27
Arginine	1.15	1.21	5.22
Asparagine	0.37	0.38	2.7
Aspartate	0.15	0.11	26.67
Glutamate	0.14	0.18	28.57
Glutamine	2.05	1.81	11.71
Glycine	0.13	0.12	7.69
Isoleucine	0.38	0.42	10.53
Leucine	0.38	0.43	13.16
Lysine	0.22	0.26	18.18
Methionine	0.1	0.09	10
MyoInositol	0.19	0.23	21.05
Serine	0.28	0.19	32.14
Valine	0.17	0.16	5.88
HEPES	25	25.99	3.96

3.3.5 Pilot study: Glycolysis and glutaminolysis are drivers of the biomass production, a trophozoite study

The shortcomings of the lower limit of detection of the quantification method were a limitation for future experiments. Even when it was not possible to resolve actual concentrations in the micromolar range, then at least trend changes should be detected.

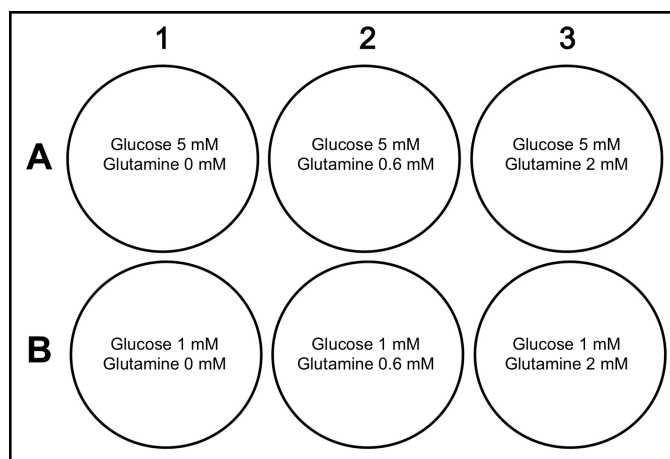


Figure 3.11: **Experimental conditions tested.** Note that there were two identical plates one with U-¹³C-D-glucose and other with D-glucose.

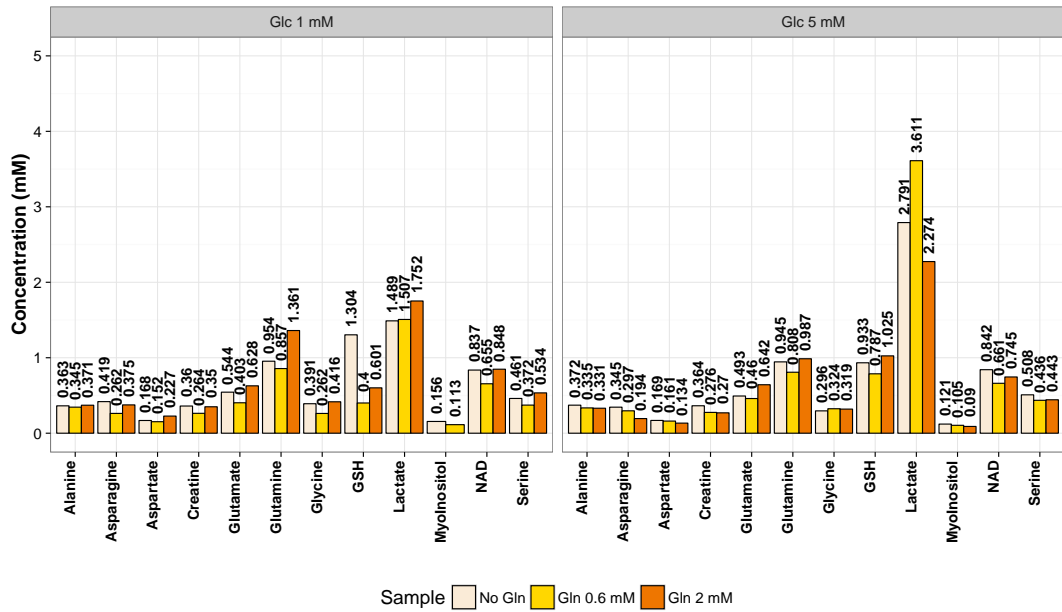
3.3.5.1 Experimental

To test that this was possible and also gain some insight on the effect of nutrient deprivation in the parasite metabolic flux I designed an experiment that consisted of incubating iRBCs in trophozoite stage for 2.5 h in Ringers solution containing either 5 or 1 mM glucose and glutamine in a range of concentrations: 0, 0.6 and 2 mM (see Figure 3.11). These concentrations of glutamine were chosen because they are representative as what is found in culture media (2 mM) and blood (0.6 mM). Glucose concentrations were chosen as typical mean value in blood (5 mM) and severe hypoglycaemia (1 mM). Samples of supernatant and cell fraction were extracted and processed as described in Chapter 2, Section *b*). Spectra were acquired and processed as described in Section 3.3.3. Concentration values for the unlabelled samples were obtained as described in Section 3.3.4 and are collated in Appendix A, Tables A.1 and A.2. Results are shown in Figures 3.12.

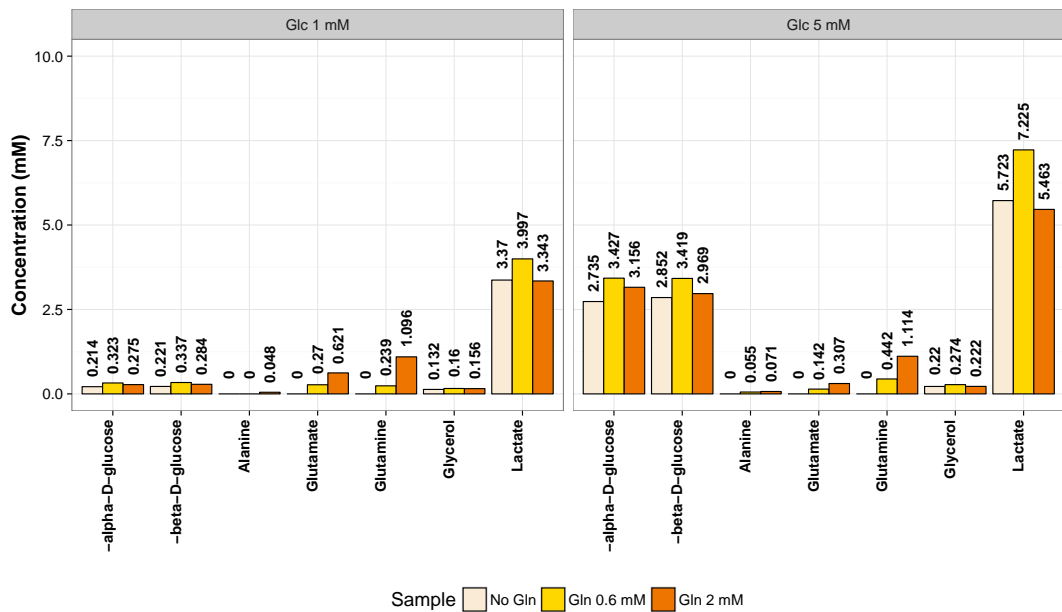
3.3.5.2 Results and discussion

Independently of glucose and glutamine, the biggest differences across conditions were observed in lactate, alanine and myoinositol concentrations. Intracellular extracts (Figure 3.12 (a)) show that myoinositol was consumed to some extent, proportionally to the glutamine available. In cells incubated with more glutamine, we found lower concentration of myoinositol, independent of the glucose available. Intracellular lactate was much higher in cells incubated with more glucose. Lactate also presented different trends in both conditions. When starting concentrations of

glucose were just 1 mM, intracellular lactate slightly increased with glutamine availability. However, when initial glucose levels were higher (5 mM), the intracellular lactate reached a peak when at lower glutamine concentrations (0.6 mM) in contrast to when the highest glutamine levels were available (2 mM). Nevertheless, intracellular concentrations of metabolites at a single time point are not that informative due to periodic oscillations in the metabolism. For example, glycolytic oscillations (which are well documented in yeast and muscle [272]) implicate the repetitive fluctuation of the metabolite concentrations [273] in periods of approximately 15 minutes [274]. Thus, small changes in sampling times between treatments might artificially suggest a difference in concentrations due to a treatment effect while there are just observations of the natural oscillations of a metabolite. Consequently, when lacking a time course to confirm if a difference is consistent over time, extracellular metabolite levels from the supernatant extracts can be more informative. These are shown in Figure 3.12 (b). Glucose consumption was relatively different across conditions. When more glucose was available, more glucose was consumed (consumption in 1 mM starting concentration was of up to 0.7 mM meanwhile consumption in 5 mM starting condition was of up to 2.3 mM). Thus the parasite is somewhat responsive to the nutrient availability. When looking at the effect that glutamine availability had on glucose consumption, more glucose was consumed when glutamine was not available in the media. However, consumption of glucose did not increase nor decrease proportionally with glutamine availability. When 0.6 mM glutamine was available, glucose was not consumed as greatly as when 2 mM glutamine was. Significantly, even though less glucose was consumed in the 0.6 mM glutamine condition, more lactate and glycerol were produced than in the 2 mM homologous experiment. This indicates that these typically considered waste products might play a role in metabolism regulation.



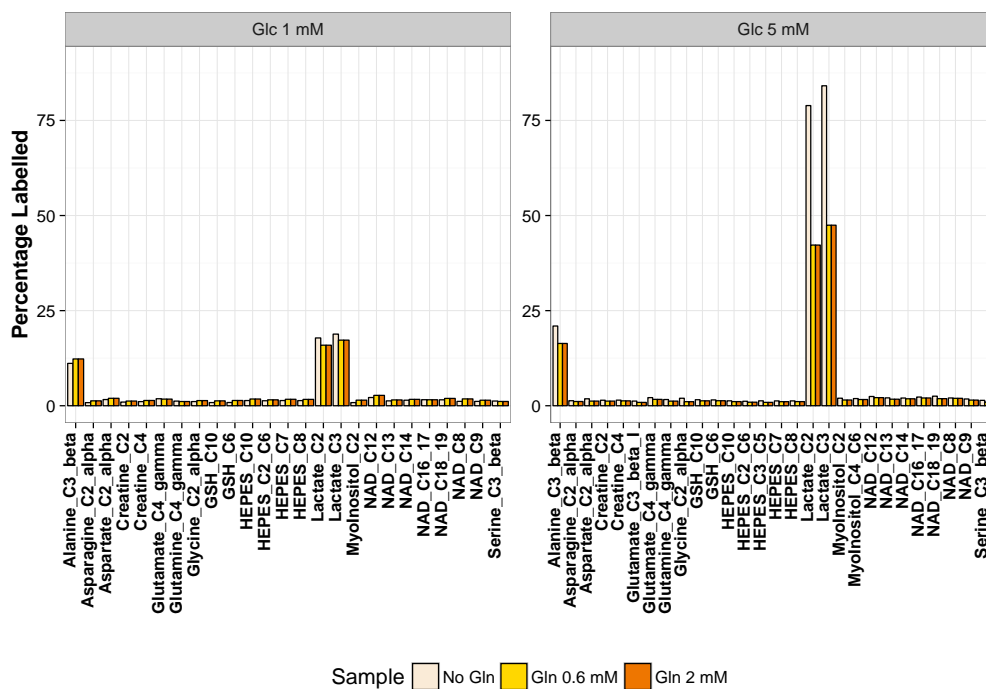
(a)



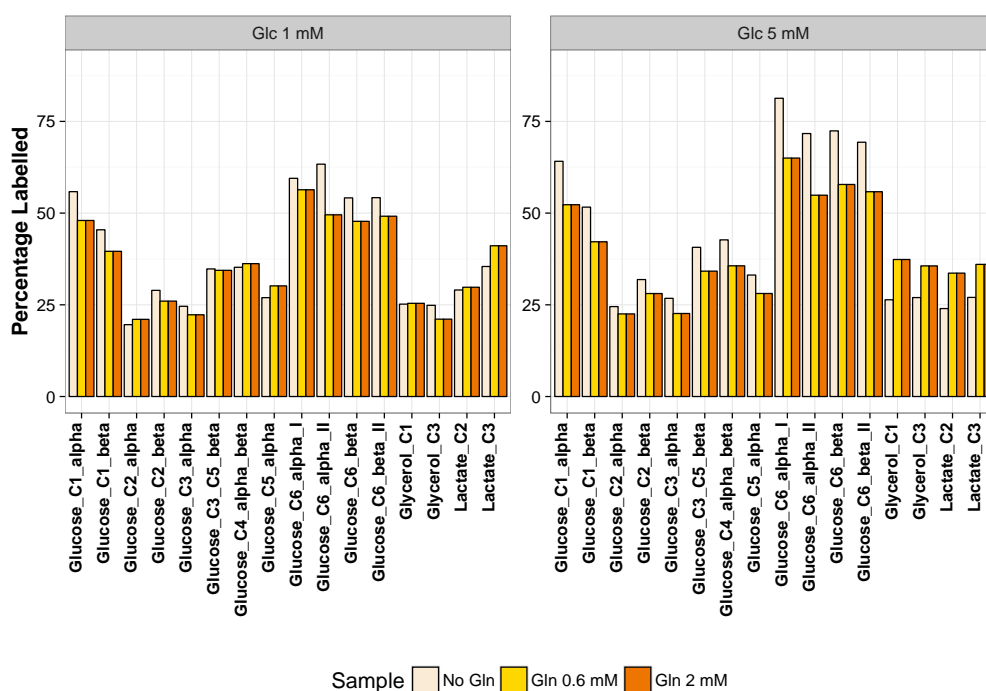
(b)

Figure 3.12: **Concentrations of metabolite extracts.** (a) Intracellular extracts (b) Media. Note Glc=Glucose and Gln=Glutamine. It can be appreciated that the parasites adapted to the environment by reducing or increasing their glucose consumption. Note that in different starting concentrations of glutamine, the central carbon metabolism is affected and a change in lactate excretion can be observed.

In order to further investigate this observation, we calculated the percentage of artificial ^{13}C labelling incorporated in each signal. To do this, spectra from both samples that had been incubated with U- ^{13}C -D-glucose and D-glucose were used. First, signals were normalised by TSP, then appropriate nomenclature was assigned to each signal and common carbons between both spectra were selected. Then, the signals of the labelled sample were multiplied by 1.1 % which is the natural ^{13}C abundance and divided by 99 % which is the amount of ^{13}C labelling in the stock glucose. This should account for 100 % labelling for a carbon that is fully labelled like those in U- ^{13}C -D-glucose. Results of these calculations for cell and supernatant samples are shown in Figure 3.13. Metabolites with significant labelling in the cellular fraction are alanine and lactate. However lactate seems much more labelled in the sample with 5 mM glucose and 0 mM glutamine as the starting condition. When looking at the supernatant samples it was striking to appreciate that glucose did not present 100% labelling, moreover there was a difference in carbons labelling within the same molecule what was not possible if the stock was homogeneously labelled. Carbons in the exterior of the molecule presented higher signal than the ones bound to two other carbons. The explanation behind this observation lies in the different magnetisation transfer between atoms. The magnetisation of a ^1H bound to ^{13}C dissipates (known as relaxation) faster than a ^1H bound to ^{12}C . The faster the relaxation of the magnetisation the broader (and in some respects less intense) the signal, as the window of detection is shorter. This principle is what is observed when comparing the peaks from ^{13}C uniform labelled and ^{13}C natural abundance in different atoms of glucose. A ^{13}C at natural abundance can be assumed to be surrounded by ^{12}C (as ^{13}C isotope at natural abundance is 1.1%) thus the ^{13}C relaxation is not enhanced by direct binding to other NMR active ^{13}C . In the case of uniform ^{13}C (99% ^{13}C), it can be assumed that any ^{13}C nucleus is surrounded by other NMR active ^{13}C nuclei and the relaxation of the magnetisation is thus enhanced. In the uniform labelled glucose this accounted for the differences in labelled signal comparing differing atoms in the glucose (see Figure 3.14) as the intensity was reduced more in the carbons bonded to two ^{13}C (i.e. in the centre of the chain C2, C3 C4 and C5) than those bonded to one ^{13}C (i.e. those at the ends of the chain C1 and C6). This phenomenon does not allow a proper comparison of U ^{13}C and natural abundance samples. However it was highlighted that the metabolites labelled were glucose and its products lactate, glycerol and alanine.



(a)



(b)

Figure 3.13: Percentages of artificially introduced ^{13}C after incubation with $\text{U-}^{13}\text{C-D-glucose}$. (a) Cellular extracts. Samples confirm alanine and glycerol as glucose products (b) Supernatant. Glucose labelling seems to not be uniform what points towards a problem.

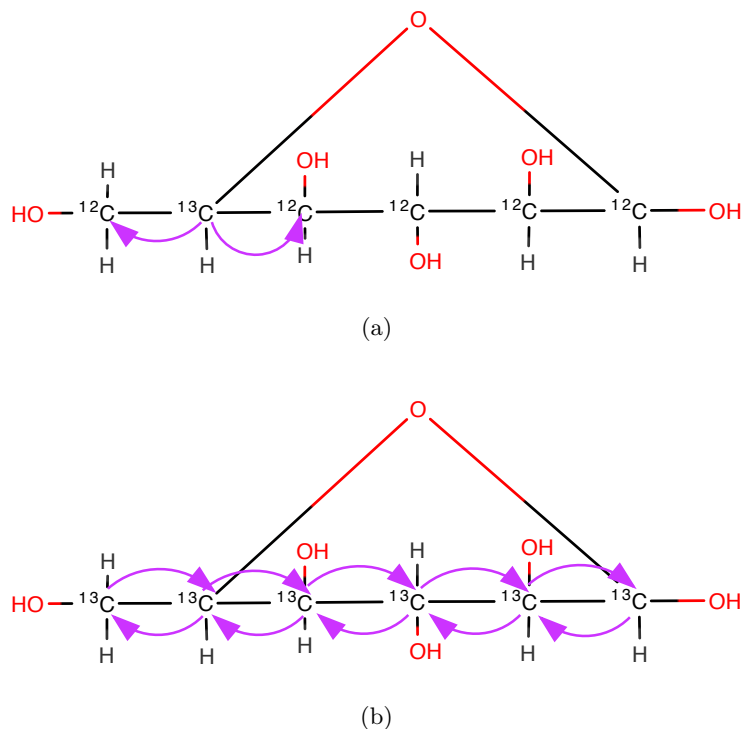


Figure 3.14: **Representation of carbon magnetisation pathways of glucose (purple arrows).** (a) Glucose with only one ^{13}C (b) $\text{U-}^{13}\text{C}$ Glucose. Note that when more than one ^{13}C isotope is present, they influence each other. Thus carbons in the outside of the molecule presented a reduced effect on this magnetisation. When using natural abundance glucose, only 1.1% of the carbon is ^{13}C and this effect is negligible.

Excreted glucose products were confirmed by tracing $1\text{-}^{13}\text{C}\text{-D-glucose}$.

In order to confirm which excreted products are produced at least partially from glucose, a similar experiment using $1\text{-}^{13}\text{C}\text{-D-glucose}$ was performed. Parasites were incubated in culture media containing either 11 mM $1\text{-}^{13}\text{C}\text{-D-glucose}$ or D-glucose . Samples of supernatant before and after incubation were taken, processed and analysed identically to the previous experiment. Labelling percentages were calculated and they are shown in Figure 3.15. As only one carbon of the glucose was labelled in these samples the relaxation differences did not affect the signal and it can be seen how C1 of glucose was labelled prior to incubation and after incubation. The glucose catabolic end products were also labelled to some extent: alanine, glycerol and lactate.

Even though molecules with more than one ^{13}C cannot be used for analysis,

these results confirm the suitability of our method to identify changes in metabolic responses to the environment which is the crucial point needed to address the fundamental question of this project on how the malaria parasite reacts to a changing nutritional environment.

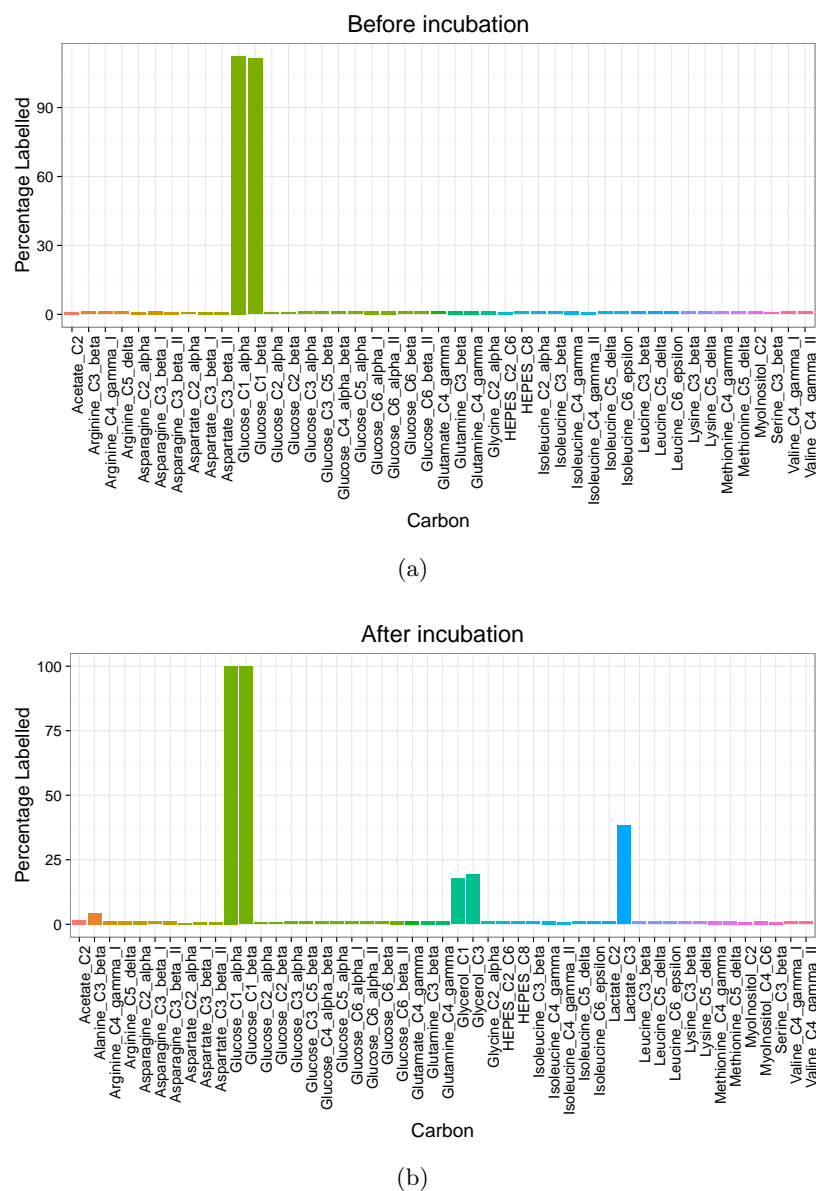


Figure 3.15: Percentages of artificially introduced ^{13}C before (a) and after (b) incubation with $1\text{-}^{13}\text{C}\text{-D-glucose}$. Only glucose is labelled at the start of incubation (a), its consumption results in some of its direct catabolic products being excreted: alanine, glycerol and lactate.

3.4 Conclusions

Upon review of the current published methodologies used to investigate the metabolism of *P. falciparum* in a holistic way we identified a lack of studies of parasites in physiological conditions as well as the lack of provision of open source platforms to proceed with metabolomics analysis. Both of these points are paramount to make research translatable into the field and accessible to different collectives.

Thus we have designed, developed and tested a pipeline that allowed the identification and quantification of 23 metabolites using open source software and *in-house* developed code. This is the first time such approach has been used to absolutely quantify both intra- and extracellular concentrations of the malaria parasite *P. falciparum* using NMR spectroscopy, instead of reporting predicted concentrations based on a fitting algorithm as presented by Teng *et al.* [219, 217]. Moreover this pipeline has the potential to be expanded to an unlimited number of metabolites and applicable to many other metabolomics studies. Its implementation in 2D spectra provides high resolution of metabolites and higher confidence on assignment with respect to the 1D spectra.

Furthermore we have identified the shortcomings of this method i.e. limited number of metabolites identified and limited limit of detection but we have proven its suitability to detect subtle differences between parasites growing in challenging conditions, thus proving the method fit for purpose. The use of labelled substrates was exploited for metabolite identification as well as confirmation of the main metabolic products from glucose namely lactate, glycerol and alanine. However, technical experimental limitations such as the differences in relaxation between different carbon isotopes, made the identification and quantification of glucose and its catabolic isotopomers not possible under the current set-up.

Future work should involve further study of the signals detected with the aim to expand the metabolites identified and consequent expansion of the calibration curves. Further work should aim to either include more steps on the pipeline in order to avoid the use of CCPNmr software (currently used to aid in phasing and metabolite mapping) or the implementation of such pipeline in python as a plug-in for the mentioned open source CCPNmr software, thus allowing a large number of users the access to immediate metabolite quantification. An attempt to adapt the method to be used with ^1H spectra must also be considered given that it is more sensitive and typically requires less acquisition time for reasonable resolution.

The use of sparse sampling techniques could also improve the current method by reducing the spectra acquisition time which would also allow an increase in the number of scans for a better resolution. Finally, the method should be adapted to use enriched ^{13}C substrates for flux analysis. To do so, experimental acquisition of the 2D ^1H - ^{13}C HSQC can be modified increasing acquisition times (to 0.15 s in the indirect dimension and 40 ms in the direct one as shown in [275]) which together with improved resolution (increase in number of scans) shows the ^{13}C - ^{13}C couplings from which the presence of label at carbonyl carbons can be elucidated. However, this experiment provides little information about the level of enrichment. Other methods have been proposed to tackle this problem [276, 277, 278] but they are not implemented in an open-source platform making them currently unsuitable for our purposes.

Chapter 4

Comparative metabolomics of early and late developmental stages of intra-erythrocytic *Plasmodium falciparum*

4.1 Introduction: Paucity of metabolic studies involving early intra-erythrocytic stages of *P. falciparum*

The intra-erythrocytic stages of *Plasmodium falciparum* afford the parasite a level of protection against the host's immune system, as well as the availability of nutrients for parasite development and multiplication. As reviewed in Chapter 1, Section 1.3, upon invasion, major modifications to the host erythrocyte are induced (known as the New Permeation Pathways, NPP) in order to allow the exchange of metabolites [279]. The parasite starts the consumption of haemoglobin from the erythrocyte cytoplasm that serves for osmotic control [280, 140] and provides initial nutritional value (through amino acid uptake [63]) before fuelling the parasite expansion within the host [141]. Aerobic glycolysis/fermentation is high and mitochondrial function is reduced [111]. As described in Chapter 3, Section 1, most of the metabolic studies of the parasite have been undertaken almost exclusively with mature trophozoite stages [219, 104, 281, 103, 282, 80, 223, 105] and most of them require a step to either concentrate the infected RBCs (usually by magnetic separation [235]) or release parasites from their host (using saponin). Both approaches are not only time consuming, but also involve removing the parasite from physiological conditions and

may therefore provoke mechanical or biotic stress responses in the parasite.

Studies involving solely the mature trophozoite stages provide limited information as they only represent a small biological window in the 48 h parasite life cycle. Following invasion, all modifications and changes occur within a specific time frame, and early invasion stages are very different from late ones. For example, erythrocyte-binding antigens are only expressed during ring and schizont/merozoite stages, but not during trophozoite stages [283], which emphasizes the importance of studies in ring stage parasites. Furthermore, asexual stages are the most vulnerable to the volatile conditions of the host environment in which fluctuations of temperature, oxidative damage and nutrient instability trigger stress response mechanisms [284]. It is the ring stage which can adapt and resist some of these. For example, a stress response triggered by the exposure to artemisinin, involves the development of a reversible dormant stage at the ring stage [285, 229]. When ring stages are exposed to nutrient starvation such as isoleucine deprivation, an arrest in development is also observed without typical dormancy morphology, but with parasites unable to progress from trophozoite stage [232].

As previously described, metabolic data of early ring asexual stages is very limited. Up to date, there is only one study in which these were included. In 2009, Olszewski *et al.* [195] presented a study that measured the accumulation of 92 metabolites in both intra and extra-cellular fractions with respect to uninfected samples at 7 time-points over the course of the intra-erythrocytic life cycle. A number of metabolites were observed to display increased levels of accumulation during late trophozoite development. This study was done by untargeted LC-MS/MS approach and it was the first to use parasite cultures at only 10% parasitaemia. However, all the results were semi-quantitative as they were reported as a normalised fold change with respect to uninfected red blood cells, which did not allow for absolute quantification. In addition, sampling intervals of 8 h did not allow for stage-specific rates of metabolite consumption/accumulation to be accurately determined. By using the method described in Chapter 3 to identify and absolutely quantify intra- and extra- cellular metabolites by NMR spectroscopy, we set out to determine whether ring-stage central energy metabolism could be detected and critically, whether it could be distinguished from that of late trophozoite stages and uninfected erythrocytes. If differences were detectable, we could proceed to study the plasticity of the malaria parasite's metabolism to physiologically relevant perturbations with our experimental method, for which sampling at more frequent intervals will be designed (see Chapter 6).

4.2 Experimental

Tightly synchronised RBCs infected with *P. falciparum* 3D7 (iRBCs) (as described in Chapter 2, Section 2.3.4.1) were split into six cultures at trophozoite stage and cultured in usual *in vitro* conditions (Chapter 2, Section 2.2). In the next life cycle parasitaemia reached 16%. Three of these cultures were analysed when in ring stage and the other three when in trophozoite stage(troph). Two hours prior to sampling, parasites were transferred to fresh medium of which samples were collected pre- and post- incubation for further analysis. Past the incubation period, 1 mL of cell pellet from each flask (equivalent to 1.7×10^9 cells) was washed with ice cold PBS to prevent further metabolic reactions and used for the metabolite extraction as described in Chapter 2 Section 2.5. In parallel three cultures of uninfected RBCs (RBCs) were kept in culture conditions for 24 hours prior to the two hour incubation with fresh medium and following metabolite extraction. Samples were analysed by NMR spectroscopy, 1D ^1H and 2D $^{13}\text{C}^1\text{H}$ spectra were acquired using a Bruker 600 MHz spectrometer, as described in Chapter 2, Section 2.7.2. Data were analysed and key metabolites identified and quantified as described in Chapter 3. Final concentrations were averaged and standard errors calculated. Where calculations included these values, errors were recalculated using the correspondent error propagation formula (see Chapter 2 Section 2.10.3). Statistical significance were tested as described in Chapter 2 Section 2.10. Data is reported in Appendix A, Tables A.3 and A.4.

4.3 Results and Discussion

4.3.1 Intracellular metabolite fingerprint showed unique and distinguishable features between RBCs and iRBCs at the different asexual stages ring and trophozoite

Initial data exploration included Principal Component Analysis which allows an analysis of hidden structure ‘ the data. PCA is a data transformation that produces new uncorrelated variables called Principal Components (PCs), that capture the maximum amount of variance in the data in decreasing order (the first principal component captures the most, last - the least). This effectively “compresses” the information allowing most of the information to be presented in just a few variables, which is easily visualised. For this dataset, variables were the metabolites and each replica a sample. Data was mean-centred and unit variance scaled prior to calculation. Score plots are shown in Figure 4.1. In Figure 4.1 (a) most of the samples are in the right hand side of the plot while only one of the RBC samples is located far

from the others. This is one of the uses of PCA, it allows for quick identification of outliers. Upon a more detailed analysis of the sample, it was identified as an outlier and removed from the analysis. PCA of the remaining samples presented a clear separation between infected (left) and uninfected (right) samples (Figure 4.1 (b)). Separation between early (ring) and late trophozoites (troph) was not very clear when looking at the first 2 dimensions. However, when a third component was taken into account (Figure 4.1 (c)), rings and trophs were clearly separated.

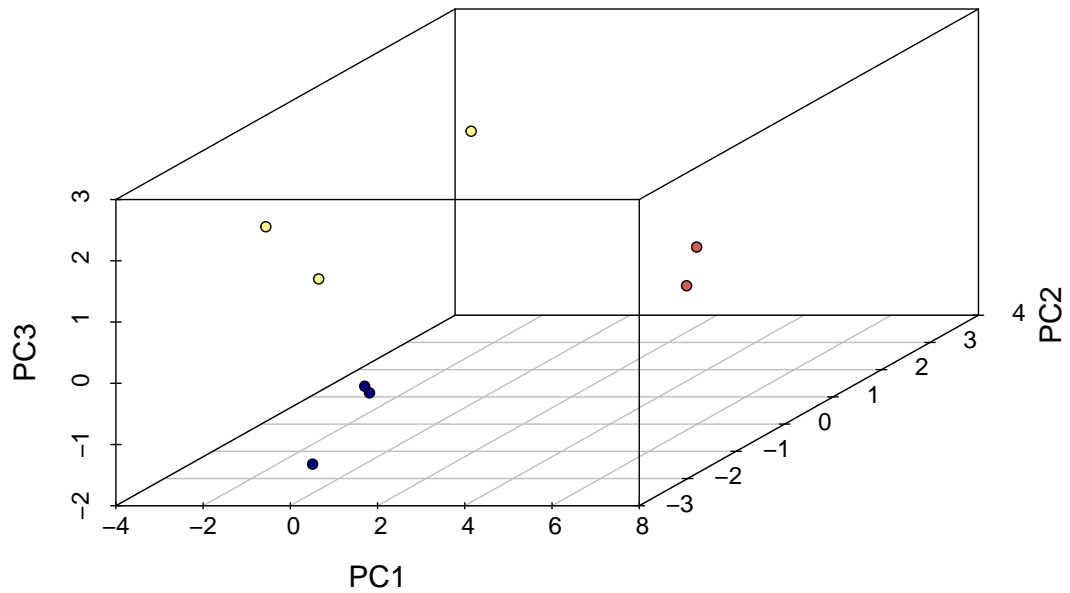
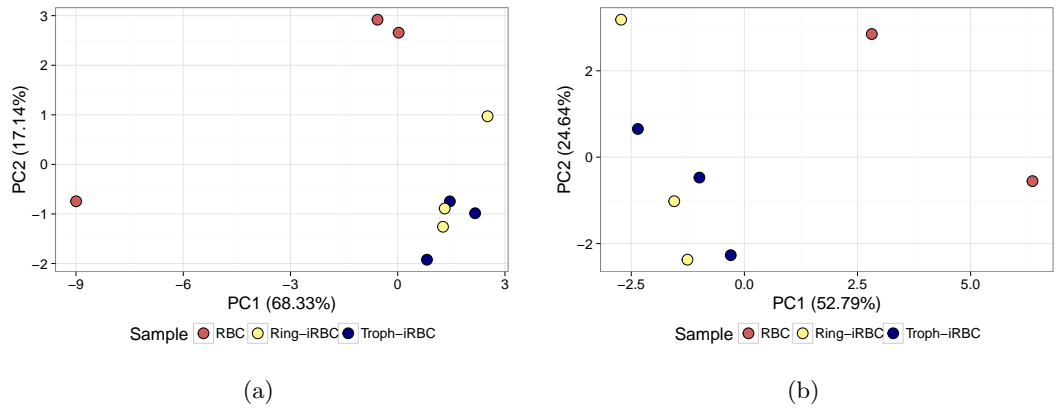


Figure 4.1: **PCA score plots of intracellular concentrations.** (a) 2D score plot of all samples where it can be observed that one of the samples is much different from the rest (RBC sample on left side of the plot) (b) 2D score plot after removal of the RBC outlier. Separation between infected and non-infected samples is very clear (right and left) (c) 3D score plot after removal of the RBC outlier. Now a separation between infected and non-infected cells is not only clear, but also a separation between infected cells in the ring and trophozoite stages are different. Note that each dot represents a sample.

The metabolites that contributed the most to the separation seen in the 2D plot (between RBC and infected RBC (iRBC)) are shown in the loadings plot (Figure 4.2). Loadings show the variables of the original dataset that contributed the most to form each of the new variables or principal components. NAD, Lactate, Alanine and Valine were the highest in iRBC samples and Aspartate, Glycine, Arginine, Glutamate and Creatine were the highest in RBCs. Differences between ring and trophozoite were mostly determined by Isoleucine, Acetate, Lysine and Leucine. All findings are consistent with Figure 4.3.

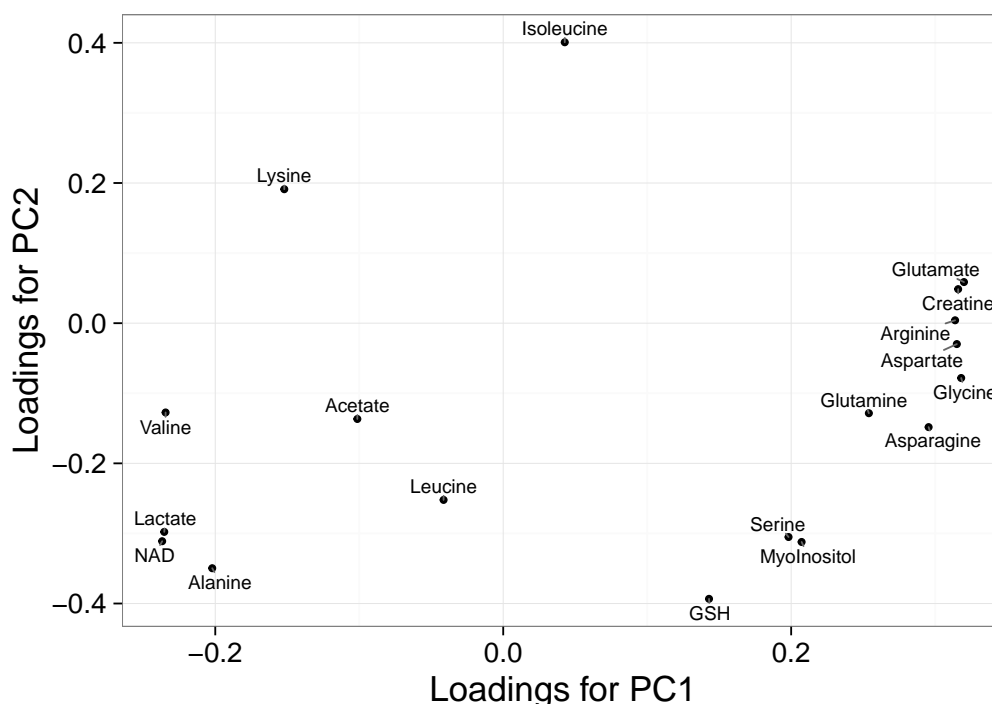


Figure 4.2: **PCA loading plot of cellular extracts.** The metabolites that are most different in infected cells with respect to non-infected are valine, lactate, NAD, alanine, lysine, acetate and leucine.

PCA showed differences between samples and highlighted which metabolites contributed the most to sample separation. In order to explore further the nature of these differences, pairwise Student's t-test was calculated for each metabolite and p-values adjusted by the Benjamini-Hochberg method. Quantifiable metabolites and results of statistical tests are shown in Figure 4.3. Differences between RBCs and infected RBCs are evident. Levels of alanine and lactate were significantly higher in iRBCs, products of the well-known increase in glycolytic flux [77]. Elevated NAD levels in infected RBCs were also observed and significantly different, which is con-

sistent with the literature [286]. However, most of the metabolites quantified were lower in abundance in the cellular extracts of infected RBCs. This was especially apparent in most of the amino acid concentrations. This might be related to the higher demand that the parasite has for amino acids, which is widely documented in the literature: arginine [195], aspartate and asparagine (usually in high demand due to the high asparagine content of *Plasmodium* proteins [231]), glycine and serine (involved in anabolic reactions for folate synthesis [287]) and glutamate and glutamine (in demand for glutaminolysis [111]). Myoinositol and creatine were also found less concentrated in infected samples, although only creatine showed a significant difference. Myoinositol is required for fatty acid synthesis for membrane creation [282] and creatine has also been found to decrease during *Plasmodium* infection [218] due to a higher metabolic demand. Although not significant, the main differences between early (ring) and late trophozoite (troph) stages, were in lower concentrations of glutamine, asparagine and aspartate in rings than in trophs. These metabolites are involved in the synthesis of proteins (asparagine) and nucleic acids (glutamine and aspartate are precursors of Carbamoyl-L-Aspartate which is upstream in the pyrimidine biosynthesis pathway). Another difference was the lower abundance of isoleucine in the ring stage and undetectable in the trophozoite stage, both probably linked to the high demand of the amino acid given that its only source is the extracellular media and it is not found in haemoglobin. Finally, GSH was found lower in trophozoites. GSH is involved in oxidative damage control which by the time the parasite reaches its late stages should be much higher than in a young parasite; this observation has also been made previously [288]. Acetate was found as a contaminant in the RPMI media (discussed in Section 4.3.2). Acetate was only found in cellular extracts of trophozoites, which might be due to the increased permeability of both host and parasite during the mature stages.

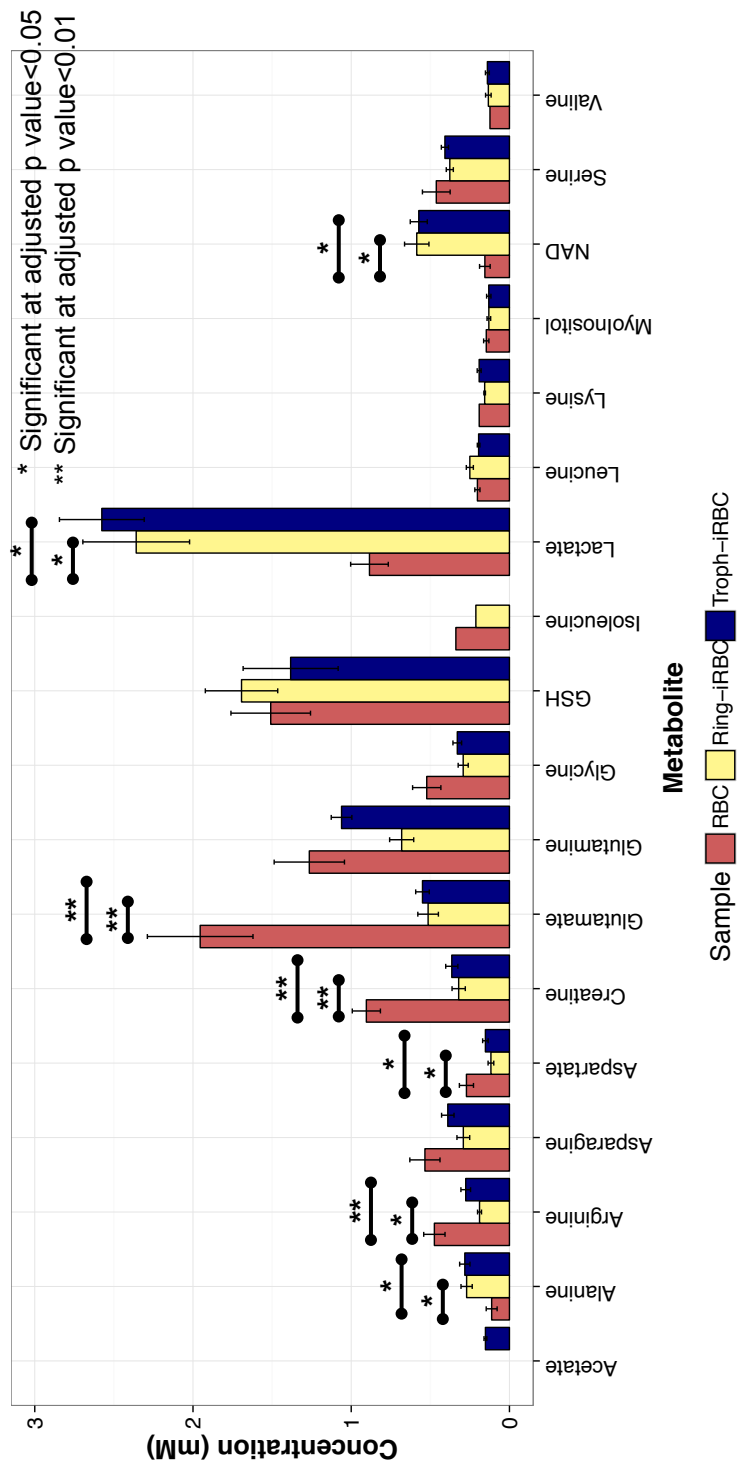


Figure 4.3: Concentrations of cellular samples. Bars represent mean values of 3 samples and error bars represent the standard error of the mean. Segments represent significant statistical test and asterisks the level of significance according to the legend.

To further contextualise our findings we decided to compare the trends of our data with those published by Olszewski *et al.* [195]. The authors reported the metabolites as the height of the peak signals from the m/z signal normalised by their internal standard and then they calculated the fold change with respect to the RBC sample at time zero. In their experiments cells were incubated for longer periods of time than in this experiment and their data processing was different. Aware of these limitations and expecting differences in values, but similarities in trends, we transformed our data as similarly as possible. Results are shown in Figure 4.4 and are also collated in Table A.5 in Appendix A. Most of the metabolites followed the same trend. Exceptions were asparagine and NAD. These differences can perhaps, be accounted by the time parasites were in culture. *Plasmodium* proteins are very rich in asparagine [231], which is used up from extracellular media and from haemoglobin degradation. These were freshly provided to our trophozoites while Olszewski *et al.* reference sample had been in the same culture medium for 32 h. NAD has been shown to oscillate during the asexual life cycle, thus different sampling times can result in different trends [289].

It can be concluded that metabolomics studies of cellular extracts by NMR spectroscopy are useful not only to identify metabolic differences between infected and uninfected RBC samples, but also differences between parasite stages inside the cell, that are in agreement with the literature. Some limitations of this approach are apparent when compared to more sensitive methods that have identified and relatively quantified a much larger number of metabolites of *P. falciparum* [103, 195], however absolute quantification has not been reported and key metabolites such as glycine, isoleucine or the isomers of glucose that present a challenge to MS studies, are resolved by NMR.

Analysis of cellular extracts has major limitations. *P. falciparum* is grown in batches in the laboratories and as such, the number of flasks that can be grown at a time limits the scope of the studies performed. Metabolite extractions are time consuming and the acquisition of samples in a timely manner is also limiting. Thus the use of solely culture media as a method for inferring parasite metabolism was also explored. NMR spectroscopy is ideal to analyse biofluids and similarly culture media has high enough concentrations that allow us to reduce the sample volume compared to cellular extracts. Consequently, extracellular products were analysed and the results are presented in Section 4.3.2.

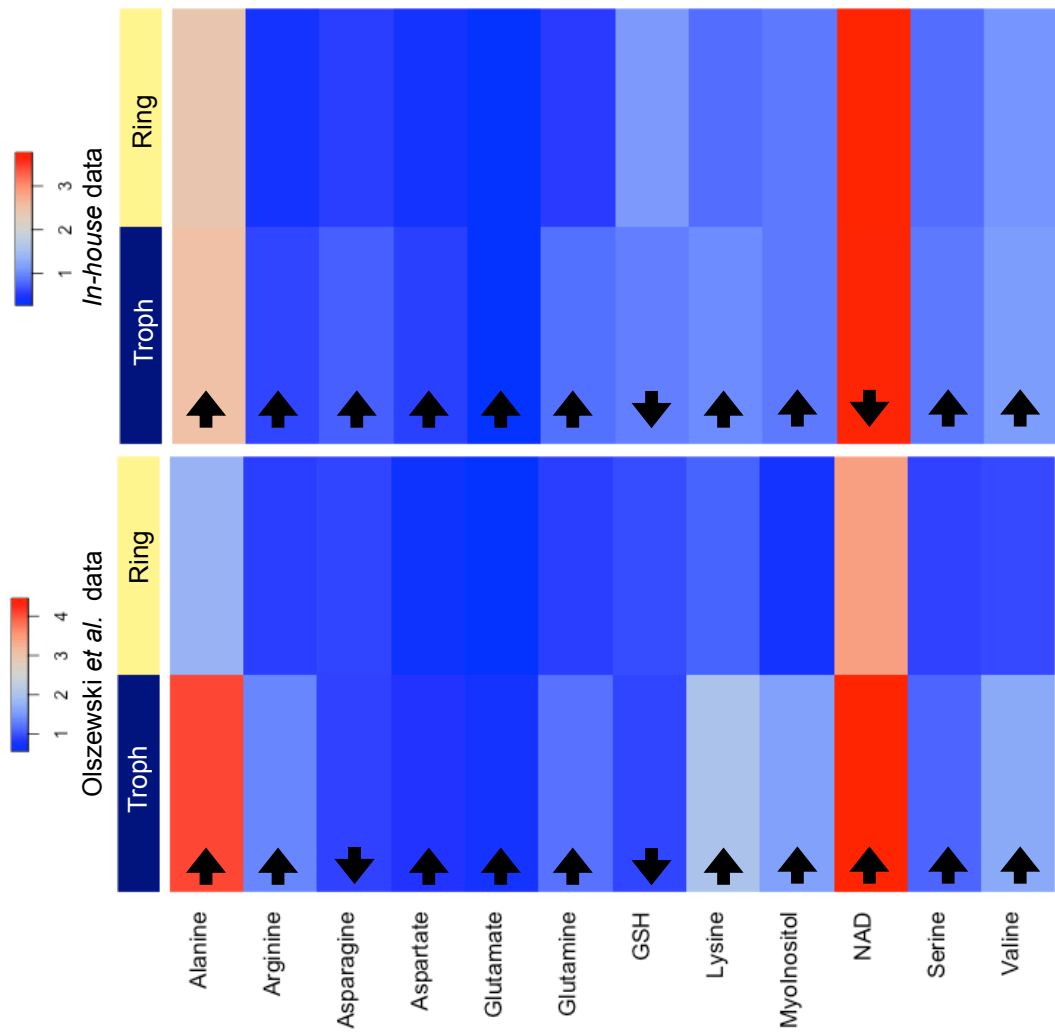
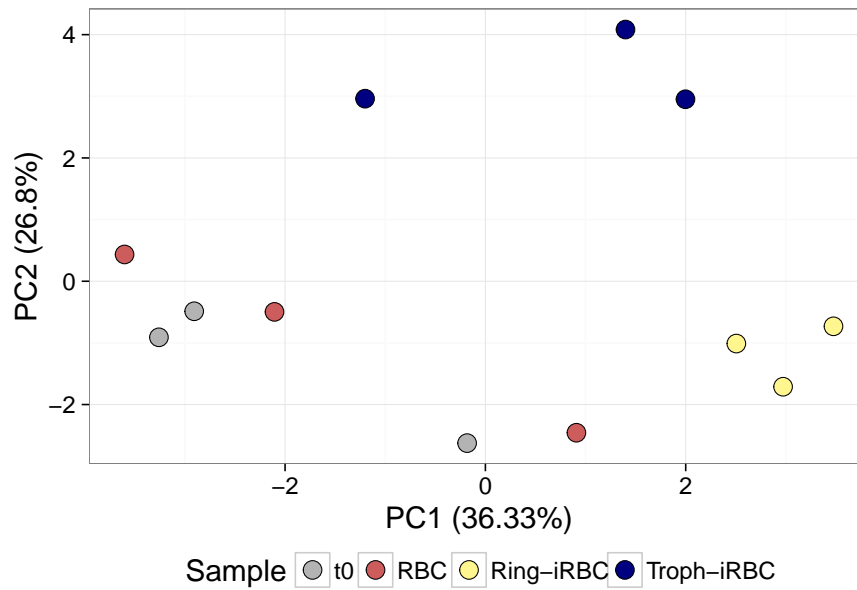


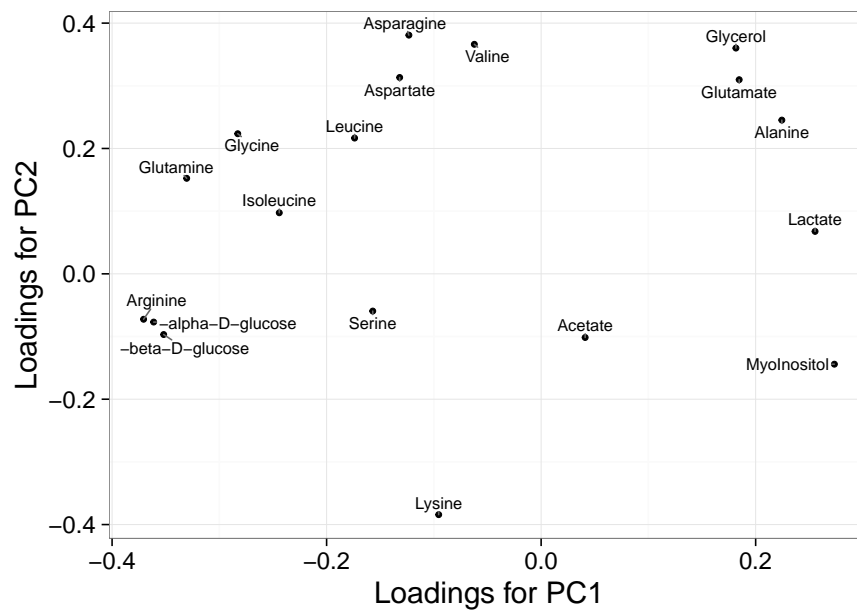
Figure 4.4: **Fold change with respect to RBCs.** Heatmap of the concentrations with respect to RBC from rings and trophozoite infected samples. Comparison between the common metabolites between the *in-house* data and those published by Olszewski *et al.*. The trends of increase/decrease of metabolites between life stages is mostly conserved (black arrows), despite experimental conditions and data acquisition being vastly different.

4.3.2 Extracellular metabolite fingerprint showed unique and distinguishable features between RBCs and iRBCs at the different ring and trophozoite asexual stages

PCA was used to discover hidden structure in the data. Media pre- and post- incubation showed an excellent sample classification upon calculation of PCA. Both iRBC and RBC as well as Ring-iRBC and Troph-iRBC samples could be discriminated by looking at the first two PCs (see Figure 4.5 (a)). The loading plot (Figure 4.5 (b)) shows that the metabolites that contributed the most to the separation of infected versus non-infected and t0 samples were myoinositol, lactate, alanine, glutamate and glycerol (higher in infected samples) and glucose and arginine (higher in non-infected samples). Glycerol is one of the exclusive metabolites that the parasite produces [81] and excretes, which makes it an excellent variable to discriminate between infected and non-infected samples.



(a)



(b)

Figure 4.5: **PCA media samples.** (a) Scores. Three clusters are distinguishable, one containing media pre-incubation and media post RBC incubation; the other two containing ring and trophozoite infected RBCs. (b) Loading plot points to glycerol, glutamate, alanine, lactate and myoinositol as the metabolites highest in infected cells with myoinositol and lactate contributing the most to separation between rings and trophozoites.

A detailed analysis of the concentrations found in the samples and statistical analysis results are shown in Figure 4.6. Although not significant, samples containing parasites had lower concentration of glucose, which is consistent with the increased demand of the metabolite during infection. For this incubation time, there were no differences in glucose uptake between rings and mature trophozoites (troph). Given that lactate is a direct product of the consumption of glucose, similar proportions were expected between rings and trophs. However, lactate concentrations were significant for all comparisons. Similarly, alanine and glycerol were also excreted in higher proportion in the troph stage. The other driver of central carbon metabolism, glutamine (via glutaminolysis, see Chapter 1 Section 1.3), was taken up slightly more in the ring stage but no significant differences were found. Myoinositol was significantly more consumed in trophs, which is consistent with the high demand for fatty acid synthesis for membrane creation for the daughter cells [282]. Other metabolite changes were not significant and more experiments are required to verify their changes; nevertheless, some of the trends observed are discussed next. Acetate concentration was slightly reduced in iRBCs, probably due to the increased permeability of the infected cells, especially late trophozoite stages, that might intake some of the metabolite resulting in a reduction of its concentration in media. Arginine and glutamine were depleted by iRBCs being consumed slightly more in the ring stage. It is interesting to report that valine and glutamate were excreted in iRBC, especially in the late trophozoite stages. This is an apparent signature of haemoglobin degradation that can be linked with parasite commitment to schizogony and it is discussed in Chapter 6.

In order to assess the differences in carbon circulation between the asexual life stages, we calculated the moles of glucose and glutamine consumed and predicted a maximum number of 3-carbon molecules that could be formed provided that they were all consumed with the sole purpose of its conversion into lactate, glycerol or alanine and subsequent excretion. Then we calculated the actual moles of excreted products (alanine, glycerol and lactate) and the percentage of these with respect to the possible predicted ones (values shown in table 4.1). This estimation shows that 71.63% of glucose and glutamine consumed were transformed into these excreted, “wasteful” products meanwhile only 43.35% in the early stages.

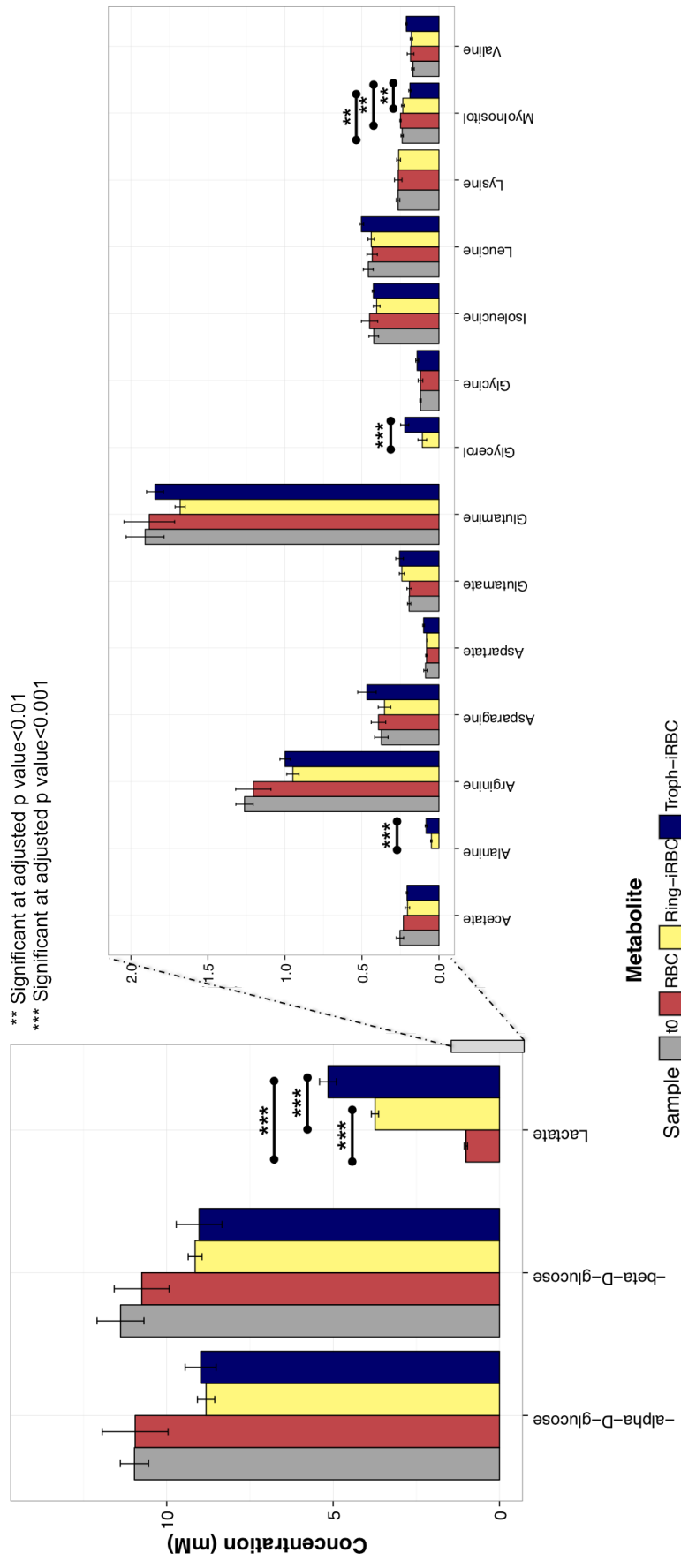


Figure 4.6: Concentrations in media before and after incubation with cells. Bars represent mean values of three samples and error bars represent standard error of the mean. Segments represent significant statistical test and asterisks the level of significance according to the legend.

Further analysis steps included the calculation of consumption and excretion of metabolites per parasite at each of the life stages. These calculations take into account small differences in parasitaemia. For example flasks used for ring stage analysis had slightly higher parasitaemia (17%) than flasks used for trophozoite stage analysis (16%). Equations 4.1 and 4.2 were used to calculate consumption and excretion of metabolites per parasite when a specific metabolite was present in medium pre-incubation or not respectively. Non-infected samples were used to estimate the contribution of just infected cells to the metabolite pool similarly to that in Teng *et al.* [219]. Then these values were divided by the incubation time to estimate the consumption and excretion per hour. In order to calculate concentrations in this way several assumptions were made:

1. Same volumes of cell pellet contain the same number of cells.
2. Steps in the extraction and sample preparation did not affect preferentially one kind of sample.
3. Non-infected RBCs are not affected by other RBCs being infected in the same culture.
4. Incubation time does not affect metabolism.

The results of these calculations are shown in Figure 4.7. Negative values represent metabolites that were consumed and positive - excreted. Pairwise t-test significant outcomes are represented with line segments. Although glucose was moderately more consumed by trophozoites (but still not significant), the proportions of glucose and glutamine consumed and ‘wasteful’ products produced (lactate, glycerol and alanine) per parasite were comparable to the medium pool (Table 4.2). Given that this estimation of consumption and excretion per cell did not add insight into the mechanistic metabolic processes observed during the incubation time, it was more realistic to use solely concentration measurements of the samples. Especially as there was evidence that not only do *Plasmodium*-infected erythrocytes inhibit glucose utilisation in uninfected erythrocytes [80], but they also modulate host enzymes in their favour [223]. Thus we cannot assume that non infected RBCs are not affected by iRBCs and consequently, for further experiments shown in Chapters 5 and 6 moles per cell were not calculated.

$$Conc_{pp} = \frac{Conc_{t_0} - (Conc_{iRBC} + ((1 - parasit)(Conc_{t_0} - Conc_{RBC}))}{N_{parasites}} \quad (4.1)$$

$$Conc_{pp} = \frac{Conc_{iRBC} + ((1 - parasit) \times Conc_{RBC})}{N_{parasites}} \quad (4.2)$$

The relative increase of wasteful products with the development of the parasite, fits the hypothesis presented by Newsholme *et al.* [117] where they proposed a role for high rates of glucose and glutamine utilisation in rapidly dividing cells (see Chapter 1 Section 1.3.1.3). Assuming a bifurcated pathway in which one branch works towards biomass production (for example through glucose into pentoses phosphate and consequent pathways for nucleic acid synthesis) and the other towards a wasteful product (lactate); a huge flux to waste could serve as a way to keep tight control on the biomass production and when an adequate signal of proliferation is received, the cell could redirect part of that flux to biomass production without having to have a feedback mechanism in the production of the precursor. Changes in flux to lactate or to biomass would allow rapid response to stimuli and consequent successful environmental adaptation. Thus, when the parasite is young and in need to create large amounts of biomass, the flux redirected towards its production should be larger than when the parasite has expanded and already built most of its biomass. This idea is further discussed in Chapter 6.

Table 4.1: Consumption/Excretion concentrations (in mM) of the main drivers of glycolysis. Average of three samples.

Stage	α -D-glucose	β -D-glucose	Glutamine	Alanine	Glycerol	Lactate	Total Consumed	Total Excreted	Possible Excreted	Percentage Excreted
Ring	2.13	2.15	0.228	0.05	0.13	3.63	4.508	3.81	8.788	43.35%
Troph	1.9	2.2	0.065	0.08	0.22	5.62	4.165	5.92	8.265	71.63%

Table 4.2: Picomoles consumed and excreted per cell of the main drivers of glycolysis.

Stage	α -D-glucose	β -D-glucose	Glutamine	Alanine	Glycerol	Lactate	Total Consumed	Total Excreted	Possible Excreted	Percentage Excreted
Ring	0.108	0.092	0.0118	0.003	0.007	0.156	0.2118	0.166	0.4118	40.31%
Troph	0.148	0.154	0.0036	0.007	0.019	0.407	0.3056	0.433	0.6076	71.26%

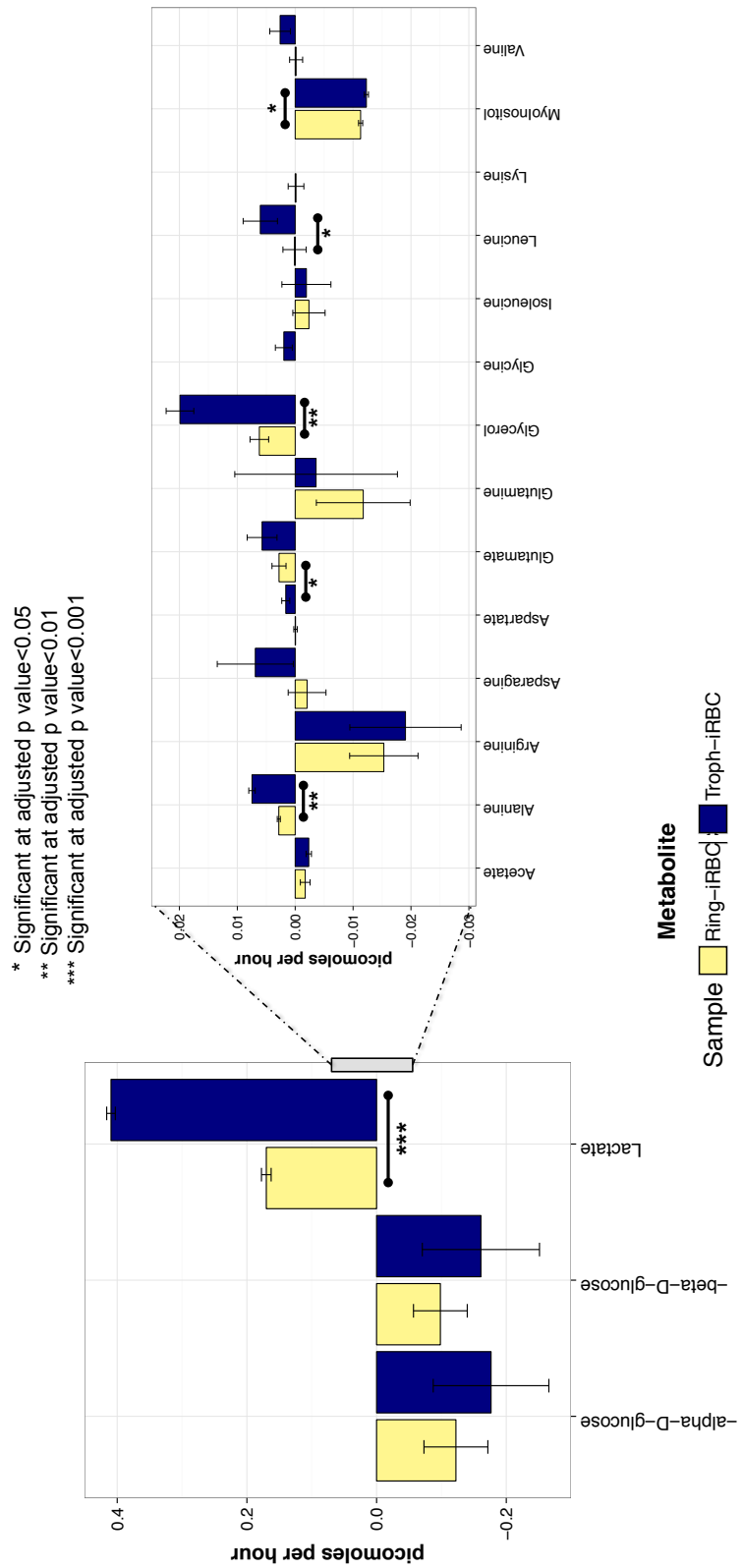


Figure 4.7: Consumption/Excretion of metabolites per parasite per hour. Bars represent mean values of 3 samples and error bars represent the standard error of the mean. Segments represent significant statistical test and asterisks the level of significance according to the legend.

4.4 Conclusions

In this Chapter I have presented the first study by NMR metabolomics showing qualitative and quantitative discrimination between not only infected and non-infected samples but also between different life stages of the intra-erythrocytic life cycle of *P. falciparum* using cultures that did not undergo any artificial enrichment of parasites. Differences in cellular extracts were found and were consistent with the literature. These can be summarise in:

- (a) An increase in the lactic acid abundance in infected cells, likely product of the increase glycolysis with respect to the erythrocyte [290]. This finding is even more interesting in cultures with only 10% parasitaemia given that the malaria parasite inhibits glucose utilisation of other uninfected erythrocytes in co-culture [223]
- (b) An increase in alanine in infected cells, likely product of both glycolysis (with alanine being produced from pyruvate as shown in Chapter 3, Figure 3.15) and possible haemoglobin degradation as alanine is one of the most abundant amino acids in the globin part (NCBI Protein database [291]).
- (c) An increase of NAD in infected red blood cells, which has been suggested to be linked to the increased glycolysis where NAD is a needed cofactor [286].
- (d) A decrease in most of the amino acids with significance in arginine, aspartate and glutamate which demand increases in infected red blood cells [111, 195, 231].
- (e) A decrease in creatine which has been found to severely decrease in mice expose to *P. berghei* infections [218].

Currently, the parasite is grown in batches what results in large numbers of flasks required for adequate sampling when doing time course studies. This increases the variance due to batch effect and might severely bias the observed results. By using just extracellular products, experiment variability can be further controlled, providing more robust outcomes. The information that can be derived from the study of the metabolic uptake of the parasite is far more informative than those obtained from cellular extracts unless metabolites are traced using ^{13}C . Thus, we also analysed media pre- and post- incubation with both infected and non infected red blood cells. Interestingly, metabolic differences were also found by looking solely at those extracellular products. These were enough to discriminate samples of infected

and non-infected cells as well as different life stages of the parasite. Analysis of media extracts are less time consuming and require less resources than cellular extractions and so these experiments set the basis for further experimentation presented in this Thesis. Key metabolites involved in such discrimination were glucose and its glycolytic products lactate, alanine and glycerol and myoinositol which is a key precursor for lipid biosynthesis and in high demand in developing parasites [282].

The shortcomings of this work rely mainly on the low sensitivity of the technique of choice, NMR metabolomics, that does not allow for identification and quantification of large number of metabolites. In this sense the use of Mass Spectrometry could improve the information acquired with respect to the cellular extracts. However and for the study of biofluids, NMR is a much sensible choice, given its robustness and easy and consistent sample preparation and analysis. Other limitation of this particular study is the limited time points analysed. This particular issue will be address in Chapter 6, where the monitoring of a whole life cycle would enable stage specific flux analysis.

Here we have shown that by using NMR metabolomics, we can discriminate between RBCs and iRBCs at different stages analysing both intra- and extracellular products by NMR spectroscopy. Differences in metabolic make up between rings and trophozoites point to stage-specific differences in carbon flux. These are investigated in the following chapters.

Chapter 5

Morphological and initial metabolic characterisation of *Plasmodium falciparum* in physiological (blood-like) medium

5.1 Introduction: *Plasmodium in vitro* culturing conditions

In vitro conditions used for *P. falciparum* axenic culture are substantially different to *in vivo* conditions in the human host. Continuous culture of *Plasmodium* spp. has proved challenging since its first attempts. It took over half a century to advance from the first culturing attempts, in which parasites growing for only a few life cycles could be obtained [292], until a robust continuous culture method was published [177]. This method was based on the use of RPMI 1640 based media, which was developed by Moore *et al.* [293]. Formulated for use at a 5% CO₂ atmosphere, its primary goal was the growth of human lymphoid cells. The richness of this medium makes it suitable for the growth of many other kind of cells upon supplementation.

RPMI 1640 medium provides a suitable environment for the continuous growth of the malaria parasite, however it contains levels of nutrients that notably differ from those seen in physiological conditions in the human host. For example, in RPMI 1640, glucose and glutamine, the main drivers of the central carbon

metabolism of *P. falciparum* during the intra-erythrocytic stages, are over twice the concentration commonly measured in human plasma [178]. Most of the vitamins present in RPMI 1640 are more concentrated than in human plasma and so are most of the metabolites. Some exceptions include valine and glycine which are slightly more abundant in human blood. A detailed comparison of RPMI 1640 components with respect to human blood has been reported by LeRoux *et al.* [178].

Many factors are involved in the differences between *in vivo* and *in vitro* conditions. The *in vitro* culturing method intrinsically limits the factors that can be improved, for example the lack of a well-established chemostat for growing *Plasmodium* spp. constrains a stable and constant nutrient availability and waste disposal. The actual nutrient availability presents a conundrum to the established studies. On the one hand the parasites readily grow in the current conditions such as the ones described in the General Materials and Methods, which is good to keep robust cultures that are consistently available for experimentation and which are easily reproducible between laboratories and therefore comparable. On the other hand growing parasites in conditions far from physiological selects parasites and alters metabolic flux dynamics and potentially responses to treatments. Moreover, the well documented differences between lab-cultured and field strains of *Plasmodium* in for example switching patterns of *var* genes [294], might be related to this adaptation to a very favourable but unrealistic culture media.

Despite its efficiency, the suitability of RPMI 1640 based media to grow the malaria parasite can be argued. When the aim of culturing the malarial parasite is to test chemical compounds that would alter its development or its interaction with the environment (i.e. drugs and vaccine candidates), the need for a research model as close as possible to the human host, is vital. The minimum nutritional requirements of *P. falciparum* in culture have been reported decades ago [233, 234, 128], however there are not studies available on the differences between malaria parasites growing in a more physiological media with respect to the current established method.

Main aims. The aims of the work presented in this Chapter were (a) to develop an *in-house* media with concentrations similar to the ones of human blood; (b) to test the viability of parasites growing in it and assess whether we could observe phenotypic differences in a quantitative manner; (c) to perform preliminary metabolomics analyses (as described in Chapter 3) to test the effect of these media on metabolic uptake between infected and non-infected cells.

5.2 Experimental

5.2.1 Media preparation

In-house produced RPMI and blood-like RPMI preparations are described in detail in Section 2.4 in Chapter 2. In brief, each component was prepared in a concentrated solution, filtered sterilised and aliquoted prior freezing. For each media batch one aliquot of each component was defrosted and used to prepare the corresponding media by mixing them at the adequate proportion, followed by pH adjustment and sterilisation. With this method, multiple combinations of media can be prepared.

5.2.1.1 Media viability test

A synchronised culture of *P. falciparum* 3D7 infected red blood cells was split in two, one was kept in commercial RPMI 1640 based medium and the other in *in-house* produced RPMI 1640, both supplemented with standard amounts of HEPES, Albumax, gentamycin and hypoxanthine (see Section 2.2 of Chapter 2). Parasite viability and growth were monitored during three life cycles by bright field microscopy.

5.2.1.2 Media effect test

A synchronised culture of *P. falciparum* 3D7 infected red blood cells was split in three, one was kept in commercial RPMI 1640 based medium (CM) and the other two in *in-house* produced blood-like medium, one supplemented with 0.04 mM hypoxanthine (BL+H) and another with 0.004 mM (BL). All of the cultures were supplemented with the usual values of HEPES, Albumax and gentamycin. Parasite viability and growth were monitored by bright field microscopy for 2 weeks. Furthermore, slides were prepared for further analysis at 24 hours and then every 48 hours for the first three cycles.

5.2.2 Image analysis

Giemsa stained parasite smears were digitalised using a Nikon camera attached to a Olympus bX-60 microscope and saved in tiff format. These images were then imported in the open source software Fiji (Image J) [295] and analysed as described in Chapter 2, Section 2.8.2.

5.2.3 Metabolomics experiment

Three tightly synchronised cultures of *P. falciparum* 3D7 at 12% parasitaemia were incubated for 24 h in blood-like medium as well as a culture of uninfected

RBCs. When at the trophozoite stage, parasites were changed into fresh media and incubated for three hours prior sampling. Media samples of 1 mL were collected in a tube containing 2.5 mM TSP (Trimethylsilyl)-propionic-2,2,3,3-d₄ acid) and snap frozen. They were lyophilised and then resuspended in 300 μ L of deuteriumoxide and transferred to an NMR tube (3 mm diameter), where 1D ¹H and 2D ¹H-¹³C were acquired in 600 MHz Bruker spectrometer as detailed in Section 2.7 of Chapter 2. Spectra were normalised by TSP, metabolites were identified and quantified as previously described (Section 2.7). Data are provided in Appendix A, Table A.6 and were analysed followed procedures described in Chapter 2, Section 2.10.

5.3 Results and discussion

5.3.1 A qualitative and quantitative analysis on the effects of physiological media on *P. falciparum* trophozoites

A “blood-like” media that would consist on the same components of RPMI 1640 but at the levels reported in human blood was designed based in the publication by LeRoux *et al.* [178] in which a comparison of the concentrations of factors present in RPMI 1640 and human blood was reviewed. Concentrations of these factors in human blood vary within different individuals. The values for our study, taken from LeRoux *et al.*, are mean values from the ones recorded in the Human Metabolome Database (HMDB) [184]. Exceptions were choline, myoinositol, niacinamide and glutathione, which were not reviewed in the publication and therefore we chose the upper value reported in HMDB (final concentrations and preparation method reported in Section 2.4 in Chapter 2).

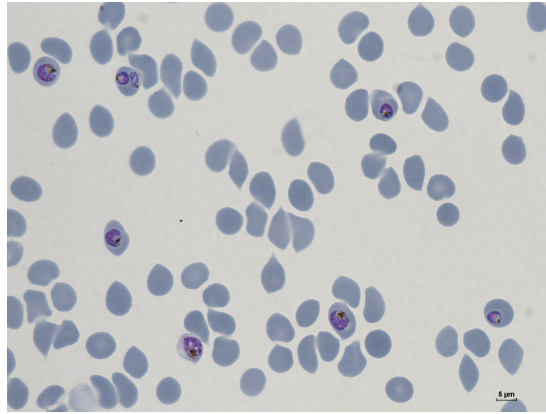
For *P. falciparum* serum free cultivation, RPMI 1640 is supplemented with HEPES, Albumax, gentamycin and most importantly hypoxanthine (see Section 2.2 in Chapter 2). *Plasmodium* spp. are not able to synthesize purine rings *de novo* [296] and therefore rely on salvage of purines from the host. They can metabolise a variety of exogenous purines although with a preference for hypoxanthine [297]. Optimal hypoxanthine levels for parasite growth have been reported between 0.015 and 0.12 mM [297]. Current accepted and spread supplementation is 0.04 mM whilst the hypoxanthine available in human serum is just 0.004 mM. Such low levels of hypoxanthine are known to affect the growth rate of *Plasmodium* [184]. In the context of this study, aiming at the development of a tailor made RPMI-like media mimicking blood nutritional levels, hypoxanthine supplementation was kept at a 0.04 mM concentration as this metabolite is already known to affect parasite growth rate.

In this framework, experiments were designed to assess: (a) whether the *in-*

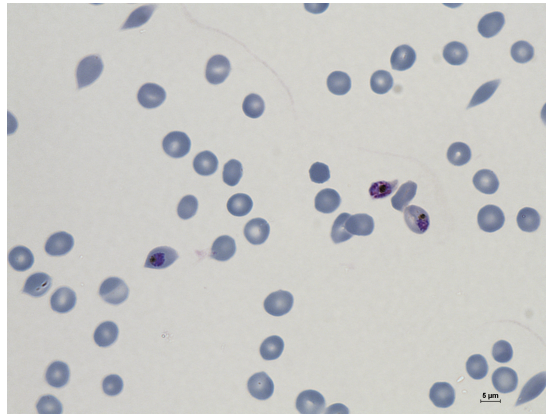
house produced medium was comparable to the commercially available, (b) whether there were phenotypic differences between parasites growing in complete media and blood-like media and (c) whether parasites growing in blood-like media supplemented with either 0.04 mM or 0.004 mM hypoxanthine were different.

5.3.1.1 *In-house* RPMI-like medium is comparable to commercially available RPMI

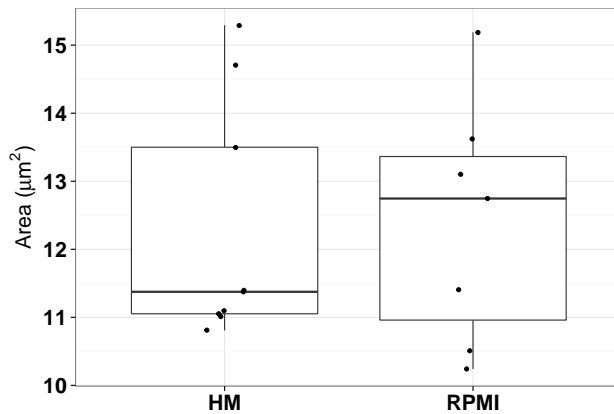
The output of the experiment described in Section 5.2.1.1, showed that parasite viability and growth was not significantly different between parasites growing in commercial RPMI and our *in-house* RPMI. Parasites were monitored for three life cycles. Representative images of Giemsa-stained parasite smears (example shown in Figure 5.1) were analysed as described in Section 5.2.2 and a Mann-Whitney-Wilcoxon statistical test was performed resulting in non significant differences between both groups (p value of 0.9182 with a 95% confidence interval of (-2.226-1.667)), proving that this method to prepare media was up to experimentation standards.



(a)



(b)



(c)

Figure 5.1: **Bright field imaging of parasites growing in different media.** (a) *In-house* produced RPMI 1640, (b) Commercial RPMI 1640; (c) Box plots of area measurements of a subset of parasites grown in either *in house* RPMI (HM) or commercial RPMI. Box plots represent median of the data (black line) contained into the first and third quantiles (box). Segments reach the maximum and minimum value.

5.3.1.2 Parasites growing in blood-like medium have different phenotype compared to those growing in complete medium

To test whether I could observe phenotypic differences between parasites grown in RPMI-1640 based media (CM) and blood-like media (BL, BL+H) the experiment described in Section 5.2.1.2 was performed. A representative image of the appearance of the parasites after 124 h of incubation is shown in Figure 5.2. Size differences between CM and BLs parasites were evident. Further confirmation was attained after image analysis as described in Section 5.2.2.

Pictures of at least 30 parasites per treatment were taken and images were analysed with Fiji (Image J) [295]. Different parameters were quantified, including area, intensity, circularity and intensity. These are shown in Figure 5.3. At each time point, the sizes of the parasites growing in a more challenging nutritional environments (BL or BL+H) were smaller with respect to the parasites growing in CM. However, the areas between parasites growing in BL or BL+H did not show an evident difference. The differences between the latter two, not surprisingly lie on the progeny numbers. As expected, parasites with lower than optimal hypoxanthine levels, showed a severe drop in progeny generated (measured as parasitaemia change between life-cycles), but amongst the viable parasites, there were no significant differences with the parasites growing in media supplemented with hypoxanthine. To determine whether the observed phenotype differences between treatments were significant, statistical tests were performed.

The normality of the data was tested using a Shapiro-Wilk test and upon significance a Mann-Whitney-Wilcoxon test was used to test the hypothesis. The p values were adjusted by the Benjamini and Hochberg method [298]. The results are reported in Table 5.1. Overall, parasites growing in CM were significantly bigger than those growing in BL or BL+H media. However, there were not significant size differences between parasites growing in BL supplemented or not with more hypoxanthine. Parallel to size, intensity and solidity were also significantly different between CM and BLs. Solidity differences might be the product of lower cellular density due to a decrease in the biomass produced. Finally circularity was similar between all the treatments.

Interestingly, at the last time point analysed, the difference of both BL growing parasites with respect to complete media growing parasites seems to be larger than in previous time points. This might suggest that there might be not only a difference in size but also a delay in the life cycle. This hypothesis will be further investigated in the next Chapter.

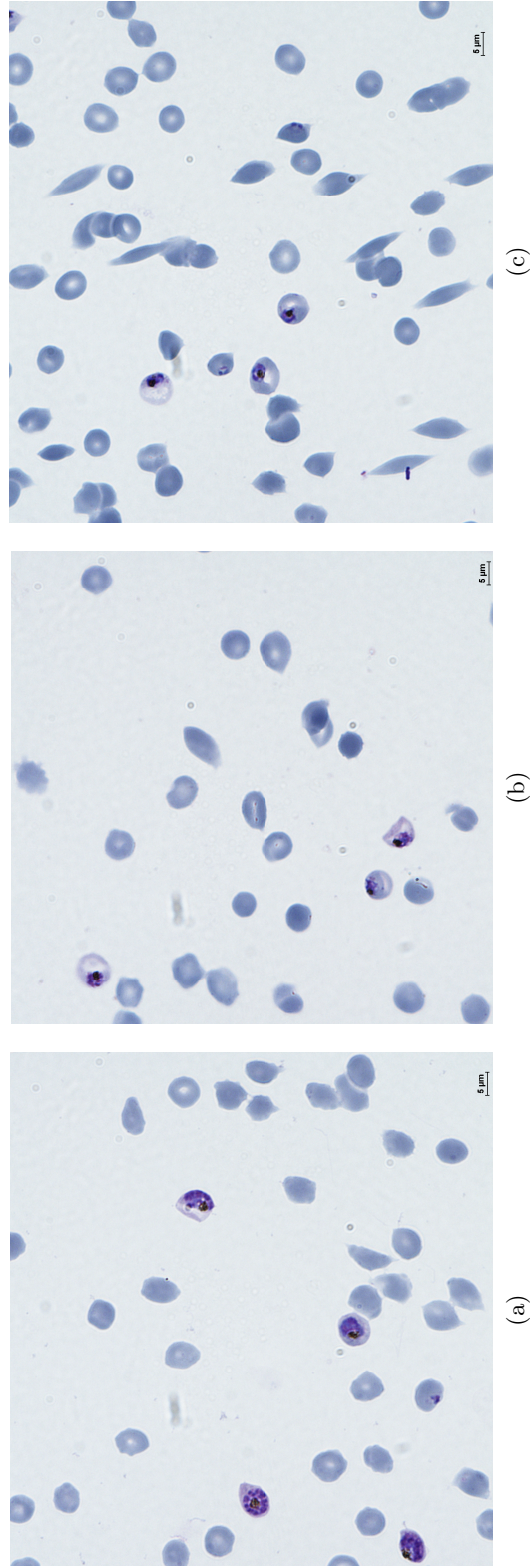


Figure 5.2: **Bright field imaging of parasites growing in different media 124 h after exposure.** (a) Complete media (CM, based on RPMI 1640) (b) Blood-like supplemented with hypoxanthine media (BL+H). The size of CM parasites is notably larger than either BL and BL+H. Note that a 5 μm scale is in the right bottom corner of each picture.

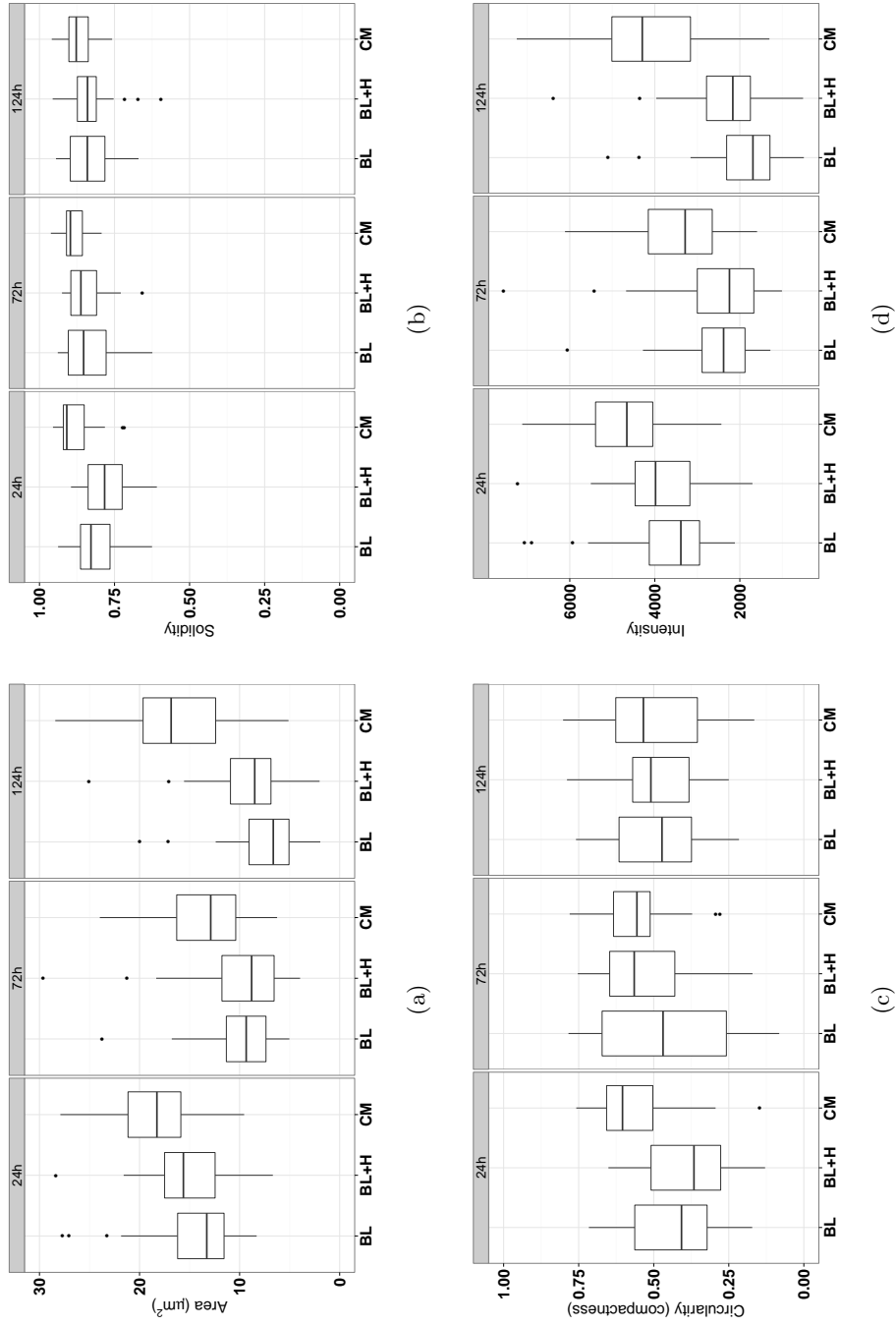


Figure 5.3: **Bright field imaging quantitative analysis of parasites growing in different media.** Parasites measured growing in different media: complete media (CM), blood-like media (BL) and blood-like media supplemented with hypoxanthine (BL+H). Trophozoite stages from slides taken at three different life cycles 24h, 72h and 124h after exposure to the media. (a) Area of the parasites, (b) Solidity, (c) Circularity, (d) Intensity. Box plots represent median of the data (black line) contained into the first and third quantiles (box). Segments reach the maximum and minimum value excluding outliers and dots represent outliers.

Table 5.1: Mann-Whitney-Wilcoxon test results

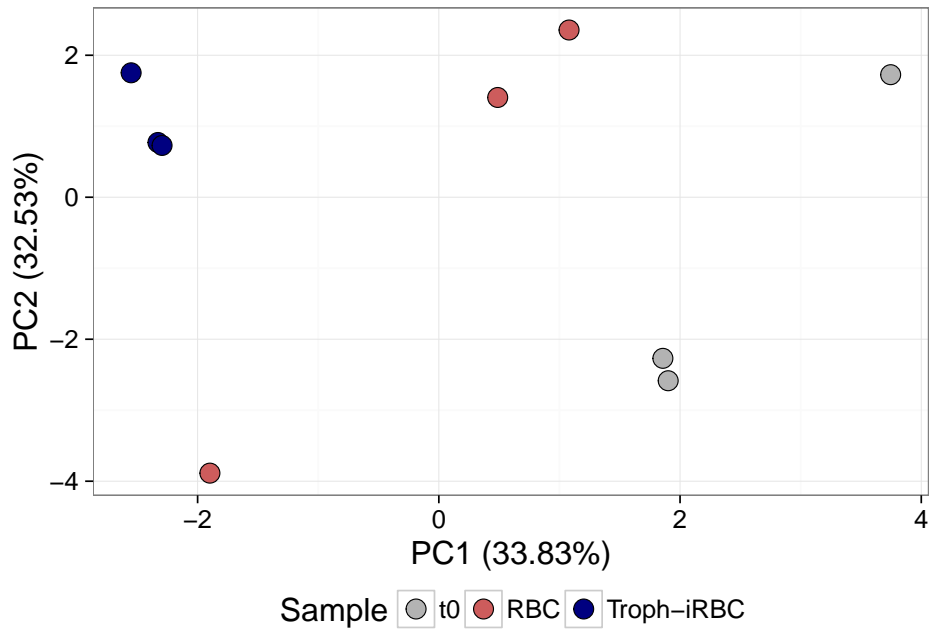
Group	Time [h]	Variable	Adjusted p-value	Confidence Interval	Significance
CM vs BL	24	Area	0.0016	(-6.376, -1.800)	**
	72	Area	0.0005	(-5.481, -1.791)	***
	124	Area	p<0.0001	(-10.954, -6.972)	***
	24	Solidity	0.0003	(-0.104, -0.034)	***
	72	Solidity	0.0026	(-0.081, -0.021)	**
	124	Solidity	0.0350	(-0.059, -0.005)	*
	24	Circularity	0.0018	(-0.200, -0.054)	**
	72	Circularity	0.0186	(-0.179, -0.025)	*
	124	Circularity	0.8456	(-0.078, -0.060)	
	24	Intensity	0.0016	(-1625.912, -456.589)	*
	72	Intensity	0.0005	(-1397.633, -456.589)	***
	124	Intensity	p<0.0001	(-2793.244, -1777.779)	***
CM vs BL+H	24	Area	0.0065	(-5.842, -1.223)	**
	72	Area	0.0010	(-5.710, -1.711)	**
	124	Area	p<0.0001	(-9.189, -5.212)	***
	24	Solidity	p<0.0001	(-0.145, 0.076)	***
	72	Solidity	0.0016	(-0.060, 0.017)	**
	124	Solidity	0.0155	(-0.055, 0.008)	*
	24	Circularity	0.0001	(-0.254, -0.101)	***
	72	Circularity	0.2097	(-0.100, 0.0135)	
	124	Circularity	0.7847	(-0.074, 0.046)	
	24	Intensity	0.0065	(-1489.69, -313.202)	**
	72	Intensity	0.0010	(-1456.199, -436.290)	**
	124	Intensity	p<0.0001	(-2343.085, -1329.038)	***
BL vs BL+H	24	Area	0.7847	(-3.063, 1.961)	
	72	Area	0.9476	(-1.678, 1.828)	
	124	Area	0.0551	(-3.373, -0.152)	
	24	Solidity	0.0701	(0.001, 0.078)	
	72	Solidity	0.5671	(-0.045, 0.019)	
	124	Solidity	0.9710	(-0.03, 0.029)	
	24	Circularity	0.2749	(-0.027, 0.133)	
	72	Circularity	0.2148	(-0.138, 0.02)	
	124	Circularity	0.9242	(-0.058, 0.068)	
	24	Intensity	0.7847	(-781.045, 500.121)	
	72	Intensity	0.9476	(-427.861, 466.126)	
	124	Intensity	0.0551	(-860.163, -38.736)	

*Statistically significant at $p<0.05$; **Statistically significant at $p<0.01$; ***Statistically significant at $p<0.001$;

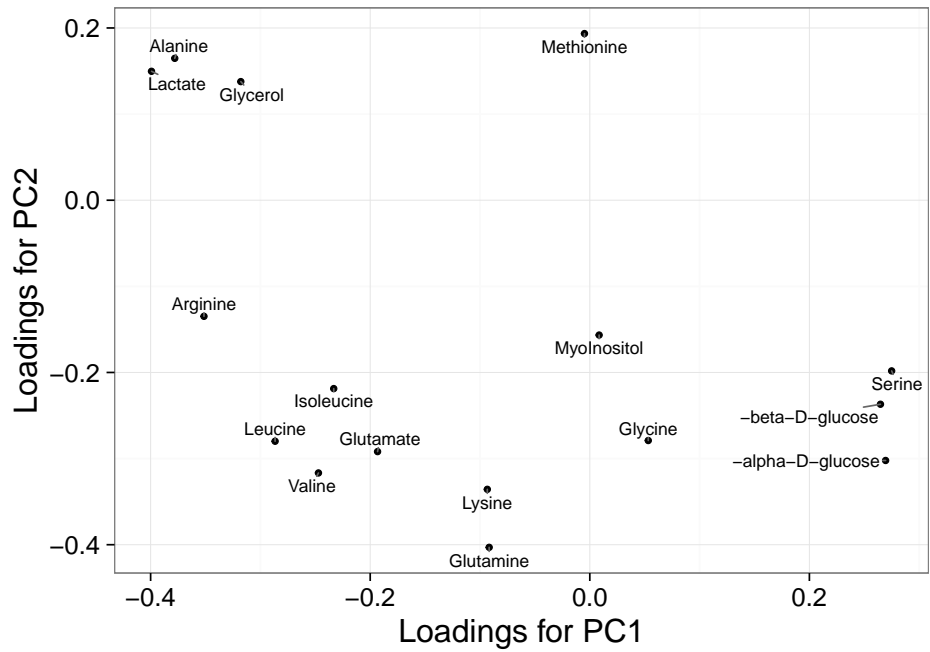
5.3.2 Uninfected RBCs and iRBCs present distinguishable metabolic profiles when in blood-like medium

In order to probe the use of metabolomics for identification of differential nutrient acquisition and excretion by parasites in different nutrient environments, it is essential to identify whether relevant metabolites can be identified using NMR spectroscopy when the concentration of the metabolites are lower than those found in complete media. We designed an experiment in which samples of media pre- and post- 3 h incubation in blood-like media of RBC and iRBCs were taken. We wanted to confirm whether: (a) we can identify and quantify some of the key metabolites feeding the central carbon metabolism, (b) we see differences pre- and post- incubation with either RBC and trophozoite-iRBCs and (c) we see differences between RBCs and trophozoite-iRBCs samples. The experiment described in Section 5.2.3 was designed for this purpose.

Preliminary data exploration was performed using principal component analysis (PCA), within the dataset each variable was an identified metabolite. The data was scaled and PCA was calculated by singular value decomposition in R [299]. Results are shown in Figure 5.4. Figure 5.4 (a) shows a scatterplot of the first two components. The analysis highlighted that there is a large difference between RBC samples (when compared to the distance between either trophozoite or pre-exposure media (time zero,t0)), thus indicating a high variance between RBC replicates. This could be explained by the loss of material in the drying process, resulting in slightly different concentrations measured. Secondly it can be appreciated how all samples pre-incubation are grouped at the right of the plot, followed by the RBCs and finally the trophozoite-infected RBC. There are noticeable differences between samples from media that had been cultured with cells and media that had not. There are also prominent differences between media incubated with infected red blood cells versus non-infected red blood cells. Because PCA is a transformation of a previous coordinate system (metabolites) into a new coordinate system (Principal Components), it can be estimated how much of each of the old variables (metabolites) contributes to each of the new ones (PCs). These are the loading plots (Figure 5.4 b, loadings of the principal components 1 and 2). Glucose and its glycolytic products: lactate, alanine and glycerol are the main contributors in the separation across the x-axis, which indicates biological relevance. Metabolites scattered across the y-axis contribute mainly to the separation of replicates. These are metabolites at much lower concentrations and therefore the variance between samples that have suffered some loss in the drying process can affect them severely.



(a)



(b)

Figure 5.4: **PCA scatterplot of metabolite concentrations in Blood-like media.** (a) Scores of first two principal components. Percentages show the amount of variance accounted for in each principal component, each point correspond to one sample (set of metabolites quantified) coloured according to the group it corresponds. (b) Loadings from first two principal components. Note that troph stands for trophozoite.

Next, we calculated pairwise Student's t-test for each metabolite and p-values were adjusted by the Benjamini and Hochberg method. The means and standard errors together with the significant statistics results are shown in Figure 5.5. As expected, both populations of cells (RBCs and Troph-iRBCs) rely on glucose as their main source of energy, as shown by the higher and significant glucose depletion in iRBC-exposed medium. Proportionally more lactate and alanine were generated although only lactate presented a significant increase with respect to RBCs for the given incubation time. Glycerol is a metabolite characteristic of the malaria parasite that is only found in human blood when adipocytes release it towards the liver to serve as substrate for gluconeogenesis [300], usually under disease conditions. Thus, it was only present in the iRBCs sample (Troph).

Low concentration metabolites did not present any significant difference. This is the likely product of the sensitivity limitation of the technique: at low concentrations, signals show a higher noise, thus increasing sampling variance. However trends can be observed such as the well-known consumption of isoleucine, by iRBC as compared to RBC. A time-course experiment could provide insight in this matter as it would allow us to measure the tendency of consumption or excretion for each metabolite detected. Consequently a time course experiment was designed, performed and analysed and it is discussed in Chapter 6.

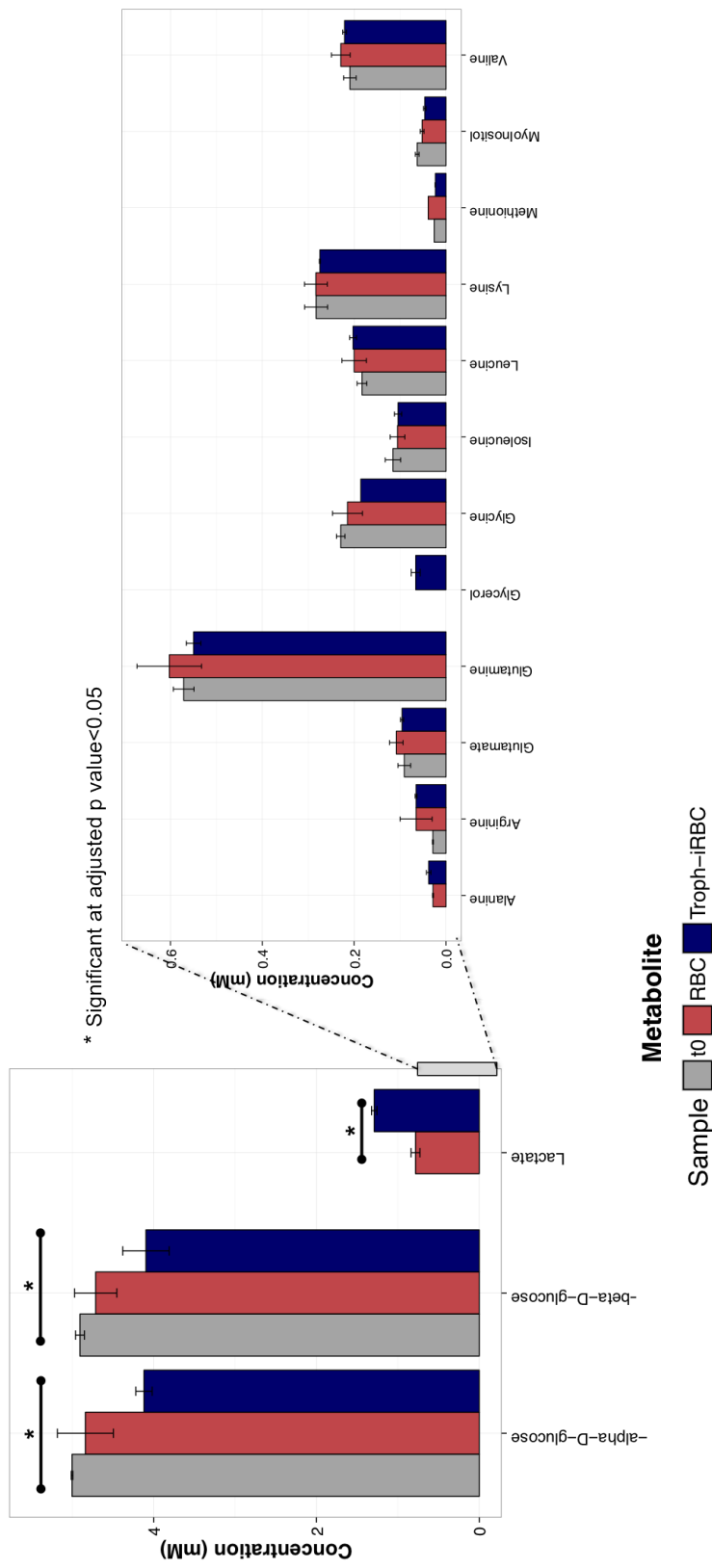


Figure 5.5: **Concentrations of metabolites found in Blood-like media** Measurements pre-incubation with cells (t0) and post 3 h incubation of red blood cells (RBC) or infected RBC with *P. falciparum* 3D7 in trophozoite stage at 12% parasitaemia. Bars represent sample mean, error bars standard error of the mean and asterisks results of statistical test.

5.4 Conclusions

In the last century, many challenges have been overcome in order to achieve continuous cultures of the malaria parasite. However current techniques are all based on the method developed in 1976 by Trager and Jensen [177]. It is a fine method that gives good yields of *Plasmodium* replication, which is valued for experimentation. However, RPMI 1640 based media for *Plasmodium* culture provides unrealistic conditions for the parasite growth [178].

We have developed in-house media at various concentrations of nutrients and shown that parasites growing in more physiological conditions presented different phenotypes and metabolic profiles than parasites growing in typical RPMI 1640. These included a parasite size reduction and proportional decrease of metabolite consumption and excretion, evidence for parasite adaptation to its environment.

Some of the key shortcomings of this work are intrinsic to the *in vitro* culturing limitations. The physiological-like medium used still lacks many of the *in vivo* elements such as the presence of other sources of carbon such as fructose or mannose or molecular signals such as interleukins or interferon. Moreover, this medium still contains buffers such as HEPES and the antibiotic gentamycin to avoid contamination. Future work should be aimed at assessment of the effects these components have on parasite development and reproductive success.

Moreover the results presented in this Chapter suggest that nutritional conditions might have an effect not only on parasite size but also on life cycle duration and progeny numbers. These will be further explored in Chapter 6.

Despite limitations, this work has shown that nutritional conditions play an important role in parasite development and reproduction what emphasizes the need to move towards more physiological culturing techniques in which the human host conditions are mimicked in order to achieve more realistic *in vitro* results that could be easily translated into the field.

Chapter 6

Developmental and metabolic consequences of nutrient availability in intra-erythrocytic stages of *Plasmodium falciparum*

6.1 Introduction: The role of metabolites beyond pathways intermediates

Millions of pounds are invested every year in nutritional studies seeking the perfect diet for *Homo sapiens*. Studying harmful or beneficial diet types with respect to disease [301], development [302], ageing [303] and offspring bearing [304] has consistently been a crucial research goal in the scientific community. Translatable to the mammalian research models *Mus musculus* and *Rattus norvegicus*, there are numerous studies on the effects on lipid-content diets and feeding frequency on the growth of rats [305], weight gaining in relation to tumorigenesis [306] or maternal malnutrition on organ development [307] amongst others.

However, diet or usual nutritional availability is a non-genetic factor that together with others such as environmental toxins or body weight modulate gene expression through epigenetic signalling [308]. These factors are not isolated compartments that can regulate the body response to health and disease, they are both influenced and can influence the gut microbiome through the production of metabo-

lites such as folate, butyrate, biotin and acetate [309]. For instance butyrate can activate epigenetically silenced genes in cancer cells [310] and has also been shown to repress angiogenesis [311].

The importance of metabolites as regulatory molecules either as precursors of other molecules, or as triggers of signalling processes is present across the Kingdoms. For example the female seahorse, *Hippocampus kuda*, fed a diet enriched in fatty acids produces larger eggs with a higher content of polyunsaturated fatty acids [312], which results in higher survival and growth rates of the offspring. Another example is the response to nutrient deprivation of yeast by inducing autophagy. This response can be inhibited by the metabolites methionine and S-adenosylmethionine [313].

Metabolites have then a major role to play in regulation. As discussed above, their importance is highlighted in species such as *M. musculus* or *Saccharomyces cerevisiae*, both of which have also very strong responses to the environment at the transcriptional level. However, evidence based on nuclear architecture and transcriptomic stage specificity suggest that *Plasmodium* might have low transcriptional response to stimuli and providing that the key to evolutionary success relies on the ability to rapidly adapt to a changing environment, metabolites are likely to play a crucial role in the malaria parasite regulation. In *Plasmodium*, chromatin loosens after erythrocyte invasion and stays unpacked (genome-wide) until moments prior the next cycle [314, 315, 316]. Transcription is tightly regulated in order to successfully result in parasite development into the next generation. The parasite has evolved an extremely specialised transcriptional regulation process that expresses genes in order, first cellular processes and then *Plasmodium*-specific functionalities. The asexual development of *P. falciparum* is directed by a cascade of gene regulation similar to a “just-in-time” factory, where a specific gene is induced only once per cycle and only when it is required [317]. Eukaryotic growth control is regulated by various mechanisms. Most eukaryotes express the signalling protein TOR (Target of Rapamycin) that functions as a regulator promoting growth when in favourable conditions [318]. TOR is also negatively regulated by unfavourable environmental stimuli, such as starvation [319]. However, genome sequence data indicates that TOR is absent in *Plasmodium* [320]. Another growth regulatory mechanism in eukaryotes is through the initiation factor 2- α (eIF2 α) which mediates an adaptive transcriptional response to nutrient deprivation by inhibiting translation, which results in growth inhibition [321]. Orthologs of eIF2 α have been found in the asexual stages of *Plasmodium*, with a role in amino acid starvation sensing (GCN2 [322, 323]). However, orthologues of the downstream effectors from GCN2 have not yet been found. [232]. Thus, *Plasmodium* which is already deficient in regulatory transcrip-

tions factors [324] and does not present either TOR or the eIF2 α , likely relies on other mechanisms to respond to the changing environment. This transcriptional rigidity is manifested in cases in which the parasite does not show a significant transcriptional difference during relevant exposure times to drugs, such as antifolates or T4 [325, 326]. In this instance, the parasite failed to mount protective transcriptional responses in time but was able to adapt to longer exposure times to the drugs [325]. A further example includes the temporary arrest of the growth of ring stage *P. falciparum* (dormancy) after artemisinin exposure [285]. Parasite control of growth has also been explored in studies of amino acid starvation, particularly of isoleucine (Ile), for which the parasite is auxotrophic. When isoleucine cannot be scavenged from the culture medium during the ring asexual stage, *P. falciparum* growth is arrested in trophozoite stage with no noticeable phenotypic changes for up to 72 h and is later resumed if the amino acid is supplemented [232]. Even though phosphorylation of eIF2 α was observed under Ile deprivation, knock-out clones showed the same phenotype, further confirming the lack of involvement of this pathway in *Plasmodium* growth adaptation to the environment.

Mechanisms of environmental response might then involve post-transcriptional modifications [327] or epigenetic mechanisms (which would be dependent on nutrients and thus metabolic response). Post-translational modifications play an important role in regulation, but the relatively unexplored metabolic driven epigenetic modifications might be the key to environmentally triggered responses. It has been recently shown that epigenetic modifications play a major role in gene expression regulation [328]. Moreover, epigenetic regulation is believed to be involved in the nutrient uptake regulation and response to stress through the control of the genes *clag3* [176, 174, 171]. The effect that nutrient availability has in metabolic rewiring has not yet been explored in *P. falciparum*.

Metabolomic studies have proved useful in unravelling the metabolic make-up of the malaria parasite, which has been object of research, discussion and debate in the last decade. Briefly, summarising from Chapter 3, Section 1, *P. falciparum* metabolism during its asexual stages presents a high glycolytic flux, increasing the glucose uptake 50-100 \times with respect to the uninfected red blood cell [290]. However the glycolytic product pyruvate does not follow canonical metabolism into acetyl coenzyme A (acetyl-CoA) into the mitochondria to enter the Krebs cycle. Pyruvate is mostly fermented into lactic acid that is excreted [102]. There is a small flux of pyruvate that is converted into acetyl-CoA and that follows metabolism in the Krebs cycle [103]. This is a recent finding after controversy against the nature of the Krebs cycle in *Plasmodium* resulted in the retraction of a publication in *Nature*

which described the *Plasmodium* Krebs cycle as being bifurcated [104]. The Krebs cycle has always been a questionable element in the biochemistry of the parasite. During the asexual stages there is almost no flux into it; however, this is opposite during the asexual stages where a programmed remodeling of central carbon metabolism is observed [103] and which might be related to parasite survival in the mosquito vector. The pyruvate dehydrogenase (PDH) is localised in the apicoplast and as such cannot contribute to the mitochondrial acetyl-CoA and its consequent incorporation in the Krebs cycle. However a branch chain ketoacid dehydrogenase (BCKDH), with PDH activity, contributes to acetyl-CoA entering the Krebs cycle [105]. Other peculiarities of the central carbon metabolism of the malaria parasite include the production and excretion of glycerol [81] and alanine. We have reviewed extensively the central carbon metabolism of the asexual stages of *P.falciparum* [111] and hypothesised that a high glycolytic flux supports the rapid proliferation that occurs in each life cycle in which one merozoite can infect an erythrocyte and grow to produce up to 36 daughter cells. Deregulated glycolytic activity coupled with impaired mitochondrial metabolism is a metabolic strategy to generate glycolytic intermediates essential for rapid biomass generation for schizogony. We also hypothesised that metabolism may be causal and can trigger events that lead to changes in development. Thus we wanted to change the *in vitro* conditions of *P.falciparum* to assess how the parasite adapts to the environment and whether there is a metabolic rewiring to do so.

Aims To further study our hypotheses and contextualise them with the findings presented in Chapters 4 and 5, we designed an experiment to test: (a) whether parasites growing in different nutritional conditions present phenotypic and metabolic differences during all the asexual life cycle (ring stages included); (b) whether parasites growing in physiological media (blood-like media, BL) present not only morphological differences but also a reduced number of daughter cells; (c) whether *P.falciparum* adapts and grows in low glucose conditions *in vitro*; (d) the impact on glucose availability by comparing parasites growing in a low-glucose blood-like media (LG) with BL; (e) assess the rates of consumption and excretion of the main metabolites in culture media and (f) potentially identify metabolites that might play a role as signals for adaptation to stimuli.

6.2 Experimental

The experiment consisted of exposure of highly synchronous cultures of *P. falciparum* 3D7 to different nutritional conditions namely: complete medium (CM, pictured in red in future graphical representations), blood-like medium (BL, pictured in green in future graphical representations) and low-glucose blood-like medium (LG, pictured in yellow in future graphical representations) prepared according to Section 2.4 in Chapter 2. Parasites were synchronised in consecutive life-cycles (as in Section 2.3 of Chapter 2) and 45 h after the second synchronisation step parasites were pooled together and split into 9 flasks, triplicates of the above-mentioned media. Parasites were incubated for a life cycle prior to sampling. This took a total of 45 h, which is the estimated 3D7 life cycle length with entry into schizogony at approximately 32 h [227]. At time 0 (equivalent to 45h post incubation) samples were taken every 3 hours. At each time point, flasks were mixed and a 1.2 mL aliquot was taken in an Eppendorf. The tube was centrifuged at 13000g for 2 minutes and supernatant was used for NMR metabolomics, while cell pellets were used for imaging.

6.2.1 NMR metabolomics

1.2 mL of supernatant were transferred to a tube containing 2.5 mM 3-(trimethylsilyl)-2,2',3,3'-tetradeuteriopropionic acid (TSP) which was immediately frozen. Samples were freeze-dried and kept at -80 °C until NMR spectroscopy analysis when samples were resuspended in 300 μ L of deuteriumoxide and 280 μ L of solution was transferred to a 3 mm NMR tube. 1D ^1H and 2D $^{13}\text{C}^1\text{H}$ spectra were acquired in a Bruker 600 MHz spectrometer, as described in Chapter 2, Section 2.7.2.

1D spectra 1D spectra were uniformly bucketed, this process consists of dividing the spectra into equally size intervals (in this case, intervals of 0.05 ppm) and calculating the area under the curve. Each bucket was scaled by the TSP, and water signal (between 3.6 and 4.8 ppm) were ignored.

2D spectra 2D spectra were inputted in the Collaborative Computing Project for NMR (CcpNmr Analysis) software where peaks of previously identified metabolites were selected and their height and volume were calculated. These data were exported and imputed in R, where each peak of each metabolite was normalised by the TSP signal and adequate nomenclature was assigned to it. Then by using the calibration curves described in Chapter 3, concentrations were calculated and means for each treatment and time point calculated as well as the standard errors. Results of

these and further analysis are presented in Section 6.3.3. Datasets are provided in Appendix A, Table A.7 and their statistical analyses are detailed in Chapter 2, Section 2.10 and in the Results and Discussion section below.

6.2.2 Imaging

Cell pellets were used for microscopy: (a) 5 μL were used to prepare a smear on a slide which was fixed with methanol and stained in Giemsa (Section 2.2.3.1, Chapter 2) and analysed as previously described in Section 5.2.2 of Chapter 5 (b) 2 μL were used to prepare a sample for the Operetta analysis described in Chapter 2 Section 2.8.1. High Content Imaging (HCI) was used to identify the overall growth pattern and to select a few interesting time points that were also analysed quantitatively by bright field microscopy to confirm phenotypes and further assess size.

Metabolite analyses were used to shed light into the biological adaptation to the conditions. Results, data analyses and interpretation are discussed below.

6.3 Results and discussion

6.3.1 Characterisation of parasite growth phenotypes in response to nutrient availability using HCI

HCI is the application of automated microscopy and image analysis to cell biology (and/or drug discovery). HCI is widely used to screen antimalarial drugs [329, 330, 331] and there are sophisticated methods for identification of parasite viability and quantification by HCI [332]. In this particular case, HCI was used with the aim to identify the dominant population size of parasites at each sampling point and compare these findings between treatments in a robust way. It was also used with the aim to identify key time points to also be analysed by bright field microscopy. Details on the methods are described in section 2.8.1 of Chapter 2.

6.3.1.1 Nature of the dyes and limitations of their binding

The chosen dyes for this study were Hoechst 33342 and tetramethyl-rhodamine-ethyl-ester (TMRE). Hoechst is a cell-permeant nucleic acid stain that emits blue fluorescence when it binds double stranded deoxyribonucleic acid (dsDNA). The rhodamine derivative TMRE is a cell-permeant, cationic, red-orange fluorescent dye that accumulates inside energised membranes, typically mitochondria. However in *P. falciparum*, a strong fluorescence signal can also be observed from the parasite

cytosol due to the high membrane potential of the parasite [246]. Mitochondrion-only signals can be obtained by depolarisation of the plasma membrane potential by addition of V-type H⁺ ATPase inhibitors [333]. For this experiment TMRE was used to assess overall parasite size with some limitations. TMRE is excluded from the parasite's food vacuole where the haem crystal produced upon digestion of haemoglobin (hemozoin) is stored (shown in Figure 6.1). This affects the size measurement and therefore it is expected to find some discrepancies with absolute size measured by bright field microscopy.

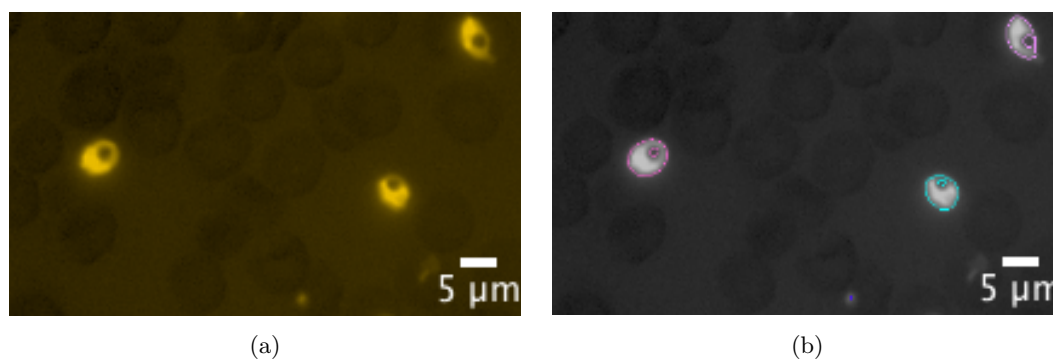


Figure 6.1: **TMRE stained *P. falciparum* trophozoite infected erythrocytes.** (a) Area bound by TMRE; (b) Selected Area for analysis. Note that the area correspondent to the hemozoin is not stained (a) and therefore is not taken into account in the selection process (b).

6.3.1.2 Data filtering and analysis

At each time point a set of 9 samples were stained and plated in a Cell Carrier-384 black plate (with optically clear bottom). To avoid position bias, samples were plated alternatively: CM, BL, LG, CM, BL, LG, CM, BL and LG. Images were acquired per channel and converted into quantitative data as described in Chapter 2 Section 2.8.1 in the Perkin Elmer software Harmony v3.5. Briefly, we used an algorithm that identifies regions that have a greater fluorescent intensity than the background and constraints those regions found to be within size and shape boundaries typical of red blood cells. Intensity cut-offs were used to discard signals that were significantly higher than the average maximum of any parasite.

Data from each channel (TMRE and Hoechst) were extracted as a text file and another phase of filtering was implemented in R (version 3.2.1). In this second phase, the data for both channels for all the time points was joined, and each time point was labelled with its treatment (CM, BL or LG). Then further size constraints

were implemented by establishing cut off ranges between 3.2-30 μm and 1.2 and 10 μm for TMRE and Hoechst data respectively. These cut off ranges were estimated by the minimum calculated from the area of 50 parasites known to be in early stages and maximum of 50 known to be in late stages of development, thus reducing the window to the possible biggest and smallest parasites. Then, erroneous fields were identified and removed from the analysis. In some cases the parameter constraint implemented in Harmony is insufficient to correctly filter all the fields due to the presence of artefacts and therefore those fields have to either be manually corrected or removed from the analysis. In this case I opted for the latter and implemented a program to find fields with a number of particles over the 97 percentile per time point and treatment and remove them from the study. Some examples of rejected fields are shown in Figure 6.2. Finally, for each time point, outliers were removed. For each variable, any points that fell outside the 10 and 90th percentiles were discarded to produce the final dataset. Then plots and statistical analyses were implemented, which are discussed in the next section.

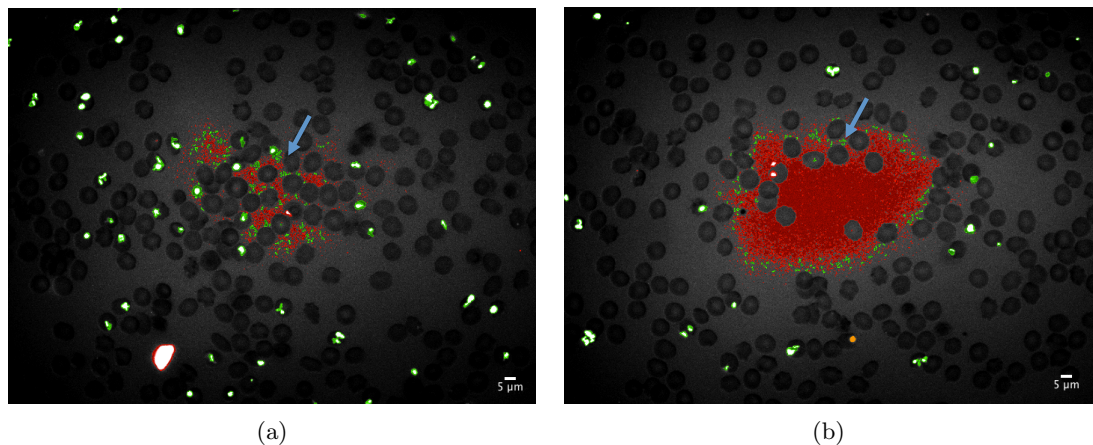


Figure 6.2: **Examples of rejected fields.** Both subfigures show regions selected by Harmony. Regions in green are selected to be retained in the analysis. Regions in red are particles discarded by the parameter implementation. Note the artefacts that are still selected in green in the middle of the picture (pointed by the blue arrow). These were not possible to eliminate using the parameters available in Harmony, thus they were eliminated from further analyses.

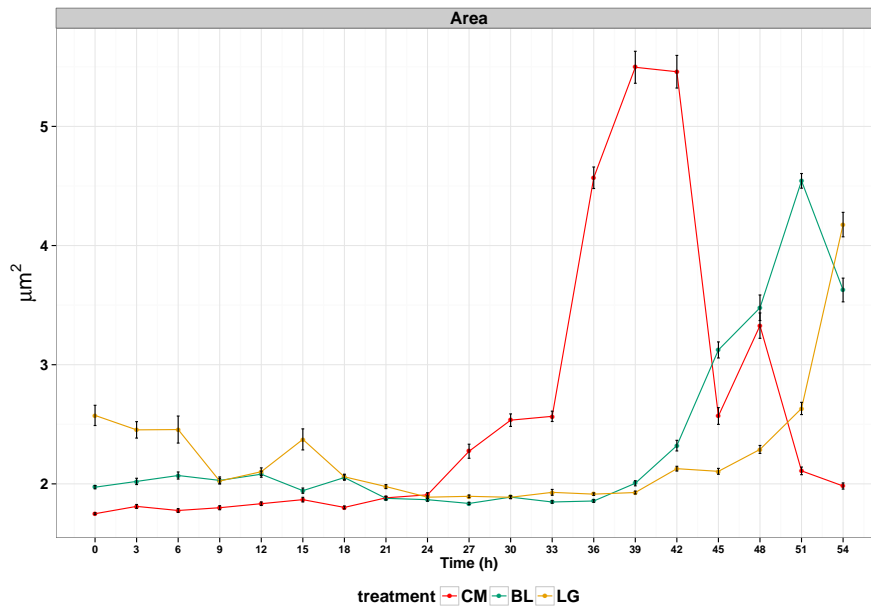
6.3.1.3 HCI showed that nutrient availability affects the duration of the parasite asexual cycle

After implementation of the data filtering process, for each time point and condition, the mean and standard errors of the area were calculated and plotted and are shown

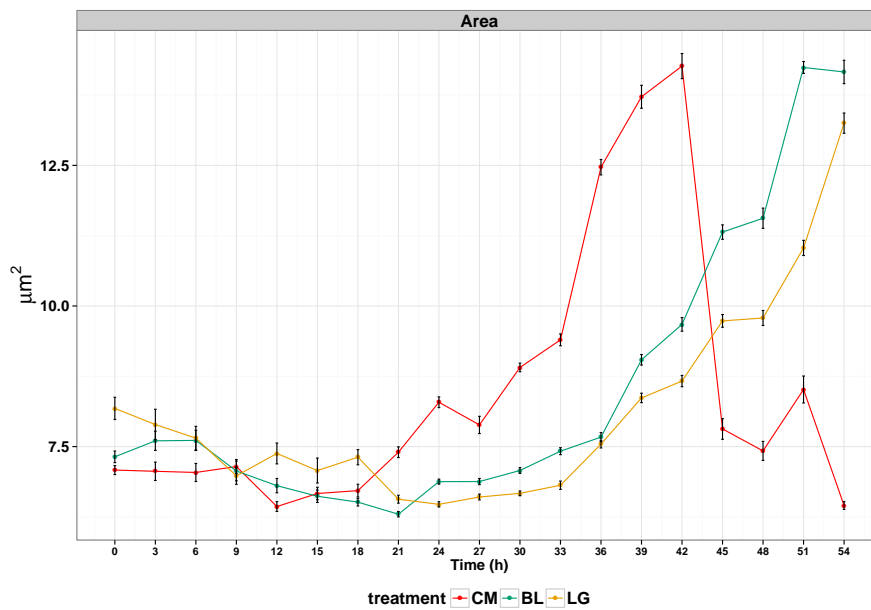
in Figure 6.3. Area in the Hoechst channel, increases with DNA content. Parasite sizes remained relatively constant until they dramatically increased at the time when the schizonts were formed and in the same manner dramatically decreased when new invasions began. Parasites growing in CM started augmenting their nuclei size at 24 h, initially very slightly until at time 39-42 h the maximum nuclei area was observed. Replication occurs in asynchronous rounds of mitosis [64], usually leading to uneven number of merozoites [334]. In times 24-36 h most of the population was in trophozoite stage but some of the parasites started showing schizogony, contributing to the increase in size. By the time most of the population reached schizogony the maximum nuclei area was observed (39-42 h) and once schizonts started to burst the nuclei area dropped drastically. When comparing this to the other two conditions there seems to be a lag in the process. Parasites growing in BL presented a constant nuclei size until time 39 h when they started to replicate. Similar to CM there is a notable increase at a specific time of the life cycle. In this case this time is 12 h later. Meanwhile CM parasites took 15 hours (24-39 h) to start replicating and reach their maximum nuclei size, BL parasites also took 15 h (39-51 h) but they started the process 12 h later. This delay is very similar for LG parasites, that also seem to start replicating at 39 h, however it seems that the glucose availability massively affects the replication and by the time the experiment was ended at time 54 h, LG parasites were just starting to reach maturity. The availability of glucose impacts the production of nucleic acids by reducing the possible flux towards the pentose-phosphate pathway from glucose-6P and consequent reduction on the amount of nucleic acid produced via phosphoribosyl pyrophosphate (PRPP).

When looking at the parasite area (Figure 6.3 b), the same lag in the life cycle can be observed. Meanwhile CM parasites grew to a maximum in the first 39-42 h, BL parasites show a maximum at times 51 and 54 hours and LG parasites start reaching the maximum by the end of the time course experiment. Given that the only difference between BL and LG is glucose, it and its direct products must be a definitive factor in the progression into the life cycle. However in this case it seems there are no significant size differences in the maximum sizes (between CM and BL parasites, t-test performed with no significant p-values, data not shown). Thus TMRE labelled regions do not differ between CM and BL parasites. However, nuclei areas are of different sizes between treatments and this must influence the overall size of the parasite. BL parasites might be growing larger organelles, such as apicoplast or food vacuole. Another possibility is that the limitations of TMRE binding properties to the parasite (such as lack of hemozoin binding) mask an actual size different between treatments. Further analysis of the bright field microscopy

slides addressed this question (Section 6.3.2).



(a)



(b)

Figure 6.3: *P. falciparum* 3D7 area stained by Hoechst (a) and TMRE (b). Points represent mean values per time point and treatment, bars represent the standard errors and lines join the points to ease interpretation. Parasites growing in CM reach the maximum size at least 9 hours prior to parasites growing in BL or LG. Note that the remarkable decrease in size corresponds to parasites bursting into merozoites. This process is observed in the final two time points for BL but occurs after the time scale shown for LG.

Despite the delay of the life cycle, the transitions between the minimum sizes and the maximum sizes seem to be very similar. In order to test whether the growth rates were comparable an analysis of covariance (ANCOVA) was performed. ANCOVA combines features of ANOVA (analysis of variance) and regression. It augments the ANOVA model with more additional quantitative variables (covariates), which are related to the response variable, in this case size measured by area. ANCOVA can be used to compare two or more regression lines by testing the effect of a factor (in this case the three media CM, BL and LG) on a dependent variable (in this case the size of the parasite measured as the area) while controlling for the effect of a continuous co-variable (in this case time). ANCOVA allows us to find out if intercepts and slopes are different between factors. The time points selected for this test were 12 to 42 h for CM, 21 to 51 h for BL and 24 to 54 h for LG. The parameters of the linear model fitted to each treatment are shown in Table 6.1. ANCOVA comparisons of CM-BL, CM-LG and BL-LG were performed and all resulted in not significant p-values (data not shown), indicating that the slope of the regression between time and area is similar for all nutritional conditions. This suggests that there might be a checkpoint in which it is decided whether to progress to schizogony; once the parasite however is committed, the progression will be done in a standard manner.

6.3.2 Bright field microscopy reveals the effect of nutrient availability in cycle length and progeny numbers

At each sampling time, a slide of each flask was made in standard manner (see Section 2.2.3.1 of Chapter 2). All slides were observed under the microscope (100X lens, oil immersion) and photographs were taken at times 0, 12, 24, 36, 48, 51 and 54 h. The maximum growth time points, as revealed by the HCI analysis (42, 48, 51 and 54 h) were used for quantification. Photographs of at least 30 parasites per time point and treatment were taken and areas were measured in Fiji (Image J) as described in Section 2 of Chapter 4. Data was then cleaned by removing outliers

Table 6.1: TMRE area linear model parameters

Treatment	Times	Slope	Intercept
CM	12-42 h	0.270	1.986
BL	21-51 h	0.238	0.342
LG	24-54 h	0.206	0.604

(defined as parasites bigger or smaller than 3 standard deviations from the mean) and statistical analyses were performed. Schizonts at the relevant time points were also selected and the merozoites inside were counted. Results are presented below.

6.3.2.1 Nutrient availability determines the duration of the parasite life cycle.

P. falciparum intra-erythrocytic life cycle typically lasts 48 h. However different strains differ on their complete life-cycle times, for example laboratory adapted strain 3D7, has a shorter life cycle of around 45 h [227]. Thus the initial experimental design consisted of 48 h life-cycle monitoring. As expected, CM parasites were already showing early stages of the next generation by 48 h. However BL and LG parasites presented a much delayed life-cycle. At 48 h none of the other treatments presented schizonts, thus the experiment was continued for a further 6 hours. A comparative visualisation of the different life stages at key sampling points is shown in Figure 6.4. Parasites were incubated for 45 h prior to sampling. At sampling time 0 h (equivalent to 45 h incubation), there was already a slight delay in the life cycle of parasites growing in LG. Meanwhile the other treatments showed a vast majority of early trophozoites (rings), LG parasites presented a mixed population of schizonts and rings. At sampling time 12 h all the parasites growing in BL and LG were in ring stage and CM parasites started presenting late trophozoite stage. Parasitaemia, however, was not noticeably different. At 24 h, CM parasites were fully developed trophozoites with clearly defined hemozoin pigments. BL parasites were starting to be trophozoites and hemozoin was just noticeable. LG parasites were in late ring stages, starting to become trophozoites. At 36 h, CM parasites started presenting some schizonts, with the vast majority of parasites in very late trophozoite stage. BL and LG parasites were in late trophozoite stage. It is noteworthy that these parasites presented a very well defined and larger food vacuole. The food vacuole accumulates undigested haemoglobin. When it is processed, the heme component is converted into hemozoin pigment and the globin is hydrolysed to its constituent amino acids, which are used for protein synthesis [335, 63], to maintain osmotic stability [280, 140] or to provide space for the growing parasite [141]. Phenotypes of swelled food vacuoles are typically observed on parasites subjected to protease inhibitors such as the compound E64 [336]. In this particular case this morphology might suggest an increase in the haemoglobin uptake by parasites growing in lower nutrient availability or a decrease in its degradation, causing accumulation of unprocessed haemoglobin in the food vacuole. This hypothesis is further discussed in Section 6.3.3. As mentioned above at sampling time 48 h, CM parasites presented early rings and schizonts

while BL and LG parasites did not. Three hours later, most of the CM schizonts had ruptured, whilst BL parasites started presenting schizonts and LG did not show signs of schizogony. In the final sampling point (54 h), BL schizonts started bursting while LG parasites started presenting some schizonts.

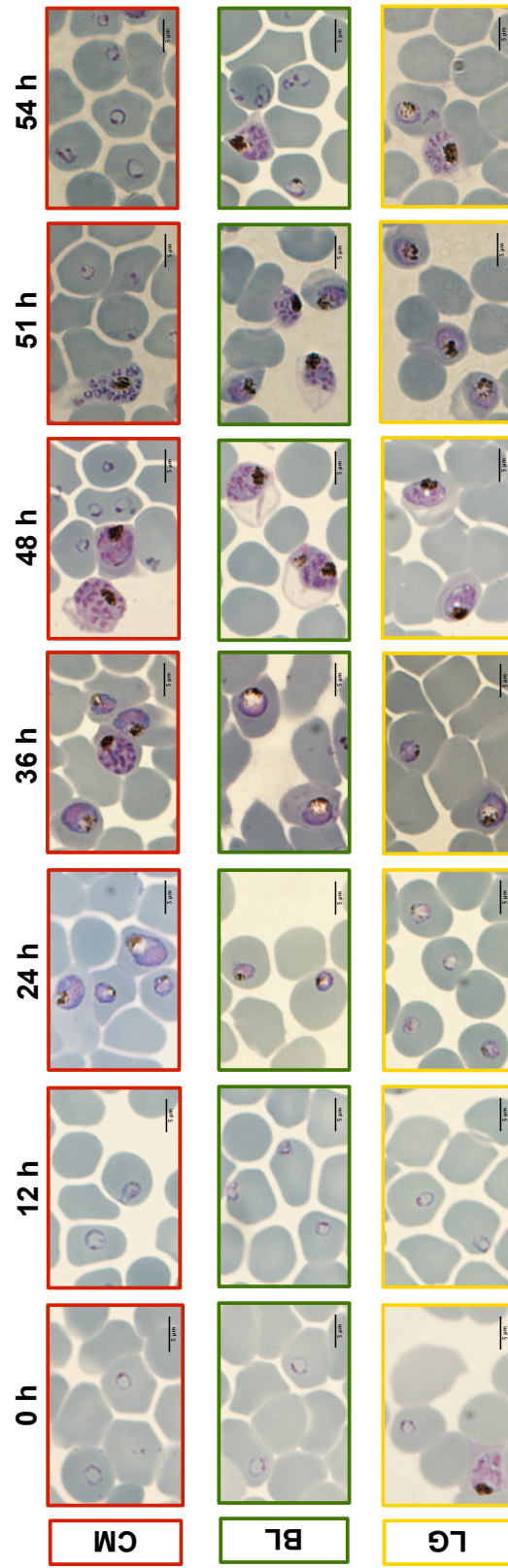
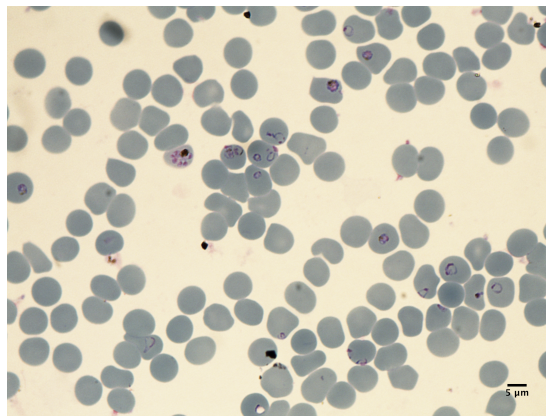
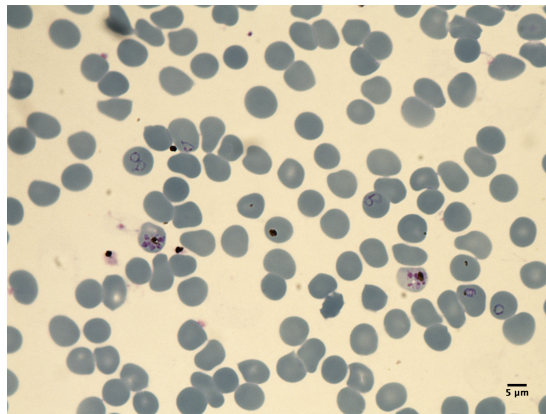


Figure 6.4: **Bright field microscopy images of selected time points.** While CM parasites complete their life cycle within 48 h, BL parasites are just starting to burst by the end of the time course and LG parasites are starting to present some schizonts. Note that the scale in the low left corner represents 5 μm

After the experiment was finished, a subset of BL and LG parasites were kept for a further 20 h to ensure the next generation was viable (Figure 6.5). Overall, compared to CM parasites, BL presented at least 10 h delay in their life cycle while LG parasites were at least 18 h delayed. This emphasises the possible control mechanism that glucose availability has in *P. falciparum*. What is more, after 74 h most of the parasites in the BL and LG cultures were in the ring stage. However, the few schizonts that had not burst yet, presented under 10 merozoites. It is possible that as nutrients were consumed, parasites that were reaching the final stages of development slightly later within the same population would decrease the progeny generated as an adaptation mechanism to the less favourable nutrient conditions.



(a)



(b)

Figure 6.5: *P. falciparum* 3D7 parasites after 119 h incubation (74 h post sampling). (a) BL (b) LG. Most of the parasites were in the ring stage. However some schizonts could still be detected. Overall these schizonts contained under 10 merozoites. Note the 5 μm scale in the bottom right corner.

6.3.2.2 Parasites growing in nutrient-limited conditions are smaller and produce fewer daughter cells

As presented above, HCI and bright field microscopy parasite measurements (Figure 6.4), demonstrated that the parasite life-cycle was delayed in nutrient-limited conditions. However, this is not the only effect observed. HCI measurements further suggested that parasite nuclear area in BL- and LG-grown parasites was smaller than CM-grown. Thus it is reasonable to assume that the resulting number of merozoites produced per schizont may be fewer in BL and LG parasites than in CM. To test this hypothesis, merozoites inside schizonts were counted for the three treatments, sample sizes were 52 for CM, 49 for BL and 22 for LG (due to not many parasites being in this stage by the end of the experiment). Results are shown in Figure 6.6, it is evident that CM parasites were able to produce a bigger progeny than BL and LG parasites. However the latter did not show a major difference with respect to its higher glucose counterpart, suggesting that even though solely glucose has an effect on the life-cycle length, it does not have an effect on progeny numbers. This was further confirmed by Mann-Whitney-Wilcoxon test as shown in Table 6.2.

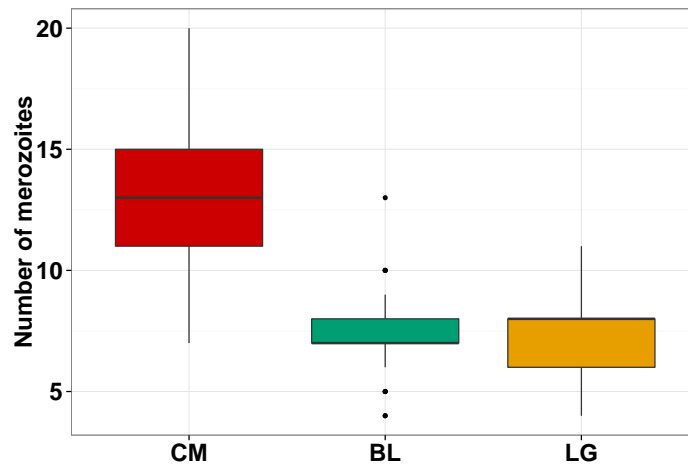


Figure 6.6: **Number of merozoites in schizonts in second generation parasites.** Box plots represent median of the data (black line) contained into the first and third quantiles (box). Segments reach the maximum and minimum value excluding outliers and dots represent outliers.

Bright field imaging was also used to address whether parasites show a difference in overall size. TMRE results from HCI suggested that the maximum size of the parasites across treatments is not that different. However, as discussed above,

Table 6.2: Number of merozoites per schizont. Mann-Whitney-Wilcoxon test results.

Group	Adjusted p-value	Confidence Interval	Significance
CM vs BL	<0.000001	(5,7)	***
CM vs LG	<0.000001	(4,7)	***
BL vs LG	0.6722	(-1,1)	

***Statistically significant at $p < 0.001$

TMRE has some limitations such as the inability to stain hemozoin. Areas of at least 30 parasites per treatment and time point selected were measured (see Figure 6.7) and statistical analyses are shown in Table 6.3. CM parasites are bigger than either BL or LG parasites and BL parasites are slightly bigger than LG parasites. Based on the size differences with respect to HCI, TMRE channel (from 12.5 to up to $23 \mu\text{m}^2$), this size difference must be somehow linked to the consumption of haemoglobin, which based on the size difference revealed by this study and compared with the HCI results, seems to be more avid in CM parasites than in BL or LG and also slightly up in BL than LG parasites. The metabolomics part of this experiment should shed light upon these observations.

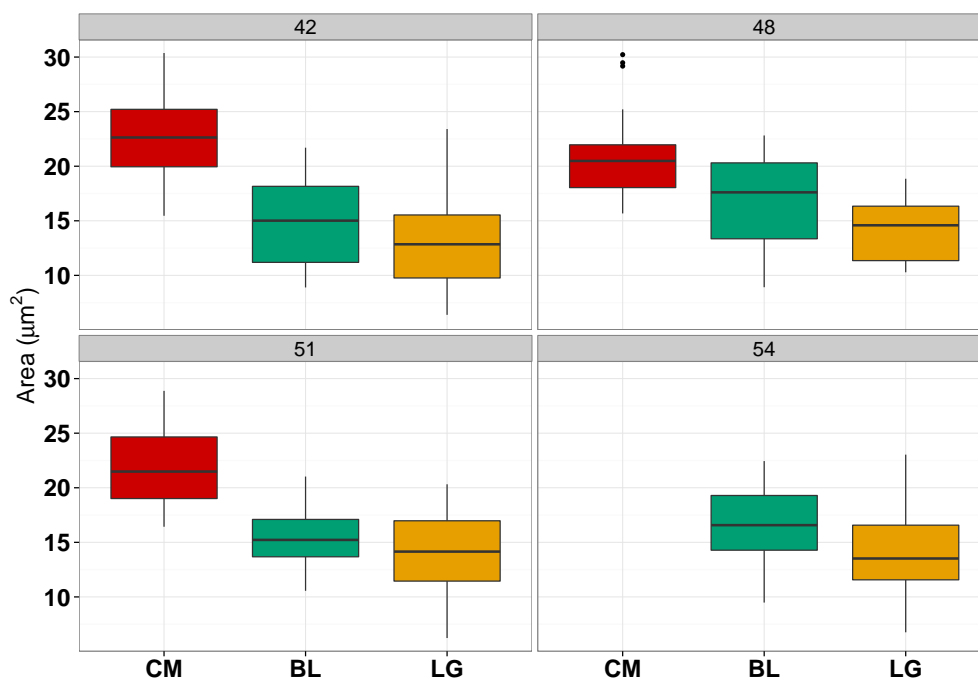


Figure 6.7: **Area of second generation parasites.** Times 42, 48, 51 and 54 h. Note there is no data from second generation CM parasites at time 54 h because the overall population was early rings on the third generation. Box plots represent median of the data (black line) contained into the first and third quartiles (box). Segments reach the maximum and minimum value excluding outliers and dots represent outliers.

6.3.3 NMR metabolomics shows how nutrient availability alters consumption and excretion of metabolites

6.3.3.1 Initial data exploration: Principal Component Analysis

The first step in the data analysis was to use the bucketed data from 1D spectra and perform Principal Component Analysis (PCA) as described in Section 4.3.1 Chapter 4. PCA is a data transformation that produces new variables called Principal Components (PCs), which capture the maximum amount of variance in the data in decreasing order. This effectively “compresses” the information showing most of the information of the data in just a few variables, which is easily visualised. In this case, each bucket was treated as a variable. Prior to PCA, each time point of each condition was normalised by subtracting the signal of media pre-incubation (t_0). Thus, any differences observed must be the product of varying consumption and excretion

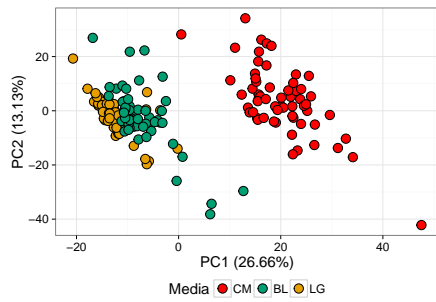
Table 6.3: Area comparison. Mann-Whitney-Wilcoxon test results.

Group	Time [h]	Adjusted p-value	Confidence Interval	Significance
CM vs BL	42	<0.000001	(5.953, 9.491)	***
	48	0.0032	(1.262, 5.748)	**
	51	<0.000001	(4.409, 8.719)	***
CM vs LG	42	<0.000001	(7.946, 11.668)	***
	48	<0.000001	(4.542, 7.868)	***
	51	<0.000001	(5.621, 10.282)	***
BL vs LG	42	0.0205	(0.314, 3.979)	*
	48	0.0018	(1.379, 4.794)	**
	51	0.0806	(-0.242, 2.916)	
	54	0.0020	(1.181, 4.438)	**

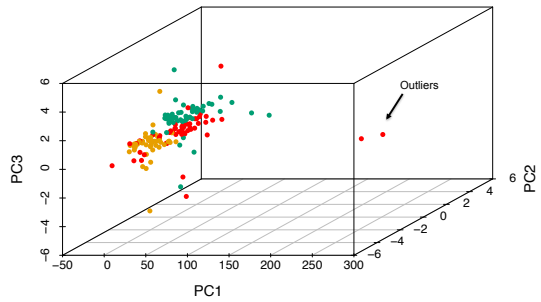
*Statistically significant at $p < 0.05$; **Statistically significant at $p < 0.01$; ***Statistically significant at $p < 0.001$

patterns of metabolites, instead of the known different initial conditions. Graphical analysis of the two first PCs scores resulted in very closely related groups (Figure 6.8 a) and when exploring a third PC (Figure 6.8 b) two outliers were identified. These samples were identified and spectra analysed. These samples had very low signal, probably due to losses of material during the drying procedure. Thus, they were removed from the analysis and PCA was performed again. The score results of the two first PCs showed a dramatic difference between CM media and BL and LG (Figure 6.8 c). When adding a third PC into the plot, the three groups separate without overlap (Figure 6.8 d). These results indicate that the consumption and excretion rates of parasites growing in the different media are different.

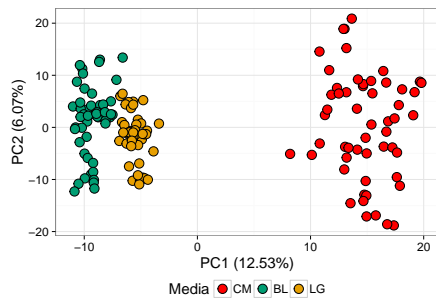
In order to assess which metabolites have a major role in the separation of the groups, the mean metabolite concentrations calculated from the 2D spectra were used to do PCA again (after subtraction of the metabolite concentrations at t_0). Results are shown in Figure 6.9 where (a) presents the score plots of the first two PCs and (b) their loadings. Loadings show the variables that contributed the most to the formation of the PCs, hence the variables that contribute the most to the group separation observed. The amino acids lysine, glycine and valine contribute the most to the separation between CM and both BL and LG. Glucose, lactate, glycerol and alanine contribute somewhat to that separation but they are mostly influencing the separation between samples/time points. Glucose and its products (lactate, alanine and glycerol) were expected to be major contributors to the differences observed due to the important role of glycolysis. However, the main contributors to the separation between conditions were found to be Lysine, Glycine and Valine (Figure 6.9 b).



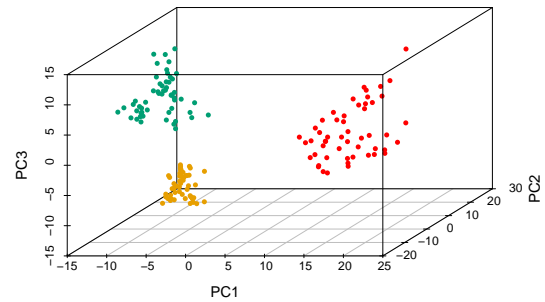
(a)



(b)

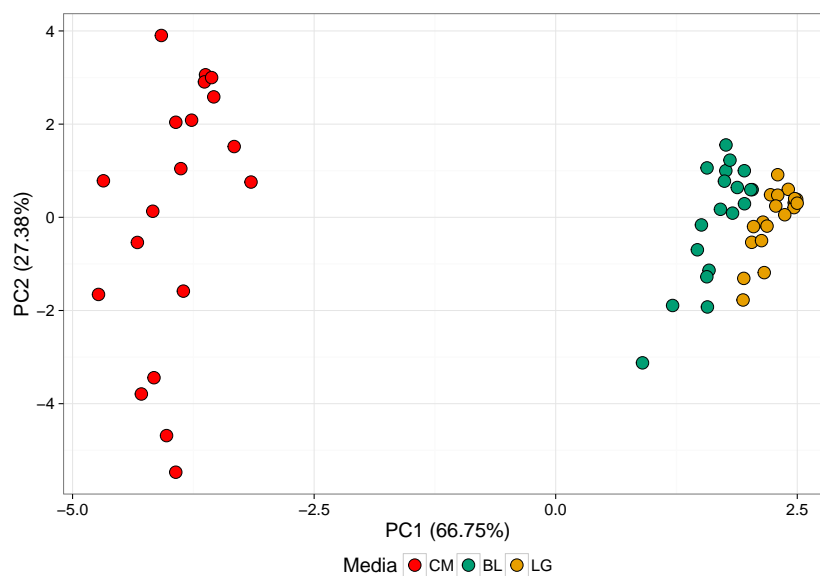


(c)

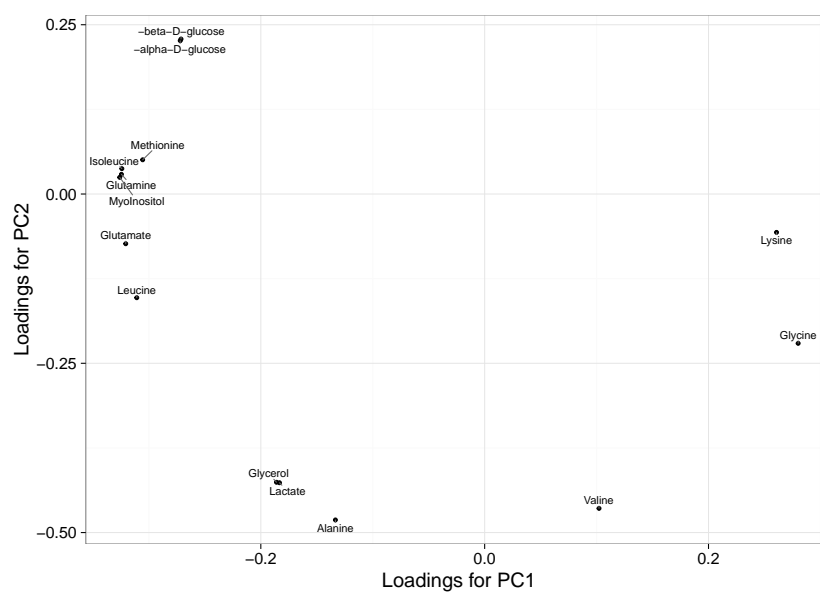


(d)

Figure 6.8: **Principal Component Analysis Score plots from spectra bucket tables.** For each spectra and time point the spectra of media prior experimentation was removed as well as the signal from a sample containing only RBCs in the same conditions. (a) PCA score plot of the first two principal components of the data. Outliers can be identified in the right bottom corner of the plot. These can be further identified in a 3D plot (b, arrow). When outliers are removed, PCA results in a more identifiable separation of the samples between treatments: (c) Two dimensional score plot and (d) Three dimensional score plot.



(a)



(b)

Figure 6.9: **Principal Component Analysis results from means of metabolite concentration in media.** (a) PCA score plot of the first two principal components of the data. Each point represents a spectra. (b) Loading plot from PC1 and PC2. The distance of the metabolites from the main cloud represents how much each influenced in the creation of the new coordinate system of PCs. The metabolites more involved in the separation between treatments are as expected, glycolysis-involved metabolites such as lactate, glucose, glycerol and alanine. However the metabolites glycine, lysine and valine seem to determine most of the separation in the first principal component.

Lysine (K), glycine (G), valine (V) and alanine (A) are, together with leucine (L) and histidine (H), the most abundant amino acids in *H. sapiens* haemoglobin (see Figure 6.10). HCl and bright field imaging data had already suggested an effect on haemoglobin digestion by the different nutritional environments the parasites are growing. PCA results of metabolic readouts further emphasises a role of haemoglobin digestion in the differential phenotype and reduced progeny observed across the treatments BL and LG. In depth study on the changes of concentrations over time is discussed in Section 6.3.3.2.

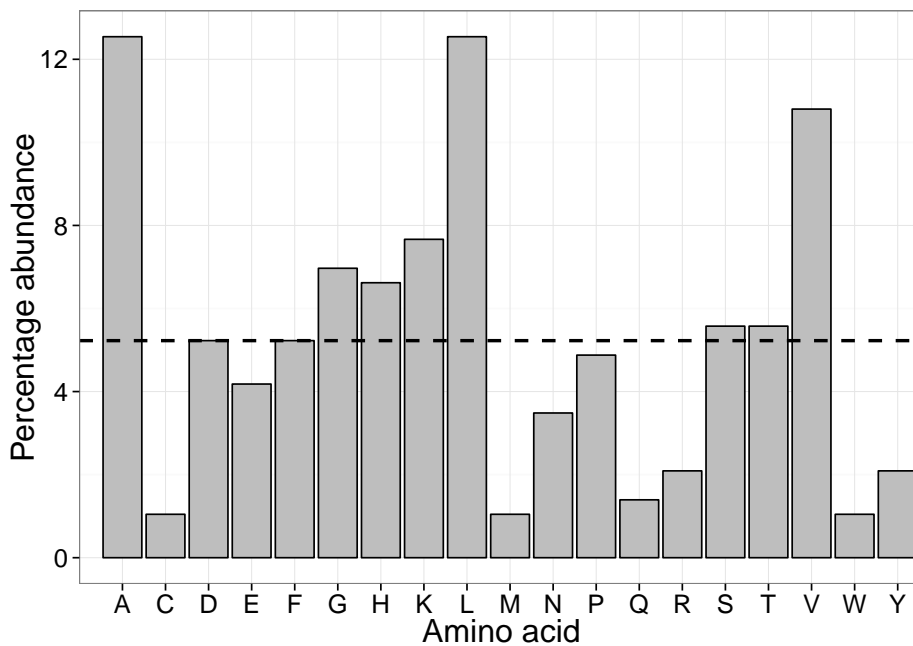


Figure 6.10: **Percentage of amino acid abundance in *H. sapiens* haemoglobin.** Data extracted from the National Centre for Biotechnology Information (NCBI), database protein [337]. Sequences of the four chains of haemoglobin were extracted (T state, oxygen bound at all four haems), collated and the proportion of each amino acid calculated and plotted. Note that the dashed line represents the median of the amino acid abundance percentage and amino acids are represented by their International Union of Pure and Applied Chemistry (IUPAC) symbols.

6.3.3.2 Concentration changes over time under the three nutritional conditions

Intra-erythrocytic asexual stages of *P. falciparum* rely on glucose as fuel for their central carbon metabolism that flows into lactate as final product of fermentation [111]. This, together with other products of glycolysis such as glycerol and alanine

are excreted and their function, if any, is unknown. *P. falciparum* has limited *de novo* synthesis of amino acids and most of them are taken from the haemoglobin. However, not all the amino acids are used up for protein synthesis and fuel [131], they also serve as osmotic regulators [280, 140] and at a specific time they are excreted to leave space to the growing parasite [338, 141]. Here the usual nutrient trafficking of nutrients present in RPMI 1640 is reported and compared with more physiological conditions.

Usual laboratory conditions: CM

Figure 6.11 shows the concentrations over time of the metabolites that were identified and quantified in CM. Every 12 h there was a discontinuity due to media change. The experiment was started when the parasites were early rings and finished when parasites were rings again after a whole life cycle. Of note, we found that RPMI 1640 had a contamination of acetate, which was avidly consumed by the parasites. During the first 24 h, consumption of glucose was markedly more moderated than during the next 24 h. Consequently, the glycolytic excreted end products lactate, glycerol and alanine had a similar behaviour.

Isoleucine, methionine, glutamine, glutamate, cystine and tyrosine are essential amino acids and they must be supplemented in the media for adequate parasite growth (Table I in [128]). Isoleucine is not present in the haemoglobin chain and therefore it is the most essential of the amino acids. Our data shows that consumption started from the early stages but it was much higher in the mature stages of the parasites. Methionine consumption from the media was not required until the mature stages. It is possible that its demand during the early stages might be met by the haemoglobin degradation. Glutamine feeds the glutaminolysis pathway, an important anaplerotic pathway in the central carbon metabolism of the parasite and as such, its consumption remained relatively constant in the early stages but it increased during the mature stages. On the contrary, glutamate remained fairly constant, with a slight tendency for excretion towards the end of the time course.

The most abundant amino acids (refer to Figure 6.10) in haemoglobin; leucine, valine, and glycine and the reasonably abundant serine, were excreted from time 15 h, when the parasites were reaching the mature trophozoite stage and at a time when the New Permeation Pathway (NPP) is known to operate [339]. Alanine is the most abundant amino acid in haemoglobin and its excretion as a glycolytic product might be also joined by excess from haemoglobin degradation. However lysine, which is also very abundant in haemoglobin was consumed even during the mature trophozoite stages. Lysine might play a role in infection regulation. For example,

an increase of pipercolic acid, which is a product from lysine degradation, was found in mice infected with *Plasmodium berghei* [218].

Arginine, as expected, was depleted rapidly as it is known to be taken up and converted into ornithine [195], a phenomenon that causes hypoargininemia in patients and which has been associated with cerebral malaria. Aspartate was also taken up consistently over the parasite life cycle. Aspartate is one of the precursors of pyrimidine biosynthesis via carbamoyl-L-aspartate and therefore essential for parasite replication. Finally, also noteworthy was the dramatic increased intake of myoinositol in the mature stages of the life-cycle. This metabolite is essential for synthesis of phosphatidylinositol (PI), which occurs by either scavenging exogenous myoinositol or *de novo* production. *De novo* myoinositol is made from glucose, via glucose-6P and inositol-3P and it is used to create a pool of PI that is the precursor for free and protein-linked glycosylphosphatidylinositol (GPI) glycolipids [282], which have important roles in host-parasite interactions [340]. Scavenged myoinositol is not used to create PI for glycolipids. It is primarily used for synthesis of bulk PI to serve in membrane architecture.

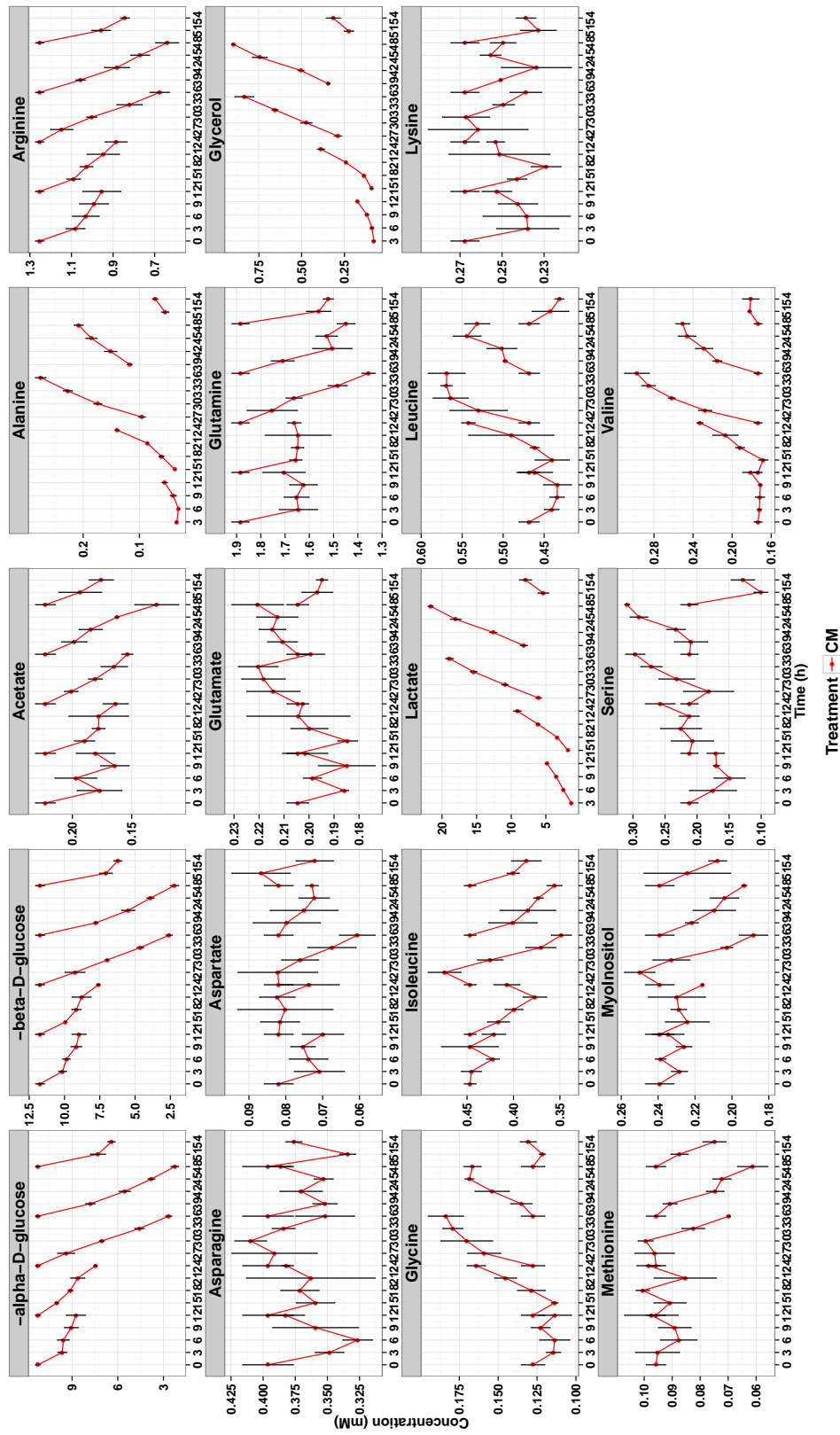


Figure 6.11: Concentration changes over time in complete culture medium containing *P. falciparum* infected RBCs. Points represent the mean value of three replicates and bars the standard error of the mean.

Physiological conditions (BL) and low-glucose physiological conditions (LG)

Analysis of the media from a more physiological nutritional environment (BL) and a low glucose counterpart (LG) provides insight into the importance of glucose as a driver of biomass production. These two conditions only differ in the initial concentration of glucose: 5 mM for BL and 2 mM for LG. After incubation of the parasites in these media, analysis of metabolites was performed, results are shown in Figure 6.12. The amino acids aspartate, asparagine, arginine and serine were found to be under the limit of detection of these media conditions.

Glucose is rapidly consumed over the time course in a similar pattern as for CM parasites; moderately during the young trophozoite stages and more avidly during the mature stages. During the initial life stages, roughly the same amounts of glucose were consumed by BL and LG parasites. It was only in the 36 to 48 h time frame when LG parasites seem to struggle and they almost completely depleted the available glucose. Parallel glycolytic products lactate, glycerol and alanine were excreted following the same patterns. Less during the early stages, more during the late stages of development and proportional to the glucose consumed, being excreted more in BL cultures than in LGs. Another of the main contributors to central carbon metabolism, glutamine is also consumed.

Valine and leucine, some of the most abundant amino acids in haemoglobin, are excreted from time 24 h in the case of BL and time 30 h in the case of LG. Glycine is only excreted in BL and methionine is not excreted. Lysine is used up in both cases and a bit more intensely in BL cultures, however the measurement error is high and no absolute conclusions can be drawn.

Interestingly, myoinositol, although consumed in both BL and LG cultures, is salvaged more in LG cultures. As mentioned in Section 6.3.3.2, *de novo* myoinositol is synthesised from glucose-6P via inositol-3P. If the glucose availability decreases then more myoinositol needs to be scavenged to fulfil the needs of PI for membrane formation and thus the number of daughter cells created might be influenced by the possible amount of membrane the parasites can build from the resources they have.

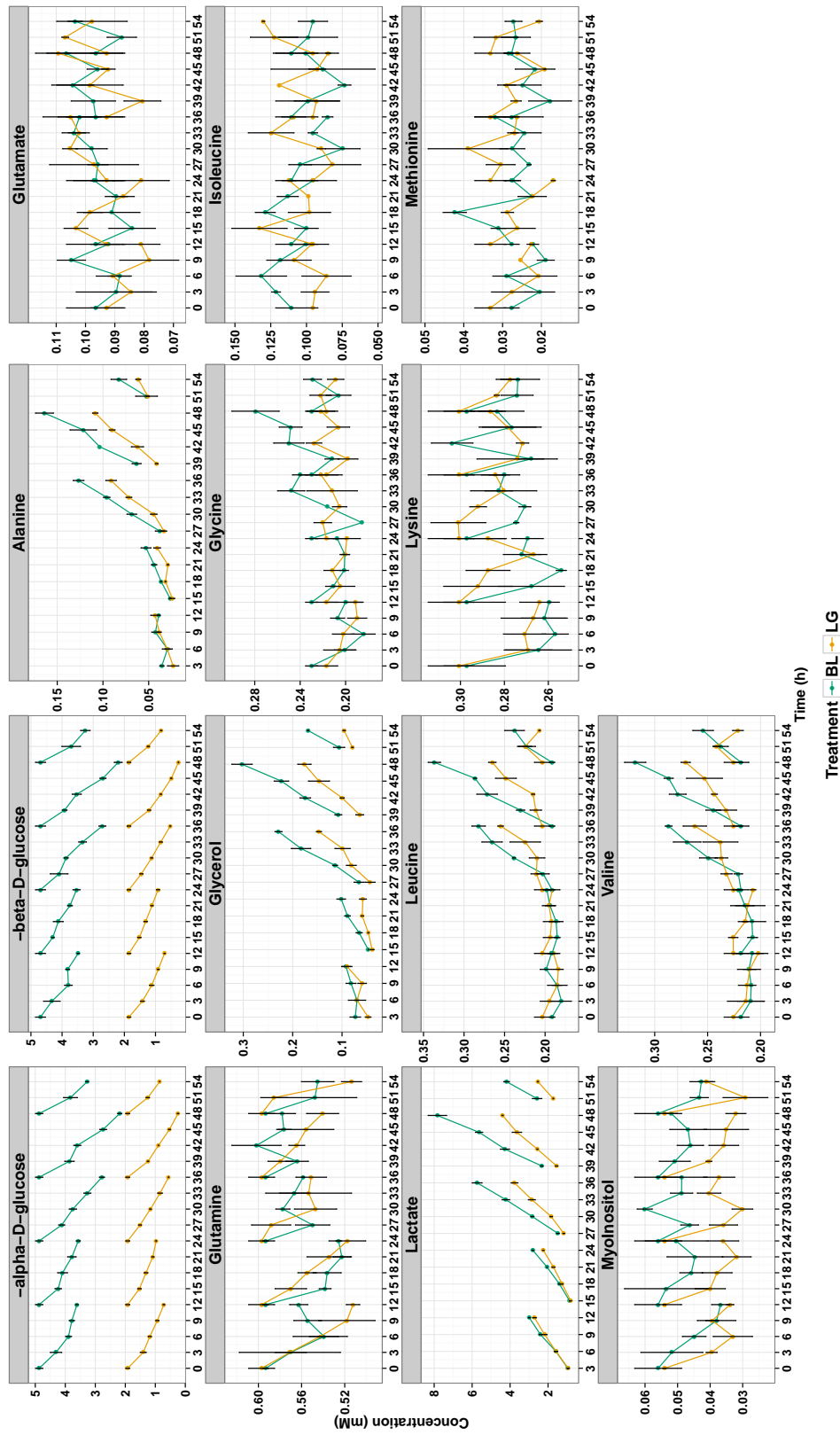


Figure 6.12: Concentration changes in blood-like and low glucose blood-like media containing *P. falciparum* infected RBCs over time. Points represent the mean value of three replicates and bars the standard error of the mean.

An overview of consumption and excretion over all conditions.

The absolute change with respect to the initial conditions was calculated for each time point and treatment in order to compare CM parasites ‘in’ and ‘out’ flux of nutrients with BL and LG parasites (see Figure 6.13). Noticeable is the much vaster glucose amount that they consume. Whilst BL and LG consume similar amounts of glucose in the first 24 hours of development, CM consumes at least $1.5\times$ more. This is dramatically higher during the late trophozoite and schizont stages in all conditions but especially in CM parasites with over 2 times higher glucose consumption than the other conditions. Meanwhile BL parasites consumed only ~ 3 mM (of the 5 available), CM parasites consumed 8 mM within the same interval. Despite more glucose being available, BL parasites did not take more than a certain limit. This can be explained by the kinetics of the transporters, GLUT1 transports glucose into the RBC and has a K_m of 26.2 mM [341], while PfHT has a K_m of 5 mM [83]. In the case of CM parasites the glucose availability was over double the PfHT K_m , thus V_{max} could be reached. The differences of consumption in the early stages between BL and LG parasites were minimal despite the over double glucose availability for BL parasites. The demand of glucose in the late trophozoite stages is larger and it was reflected on the consumption of glucose, far larger in BL conditions (~ 3 mM) and limited in LG parasites (~ 2 mM) which resulted in a further delay in their life cycle. These observations point towards a more complex regulation in which environmental signals on nutrient availability might regulate the influx on glucose into the cell as a mechanism to preserve resources for the next generation. Life cycle delays observed between CM and both BL and LG but also between BL and LG (with no impact in the latter in progeny numbers) suggest the existence of at least one control point that, similarly to the well known check points in mitosis, would serve for the cell to assess integrity and resources in order to proceed to the next generation. This control point seems to be early in the life cycle before the parasite is committed to schizogony.

Glycolytic products alanine, glycerol and lactate were all excreted at proportional rates across treatments. It is worth mentioning that despite the differences in initial conditions, during the ring stages, alanine excretion was similar across treatments. Finally, the amino acids excreted due to haemoglobin degradation showed a big difference between treatments. CM parasites excreted these from time 15 h, meanwhile BL parasites did not start excretion until 24 h and LG until 30 h. These provide reasonable biomarkers for parasite development and commitment to the next generation.

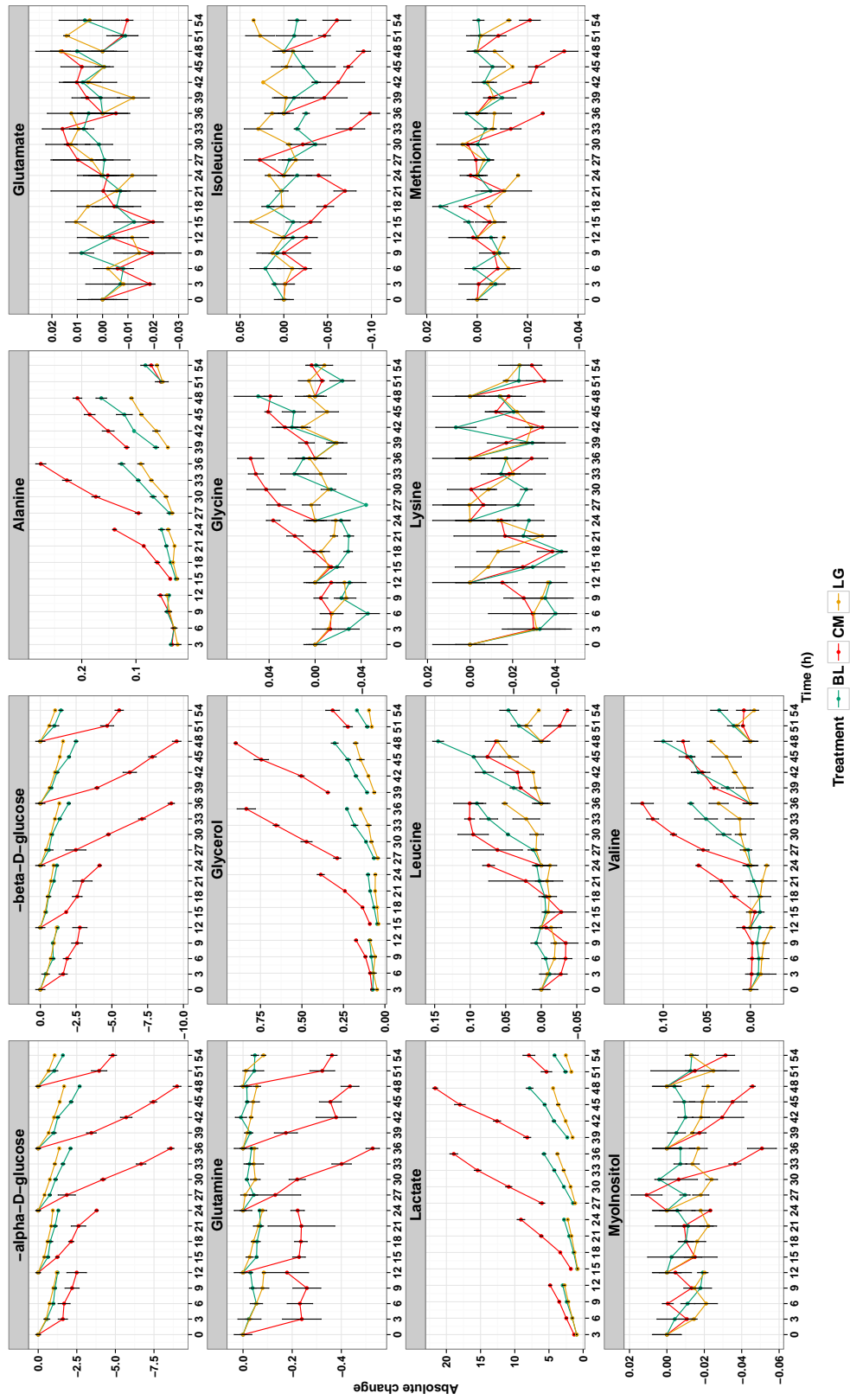


Figure 6.13: Absolute change from the initial conditions over time in all media containing *P. falciparum* infected RBCs.

6.3.3.3 Rates of metabolite consumption and production.

To assess the rate of metabolite consumption and production for the various growth conditions, linear models were fitted to each 12 h interval (see Figure 6.14) and the slopes of each model were used to assess the differences in consumption and excretion of the different metabolites per time interval. These are shown in Figure 6.15. ANCOVA was used to determine whether the slopes (rates) were different between treatments at specific time intervals and results are shown in Table 6.4. Metabolically, not many changes occurred during the first 12 h of the experiment, which coincided with the ring stage. Common to all treatment comparisons was the differential rate of consumption of both α and β -D-glucose with consequential differences in the excretion of lactate, alanine and glycerol. Other expected differences are in valine, leucine and glycine. Valine is also different between BL and LG.

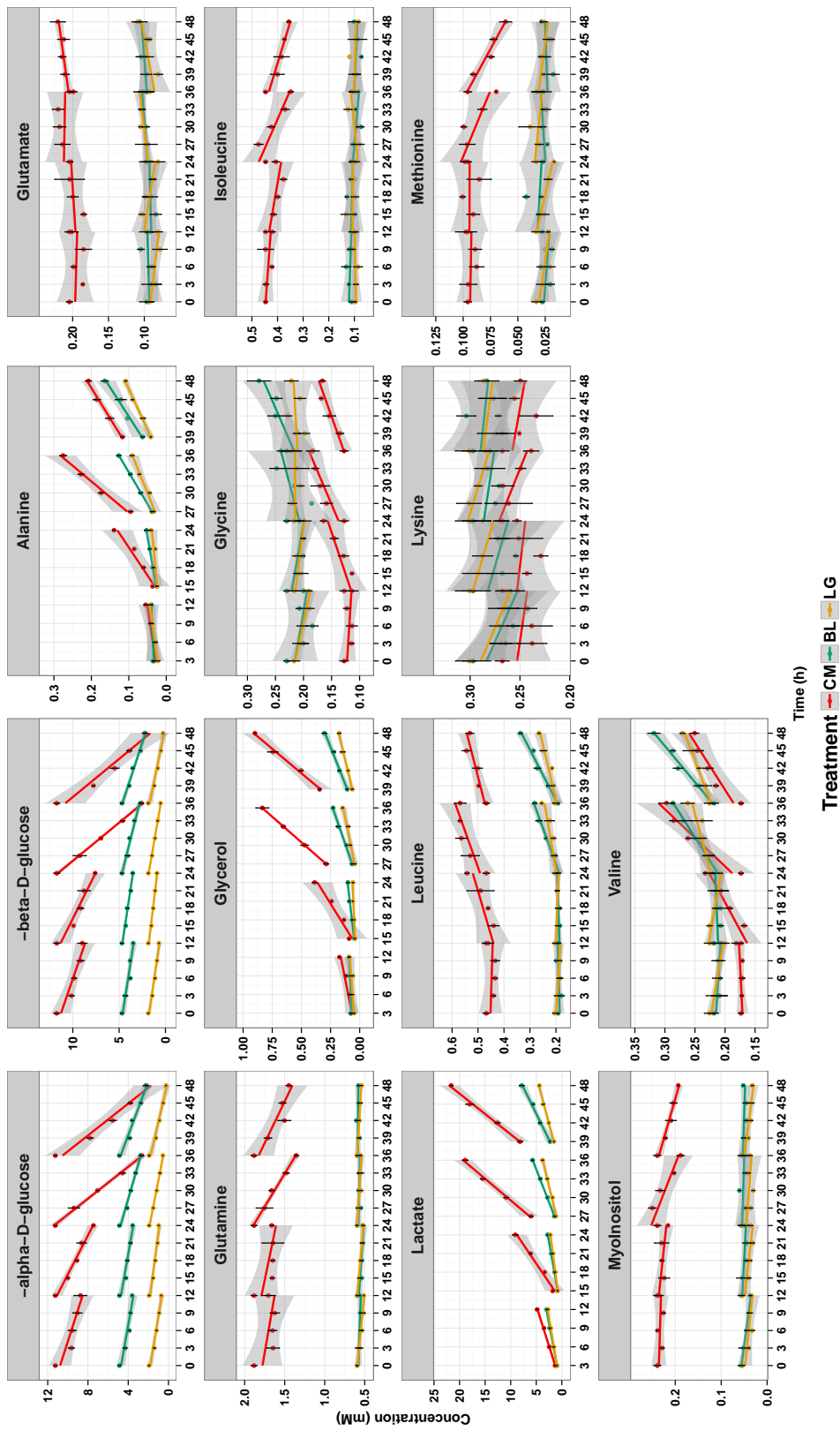


Figure 6.14: **Illustration of the linear models fitted.** Colourful lines represent the linear model fitted and grey areas the 95 % interval. Note that the last interval (48-51 h) had only 2-3 points, thus implementation of a linear model was not suitable and was not performed.

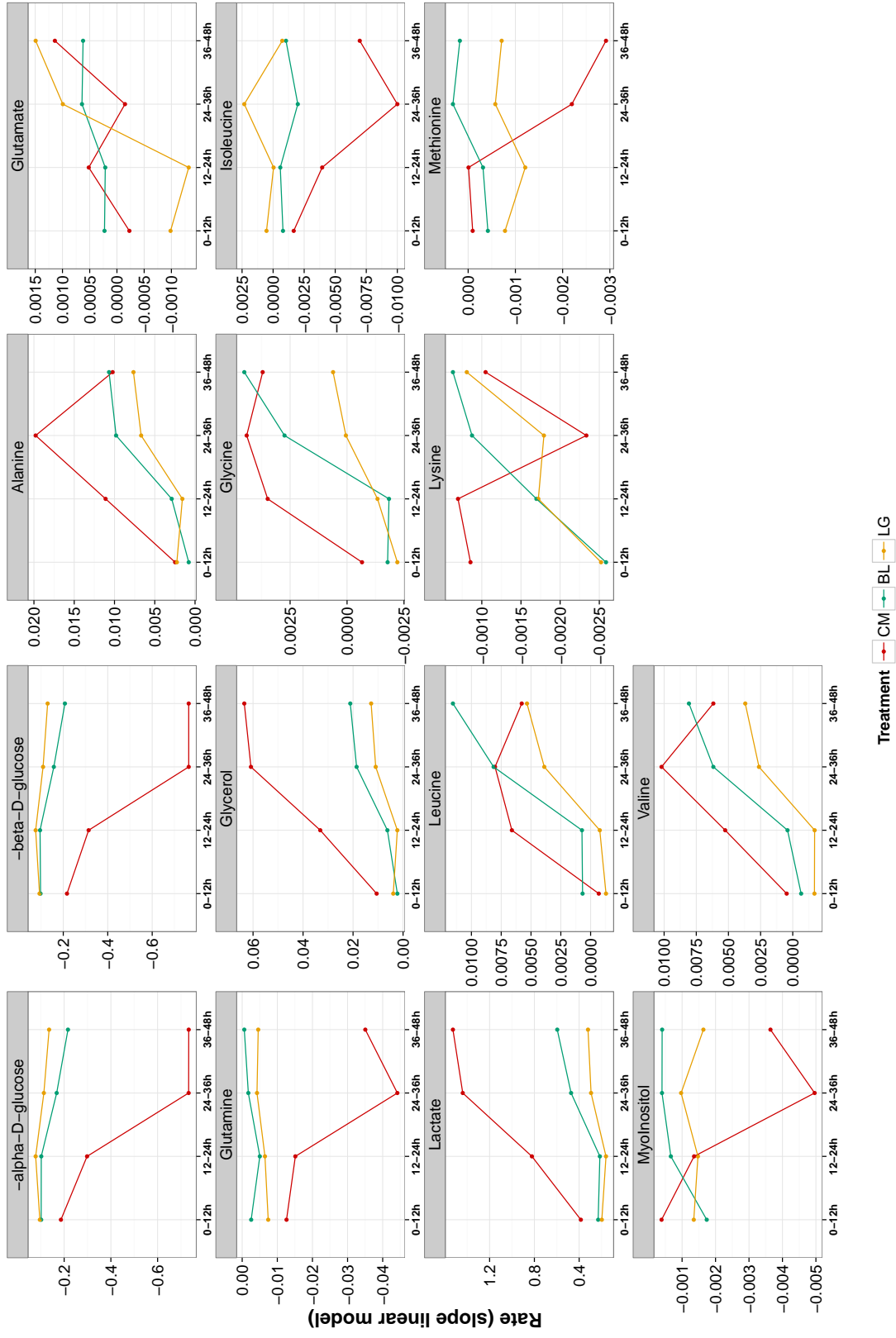


Figure 6.15: Slopes of the linear models. Values are connected by a line to ease interpretation.

Table 6.4: ANCOVA significance values for the comparison of fitted linear model slopes.

Metabolite	0-12 h			12-24 h			24-36 h			36-48 h		
	CM vs BL	CM vs LG	BL vs LG	CM vs BL	CM vs LG	BL vs LG	CM vs BL	CM vs LG	BL vs LG	CM vs BL	CM vs LG	BL vs LG
α -D-glucose	-	-	-	***	***	***	***	***	***	***	***	***
β -D-glucose	-	*	-	**	**	**	***	***	***	**	***	**
Lactate	***	***	*	**	**	*	***	***	***	***	***	**
Alanine	-	**	-	**	**	-	**	**	*	-	**	-
Glutamine	*	-	-	**	**	**	***	***	*	***	***	**
Glycerol	-	-	-	-	-	-	***	***	-	**	*	-
Leucine	-	-	-	-	*	-	*	-	*	*	-	**
Valine	-	**	-	**	***	*	-	**	*	-	**	**
Glycine	-	-	-	*	*	-	-	*	-	-	-	-
Myoinositol	-	-	-	-	-	-	*	*	-	**	*	-
Isoleucine	-	-	-	-	-	-	*	**	-	*	*	-
Methionine	-	-	-	-	-	-	*	-	-	**	**	-

-Not significant *Statistically significant at $p < 0.05$, **Statistically significant at $p < 0.01$; ***Statistically significant at $p < 0.001$;

6.3.3.4 Excreted products per glucose consumed vary with respect to life-stage and treatment.

Despite the adverse nutritional conditions in some of the media, all parasites still produced “wasteful” products (i.e. alanine, glycerol and lactate). Overall, BL and LG parasites had less nutrients available than CM and in comparison less nutrients were consumed and less nutrients were excreted. However, we wanted to explore the proportions of the so named “wasteful” products in relation to the nutrient consumption.

As described in Section 4.3.2 of Chapter 4, calculations were implemented to determine the level of waste produced with respect to the key drivers of the central carbon metabolism (glucose and glutamine) during early and late trophozoites in the differing nutritional environments. The uptake of glucose and glutamine was compared to the level of excretion of lactate, glycerol and alanine in order to determine a percentage of waste production (Figure 6.16). The overall percentage of waste produced increased from early life stages to later ones as in agreement with results shown in Chapter 4. This also fits with the hypothesis presented by Newsholme *et al.* [117] in which they give purpose to the existence of a bifurcated pathway where one branch leads to a product excreted as “waste” and the other results in biomass production. Using this bifurcated pathway, a signal at any time point can shift the pathway from waste production to biomass generation.

Upon comparison of the “waste” to biomass ratios it was observed that “waste” production trend was higher in both BL and LG parasites in the ring stage when compared to CM. This was an unexpected observation as it could be expected that in a limited glucose environment resources would be mostly invested in biomass production as opposed to the production of waste. This might be a consequence of the decrease production of biomass. If less glucose finishes as biomass, then more “waste” is produced. However, it is possible that the “waste” products, specifically lactate, play a crucial extracellular role. Indeed the excretion of these products is dramatically reduced as the parasites enter the sexual stages [342] thus indicating a potential role in human colonisation that should be further investigated.

One of the important extracellular roles undertaken by waste products, is their action as osmolytes. For example, glycerol inhibits water permeation through the aquaglycerolporin (PfAQP) [343] and alanine is a solute commonly used for synchronisation or parasites due to its osmotic selectivity in the early trophozoite stages [344].

As previously highlighted, the metabolism of *P. falciparum* parasites during the asexual intraerythrocytic stages is similar to that observed in cancer cells or

yeast [115]. There is an increased uptake of glucose and an accumulation of lactate, known as the Warburg Effect. In cancer, this occurs even in normoxic conditions thus indicating that the build up is not due to lactate fermentation caused by low oxygen availability [345]. Moreover, lactate has been found to play a crucial role in tumorigenesis, and there is a high degree of malignancy in high-lactate tumors where lactate is responsible for migration of tumor cells and cell clusters, it has antioxidative properties [346] and it contributes to immune escape [347, 348]. Lactate also promotes angiogenesis by inducing secretion of Vascular Endothelial Growth Factor (VEGF) [349, 345, 350].

Furthermore, in tumours containing fermentative and aerobic cells, when glucose is insufficient for both populations, the aerobic cells can uptake lactate through a special transporter and utilise it for oxidative phosphorylation [125, 126]. In samples of patients infected with *P. falciparum* different transcriptional stages have been found, two of them corresponding to either glycolytic metabolism or starvation response accompanied by metabolism of alternative carbon sources [351]. These variations are similar to the ones found in tumours and may affect disease manifestations and treatment.

As *P. falciparum* produces large amounts of lactate even in poor nutritional environments and given not only the success of the malaria parasite but the beneficial effects of high lactate in other disease states, it can be argued that lactate has a function that enhances the generation success of the parasite. Whether it helps the parasite to evade the immune system, reduced oxidative damage and/or increases the parasites ability to spread to uninfected RBCs is unknown but this is an area worth pursuing.

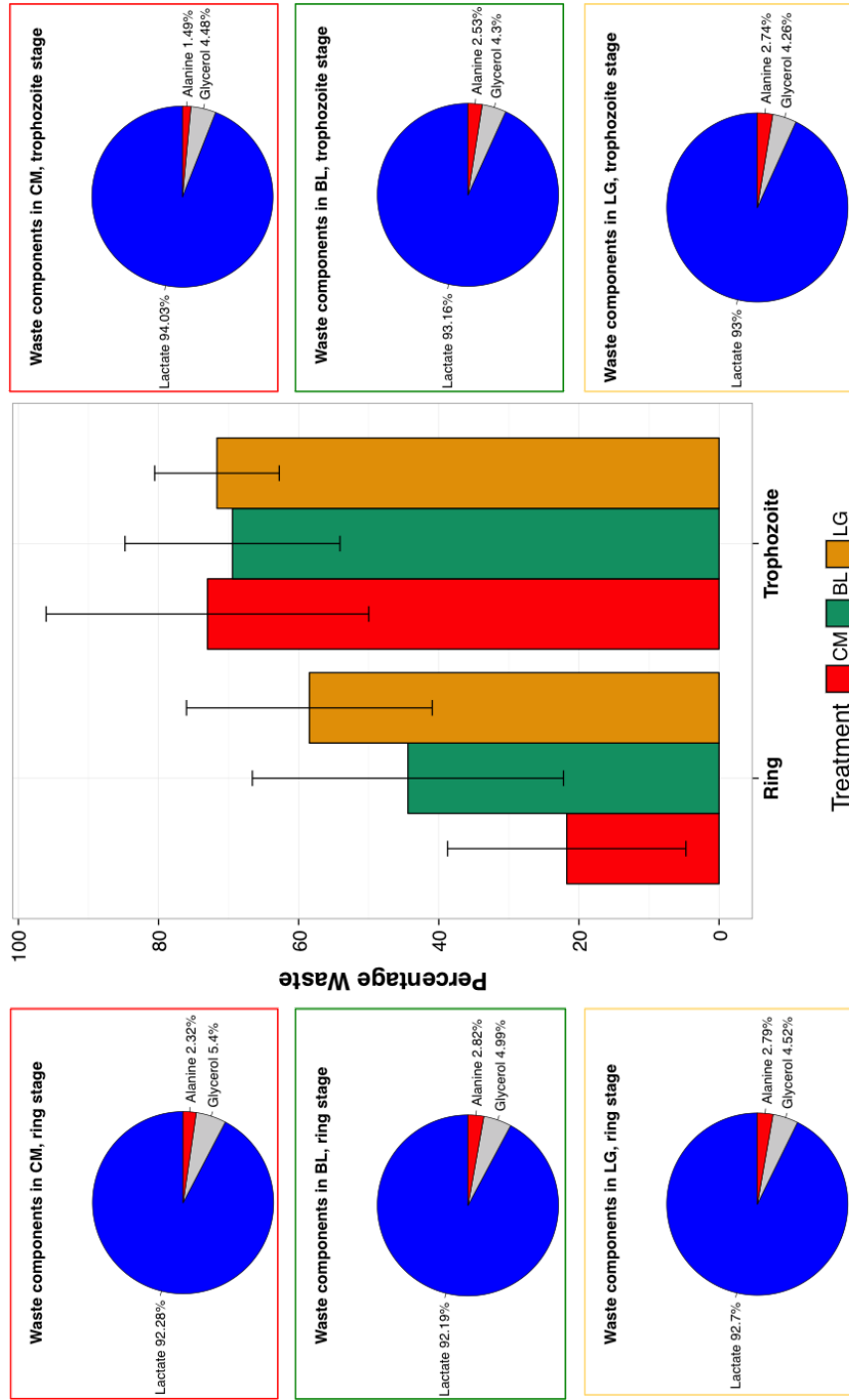


Figure 6.16: **Fold change with respect to first incubation interval.** Percentage of excreted products with respect to glucose and glutamine consumed in the early (ring) and late trophozoite per treatment. Note that the pie charts represent the proportion of each wasteful product to the final contribution. Lactate represents the highest contribution followed by glycerol and alanine.

6.4 Conclusion

In this work we have presented the first study to completely characterise *P. falciparum* life cycle nuclei size, parasite size, merozoite numbers and metabolic uptake and excretion. Moreover, we have followed the effects of nutrient excess and deprivation in all those factors gaining insight into the parasite's ability to adapt to new environments.

By adjusting *in vitro* nutrient availability of *P. falciparum* to a more physiological range, we have altered the life cycle length, the progeny numbers and the rates of consumption and excretion of metabolites. We have found differential rates for metabolite markers of processes such as haemoglobin degradation (leucine, glycine and valine), nucleic acid production (glucose, glutamine and aspartate) and waste excretion (lactate, glycerol, alanine). We have linked these findings with phenotypic traits using image analysis. For example the parasites growing in BL conditions showed more defined vacuole. By further decreasing the glucose availability, the *P. falciparum* life-cycle was further elongated, unveiling the importance of metabolite signalling in growth adaptation.

Furthermore, we have found a modulation of metabolism triggered by nutrient availability that involved the overproduction of daughter cells and shortening of life cycle in parasites growing in usual *in vitro* conditions. This unveils a shortcoming in current experimentation in which pre-clinical tests are done, using parasites that behave and adapt to life conditions far from physiological and where responses to treatment might be compromised. Methodologies that allow for precise determination of the killing rate of antimalarial compounds *in vitro* [352] base results on scrutiny of parasites during periods of several life cycles. Some of the limitations of drug dose predictions may be explained by the different replication rates and life cycle lengths between *in vitro* and *in vivo* conditions. Furthermore the diet differences in animals and humans might also compromise the experimental results used for pharmacokinetic/pharmacodynamic modelling. These models are fitted with data that is mainly acquired using animal models. By further adaptation of experimental *in vitro* methods to physiological conditions, higher translatability between animal and cellular cultures behaviours might allow the reduction of the number of animals used for experimentation.

Future work should focus on the complete characterisation of the effects that each nutrient might have in parasite reproduction. This will shed light not only

on parasite biology and reproduction rates in different conditions but also might highlight essential metabolic processes and signalling pathways that might serve as new drug targets.

Chapter 7

General conclusions

Phenotype equals the effects of genotype and the environment, and for any given parasite its environment is directly determined by its host/s. In order to improve how to diagnose, treat and ultimately eradicate a parasitic disease, the effect that the host (environment) might have upon such organisms has to be studied. The deadliest malaria parasite *Plasmodium falciparum* has been extensively studied *in vitro*. However the conditions used provide the parasite with an environment far from physiological, with nutrients present at concentrations up to an order of magnitude higher than in the human host [178]. The aims of this study were to move a step forward towards complete understanding of *P. falciparum* phenotype by comparing its growth, development and metabolism in more physiological conditions as well as in hypoglycaemic conditions.

Phenotype is perhaps best studied at the metabolome level given that any changes or fluctuations in gene expression, protein modification or environmental signal response have an impact at this level of organisation. Nuclear Magnetic Resonance (NMR) spectroscopy was used to study the metabolic make-up of the parasite. As described in Chapter 3, a method to monitor metabolites in samples containing 10-16% parasitaemia was developed. Some of the shortcomings of this technique involve the lack of freely available and curated tools to identify and quantify metabolites. With help of the open source software CCPNmr [243], the metabolite specific databases HMDB [184] and MQMCD [199] 23 metabolites were identified in *P. falciparum* infected red blood cells (iRBCs). This number is rather low in comparison with other publications in which the software Chenomx [219, 217] or Mass Spectrometry [195, 103] have been used. The limited number of identified metabolites has presented one of the shortcomings of this work, although the current platform allows for expansion. One of the advantages of NMR metabolomics is that standards

do not need to be run with the experiments to be informative. The robustness of the technique allows for spectra to be acquired even in another machine and still be comparable. Spectra acquired for these experiments included both 2D C-H and 1D H spectra. Thus, provided time and resources, further identification of metabolites and confirmation with standards can be achieved. Another shortcoming of the current methodology was that ^{13}C break down could not be tracked. The current NMR parameters used did not allow for discrimination between the proportions of ^{13}C from either natural abundance or artificial labelling. To overcome this problem new experiments can be designed with modified NMR acquisition parameters that would avoid the relaxation interaction between ^{13}C with its consequent masking of signal (see Chapter 3 Section 3.6). Finally, absolute quantification was achieved by using calibration curves. Pipelines to calculate the equations and use them to calculate concentrations from query spectra as well as normalisation, scaling and adequate nomenclature of metabolites were implemented in the software environment R [299]. These can be easily expanded to include more metabolites and can also be customized to suit needs of other experiments thus highlighting the potential of this method.

In Chapter 4 we proved that we could distinguish between infected and non-infected samples using NMR metabolomics and also between parasite life stages. Furthermore we showed we could use the extracellular media to do so. By monitoring culture media samples we studied parasite metabolism with minimal disruption of optimal growing conditions. The establishment of *in vitro* cultures of *Plasmodium* took over half a century [292, 177]. The method is based on the use of RPMI 1640 - a very rich medium with nutrient concentrations far from physiological [178]. To try and investigate the possible response to a more physiological media we developed an *in-house* version of RPMI that presented nutrient concentrations typically found in humans referred to as "blood-like" medium (BL). In Chapter 5 we showed that the viability of the parasites was not compromised by the new medium but phenotype was different, presenting smaller cell size and different intake of nutrients. Some of the shortcomings of this attempt to mimic host conditions rely on the still vast differences with respect to humans as for example the use of pH buffers. The main reason for these concessions is the lack of a suitable chemostat that would allow the growth of *P. falciparum* in continuous culture. Instead parasites are grown in batches which does not allow the dynamic exchange of substrates and waste products, complicating optimisation of some conditions. Future directions should involve the complete optimisation of *P. falciparum* growth in physiological conditions and an attempt to use dynamic culture conditions such as the use of chemostats and

hollow fibre models.

The role of nutrient availability not only in growth but also in regulation was explored in Chapter 6 in which a novel combination of high content imaging, bright field microscopy and NMR metabolomics were used to monitor parasites growing in three types of media: usual RPMI (CM), BL and low glucose BL (LG). *P. falciparum* iRBCs were followed for the duration of the life cycle to assess the rates of nutrient uptake and their role in life cycle control. We observed the metabolic uptake of nutrients and excretion of products by the parasite that was in agreement with the literature with high rates of glucose consumed and large amounts of lactate excreted together with glycerol and alanine. In addition, excretion of some of the most abundant amino acids found in haemoglobin was observed. It has been documented that at a certain developmental stage, the need for space is larger than the demand of certain amino acids and haemoglobin degradation becomes a way to make space for the growing parasite resulting in an excretion of the amino acids that constitute its globular part [140]. Interestingly, despite lysine being one of the most abundant metabolites of haemoglobin, it was not excreted as otherwise leucine, valine and glycine were.

We found that when the laboratory strain 3D7, which has slightly shorter life cycle than field strains (42 to 45 hours), was grown in BL conditions the life cycle was elongated towards more *in vivo* conditions (48 to 51 hours) and the life cycle was further elongated when mimicking hypoglycaemic conditions, emphasising the importance of glucose in parasite development. This was accompanied with a 40% reduction of parasite size and a consequent significant reduction in daughter cell production (up to 50%). Haemoglobin derived amino acids were not excreted until parasite maturity was reached, with a difference of 9 and 15 hours between CM and BL or LG parasites respectively. These metabolites could be used as markers for life cycle progression. Rates of consumption and excretion of most metabolites monitored were different. Including myoinositol, demand for which was much higher in CM parasites, probably due to its role as precursor of phosphatidylinositol, involved in membrane architecture, whose demand must be higher in CM parasites producing a mean of double the amount of daughter cells.

Notably glucose consumption was altered and adapted to the new conditions. Parasites growing in BL did not exhaust the available glucose, which indicated a role for metabolite signalling in parasite adaptation. These have already been posed in the literature with the identification of *clag3* genes whose expression is modulated by nutrient availability through epigenetic modifications [174, 171]. These results further confirmed the effect of nutritional environment in parasite adaptation, re-

production and response, opening a new window of research for future projects. Furthermore, both BL and LG parasites presented a moderate higher proportion of excreted products being produced per molecule of glucose consumed (lactate, glycerol and alanine) during the early developmental stages. This might point to a more important role associated with these, initially considered wasteful, products. For example a beneficial role for lactic acid has already been described in cancer [123] where it has also been shown to inhibit TNF (Tumor Necrosis Factor) secretion of monocytes [353]. It has been recently published that TNF reduces *P. falciparum* parasitaemia in *in vitro* experiments [354], thus indicating a possible role for lactate excretion. Future experimentation should aim to assess the possible protective role that excreted products have to *P. falciparum* development.

This work presents a first, albeit decisive step towards breaching the gap between *in vitro* and *in vivo* experimentation. We have not only shown that parasites growing in different conditions present different phenotype and metabolic fluxes but also that their adaptation to the environment results in different life-cycle's length and multiplication rates. The latter might point towards an important consequence in drug killing rates estimations, which emphasises the need to adapt experimentation of the malaria parasite to more physiological conditions in order to improve the robustness of scientific results and make them more extrapolative to clinical settings. Furthermore, by adapting experimental methods to more nutritional challenging conditions other properties of the infection can be discovered. For example the bacteria *Pseudomonas aeruginosa*, when grown in limited nutrient conditions, is shown to become highly tolerant to antibiotics [355]. *Plasmodium*-infected mosquitoes present lower starvation resistance than uninfected ones, which has implications for disease transmission in the field [356].

Humans are different across the world and so is *P. falciparum*. In different parts of the world there are different environments and humans have access to more or less food, health care and are exposed to multitude of diseases. Here we have shown that the nutritional environment of the parasite plays a significant role in its development, which may have further effects on parasite virulence. However, currently implemented malaria treatments do not take into account the geographical nutritional peculiarities. From vitamin deficiencies to genetic disposition, human hosts will have a range of environmental conditions in which the parasites reside and adapt through generations. Thus, these selective pressures might aid the parasite to adapt to and circumvent the action of certain drugs. Consequently, it will be beneficial to attempt mimicking such conditions *in vitro* to assess whether current drug doses and screening procedures are suitable for each sub-population.

Bibliography

- [1] World Health Organization. World Health Statistics . *WHO*, 2015.
- [2] Marianne E Sinka. Global distribution of the dominant vector species of malaria, *Anopheles* mosquitoes. *New insights into malaria vectors*, July 2013.
- [3] William N T Wylie. Poverty, Distress, and Disease: Labour and the construction of the Rideau canal, 1826-32. *Labour / Le Travail*, 11:7–29, 1983.
- [4] Giancarlo Majori. Short history of malaria and its eradication in Italy with short notes on the fight against the infection in the Mediterranean basin. *Mediterr. J Hematol. Infect. Dis.*, 4(1):e2012016, 2012.
- [5] Jean-Paul Chretien, Assaf Anyamba, Jennifer Small, Seth Britch, Jose L Sanchez, Alaina C Halbach, Compton Tucker, and Kenneth J Linthicum. Global climate anomalies and potential infectious disease risks: 2014-2015. *PLoS Curr*, 7, 2015.
- [6] Simon I Hay, Carlos A Guerra, Andrew J Tatem, Abdisalan M Noor, and Robert W Snow. The global distribution and population at risk of malaria: past, present, and future. *Lancet Infect Dis*, 4(6):327–336, June 2004.
- [7] Alessandro Bartoloni and Lorenzo Zammarchi. Clinical aspects of uncomplicated and severe malaria. *Mediterr. J. Hematol. Infect. Dis.*, 4(1):e2012026, 2012.
- [8] Nicholas A V Beare, Terrie E Taylor, Simon P Harding, Susan Lewallen, and Malcolm E Molyneux. Malarial retinopathy: a newly established diagnostic sign in severe malaria. *Am. J. Trop. Med. Hyg.*, 75(5):790–797, November 2006.
- [9] H W Choi, J G Breman, S M Teutsch, S Liu, A W Hightower, and J D Sexton. The effectiveness of insecticide-impregnated bed nets in reducing

cases of malaria infection: a meta-analysis of published results. *Am J Trop Med Hyg*, 52(5):377–382, 1995.

- [10] Bianca Pluess, Frank C Tanser, Christian Lengeler, and Brian L Sharp. Indoor residual spraying for preventing malaria. *Cochrane Database Syst Rev*, 14(4):CD006657, 2010.
- [11] Janet Hemingway and Hilary Ranson. Insecticide resistance in insect vectors of human disease. *Annu. Rev. Entomol.*, 45(1):371–391, January 2000.
- [12] Mark J Geels, Egeruan B Imoukhuede, Nathalie Imbault, Harry van Schooten, Terry McWade, Marita Troye-Blomberg, Roland Dobbelaer, Alister G Craig, and Odile Leroy. European Vaccine Initiative: lessons from developing malaria vaccines. *Expert Rev Vaccines*, 10(12):1697–1708, December 2011.
- [13] Stephen L Hoffman, Johan Vekemans, Thomas L Richie, and Patrick E Duffy. The March Toward Malaria Vaccines. *Am J Prev Med*, 49(6 Suppl 4):S319–33, December 2015.
- [14] Peter Winstanley and Stephen Ward. Malaria chemotherapy. *Adv. Parasitol.*, 61:47–76, 2006.
- [15] Richard J Pearce, Hirva Pota, Marie-Solange B Evehe, El-Hadj Bâ, Ghyslain Mombo-Ngoma, Allen L Malisa, Rosalynn Ord, Walter Inojosa, Alexandre Matondo, Diadier A Diallo, Wilfred Mbacham, Ingrid V van den Broek, Todd D Swarthout, Asefaw Getachew, Seyoum Dejene, Martin P Grobusch, Fanta Njie, Samuel Dunyo, Margaret Kweku, Seth Owusu-Agyei, Daniel Chandramohan, Maryline Bonnet, Jean-Paul Guthmann, Sian Clarke, Karen I Barnes, Elizabeth Streat, Stark T Katokele, Petrina Uusiku, Chris O Agboghroma, Olufunmilayo Y Elegba, Badara Cissé, Ishraga E A-Elbasit, Hayder A Giha, S Patrick Kachur, Caroline Lynch, John B Rwakimari, Pascalina Chanda, Moonga Hawela, Brian Sharp, Inbarani Naidoo, and Cally Roper. Multiple origins and regional dispersal of resistant dhps in African *Plasmodium falciparum* malaria. *PLoS Med.*, 6(4):e1000055, April 2009.
- [16] Harald Noedl, Youry Se, Kurt Schaecher, Bryan L Smith, Duong Socheat, and Mark M Fukuda. Evidence of artemisinin-resistant malaria in Western Cambodia. *N Engl J Med*, 359(24):2619–2620, December 2008.
- [17] M Foley and L Tilley. Quinoline antimalarials: mechanisms of action and resistance and prospects for new agents. *Pharmacol. Ther.*, 1998.

- [18] P Olliaro. Mode of action and mechanisms of resistance for antimalarial drugs. *Pharmacol. Ther.*, 89(2):207–219, February 2001.
- [19] P G Bray and S A Ward. A comparison of the phenomenology and genetics of multidrug resistance in cancer cells and quinoline resistance in *Plasmodium falciparum*. *Pharmacol. Ther.*, 77(1):1–28, January 1998.
- [20] P G Bray, S A Ward, and P M O’Neill. Quinolines and artemisinin: chemistry, biology and history. *Curr. Top. Microbiol. Immunol.*, 295:3–38, 2005.
- [21] Heather J Painter, Joanne M Morrissey, Michael W Mather, and Akhil B Vaidya. Specific role of mitochondrial electron transport in blood-stage *Plasmodium falciparum*. *Nature*, 446(7131):88–91, March 2007.
- [22] J Krungkrai. Purification, characterization and localization of mitochondrial dihydroorotate dehydrogenase in *Plasmodium falciparum*, human malaria parasite. *Biochim. Biophys. Acta*, 1243(3):351–360, April 1995.
- [23] N A Helsby, G Edwards, A M Breckenridge, and S A Ward. The multiple dose pharmacokinetics of proguanil. *British Journal of Clinical Pharmacology*, 35(6):653–656, January 1993.
- [24] S R Meshnick, T E Taylor, and S Kamchonwongpaisan. Artemisinin and the antimalarial endoperoxides: from herbal remedy to targeted chemotherapy. *Microbiol. Rev.*, 60(2):301–315, June 1996.
- [25] Arjen M Dondorp, François Nosten, Poravuth Yi, Debashish Das, Aung Phae Phyo, Joel Tarning, Khin Maung Lwin, Frederic Ariey, Warunee Hanpithakpong, Sue J Lee, Pascal Ringwald, Kamolrat Silamut, Mallika Imwong, Kesinee Chotivanich, Pharath Lim, Trent Herdman, Sen Sam An, Shunmay Yeung, Pratap Singhasivanon, Nicholas P J Day, Niklas Lindegardh, Duong Socheat, and Nicholas J White. Artemisinin resistance in *Plasmodium falciparum* malaria. *N Engl J Med*, 361(5):455–467, July 2009.
- [26] S R Meshnick. Artemisinin antimalarials : Mechanisms of action and resistance. *Médecine tropicale*, 58(3):13–17, 1998.
- [27] Sachel Mok, Mallika Imwong, Margaret J Mackinnon, Joan Sim, Ramya Ramadoss, Poravuth Yi, Mayfong Mayxay, Kesinee Chotivanich, Kek-Yee Liong, Bruce Russell, Duong Socheat, Paul N Newton, Nicholas P J Day, Nicholas J White, Peter R Preiser, François Nosten, Arjen M Dondorp, and Zbynek

Bozdech. Artemisinin resistance in *Plasmodium falciparum* is associated with an altered temporal pattern of transcription. *BMC Genomics*, 12:391, 2011.

- [28] G I McFadden and D S Roos. Apicomplexan plastids as drug targets. *Trends in Microbiology*, 7(8):328–333, August 1999.
- [29] K Burns, M Cannon, and E Cundliffe. A resolution of conflicting reports concerning the mode of action of fusidic acid. *FEBS Lett.*, 40(1):219–223, March 1974.
- [30] E Cundliffe and D J Burns. Long term effects of fusidic acid on bacterial protein synthesis *in vivo*. *Biochem. Biophys. Res. Commun.*, 49(3):766–774, November 1972.
- [31] Eric Pelfrene, Marie-Helene Pinheiro, and Marco Cavaleri. Artemisinin-based combination therapy in the treatment of uncomplicated malaria: review of recent regulatory experience at the European Medicines Agency. *Int Health*, 7(4):239–246, July 2015.
- [32] Richard T Eastman and David A Fidock. Artemisinin-based combination therapies: a vital tool in efforts to eliminate malaria. *Nat. Rev. Microbiol.*, 7(12):864–874, December 2009.
- [33] Ric N Price, Lorenz von Seidlein, Neena Valecha, François Nosten, J Kevin Baird, and Nicholas J White. Global extent of chloroquine-resistant *Plasmodium vivax*: a systematic review and meta-analysis. *Lancet Infect Dis*, 14(10):982–991, September 2014.
- [34] George K John, Nicholas M Douglas, Lorenz von Seidlein, François Nosten, J Kevin Baird, Nicholas J White, and Ric N Price. Primaquine radical cure of *Plasmodium vivax*: a critical review of the literature. *Malar J*, 11:280–280, 2012.
- [35] S C Parija and I Praharaaj. Drug resistance in malaria. *Indian J Med Microbiol*, 29(3):243, 2011.
- [36] David A Fidock, Richard T Eastman, Stephen A Ward, and Steven R Meshnick. Recent highlights in antimalarial drug resistance and chemotherapy research. *Trends Parasitol.*, 24(12):537–544, December 2008.
- [37] Matthias Rottmann, Case McNamara, Bryan K S Yeung, Marcus C S Lee, Bin Zou, Bruce Russell, Patrick Seitz, David M Plouffe, Neekesh V Dharia,

Jocelyn Tan, Steven B Cohen, Kathryn R Spencer, Gonzalo E González-Páez, Suresh B Lakshminarayana, Anne Goh, Rossarin Suwanarusk, Tim Jegla, Esther K Schmitt, Hans-Peter Beck, Reto Brun, François Nosten, Laurent Renia, Veronique Dartois, Thomas H Keller, David A Fidock, Elizabeth A Winzeler, and Thierry T Diagana. Spiroindolones, a new and potent chemotype for the treatment of malaria. *Science*, 329(5996):1175–1180, September 2010.

- [38] M Khogali, R Zachariah, A Keiluhu, K Van den Brande, K Tayler-Smith, L Ayada, D Jima, S G Hinderaker, and A D Harries. Detection of malaria in relation to fever and grade of malnutrition among malnourished children in Ethiopia. *Public Health Action*, 1(1):16–18, September 2011.
- [39] Giuseppe Matarese, Antonio La Cava, Veronica Sanna, Graham M Lord, Robert I Lechler, Silvia Fontana, and Serafino Zappacosta. Balancing susceptibility to infection and autoimmunity: a role for leptin? *Trends in Immunology*, 23(4):182–187, April 2002.
- [40] Renato Paschoal Prado, Bruna Fornazari dos Santos, Carla Lombardi de Souza Pinto, Kátia Regina Carvalho de Assis, Daisy Maria Fávero Salvadori, and Marcelo Sady Plácido Ladeira. Influence of diet on oxidative DNA damage, uracil misincorporation and DNA repair capability. *Mutagenesis*, 25(5):483–487, September 2010.
- [41] Laura E Caulfield, Stephanie A Richard, and Robert E Black. Undernutrition as an underlying cause of malaria morbidity and mortality in children less than five years old. *Am J Trop Med Hyg*, 71(2 Suppl):55–63, August 2004.
- [42] A H Shankar and A S Prasad. Zinc and immune function: the biological basis of altered resistance to infection. *Am. J. Clin. Nutr.*, 68(2 Suppl):447S–463S, August 1998.
- [43] Arif AJ, Mathur PD, Chandra S, Singh C, and Sen AB. Effect of zinc diet on xanthine oxidase activity of liver of mice infected with *Plasmodium berghei*. *Indian J Malariol*, 24(1):59–63, June 1987.
- [44] J Alexandra Rowe, Antoine Claessens, Ruth A Corrigan, and Mònica Arman. Adhesion of *Plasmodium falciparum*-infected erythrocytes to human cells: molecular mechanisms and therapeutic implications. *Expert Rev Mol Med*, 11:e16, 2009.
- [45] K Mendis, B J Sina, P Marchesini, and R Carter. The neglected burden of *Plasmodium vivax* malaria. *Am J Trop Med Hyg*, 64:97–105, 2001.

- [46] Renu Tuteja. Malaria - an overview. *FEBS J.*, 274(18):4670–4679, September 2007.
- [47] H E Shortt. Life-cycle of the mammalian malaria parasite. *Br. Med. Bull.*, 8(1):7–9, 1951.
- [48] Leann Tilley, Matthew W A Dixon, and Kiaran Kirk. The *Plasmodium falciparum*-infected red blood cell. *Int. J. Biochem. Cell Biol.*, 43(6):839–842, June 2011.
- [49] A R Wargo, J C de Roode, S Huijben, D R Drew, and A F Read. Transmission stage investment of malaria parasites in response to in-host competition. *Proceedings of the Royal Society B: Biological Sciences*, 274(1625):2629–2638, October 2007.
- [50] Richard Carter and Louis H Miller. Recent developments in production and purification of malaria antigens: Evidence for environmental modulation of gametocytogenesis in *Plasmodium falciparum* in continuous culture. *Bulletin of the World Health Organization*, 57(Suppl):37–52, 1979.
- [51] Albert W C A Cornelissen. Sex determination and sex differentiation in malaria parasites . *Biological Reviews*, 63(3):379–394, August 1988.
- [52] C A Lobo and N Kumar. Sexual differentiation and development in the malaria parasite. *Parasitol Today*, 14(4):146–150, April 1998.
- [53] J A Dvorak, L H Miller, W C Whitehouse, and T Shiroishi. Invasion of erythrocytes by malaria merozoites. *Science*, 187:748–750, 1975.
- [54] J N Okoyeh, C R Pillai, and C E Chitnis. *Plasmodium falciparum* field isolates commonly use erythrocyte invasion pathways that are independent of sialic acid residues of glycophorin A. *Infect. Immun.*, 67:5784–5791, 1999.
- [55] S A Dolan, L H Miller, and T E Wellems. Evidence for a switching mechanism in the invasion of erythrocytes by *Plasmodium falciparum*. *J. Clin. Invest.*, 86:618–624, 1990.
- [56] Lars Hviid and Anja T R Jensen. PfEMP1 - A Parasite Protein Family of Key Importance in *Plasmodium falciparum* Malaria Immunity and Pathogenesis. *Adv. Parasitol.*, 88:51–84, April 2015.
- [57] Chigozie J Uneke. Impact of Placental *Plasmodium falciparum* Malaria on Pregnancy and Perinatal Outcome in Sub-Saharan Africa: I: Introduction to

Placental Malaria. *The Yale Journal of Biology and Medicine*, 80(2):39–50, June 2007.

- [58] S G Langreth, J B Jensen, R T Reese, and W Trager. Fine structure of human malaria *in vitro*. *J. Protozool.*, 25(4):443–452, November 1978.
- [59] C T Atkinson and M Aikawa. Ultrastructure of malaria-infected erythrocytes. *Blood Cells*, 16(2-3):351–368, 1990.
- [60] Eric Hanssen, Peter Carlton, Samantha Deed, Nectarios Klonis, John Sedat, Joe DeRisi, and Leann Tilley. Whole cell imaging reveals novel modular features of the exomembrane system of the malaria parasite, *Plasmodium falciparum*. *Int. J. Parasitol.*, 40(1):123–134, January 2010.
- [61] M Aikawa, P K Hepler, C G Huff, and H Sprinz. The feeding mechanism of avian malarial parasites. *J Cell Biol*, 28(2):355–373, February 1966.
- [62] C Slomianny. Three-dimensional reconstruction of the feeding process of the malaria parasite. *Blood Cells*, 16(2-3):369–378, 1990.
- [63] Susan E Francis, David J Sullivan, and Daniel E Goldberg. Hemoglobin metabolism in the malaria parasite *Plasmodium falciparum*. *Annu. Rev. Microbiol.*, 51(1):97–123, 1997.
- [64] L H Bannister, J M Hopkins, R E Fowler, S Krishna, and G H Mitchell. A brief illustrated guide to the ultrastructure of *Plasmodium falciparum* asexual blood stages. *Parasitology Today*, 16(10):427–433, October 2000.
- [65] Michael Lanzer, Hannes Wickert, Georg Krohne, Laetitia Vincensini, and Catherine Braun Breton. Maurer’s clefts: A novel multi-functional organelle in the cytoplasm of *Plasmodium falciparum*-infected erythrocytes. *Int. J. Parasitol.*, 36(1):23–36, January 2006.
- [66] Tania F de Koning-Ward, Paul R Gilson, Justin A Boddey, Melanie Rug, Brian J Smith, Anthony T Papenfuss, Paul R Sanders, Rachel J Lundie, Alexander G Maier, Alan F Cowman, and Brendan S Crabb. A newly discovered protein export machine in malaria parasites. *Nature*, 459(7249):945–949, June 2009.
- [67] Rani Soni, Drista Sharma, and Tarun K Bhatt. *Plasmodium falciparum* Secretome in Erythrocyte and Beyond. *Frontiers in Microbiology*, 7:194, 2016.

- [68] Esther Mundwiler-Pachlatko and Hans-Peter Beck. Maurer’s clefts, the enigma of *Plasmodium falciparum*. *Proc. Natl. Acad. Sci. U.S.A.*, 110(50):19987–19994, December 2013.
- [69] Henry M Staines, Caroline Rae, and Kiaran Kirk. Increased permeability of the malaria-infected erythrocyte to organic cations. *Biochimica et Biophysica Acta (BBA) - Biomembranes*, 1463(1):88–98, January 2000.
- [70] Hagai Ginsburg. Transport pathways in the malaria-infected erythrocyte. Their characterization and their use as potential targets for chemotherapy. *Biochemical Pharmacology*, 48(10):1847–1856, November 1994.
- [71] Germán Plata, Tzu-Lin Hsiao, Kellen L Olszewski, Manuel Llinás, and Dennis Vitkup. Reconstruction and flux-balance analysis of the *Plasmodium falciparum* metabolic network. *Molecular Systems Biology*, 6:408, September 2010.
- [72] Carola Huthmacher, Andreas Hoppe, Sascha Bulik, and Hermann-Georg Holzhütter. Antimalarial drug targets in *Plasmodium falciparum* predicted by stage-specific metabolic network analysis. *BMC Syst Biol*, 4(1):120, 2010.
- [73] Cristina Aurrecochea, John Brestelli, Brian P Brunk, Jennifer Dommer, Steve Fischer, Bindu Gajria, Xin Gao, Alan Gingle, Greg Grant, Omar S Harb, Mark Heiges, Frank Innamorato, John Iodice, Jessica C Kissinger, Eileen Kraemer, Wei Li, John A Miller, Vishal Nayak, Cary Pennington, Deborah F Pinney, David S Roos, Chris Ross, Christian J Stoeckert, Charles Treatman, and Haiming Wang. PlasmoDB: a functional genomic database for malaria parasites. *Nucleic acids Research*, 37(Database issue):D539–43, January 2009.
- [74] Hagai Ginsburg. Progress in *in silico* functional genomics: the malaria Metabolic Pathways database. *Trends Parasitol.*, 22(6):238–240, June 2006.
- [75] Hagai Ginsburg. Caveat emptor: limitations of the automated reconstruction of metabolic pathways in *Plasmodium*. *Trends Parasitol.*, 25(1):37–43, January 2009.
- [76] Iwei Yeh, Theodor Hanekamp, Sophia Tsoka, Peter D Karp, and Russ B Altman. Computational analysis of *Plasmodium falciparum* metabolism: organizing genomic information to facilitate drug discovery. *Genome Res.*, 14(5):917–924, May 2004.

- [77] E F Roth, C Raventos-Suarez, M Perkins, and R L Nagel. Glutathione stability and oxidative stress in *P. falciparum* infection *in vitro*: responses of normal and G6PD deficient cells. *Biochem. Biophys. Res. Commun.*, 109(2):355–362, November 1982.
- [78] E F Roth, M C Calvin, I Max-Audit, J Rosa, and R Rosa. The enzymes of the glycolytic pathway in erythrocytes infected with *Plasmodium falciparum* malaria parasites. *Blood*, 72(6):1922–1925, December 1988.
- [79] C A Homewood. Carbohydrate metabolism of malarial parasites. *Bulletin of the World Health Organization*, 55(2-3):229, 1977.
- [80] Monika Mehta, Haripalsingh M Sonawat, and Shobhona Sharma. Malaria parasite-infected erythrocytes inhibit glucose utilization in uninfected red cells. *FEBS Lett.*, 579(27):6151–6158, November 2005.
- [81] Lu-Yun Lian, Mohammed Al-Helal, Abd Majid Roslaini, Nicholas Fisher, Patrick G Bray, Stephen A Ward, and Giancarlo A Biagini. Glycerol: an unexpected major metabolite of energy metabolism by the human malaria parasite. *Malar J*, 8:38, 2009.
- [82] C J Woodrow, R J Burchmore, and S Krishna. Hexose permeation pathways in *Plasmodium falciparum*-infected erythrocytes. *Proc. Natl. Acad. Sci. U.S.A.*, 97(18):9931–9936, August 2000.
- [83] C J Woodrow, J I Penny, and S Krishna. Intraerythrocytic *Plasmodium falciparum* expresses a high affinity facilitative hexose transporter. *J. Biol. Chem.*, 274(11):7272–7277, March 1999.
- [84] E F Roth. Malarial parasite hexokinase and hexokinase-dependent glutathione reduction in the *Plasmodium falciparum*-infected human erythrocyte. *J. Biol. Chem.*, 262(32):15678–15682, November 1987.
- [85] I K Srivastava, M Schmidt, M Grall, U Certa, A M Garcia, and L H Perrin. Identification and purification of glucose phosphate isomerase of *Plasmodium falciparum*. *Mol. Biochem. Parasitol.*, 54(2):153–164, September 1992.
- [86] D Buckwitz, G Jacobasch, C Gerth, H G Holzhütter, and R Thamm. A kinetic model of phosphofructokinase from *Plasmodium berghei*. Influence of ATP and fructose-6-phosphate. *Mol. Biochem. Parasitol.*, 27(2-3):225–232, January 1988.

- [87] D Buckwitz, G Jacobasch, and C Gerth. Phosphofruktokinase from *Plasmodium berghei*. Influence of Mg²⁺, ATP and Mg²⁺(+)-complexed ATP. *Biochem. J.*, 267(2):353–357, April 1990.
- [88] Binny M Mony, Monika Mehta, Gotam K Jarori, and Shobhona Sharma. Plant-like phosphofruktokinase from *Plasmodium falciparum* belongs to a novel class of ATP-dependent enzymes. *Int. J. Parasitol.*, 39(13):1441–1453, November 2009.
- [89] H Döbeli, A Trzeciak, D Gillessen, H Matile, I K Srivastava, L H Perrin, P E Jakob, and U Certa. Expression, purification, biochemical characterization and inhibition of recombinant *Plasmodium falciparum* aldolase. *Mol. Biochem. Parasitol.*, 41(2):259–268, June 1990.
- [90] H Döbeli, C Itin, B Meier, and U Certa. Is *Plasmodium falciparum* aldolase useful for rational drug design? *Acta Leiden.*, 60(1):135–140, 1991.
- [91] S S Velanker, S S Ray, R S Gokhale, S Suma, H Balaram, P Balaram, and M R Murthy. Triosephosphate isomerase from *Plasmodium falciparum*: the crystal structure provides insights into antimalarial drug design. *Structure*, 5(6):751–761, June 1997.
- [92] G Ravindra and P Balaram. *Plasmodium falciparum* triosephosphate isomerase: new insights into an old enzyme - Publications of the IAS Fellows. *Pure and applied chemistry*, 2005.
- [93] Jacqueline F Satchell, Robyn L Malby, Cindy S Luo, Akinola Adisa, Aysun E Alpyurek, Nectarios Klonis, Brian J Smith, Leann Tilley, and Peter M Colman. Structure of glyceraldehyde-3-phosphate dehydrogenase from *Plasmodium falciparum*. *Acta Crystallogr. D Biol. Crystallogr.*, 61(Pt 9):1213–1221, September 2005.
- [94] Biswajit Pal, Brandon Pybus, Donald D Muccio, and Debasish Chattopadhyay. Biochemical characterization and crystallization of recombinant 3-phosphoglycerate kinase of *Plasmodium falciparum*. *Biochimica et Biophysica Acta (BBA) - Proteins and Proteomics*, 1699(1-2):277–280, June 2004.
- [95] M Grall, I K Srivastava, M Schmidt, A M Garcia, J Mauël, and L H Perrin. *Plasmodium falciparum*: identification and purification of the phosphoglycerate kinase of the malaria parasite. *Exp. Parasitol.*, 75(1):10–18, August 1992.

- [96] Ipsita Pal-Bhowmick, K Sadagopan, Hardeep K Vora, Alfica Sehgal, Shobhona Sharma, and Gotam K Jarori. Cloning, over-expression, purification and characterization of *Plasmodium falciparum* enolase. *Eur. J. Biochem.*, 271(23-24):4845–4854, December 2004.
- [97] Sujaan Das, Saudamini Shevade, Douglas J LaCount, and Gotam K Jarori. *Plasmodium falciparum* enolase complements yeast enolase functions and associates with the parasite food vacuole. *Mol. Biochem. Parasitol.*, 179(1):8–17, September 2011.
- [98] Maurice Chan and Tiow-Suan Sim. Functional analysis, overexpression, and kinetic characterization of pyruvate kinase from *Plasmodium falciparum*. *Biochem. Biophys. Res. Commun.*, 326(1):188–196, January 2005.
- [99] Sybille Mazurek. Pyruvate kinase type M2: a key regulator of the metabolic budget system in tumor cells. *Int. J. Biochem. Cell Biol.*, 43(7):969–980, July 2011.
- [100] V J Winter, A Cameron, R Tranter, R B Sessions, and R L Brady. Crystal structure of *Plasmodium berghei* lactate dehydrogenase indicates the unique structural differences of these enzymes are shared across the Plasmodium genus. *Mol. Biochem. Parasitol.*, 131(1):1–10, September 2003.
- [101] D J Bzik, B A Fox, and K Gonyer. Expression of *Plasmodium falciparum* lactate dehydrogenase in Escherichia coli. *Mol. Biochem. Parasitol.*, 59(1):155–166, May 1993.
- [102] Rosa V Marchetti, Adele M Lehane, Sarah H Shafik, Markus Winterberg, Rowena E Martin, and Kiaran Kirk. A lactate and formate transporter in the intraerythrocytic malaria parasite, *Plasmodium falciparum*. *Nat Commun*, 6:6721, 2015.
- [103] James I Macrae, Matthew Wa Dixon, Megan K Dearnley, Hwa H Chua, Jennifer M Chambers, Shannon Kenny, Iveta Bottova, Leann Tilley, and Malcolm J McConville. Mitochondrial metabolism of sexual and asexual blood stages of the malaria parasite *Plasmodium falciparum*. *BMC Biol.*, 11:67, 2013.
- [104] Kellen L Olszewski, Michael W Mather, Joanne M Morrissey, Benjamin A Garcia, Akhil B Vaidya, Joshua D Rabinowitz, and Manuel Llinás. Branched tricarboxylic acid metabolism in *Plasmodium falciparum*. *Nature*, 466(7307):774–778, August 2010.

- [105] Simon A Cobbold, Ashley M Vaughan, Ian A Lewis, Heather J Painter, Nelly Camargo, David H Perlman, Matthew Fishbaugher, Julie Healer, Alan F Cowman, Stefan H I Kappe, and Manuel Llinás. Kinetic flux profiling elucidates two independent acetyl-CoA biosynthetic pathways in *Plasmodium falciparum*. *J. Biol. Chem.*, 288(51):36338–36350, October 2013.
- [106] Rebecca D Oppenheim, Darren J Creek, James I Macrae, Katarzyna K Modrzynska, Paco Pino, Julien Limenitakis, Valerie Polonais, Frank Seeber, Michael P Barrett, Oliver Billker, Malcolm J McConville, and Dominique Soldati-Favre. BCKDH: The Missing Link in Apicomplexan Mitochondrial Metabolism Is Required for Full Virulence of *Toxoplasma gondii* and *Plasmodium berghei*. *PLoS Pathog.*, 10(7):e1004263, July 2014.
- [107] Hangjun Ke, Ian A Lewis, Joanne M Morrissey, Kyle J McLean, Suresh M Ganesan, Heather J Painter, Michael W Mather, Marcelo Jacobs-Lorena, Manuel Llinás, and Akhil B Vaidya. Genetic investigation of tricarboxylic acid metabolism during the *Plasmodium falciparum* life cycle. *Cell Rep.*, 11(1):164–174, April 2015.
- [108] Nicholas Fisher, Patrick G Bray, Stephen A Ward, and Giancarlo A Biagini. The malaria parasite type II NADH:quinone oxidoreductase: an alternative enzyme for an alternative lifestyle. *Trends Parasitol.*, 23(7):305–310, July 2007.
- [109] Praveen Balabaskaran Nina, Joanne M Morrissey, Suresh M Ganesan, Hangjun Ke, April M Pershing, Michael W Mather, and Akhil B Vaidya. ATP synthase complex of *Plasmodium falciparum*: dimeric assembly in mitochondrial membranes and resistance to genetic disruption. *J. Biol. Chem.*, 286(48):41312–41322, December 2011.
- [110] Matthew G Vander Heiden, Lewis C Cantley, and Craig B Thompson. Understanding the Warburg Effect: The Metabolic Requirements of Cell Proliferation. *Science*, 324(5930):1029–1033, May 2009.
- [111] J Enrique Salcedo-Sora, Eva Caamano-Gutierrez, Stephen A Ward, and Giancarlo A Biagini. The proliferating cell hypothesis: a metabolic framework for *Plasmodium* growth and development. *Trends Parasitol.*, 30(4):170–175, April 2014.

- [112] Toshihide Mitamura and Nirianne Marie Q Palacpac. Lipid metabolism in *Plasmodium falciparum*-infected erythrocytes: possible new targets for malaria chemotherapy. *Microbes Infect*, 5(6):545–552, May 2003.
- [113] Ellen Yeh and Joseph L DeRisi. Chemical rescue of malaria parasites lacking an apicoplast defines organelle function in blood-stage *Plasmodium falciparum*. *PLoS Biol.*, 9(8):e1001138, August 2011.
- [114] J Enrique Salcedo-Sora and Steve A Ward. The folate metabolic network of Falciparum malaria. *Mol. Biochem. Parasitol.*, 188(1):51–62, March 2013.
- [115] Rodrigo Diaz-Ruiz, Michel Rigoulet, and Anne Devin. The Warburg and Crabtree effects: On the origin of cancer cell energy metabolism and of yeast glucose repression. *Biochim. Biophys. Acta*, 1807(6):568–576, June 2011.
- [116] Sophia Y Lunt and Matthew G Vander Heiden. Aerobic glycolysis: meeting the metabolic requirements of cell proliferation. *Annu. Rev. Cell Dev. Biol.*, 27:441–464, 2011.
- [117] E A Newsholme, B Crabtree, and M S Ardawi. The role of high rates of glycolysis and glutamine utilization in rapidly dividing cells. *Biosci. Rep.*, 5(5):393–400, May 1985.
- [118] R Brooks Robey, Judith Weisz, Nancy B Kuemmerle, Anna C Salzberg, Arthur Berg, Dustin G Brown, Laura Kubik, Roberta Palorini, Fahd Al-Mulla, Rabeah Al-Temaimi, Annamaria Colacci, Chiara Mondello, Jayadev Raju, Jordan Woodrick, A Ivana Scovassi, Neetu Singh, Monica Vaccari, Rabintra Roy, Stefano Forte, Lorenzo Memeo, Hosni K Salem, Amedeo Amedei, Roslida A Hamid, Graeme P Williams, Leroy Lowe, Joel Meyer, Francis L Martin, William H Bisson, Ferdinando Chiaradonna, and Elizabeth P Ryan. Metabolic reprogramming and dysregulated metabolism: cause, consequence and/or enabler of environmental carcinogenesis? *Carcinogenesis*, 36 Suppl 1:S203–31, June 2015.
- [119] E A Newsholme and M Board. Application of metabolic-control logic to fuel utilization and its significance in tumor cells. *Adv Enzyme Regul*, 31:225–246, 1991.
- [120] Chunxia Li, Guifeng Zhang, Lei Zhao, Zhijun Ma, and Hongbing Chen. Metabolic reprogramming in cancer cells: glycolysis, glutaminolysis, and Bcl-2 proteins as novel therapeutic targets for cancer. *World J Surg Oncol*, 14(1):15, 2016.

- [121] Aaron M Hosios, Vivian C Hecht, Laura V Danai, Marc O Johnson, Jeffrey C Rathmell, Matthew L Steinhauser, Scott R Manalis, and Matthew G Vander Heiden. Amino Acids Rather than Glucose Account for the Majority of Cell Mass in Proliferating Mammalian Cells. *Dev Cell*, 36(5):540–549, March 2016.
- [122] Huasheng Lu, Robert A Forbes, and Ajay Verma. Hypoxia-inducible factor 1 activation by aerobic glycolysis implicates the Warburg effect in carcinogenesis. *J. Biol. Chem.*, 277(26):23111–23115, June 2002.
- [123] Franziska Hirschhaeuser, Ulrike G A Sattler, and Wolfgang Mueller-Klieser. Lactate: A Metabolic Key Player in Cancer. *Cancer Res*, 71(22):6921–6925, November 2011.
- [124] David K Gardner. Lactate production by the mammalian blastocyst: manipulating the microenvironment for uterine implantation and invasion? *Bioessays*, 37(4):364–371, April 2015.
- [125] Pierre Sonveaux, Frédérique Végran, Thies Schroeder, Melanie C Wergin, Julien Verrax, Zahid N Rabbani, Christophe J De Saedeleer, Kelly M Kennedy, Caroline Diepart, Benedicte F Jordan, Michael J Kelley, Bernard Gallez, Miriam L Wahl, Olivier Feron, and Mark W Dewhirst. Targeting lactate-fueled respiration selectively kills hypoxic tumor cells in mice. *J. Clin. Invest.*, 118(12):3930–3942, December 2008.
- [126] Gregg L Semenza. Tumor metabolism: cancer cells give and take lactate. *J. Clin. Invest.*, 118(12):3835–3837, December 2008.
- [127] Samuel H Payne and William F Loomis. Retention and Loss of Amino Acid Biosynthetic Pathways Based on Analysis of Whole-Genome Sequences. *Eukaryotic Cell*, 5(2):272–276, February 2006.
- [128] A A Divo, T G Geary, N L Davis, and J B Jensen. Nutritional requirements of *Plasmodium falciparum* in culture. I. Exogenously supplied dialyzable components necessary for continuous growth. *J. Protozool.*, 32(1):59–64, February 1985.
- [129] D E Goldberg. Hemoglobin degradation. *Curr. Top. Microbiol. Immunol.*, 295:275–291, 2005.

- [130] J R Eckman, S Modler, J W Eaton, E Berger, and R R Engel. Host heme catabolism in drug-sensitive and drug-resistant malaria. *J Lab Clin Med*, 90(4):767–770, October 1977.
- [131] I W Sherman. Amino acid metabolism and protein synthesis in malarial parasites. *Bulletin of the World Health Organization*, 55(2-3):265–276, 1977.
- [132] P M O’Neill, P G Bray, S R Hawley, S A Ward, and B K Park. 4-Aminoquinolines—past, present, and future: a chemical perspective. *Pharmacol. Ther.*, 77(1):29–58, January 1998.
- [133] Dewal Jani, Rana Nagarkatti, Wandy Beatty, Ross Angel, Carla Slebodnick, John Andersen, Sanjai Kumar, and Dharmendar Rathore. HDP-a novel heme detoxification protein from the malaria parasite. *PLoS Pathog.*, 4(4):e1000053, April 2008.
- [134] K Bendrat, B J Berger, and A Cerami. Haem polymerization in malaria. *Nature*, 378(6553):138–139, November 1995.
- [135] D J Jr Sullivan, I Y Gluzman, and D E Goldberg. *Plasmodium* hemozoin formation mediated by histidine-rich proteins. *Science*, 271(5246):219–222, January 1996.
- [136] Monika Chugh, Vidhya Sundararaman, Saravanan Kumar, Vanga S Reddy, Waseem A Siddiqui, Kenneth D Stuart, and Pawan Malhotra. Protein complex directs hemoglobin-to-hemozoin formation in *Plasmodium falciparum*. *Proc. Natl. Acad. Sci. U.S.A.*, 110(14):5392–5397, April 2013.
- [137] R D Theakston, K A Fletcher, and B G Maegraith. The use of electron microscope autoradiography for examining the uptake and degradation of haemoglobin by *Plasmodium berghei*. *Ann Trop Med Parasitol*, 64(1):63–71, March 1970.
- [138] Jun Liu, Eva S Istvan, Ilya Y Gluzman, Julia Gross, and Daniel E Goldberg. *Plasmodium falciparum* ensures its amino acid supply with multiple acquisition pathways and redundant proteolytic enzyme systems. *Proceedings of the National Academy of Sciences*, 103(23):8840–8845, June 2006.
- [139] S E Francis, I Y Gluzman, A Oksman, A Knickerbocker, R Mueller, M L Bryant, D R Sherman, D G Russell, and D E Goldberg. Molecular characterization and inhibition of a *Plasmodium falciparum* aspartic hemoglobinase. *EMBO J*, 13(2):306–317, January 1994.

- [140] Virgilio L Lew, Lynn Macdonald, Hagai Ginsburg, Miriam Krugliak, and Teresa Tiffert. Excess haemoglobin digestion by malaria parasites: a strategy to prevent premature host cell lysis. *Blood Cells Mol Dis*, 32(3):353–359, May 2004.
- [141] Miriam Krugliak, Jianmin Zhang, and Hagai Ginsburg. Intraerythrocytic *Plasmodium falciparum* utilizes only a fraction of the amino acids derived from the digestion of host cell cytosol for the biosynthesis of its proteins. *Mol. Biochem. Parasitol.*, 119(2):249–256, February 2002.
- [142] Harry P de Koning, Daniel J Bridges, and Richard J S Burchmore. Purine and pyrimidine transport in pathogenic protozoa: from biology to therapy. *FEMS Microbiol. Rev.*, 29(5):987–1020, November 2005.
- [143] John E Hyde. Targeting purine and pyrimidine metabolism in human apicomplexan parasites. *Curr Drug Targets*, 8(1):31–47, January 2007.
- [144] Kamal El Bissati, Rachel Zufferey, William H Witola, Nicola S Carter, Buddy Ullman, and Choukri Ben Mamoun. The plasma membrane permease PfNT1 is essential for purine salvage in the human malaria parasite *Plasmodium falciparum*. *Proc. Natl. Acad. Sci. U.S.A.*, 103(24):9286–9291, June 2006.
- [145] P Reyes, P K Rathod, D J Sanchez, J E Mrema, K H Rieckmann, and H G Heidrich. Enzymes of purine and pyrimidine metabolism from the human malaria parasite, *Plasmodium falciparum*. *Mol. Biochem. Parasitol.*, 5(5):275–290, May 1982.
- [146] Wuxian Shi, Li-Min Ting, Gregory A Kicska, Andrzej Lewandowicz, Peter C Tyler, Gary B Evans, Richard H Furneaux, Kami Kim, Steve C Almo, and Vern L Schramm. *Plasmodium falciparum* purine nucleoside phosphorylase: crystal structures, immucillin inhibitors, and dual catalytic function. *J. Biol. Chem.*, 279(18):18103–18106, April 2004.
- [147] Margaret A Phillips and Pradipsinh K Rathod. *Plasmodium* dihydroorotate dehydrogenase: a promising target for novel anti-malarial chemotherapy. *Infectious disorders drug targets*, 10(3):226–239, June 2010.
- [148] Christopher V Plowe, James G Kublin, and Ogobara K Doumbo. *P. falciparum* dihydrofolate reductase and dihydropteroate synthase mutations: epidemiology and role in clinical resistance to antifolates. *Drug Resistance Updates*, 1(6):389–396, January 1998.

- [149] W Sirawaraporn, T Sathitkul, R Sirawaraporn, Y Yuthavong, and D V Santi. Antifolate-resistant mutants of *Plasmodium falciparum* dihydrofolate reductase. *Proc. Natl. Acad. Sci. U.S.A.*, 94(4):1124–1129, February 1997.
- [150] Giel G van Dooren and Boris Striepen. The algal past and parasite present of the apicoplast. *Annu. Rev. Microbiol.*, 67:271–289, 2013.
- [151] Bernardo J Foth and Geoffrey I McFadden. The apicoplast: a plastid in *Plasmodium falciparum* and other Apicomplexan parasites. *Int Rev Cytol*, 224:57–110, 2003.
- [152] S Varadharajan, S Dhanasekaran, Z Q Bonday, P N Rangarajan, and G Padmanaban. Involvement of delta-aminolaevulinate synthase encoded by the parasite gene in de novo haem synthesis by *Plasmodium falciparum*. *Biochem. J.*, 367(Pt 2):321–327, October 2002.
- [153] Stuart A Ralph, Giel G van Dooren, Ross F Waller, Michael J Crawford, Martin J Fraunholz, Bernardo J Foth, Christopher J Tonkin, David S Roos, and Geoffrey I McFadden. Tropical infectious diseases: metabolic maps and functions of the *Plasmodium falciparum* apicoplast. *Nat. Rev. Microbiol.*, 2(3):203–216, March 2004.
- [154] Ben C L van Schaijk, T R Santha Kumar, Martijn W Vos, Adam Richman, Geert-Jan van Gemert, Tao Li, Abraham G Eappen, Kim C Williamson, Belinda J Morahan, Matt Fishbaugher, Mark Kennedy, Nelly Camargo, Shahid M Khan, Chris J Janse, Kim Lee Sim, Stephen L Hoffman, Stefan H I Kappe, Robert W Sauerwein, David A Fidock, and Ashley M Vaughan. Type II fatty acid biosynthesis is essential for *Plasmodium falciparum* sporozoite development in the midgut of Anopheles mosquitoes. *Eukaryotic Cell*, 13(5):550–559, May 2014.
- [155] Alice S Tarun, Xinxia Peng, Ronald F Dumpit, Yuko Ogata, Hilda Silva-Rivera, Nelly Camargo, Thomas M Daly, Lawrence W Bergman, and Stefan H I Kappe. A combined transcriptome and proteome survey of malaria parasite liver stages. *Proceedings of the National Academy of Sciences*, 105(1):305–310, January 2008.
- [156] P A Maguire and I W Sherman. Phospholipid composition, cholesterol content and cholesterol exchange in *Plasmodium falciparum*-infected red cells. *Mol. Biochem. Parasitol.*, 38(1):105–112, January 1990.

- [157] F Matesanz, I Duran-Chica, and A Alcina. The cloning and expression of Pfacs1, a *Plasmodium falciparum* fatty acyl coenzyme A synthetase-1 targeted to the host erythrocyte cytoplasm. *J. Mol. Biol.*, 291(1):59–70, August 1999.
- [158] F Mi-Ichi, K Kita, and T Mitamura. Intraerythrocytic *Plasmodium falciparum* utilize a broad range of serum-derived fatty acids with limited modification for their growth. *Parasitology*, 133(Pt 4):399–410, October 2006.
- [159] Joel S Freundlich, Min Yu, Edinson Lucumi, Mack Kuo, Han-Chun Tsai, Juan-Carlos Valderramos, Luchezar Karagyozov, William R Jr Jacobs, Guy A Schiehsler, David A Fidock, David P Jacobus, and James C Sacchettini. Synthesis and biological activity of diaryl ether inhibitors of malarial enoyl acyl carrier protein reductase. Part 2: 2'-substituted triclosan derivatives. *Bioorg Med Chem Lett*, 16(8):2163–2169, April 2006.
- [160] Gyanendra Kumar, Prasanna Parasuraman, Shailendra Kumar Sharma, Tanushree Banerjee, Krishanpal Karmodiya, Namita Surolia, and Avadhesh Surolia. Discovery of a rhodanine class of compounds as inhibitors of *Plasmodium falciparum* enoyl-acyl carrier protein reductase. *J. Med. Chem.*, 50(11):2665–2675, May 2007.
- [161] Nadine Thomsen-Zieger, Joachim Schachtner, and Frank Seeber. Apicomplexan parasites contain a single lipoxic acid synthase located in the plastid. *FEBS Lett.*, 547(1-3):80–86, July 2003.
- [162] Melanie J Shears, Cyrille Y Botté, and Geoffrey I McFadden. Fatty acid metabolism in the *Plasmodium* apicoplast: Drugs, doubts and knockouts. *Mol. Biochem. Parasitol.*, 199(1–2):34–50, January 2015.
- [163] H K Lichtenthaler, J Schwender, A Disch, and M Rohmer. Biosynthesis of isoprenoids in higher plant chloroplasts proceeds via a mevalonate-independent pathway. *FEBS Lett.*, 400(3):271–274, January 1997.
- [164] A S Fairfield, S R Meshnick, and J W Eaton. Malaria parasites adopt host cell superoxide dismutase. *Science*, 221(4612):764–766, August 1983.
- [165] Katja Becker, Leann Tilley, Jonathan L Vennerstrom, David Roberts, Stephen Rogerson, and Hagai Ginsburg. Oxidative stress in malaria parasite-infected erythrocytes: host–parasite interactions. *Int. J. Parasitol.*, 34(2):163–189, February 2004.

- [166] Brenda L Bohnsack and Karen K Hirschi. Nutrient regulation of cell cycle progression. *Annu Rev Nutr*, 24:433–453, 2004.
- [167] Simonetta Friso and Sang-Woon Choi. Gene-nutrient interactions and DNA methylation. *J. Nutr.*, 132(8 Suppl):2382S–2387S, August 2002.
- [168] Till S Voss, Zbynek Bozdech, and Richard Bartfai. Epigenetic memory takes center stage in the survival strategy of malaria parasites. *Curr. Opin. Microbiol.*, 20:88–95, August 2014.
- [169] Sanjay A Desai. Ion and nutrient uptake by malaria parasite-infected erythrocytes. *Cell Microbiol*, 14(7):1003–1009, July 2012.
- [170] Sanjay A Desai. Targeting ion channels of *Plasmodium falciparum*-infected human erythrocytes for antimalarial development. *Curr Drug Targets Infect Disord*, 4(1):79–86, March 2004.
- [171] Wang Nguitragool, Abdullah A B Bokhari, Ajay D Pillai, Kempaiah Rayavara, Paresh Sharma, Brad Turpin, L Aravind, and Sanjay A Desai. Malaria parasite clag3 genes determine channel-mediated nutrient uptake by infected red blood cells. *Cell*, 145(5):665–677, May 2011.
- [172] Christy A Comeaux, Bradley I Coleman, Amy K Bei, Nicole Whitehurst, and Manoj T Duraisingh. Functional analysis of epigenetic regulation of tandem RhopH1/clag genes reveals a role in *Plasmodium falciparum* growth. *Mol. Microbiol.*, 80(2):378–390, April 2011.
- [173] Alfred Cortes, Celine Carret, Osamu Kaneko, Brian Y S Yim Lim, Alasdair Ivens, and Anthony A Holder. Epigenetic silencing of *Plasmodium falciparum* genes linked to erythrocyte invasion. *PLoS Pathog.*, 3(8):e107, August 2007.
- [174] Nuria Rovira-Graells, Valerie M Crowley, Cristina Bancells, Sofia Mira-Martinez, Lluís Ribas de Pouplana, and Alfred Cortes. Deciphering the principles that govern mutually exclusive expression of *Plasmodium falciparum* clag3 genes. *Nucleic acids Research*, 43(17):8243–8257, September 2015.
- [175] Paresh Sharma, Kurt Wollenberg, Morgan Sellers, Kayvan Zainabadi, Kevin Galinsky, Eli Moss, Wang Nguitragool, Daniel Neafsey, and Sanjay A Desai. An epigenetic antimalarial resistance mechanism involving parasite genes linked to nutrient uptake. *J. Biol. Chem.*, 288(27):19429–19440, July 2013.

- [176] Sofia Mira-Martinez, Nuria Rovira-Graells, Valerie M Crowley, Lindsey M Altenhofen, Manuel Llinás, and Alfred Cortes. Epigenetic switches in *clag3* genes mediate blasticidin S resistance in malaria parasites. *Cell Microbiol.*, 15(11):1913–1923, November 2013.
- [177] W Trager and J B Jensen. Human malaria parasites in continuous culture. *Science*, 193(4254):673–675, August 1976.
- [178] Michele LeRoux, Viswanathan Lakshmanan, and Johanna P Daily. *Plasmodium falciparum* biology: analysis of in vitro versus in vivo growth conditions. *Trends Parasitol.*, 25(10):474–481, October 2009.
- [179] Hauke Holtorf, Marie-Christine Guitton, and Ralf Reski. Plant functional genomics. *Naturwissenschaften*, 89(6):235–249, June 2002.
- [180] Roger Brent. Genomic Biology. *Cell*, 100(1):169–183, January 2000.
- [181] Jörg Stelling. Mathematical models in microbial systems biology. *Curr. Opin. Microbiol.*, 7(5):513–518, October 2004.
- [182] Rainer Breitling, Barbara M Bakker, Michael P Barrett, Saskia Decuypere, and Jean-Claude Dujardin. Metabolomic Systems Biology of Protozoan Parasites. In K Suhre, editor, *Genetics Meets Metabolomics*, pages 73–84. Springer New York, New York, NY, May 2012.
- [183] O Fiehn, J Kopka, P Dörmann, T Altmann, R N Trethewey, and L Willmitzer. Metabolite profiling for plant functional genomics. *Nat. Biotechnol.*, 18(11):1157–1161, November 2000.
- [184] David S Wishart, Dan Tzur, Craig Knox, Roman Eisner, An Chi Guo, Nelson Young, Dean Cheng, Kevin Jewell, David Arndt, Summit Sawhney, Chris Fung, Lisa Nikolai, Mike Lewis, Marie-Aude Coutouly, Ian Forsythe, Peter Tang, Savita Shrivastava, Kevin Jeroncic, Paul Stothard, Godwin Amegbey, David Block, David D Hau, James Wagner, Jessica Miniaci, Melisa Clements, Mulu Gebremedhin, Natalie Guo, Ying Zhang, Gavin E Duggan, Glen D Macinnis, Alim M Weljie, Reza Dowlatabadi, Fiona Bamforth, Derrick Clive, Russ Greiner, Liang Li, Tom Marrie, Brian D Sykes, Hans J Vogel, and Lori Querengesser. HMDB: the Human Metabolome Database. *Nucleic acids Research*, 35(Database issue):D521–6, January 2007.

- [185] M A Fitzgerald, S R McCouch, and R D Hall. ScienceDirect.com - Trends in Plant Science - Not just a grain of rice: the quest for quality. *Trends Plant Sci*, 2009.
- [186] Wipawee Pongsuwan, Takeshi Bamba, Tsutomu Yonetani, Akio Kobayashi, and Eiichiro Fukusaki. Quality prediction of Japanese green tea using pyrolyzer coupled GC/MS based metabolic fingerprinting. *J. Agric. Food Chem.*, 56(3):744–750, February 2008.
- [187] O Galtier, N Dupuy, Y Le Dréau, D Ollivier, and C Pinatel. Geographic origins and compositions of virgin olive oils determined by chemometric analysis of NIR spectra. *Analytica chimica Acta*, 2007.
- [188] Christof Francke, Roland J Siezen, and Bas Teusink. Reconstructing the metabolic network of a bacterium from its genome. *Trends in Microbiology*, 13(11):550–558, November 2005.
- [189] Jeremy K Nicholson and Ian D Wilson. Opinion: understanding 'global' systems biology: metabonomics and the continuum of metabolism. *Nat Rev Drug Discov*, 2(8):668–676, August 2003.
- [190] H Kitano. Computational systems biology. *Nature*, 2002.
- [191] Trey Ideker and Douglas Lauffenburger. Building with a scaffold: emerging strategies for high- to low-level cellular modeling. *Trends in Biotechnology*, 21(6):255–262, June 2003.
- [192] T P Ikeda, A E Shauger, and S Kustu. Salmonella typhimurium apparently perceives external nitrogen limitation as internal glutamine limitation. *J. Mol. Biol.*, 259(4):589–607, June 1996.
- [193] M R Mashego, L Wu, J C Van Dam, C Ras, J L Vinke, W A Van Winden, W M Van Gulik, and J J Heijnen. MIRACLE: mass isotopomer ratio analysis of U-13C-labeled extracts. A new method for accurate quantification of changes in concentrations of intracellular metabolites. *Biotechnol. Bioeng.*, 85(6):620–628, 2004.
- [194] Joshua D Rabinowitz. Cellular metabolomics of Escherchia coli. *Expert Rev Proteomics*, 4(2):187–198, April 2007.
- [195] Kellen L Olszewski, Joanne M Morrissey, Daniel Wilinski, James M Burns, Akhil B Vaidya, Joshua D Rabinowitz, and Manuel Llinás. Host-Parasite

Interactions Revealed by *Plasmodium falciparum* Metabolomics. *Cell Host & Microbe*, 5(2):191–199, February 2009.

- [196] Douglas B Kell. Systems biology, metabolic modelling and metabolomics in drug discovery and development. *Drug Discov. Today*, 11(23-24):1085–1092, December 2006.
- [197] Royston Goodacre, Seetharaman Vaidyanathan, Warwick B Dunn, George G Harrigan, and Douglas B Kell. Metabolomics by numbers: acquiring and understanding global metabolite data. *Trends in Biotechnology*, 22(5):245–252, May 2004.
- [198] Olivier Cloarec, Marc-Emmanuel Dumas, Andrew Craig, Richard H Barton, Johan Trygg, Jane Hudson, Christine Blancher, Dominique Gauguier, John C Lindon, Elaine Holmes, and Jeremy Nicholson. Statistical total correlation spectroscopy: an exploratory approach for latent biomarker identification from metabolic 1H NMR data sets. *Anal Chem*, 77(5):1282–1289, March 2005.
- [199] Qiu Cui, Ian A Lewis, Adrian D Hegeman, Mark E Anderson, Jing Li, Christopher F Schulte, William M Westler, Hamid R Eghbalian, Michael R Sussman, and John L Markley. Metabolite identification via the Madison Metabolomics Consortium Database. *Nat. Biotechnol.*, 26(2):162–164, February 2008.
- [200] Sara Forcisi, Franco Moritz, Basem Kanawati, Dimitrios Tziotis, Rainer Lehmann, and Philippe Schmitt-Kopplin. Liquid chromatography-mass spectrometry in metabolomics research: mass analyzers in ultra high pressure liquid chromatography coupling. *J Chromatogr A*, 1292:51–65, May 2013.
- [201] Susen Becker, Linda Kortz, Christin Helmschrodt, Joachim Thiery, and Uta Ceglarek. LC-MS-based metabolomics in the clinical laboratory. *J Chromatogr B Analyt Technol Biomed Life Sci*, 883-884:68–75, February 2012.
- [202] Hiroshi Tsugawa, Takeshi Bamba, Masakazu Shinohara, Shin Nishiumi, Masaru Yoshida, and Eiichiro Fukusaki. Practical non-targeted gas chromatography/mass spectrometry-based metabolomics platform for metabolic phenotype analysis. *J Biosci Bioeng*, 112(3):292–298, September 2011.
- [203] Luc Denoroy, Luc Zimmer, Bernard Renaud, and Sandrine Parrot. Ultra high performance liquid chromatography as a tool for the discovery and the analysis of biomarkers of diseases: a review. *J Chromatogr B Analyt Technol Biomed Life Sci*, 927:37–53, May 2013.

- [204] Nicola Volpi and Francesca Maccari. *Capillary Electrophoresis of Biomolecules*. Methods and Protocols. Humana Press, February 2013.
- [205] Julia Balog, Sacheen Kumar, James Alexander, Ottmar Golf, Juzheng Huang, Tom Wiggins, Nima Abbassi-Ghadi, Attila Enyedi, Sandor Kacska, James Kinross, George B Hanna, Jeremy K Nicholson, and Zoltan Takats. In Vivo Endoscopic Tissue Identification by Rapid Evaporative Ionization Mass Spectrometry (REIMS). *Angew. Chem. Int. Ed.*, 54(38):11059–11062, September 2015.
- [206] Roger S Macomber. *A complete introduction to modern NMR spectroscopy*. Wiley-Interscience, 1998.
- [207] J K Nicholson, M P O’Flynn, P J Sadler, A F Macleod, S M Juul, and P H Sönksen. Proton-nuclear-magnetic-resonance studies of serum, plasma and urine from fasting normal and diabetic subjects. *Biochem. J.*, 217(2):365–375, January 1984.
- [208] J K Nicholson, M J Buckingham, and P J Sadler. High resolution ^1H n.m.r. studies of vertebrate blood and plasma. *Biochem. J.*, 211(3):605–615, June 1983.
- [209] D J Russell, C E Hadden, G E Martin, A A Gibson, A P Zens, and J L Carolan. A comparison of inverse-detected heteronuclear NMR performance: conventional vs cryogenic microprobe performance. *J Nat Prod*, 63(8):1047–1049, August 2000.
- [210] Gwenaelle Le Gall. Sample collection and preparation of biofluids and extracts for NMR spectroscopy. *Methods Mol. Biol.*, 1277:15–28, 2015.
- [211] Anthony C Dona, Beatriz Jimenez, Hartmut Schafer, Eberhard Humpfer, Manfred Spraul, Matthew R Lewis, Jake T M Pearce, Elaine Holmes, John C Lindon, and Jeremy K Nicholson. Precision high-throughput proton NMR spectroscopy of human urine, serum, and plasma for large-scale metabolic phenotyping. *Anal Chem*, 86(19):9887–9894, October 2014.
- [212] Wenyun Lu, Elizabeth Kimball, and Joshua D Rabinowitz. A high-performance liquid chromatography-tandem mass spectrometry method for quantitation of nitrogen-containing intracellular metabolites. *J Am Soc Mass Spectrom*, 17(1):37–50, January 2006.

- [213] Teresa W-M Fan and Andrew N Lane. Structure-based profiling of metabolites and isotopomers by NMR. *Progress in Nuclear Magnetic Resonance Spectroscopy*, 52(2-3):69–117, 2008.
- [214] Guido F Pauli, Birgit U Jaki, and David C Lankin. Quantitative ^1H NMR: Development and Potential of a Method for Natural Products Analysis §. *J Nat Prod*, 68(1):133–149, January 2005.
- [215] Renata Tonhosolo, Fabio L D’Alexandri, Veridiana V de Rosso, Marcos L Gazarini, Miriam Y Matsumura, Valnice J Peres, Emilio F Merino, Jane M Carlton, Gerhard Wunderlich, Adriana Z Mercadante, Emilia A Kimura, and Alejandro M Katzin. Carotenoid biosynthesis in intraerythrocytic stages of *Plasmodium falciparum*. *J. Biol. Chem.*, 284(15):9974–9985, April 2009.
- [216] Evelin Schwarzer, Hartmut Kuhn, Elena Valente, and Paolo Arese. Malaria-parasitized erythrocytes and hemozoin nonenzymatically generate large amounts of hydroxy fatty acids that inhibit monocyte functions. *Blood*, 101(2):722–728, January 2003.
- [217] Rongwei Teng, Adele M Lehane, Markus Winterberg, Sarah H Shafik, Robert L Summers, Rowena E Martin, Donnelly A van Schalkwyk, Pauline R Junankar, and Kiaran Kirk. (^1H) -NMR metabolite profiles of different strains of *Plasmodium falciparum*. *Biosci. Rep.*, 34(6):e00150, 2014.
- [218] Jia V Li, Yulan Wang, Jasmina Saric, Jeremy K Nicholson, Stephan Dirnhofer, Burton H Singer, Marcel Tanner, Sergio Wittlin, Elaine Holmes, and Jurg Utzinger. Global metabolic responses of NMRI mice to an experimental *Plasmodium berghei* infection. *J Proteome Res*, 7(9):3948–3956, September 2008.
- [219] Rongwei Teng, Pauline R Junankar, William A Bubb, Caroline Rae, Pascal Mercier, and Kiaran Kirk. Metabolite profiling of the intraerythrocytic malaria parasite *Plasmodium falciparum* by (^1H) NMR spectroscopy. *NMR Biomed*, 22(3):292–302, April 2009.
- [220] Anna C van Brummelen, Kellen L Olszewski, Daniel Wilinski, Manuel Llinás, Abraham I Louw, and Lyn-Marie Birkholtz. Co-inhibition of *Plasmodium falciparum* S-adenosylmethionine decarboxylase/ornithine decarboxylase reveals perturbation-specific compensatory mechanisms by transcriptome, proteome, and metabolome analyses. *J. Biol. Chem.*, 284(7):4635–4646, February 2009.

- [221] Simon A Cobbold, Hwa H Chua, Brunda Nijagal, Darren J Creek, Stuart A Ralph, and Malcolm J McConville. Metabolic Dysregulation Induced in *Plasmodium falciparum* by Dihydroartemisinin and Other Front-Line Antimalarial Drugs. *J. Infect. Dis.*, 213(2):276–286, July 2015.
- [222] Sanna R Rijpma, Maarten van der Velden, Albert Bilos, Robert S Jansen, Sunny Mahakena, Frans G M Russel, Robert W Sauerwein, Koen van de Wetering, and Jan B Koenderink. MRP1 mediates folate transport and antifolate sensitivity in *Plasmodium falciparum*. *FEBS Lett.*, 590(4):482–492, February 2016.
- [223] Monika Mehta, Haripalsingh M Sonawat, and Shobhona Sharma. Glycolysis in *Plasmodium falciparum* results in modulation of host enzyme activities. *J Vector Borne Dis*, 43(3):95–103, September 2006.
- [224] Angika Basant, Mayuri Rege, Shobhona Sharma, and Haripalsingh M Sonawat. Alterations in urine, serum and brain metabolomic profiles exhibit sexual dimorphism during malaria disease progression. *Malar J*, 9:110, 2010.
- [225] Izabella Surowiec, Judy Orikiiriza, Elisabeth Karlsson, Maria Nelson, Mari Bonde, Patrick Kyamanwa, Ben Karenzi, Sven Bergstrom, Johan Trygg, and Johan Normark. Metabolic Signature Profiling as a Diagnostic and Prognostic Tool in Pediatric *Plasmodium falciparum* Malaria. *Open Forum Infect Dis*, 2(2):ofv062, April 2015.
- [226] Anubhav Srivastava, Darren J Creek, Krystal J Evans, David De Souza, Louis Schofield, Sylke Müller, Michael P Barrett, Malcolm J McConville, and Andrew P Waters. Host reticulocytes provide metabolic reservoirs that can be exploited by malaria parasites. *PLoS Pathog.*, 11(6):e1004882, June 2015.
- [227] Marylin Torrentino-Madamet, Lionel Alméras, Jérôme Desplans, Yannick Le Priol, Maya Belghazi, Matthieu Pophillat, Patrick Fourquet, Yves Jammes, and Daniel Parzy. Global response of *Plasmodium falciparum* to hyperoxia: a combined transcriptomic and proteomic approach. *Malar J*, 10:4–4, 2011.
- [228] Philip J Shaw, Sastra Chaotheing, Pavita Kaewprommal, Jittima Piriyaongsa, Chayaphat Wongsombat, Nattida Suwannakitti, Pongpisid Koonyosying, Chairat Uthaipibull, Yongyuth Yuthavong, and Sumalee Kamchonwongpaisan. *Plasmodium* parasites mount an arrest response to dihydroartemisinin, as revealed by whole transcriptome shotgun sequencing (RNA-seq) and microarray study. *BMC Genomics*, 16(1):830, 2015.

- [229] Benoit Witkowski, Joel Lelièvre, María José López Barragán, Victor Laurent, Xin-Zhuan Su, Antoine Berry, and Françoise Benoit-Vical. Increased Tolerance to Artemisinin in *Plasmodium falciparum* Is Mediated by a Quiescence Mechanism. *Antimicrob. Agents Chemother.*, 54(5):1872–1877, May 2010.
- [230] J-H Ch'ng, S R Kotturi, A G-L Chong, M J Lear, and K S-W Tan. A programmed cell death pathway in the malaria parasite *Plasmodium falciparum* has general features of mammalian apoptosis but is mediated by clan CA cysteine proteases. *Cell Death Dis*, 1:e26, 2010.
- [231] Viswanathan A Nagaraj, Dhanunjay Mukhi, Vinayagam Sathishkumar, Pradeep A Subramani, Susanta K Ghosh, Rajeev R Pandey, Manjunatha C Shetty, and Govindarajan Padmanaban. Asparagine requirement in *Plasmodium berghei* as a target to prevent malaria transmission and liver infections. *Nat Commun*, 6 SP -, November 2015.
- [232] Shalon E Babbitt, Lindsey Altenhofen, Simon A Cobbold, Eva S Istvan, Clare Fennell, Christian Doerig, Manuel Llinás, and Daniel E Goldberg. *Plasmodium falciparum* responds to amino acid starvation by entering into a hibernatory state. *Proc. Natl. Acad. Sci. U.S.A.*, 109(47):E3278–87, November 2012.
- [233] Timothy G Geary, Alan A Divo, and James B Jensen. Nutritional Requirements of *Plasmodium falciparum* in Culture. II. Effects of Antimetabolites in a Semi Defined Medium. *J Euk. Microbiol.*, 32(1):65–69, February 1985.
- [234] T G Geary, A A Divo, L C Bonanni, and J B Jensen. Nutritional requirements of *Plasmodium falciparum* in culture. III. Further observations on essential nutrients and antimetabolites. *J. Protozool.*, 32(4):608–613, November 1985.
- [235] Lydia Mata-Cantero, Maria J Lafuente, Laura Sanz, and Manuel S Rodriguez. Magnetic isolation of *Plasmodium falciparum* schizonts iRBCs to generate a high parasitaemia and synchronized in vitro culture. *Malar J*, 13(1):112, 2014.
- [236] F L Schuster. Cultivation of *Plasmodium* spp. *Clinical Microbiology Reviews*, 15(3):355–364, July 2002.
- [237] Chris Lambros and Jerome P Vanderberg. Synchronization of *Plasmodium falciparum* Erythrocytic Stages in Culture. *The Journal of Parasitology*, 65(3):418, June 1979.
- [238] D Méndez, C Moneriz, M Linares, and P Marín-García. Synchronous culture of *Plasmodium falciparum* at high parasitemia levels . *Nat Protoc*, 2009.

- [239] Kellen L Olszewski and Manuel Llinás. Extraction of hydrophilic metabolites from *Plasmodium falciparum*-infected erythrocytes for metabolomic analysis. *Methods Mol. Biol.*, 923:259–266, 2013.
- [240] Olaf Beckonert, Hector C Keun, Timothy M D Ebbels, Jacob Bundy, Elaine Holmes, John C Lindon, and Jeremy K Nicholson. Metabolic profiling, metabolomic and metabonomic procedures for NMR spectroscopy of urine, plasma, serum and tissue extracts. *Nat Protoc*, 2(11):2692–2703, 2007.
- [241] M Findeisen, T Brand, and S Berger. A ¹H-NMR thermometer suitable for cryoprobes. *Magnetic Resonance in Chemistry*, 45:175–178, 2007.
- [242] Wim F Vranken, Wayne Boucher, Tim J Stevens, Rasmus H Fogh, Anne Pajon, Miguel Llinas, Eldon L Ulrich, John L Markley, John Ionides, and Ernest D Laue. The CCPN data model for NMR spectroscopy: development of a software pipeline. *Proteins*, 59(4):687–696, June 2005.
- [243] Francesca Chignola, Silvia Mari, Tim J Stevens, Rasmus H Fogh, Valeria Mannella, Wayne Boucher, and Giovanna Musco. The CCPN Metabolomics Project: a fast protocol for metabolite identification by 2D-NMR. *Bioinformatics*, 27(6):885–886, March 2011.
- [244] Thomas Spangenberg, Jeremy N Burrows, Paul Kowalczyk, Simon McDonald, Timothy N C Wells, and Paul Willis. The open access malaria box: a drug discovery catalyst for neglected diseases. *PLoS ONE*, 8(6):e62906, 2013.
- [245] Kellen L Olszewski, Michael W Mather, Joanne M Morrissey, Benjamin A Garcia, Akhil B Vaidya, Joshua D Rabinowitz, and Manuel Llinás. Retraction: Branched tricarboxylic acid metabolism in *Plasmodium falciparum*. *Nature*, 497(7451):652, May 2013.
- [246] Richard J W Allen and Kiaran Kirk. The membrane potential of the intraerythrocytic malaria parasite *Plasmodium falciparum*. *J. Biol. Chem.*, 279(12):11264–11272, March 2004.
- [247] Clotilde Ribaut, Antoine Berry, Séverine Chevalley, Karine Reybier, Isabelle Morlais, Daniel Parzy, Françoise Nepveu, Françoise Benoit-Vical, and Alexis Valentin. Concentration and purification by magnetic separation of the erythrocytic stages of all human *Plasmodium* species. *Malar J*, 7:45–45, 2008.

- [248] N Jamshidi, J S Edwards, T Fahland, G M Church, and B O Palsson. Dynamic simulation of the human red blood cell metabolic network. *Bioinformatics*, 17(3):286–287, March 2001.
- [249] Massimo Castagnola, Irene Messina, Maria Teresa Sanna, and Bruno Giardina. Oxygen-linked modulation of erythrocyte metabolism: state of the art. *Blood Transfusion*, 8(Suppl 3):s53–s58, June 2010.
- [250] Joshua D Rabinowitz and Elizabeth Kimball. Acidic acetonitrile for cellular metabolome extraction from *Escherichia coli*. *Anal Chem*, 79(16):6167–6173, August 2007.
- [251] Norbert W Lutz, Jonathan V Sweedler, and Ron A Wevers. *Methodologies for Metabolomics: Experimental Strategies and Techniques*. Cambridge University Press, January 2013.
- [252] Chenomx Inc. Chenomx Inc. - Metabolite Discovery and Measurement Software.
- [253] Lucienne Tritten, Jennifer Keiser, Markus Godejohann, Jurg Utzinger, Mireille Vargas, Olaf Beckonert, Elaine Holmes, and Jasmina Saric. Metabolic profiling framework for discovery of candidate diagnostic markers of malaria. *Sci Rep*, 3:2769, 2013.
- [254] Arjun Sengupta, Soumita Ghosh, Shobhona Sharma, and Haripalsingh M Sonawat. ¹H NMR metabonomics indicates continued metabolic changes and sexual dimorphism post-parasite clearance in self-limiting murine malaria model. *PLoS ONE*, 8(6):e66954, 2013.
- [255] Soumita Ghosh, Arjun Sengupta, Shobhona Sharma, and Haripalsingh M Sonawat. Metabolic fingerprints of serum, brain, and liver are distinct for mice with cerebral and noncerebral malaria: a (¹H) NMR spectroscopy-based metabonomic study. *J Proteome Res*, 11(10):4992–5004, October 2012.
- [256] Arjun Sengupta, Soumita Ghosh, Angika Basant, Suhas Malusare, Parul Johri, Sulabha Pathak, Shobhona Sharma, and Haripalsingh M Sonawat. Global host metabolic response to *Plasmodium vivax* infection: a ¹H NMR based urinary metabonomic study. *Malar J*, 10:384, 2011.
- [257] Aalim M Weljie, Jack Newton, Pascal Mercier, Erin Carlson, and Carolyn M Slupsky. Targeted profiling: quantitative analysis of ¹H NMR metabolomics data. *Anal Chem*, 78(13):4430–4442, July 2006.

- [258] E L Ulrich, H Akutsu, J F Doreleijers, Y Harano, Y E Ioannidis, J Lin, M Livny, S Mading, D Maziuk, Z Miller, E Nakatani, C F Schulte, D E Tolmie, R Kent Wenger, H Yao, and J L Markley. BioMagResBank. *Nucleic acids Research*, 36(Database):D402–D408, December 2007.
- [259] Christian Ludwig, John M Easton, Alessia Lodi, Stefano Tiziani, Susan E Manzoor, Andrew D Southam, Jonathan J Byrne, Lisa M Bishop, Shan He, Theodoros N Arvanitis, Ulrich L Günther, and Mark R Viant. Birmingham Metabolite Library: a publicly accessible database of 1-D ^1H and 2-D ^1H J-resolved NMR spectra of authentic metabolite standards (BML-NMR). *Metabolomics*, 8(1):8–18, August 2011.
- [260] NMR Spectra Software — Spectroscopy (formerly Informatics) — Bio-Rad. *bio-rad.com*.
- [261] Arnald Alonso, Miguel A Rodriguez, Maria Vinaixa, Raul Tortosa, Xavier Correig, Antonio Julia, and Sara Marsal. Focus: a robust workflow for one-dimensional NMR spectral analysis. *Anal Chem*, 86(2):1160–1169, January 2014.
- [262] Matthias S Klein, Peter J Oefner, and Wolfram Gronwald. MetaboQuant: a tool combining individual peak calibration and outlier detection for accurate metabolite quantification in 1D (^1H) and (^1H)-(^{13}C) HSQC NMR spectra. *Biotechniques*, 54(5):251–256, May 2013.
- [263] Neil MacKinnon, Bagganahalli S Somashekar, Pratima Tripathi, Wencheng Ge, Thekkelnaycke M Rajendiran, Arul M Chinnaiyan, and Ayyalusamy Ramamoorthy. MetaboID: a graphical user interface package for assignment of ^1H NMR spectra of bodyfluids and tissues. *J Magn Reson*, 226:93–99, January 2013.
- [264] Josep Gomez, Jesus Brezmes, Roger Mallol, Miguel A Rodriguez, Maria Vinaixa, Reza M Salek, Xavier Correig, and Nicolau Canellas. Dolphin: a tool for automatic targeted metabolite profiling using 1D and 2D (^1H)-NMR data. *Anal Bioanal Chem*, 406(30):7967–7976, December 2014.
- [265] Dan Tulpan, Serge Léger, Luc Belliveau, Adrian Culf, and Miroslava Čuperlović-Culf. MetaboHunter: an automatic approach for identification of metabolites from (^1H)-NMR spectra of complex mixtures. *BMC Bioinformatics*, 12:400–400, 2011.

- [266] Jianguo Xia, Igor V Sinelnikov, Beomsoo Han, and David S Wishart. MetaboAnalyst 3.0—making metabolomics more meaningful. *Nucleic acids Research*, 43(W1):W251–7, July 2015.
- [267] Fengli Zhang, Steven L Robinette, Lei Bruschweiler-Li, and Rafael Bruschweiler. Web server suite for complex mixture analysis by covariance NMR. *Magn Reson Chem*, 47 Suppl 1:S118–22, December 2009.
- [268] Eisuke Chikayama, Yasuyo Sekiyama, Mami Okamoto, Yumiko Nakanishi, Yuri Tsuboi, Kenji Akiyama, Kazuki Saito, Kazuo Shinozaki, and Jun Kikuchi. Statistical indices for simultaneous large-scale metabolite detections for a single NMR spectrum. *Anal Chem*, 82(5):1653–1658, March 2010.
- [269] Ian A Lewis, Seth C Schommer, and John L Markley. rNMR: open source software for identifying and quantifying metabolites in NMR spectra. *Magnetic Resonance in Chemistry*, 47(S1):S123–S126, December 2009.
- [270] Jianguo Xia, Trent C Bjorndahl, Peter Tang, and David S Wishart. MetaboMiner—semi-automated identification of metabolites from 2D NMR spectra of complex biofluids. *BMC Bioinformatics*, 9:507, 2008.
- [271] Jie Hao, William Astle, Maria De Iorio, and Timothy M D Ebbels. BATMAN—an R package for the automated quantification of metabolites from nuclear magnetic resonance spectra using a Bayesian model. *Bioinformatics*, 28(15):2088–2090, August 2012.
- [272] Albert Goldbeter Berridge, M J, and Albert Goldbeter. *Oscillatory enzymes: simple periodic behaviour in an allosteric model for glycolytic oscillations*. publisherNameCambridge University Press, 1996.
- [273] F A Chandra, G Buzi, and J C Doyle. Glycolytic Oscillations and Limits on Robust Efficiency. *Science*, 333(6039):187–192, July 2011.
- [274] P Smolen. A model for glycolytic oscillations based on skeletal muscle phosphofructokinase kinetics. *J. Theor. Biol.*, 174(2):137–148, May 1995.
- [275] Teresa W-M Fan and Andrew N Lane. NMR-based stable isotope resolved metabolomics in systems biochemistry. *J Biomol NMR*, 49(3-4):267–280, February 2011.
- [276] A Dean Sherry, F Mark H Jeffrey, and Craig R Malloy. Analytical solutions for (^{13}C) isotopomer analysis of complex metabolic conditions: substrate oxi-

- dation, multiple pyruvate cycles, and gluconeogenesis. *Metabolic Engineering*, 6(1):12–24, January 2004.
- [277] Danhong Lu, Hindrik Mulder, Piyu Zhao, Shawn C Burgess, Mette V Jensen, Svetlana Kamzolova, Christopher B Newgard, and A Dean Sherry. ¹³C NMR isotopomer analysis reveals a connection between pyruvate cycling and glucose-stimulated insulin secretion (GSIS). *Proc. Natl. Acad. Sci. U.S.A.*, 99(5):2708–2713, March 2002.
- [278] Helen M Parsons, Christian Ludwig, and Mark R Viant. Line-shape analysis of J-resolved NMR spectra: application to metabolomics and quantification of intensity errors from signal processing and high signal congestion. *Magnetic Resonance in Chemistry*, 47(S1):S86–S95, December 2009.
- [279] K Kirk, R E Martin, S Bröer, S M Howitt, and K J Saliba. *Plasmodium* permeomics: membrane transport proteins in the malaria parasite. *Curr. Top. Microbiol. Immunol.*, 295:325–356, 2005.
- [280] Virgilio L Lew, Teresa Tiffert, and Hagai Ginsburg. Excess hemoglobin digestion and the osmotic stability of *Plasmodium falciparum*-infected red blood cells. *Blood*, 101(10):4189–4194, May 2003.
- [281] Kellen L Olszewski and Manuel Llinás. Central carbon metabolism of *Plasmodium* parasites. *Mol. Biochem. Parasitol.*, 175(2):95–103, February 2011.
- [282] James I Macrae, Sash Lopaticki, Alexander G Maier, Thusitha Rupasinghe, Amsaha Nahid, Alan F Cowman, and Malcolm J McConville. *Plasmodium falciparum* is dependent on de novo myo-inositol biosynthesis for assembly of GPI glycolipids and infectivity. *Mol. Microbiol.*, 91(4):762–776, February 2014.
- [283] Karine G Le Roch, Yingyao Zhou, Peter L Blair, Muni Grainger, J Kathleen Moch, J David Haynes, Patricia De La Vega, Anthony A Holder, Serge Batalov, Daniel J Carucci, and Elizabeth A Winzeler. Discovery of gene function by expression profiling of the malaria parasite life cycle. *Science*, 301(5639):1503–1508, September 2003.
- [284] Nathalie Vonlaufen, Stefan M Kanzok, Ronald C Wek, and William J Jr Sullivan. Stress response pathways in protozoan parasites. *Cell Microbiol.*, 10(12):2387–2399, December 2008.

- [285] Franka Teuscher, Michelle L Gatton, Nanhua Chen, Jennifer Peters, Dennis E Kyle, and Qin Cheng. Artemisinin-induced dormancy in *Plasmodium falciparum*: duration, recovery rates, and implications in treatment failure. *J. Infect. Dis.*, 202(9):1362–1368, November 2010.
- [286] C R Zerez, E F Roth, S Schulman, and K R Tanaka. Increased nicotinamide adenine dinucleotide content and synthesis in *Plasmodium falciparum*-infected human erythrocytes. *Blood*, 75(8):1705–1710, April 1990.
- [287] Enrique Salcedo, Paul F G Sims, and John E Hyde. A glycine-cleavage complex as part of the folate one-carbon metabolism of *Plasmodium falciparum*. *Trends Parasitol.*, 21(9):406–411, September 2005.
- [288] Kodjo Ayi, Marina Cappadoro, Mario Branca, Franco Turrini, and Paolo Arese. *Plasmodium falciparum* glutathione metabolism and growth are independent of glutathione system of host erythrocyte. *FEBS Lett.*, 424(3):257–261, March 1998.
- [289] Jessica K O’Hara, Lewis J Kerwin, Simon A Cobbold, Jonathan Tai, Thomas A Bedell, Paul J Reider, and Manuel Llinás. Targeting NAD⁺ metabolism in the human malaria parasite *Plasmodium falciparum*. *PLoS ONE*, 9(4):e94061, April 2014.
- [290] Roth E, Jr. *Plasmodium falciparum* carbohydrate metabolism: a connection between host cell and parasite. *Blood Cells*, 16(2-3):453–60; discussion 461–6, January 1990.
- [291] NCBI Resource Coordinators. Database resources of the National Center for Biotechnology Information. *Nucleic acids Research*, 42(Database issue):D7–17, January 2014.
- [292] C C Bass and F M Johns. The cultivation of malarial plasmodia (*Plasmodium vivax* and *Plasmodium falciparum*) in vitro. *J. Exp. Med.*, 16(4):567–579, October 1912.
- [293] G E Moore, R E Gerner, and H A Franklin. Culture of normal human leukocytes. *JAMA*, 199(8):519–524, February 1967.
- [294] Run Ye, Dongmei Zhang, Biaobang Chen, Yongqiang Zhu, Yilong Zhang, Shengyue Wang, and Weiqing Pan. Transcription of the *var* genes from a freshly-obtained field isolate of *Plasmodium falciparum* shows more variable

- switching patterns than long laboratory-adapted isolates. *Malar J*, 14:66, 2015.
- [295] Johannes Schindelin, Ignacio Arganda-Carreras, Erwin Frise, Verena Kaynig, Mark Longair, Tobias Pietzsch, Stephan Preibisch, Curtis Rueden, Stephan Saalfeld, Benjamin Schmid, Jean-Yves Tinevez, Daniel James White, Volker Hartenstein, Kevin Eliceiri, Pavel Tomancak, and Albert Cardona. Fiji: an open-source platform for biological-image analysis. *Nat Methods*, 9(7):676–682, July 2012.
- [296] Theodore Booden and Robert W Hull. Nucleic acid precursor synthesis by *Plasmodium lophurae* parasitizing chicken erythrocytes. *Exp. Parasitol.*, 34(2):220–228, October 1973.
- [297] H Asahi, T Kanazawa, Y Kajihara, K Takahashi, and T Takahashi. Hypoxanthine: a low molecular weight factor essential for growth of erythrocytic *Plasmodium falciparum* in a serum-free medium. *Parasitology*, 113 (Pt 1):19–23, July 1996.
- [298] Y Hochberg and Y Benjamini. More powerful procedures for multiple significance testing. *Stat Med*, 9(7):811–818, July 1990.
- [299] R Core Team. R: A Language and Environment for Statistical Computing. *R Foundation for Statistical Computing. Vienna, Austria.*, 2013.
- [300] Norikazu Maeda, Toshiyuki Hibuse, and Tohru Funahashi. Role of aquaporin-7 and aquaporin-9 in glycerol metabolism; involvement in obesity. *Handb Exp Pharmacol*, 190:233–249, 2009.
- [301] Mary C Playdon, Michael B Bracken, Tara B Sanft, Jennifer A Ligibel, Maura Harrigan, and Melinda L Irwin. Weight gain after breast cancer diagnosis and all-cause mortality: systematic review and meta-analysis. *J Natl Cancer Inst*, 107(12), December 2015.
- [302] A Llewellyn, M Simmonds, C G Owen, and N Woolacott. Childhood obesity as a predictor of morbidity in adulthood: a systematic review and meta-analysis. *Obes Rev*, October 2015.
- [303] Mariangela Rondanelli, Milena Anna Faliva, Gabriella Peroni, Francesca Moncaglieri, Vittoria Infantino, Maurizio Naso, and Simone Perna. Focus on pivotal role of dietary intake (diet and supplement) and blood levels of

- tocopherols and tocotrienols in obtaining successful aging. *Int J Mol Sci*, 16(10):23227–23249, 2015.
- [304] Nashita Patel, Dharmintra Pasupathy, and Lucilla Poston. Determining the consequences of maternal obesity on offspring health. *Exp Physiol*, October 2015.
- [305] J D Wood and J T Reid. The influence of dietary fat on fat metabolism and body fat deposition in meal-feeding and nibbling rats. *Br J Nutr*, 34(1):15–24, July 1975.
- [306] W T Briscoe, L P Mercer, D Gimlin, and J Ramlet. Prediction of food intakes, weight gains, organ weights, and tumor size in tumor-bearing rats by the four-parameter mathematical model for physiological responses. *Cancer Res*, 41(8):3030–3034, August 1981.
- [307] E E Faridy. Effect of maternal malnutrition on surface activity of fetal lungs in rats. *J Appl Physiol*, 39(4):535–540, October 1975.
- [308] Dana C Dolinoy, Jennifer R Weidman, and Randy L Jirtle. Epigenetic gene regulation: Linking early developmental environment to adult disease. *Fetal Basis of Adult Disease*, 23(3):297–307, April 2007.
- [309] Ian B Jeffery and Paul W O’Toole. Diet-microbiota interactions and their implications for healthy living. *Nutrients*, 5(1):234–252, January 2013.
- [310] Roberto Berni Canani, Margherita Di Costanzo, and Ludovica Leone. The epigenetic effects of butyrate: potential therapeutic implications for clinical practice. *Clin Epigenetics*, 4(1):4, 2012.
- [311] Dimitrios Zgouras, Astrid Wachtershauser, Daniela Frings, and Jurgen Stein. Butyrate impairs intestinal tumor cell-induced angiogenesis by inhibiting HIF-1 α nuclear translocation. *Biochem. Biophys. Res. Commun.*, 300(4):832–838, January 2003.
- [312] M Saavedra, M Masdeu, P Hale, C M Sibbons, and W V Holt. Dietary fatty acid enrichment increases egg size and quality of yellow seahorse *Hippocampus kuda*. *Anim Reprod Sci*, 145(1-2):54–61, February 2014.
- [313] Sunil Laxman, Benjamin M Sutter, and Benjamin P Tu. Methionine is a signal of amino acid sufficiency that inhibits autophagy through the methylation of PP2A. *Autophagy*, 10(2):386–387, February 2014.

- [314] Nadia Ponts, Elena Y Harris, Jacques Prudhomme, Ivan Wick, Colleen Eckhardt-Ludka, Glenn R Hicks, Gary Hardiman, Stefano Lonardi, and Karine G Le Roch. Nucleosome landscape and control of transcription in the human malaria parasite. *Genome Res.*, 20(2):228–238, February 2010.
- [315] Nadia Ponts, Elena Y Harris, Stefano Lonardi, and Karine G Le Roch. Nucleosome occupancy at transcription start sites in the human malaria parasite: a hard-wired evolution of virulence? *Infect. Genet. Evol.*, 11(4):716–724, June 2011.
- [316] Florence Caro, Vida Ahyong, Miguel Betegon, and Joseph L DeRisi. Genome-wide regulatory dynamics of translation in the *Plasmodium falciparum* asexual blood stages. *eLife*, 3:e04106, 2014.
- [317] Zbynek Bozdech, Manuel Llinás, Brian Lee Pulliam, Edith D Wong, Jingchun Zhu, and Joseph L DeRisi. The transcriptome of the intraerythrocytic developmental cycle of *Plasmodium falciparum*. *PLoS Biol.*, 1(1):E5, October 2003.
- [318] Stephan Wullschleger, Robbie Loewith, and Michael N Hall. TOR signaling in growth and metabolism. *Cell*, 124(3):471–484, February 2006.
- [319] Joungmok Kim and Kun-Liang Guan. Amino acid signaling in TOR activation. *Annu. Rev. Biochem.*, 80:1001–1032, 2011.
- [320] Ana Brennand, Melisa Gualdron-Lopez, Isabelle Coppens, Daniel J Rigden, Michael L Ginger, and Paul A M Michels. Autophagy in parasitic protists: unique features and drug targets. *Mol. Biochem. Parasitol.*, 177(2):83–99, June 2011.
- [321] Alan G Hinnebusch and Krishnamurthy Natarajan. Gcn4p, a master regulator of gene expression, is controlled at multiple levels by diverse signals of starvation and stress. *Eukaryotic Cell*, 1(1):22–32, February 2002.
- [322] Anamika, N Srinivasan, and A Krupa. A genomic perspective of protein kinases in *Plasmodium falciparum*. *Proteins*, 58(1):180–189, January 2005.
- [323] Pauline Ward, Leila Equinet, Jeremy Packer, and Christian Doerig. Protein kinases of the human malaria parasite *Plasmodium falciparum*: the kinome of a divergent eukaryote. *BMC Genomics*, 5:79, October 2004.

- [324] Richard M R Coulson, Neil Hall, and Christos A Ouzounis. Comparative genomics of transcriptional control in the human malaria parasite *Plasmodium falciparum*. *Genome Res.*, 14(8):1548–1554, August 2004.
- [325] Karthikeyan Ganesan, Napawan Ponmee, Lei Jiang, Joseph W Fowble, John White, Sumalee Kamchonwongpaisan, Yongyuth Yuthavong, Prapon Wilairat, and Pradipsinh K Rathod. A genetically hard-wired metabolic transcriptome in *Plasmodium falciparum* fails to mount protective responses to lethal antifolates. *PLoS Pathog.*, 4(11):e1000214, November 2008.
- [326] Karine G Le Roch, Jeffrey R Johnson, Hugues Ahiboh, Duk-Won D Chung, Jacques Prudhomme, David Plouffe, Kerstin Henson, Yingyao Zhou, William Witola, John R Yates, Choukri Ben Mamoun, Elizabeth A Winzeler, and Henri Vial. A systematic approach to understand the mechanism of action of the bisthiazolium compound T4 on the human malaria parasite, *Plasmodium falciparum*. *BMC Genomics*, 9:513, 2008.
- [327] Duk-Won Doug Chung, Nadia Ponts, Serena Cervantes, and Karine G Le Roch. Post-translational modifications in *Plasmodium*: more than you think! *Mol. Biochem. Parasitol.*, 168(2):123–134, December 2009.
- [328] Balbir K Chaal, Archana P Gupta, Brigitta D Wastuwidyaningtyas, Yen-Hoon Luah, and Zbynek Bozdech. Histone deacetylases play a major role in the transcriptional regulation of the *Plasmodium falciparum* life cycle. *PLoS Pathog.*, 6(1):e1000737, January 2010.
- [329] Serena Cervantes, Paige E Stout, Jacques Prudhomme, Sebastian Engel, Matthew Bruton, Michael Cervantes, David Carter, Young Tae-Chang, Mark E Hay, William Aalbersberg, Julia Kubanek, and Karine G Le Roch. High content live cell imaging for the discovery of new antimalarial marine natural products. *BMC Infect Dis*, 12:1, 2012.
- [330] Serena Cervantes, Jacques Prudhomme, David Carter, Krishna G Gopi, Qian Li, Young-Tae Chang, and Karine G Le Roch. High-content live cell imaging with RNA probes: advancements in high-throughput antimalarial drug discovery. *BMC Cell Biol*, 10:45, 2009.
- [331] Yan Quan Lee, Amanda S P Goh, Jun Hong Ch’ng, Francois H Nosten, Peter Rainer Preiser, Shazib Pervaiz, Sanjiv Kumar Yadav, and Kevin S W Tan. A high-content phenotypic screen reveals the disruptive potency of quinacrine

- and 3',4'-dichlorobenzamil on the digestive vacuole of *Plasmodium falciparum*. *Antimicrob. Agents Chemother.*, 58(1):550–558, 2014.
- [332] Seunghyun Moon, Sukjun Lee, Heechang Kim, Lucio H Freitas-Junior, Myungjoo Kang, Lawrence Ayong, and Michael A E Hansen. An image analysis algorithm for malaria parasite stage classification and viability quantification. *PLoS ONE*, 8(4):e61812, 2013.
- [333] Giancarlo A Biagini, Parnpen Viriyavejakul, Paul M O'Neill, Patrick G Bray, and Stephen A Ward. Functional characterization and target validation of alternative complex I of *Plasmodium falciparum* mitochondria. *Antimicrob. Agents Chemother.*, 50(5):1841–1851, May 2006.
- [334] Heather B Reilly, Hongjian Wang, John A Steuter, Anastasia M Marx, and Michael T Ferdig. Quantitative dissection of clone-specific growth rates in cultured malaria parasites. *Int. J. Parasitol.*, 37(14):1599–1607, December 2007.
- [335] J H McKerrow, E Sun, P J Rosenthal, and J Bouvier. The proteases and pathogenicity of parasitic protozoa. *Annu. Rev. Microbiol.*, 47:821–853, 1993.
- [336] E Bailly, R Jambou, J Savel, and G Jaureguiberry. *Plasmodium falciparum*: differential sensitivity in vitro to E-64 (cysteine protease inhibitor) and Pepstatin A (aspartyl protease inhibitor). *J. Protozool.*, 39(5):593–599, September 1992.
- [337] Eric W Sayers, Tanya Barrett, Dennis A Benson, Evan Bolton, Stephen H Bryant, Kathi Canese, Vyacheslav Chetvernin, Deanna M Church, Michael Dicuccio, Scott Federhen, Michael Feolo, Lewis Y Geer, Wolfgang Helmberg, Yuri Kapustin, David Landsman, David J Lipman, Zhiyong Lu, Thomas L Madden, Tom Madej, Donna R Maglott, Aron Marchler-Bauer, Vadim Miller, Ilene Mizrachi, James Ostell, Anna Panchenko, Kim D Pruitt, Gregory D Schuler, Edwin Sequeira, Stephen T Sherry, Martin Shumway, Karl Sirotkin, Douglas Slotta, Alexandre Souvorov, Grigory Starchenko, Tatiana A Tatusova, Lukas Wagner, Yanli Wang, W John Wilbur, Eugene Yaschenko, and Jian Ye. Database resources of the National Center for Biotechnology Information. *Nucleic acids Research*, 38(Database issue):D5–16, January 2010.
- [338] I W Sherman. Transport of amino acids and nucleic acid precursors in malarial parasites. *Bulletin of the World Health Organization*, 55(2-3):211–225, 1977.

- [339] K Kirk. Membrane transport in the malaria-infected erythrocyte. *Physiol Rev*, 81(2):495–537, April 2001.
- [340] Paul R Sanders, Paul R Gilson, Greg T Cantin, Doron C Greenbaum, Thomas Nebl, Daniel J Carucci, Malcolm J McConville, Louis Schofield, Anthony N Hodder, John R 3rd Yates, and Brendan S Crabb. Distinct protein classes including novel merozoite surface antigens in Raft-like membranes of *Plasmodium falciparum*. *J. Biol. Chem.*, 280(48):40169–40176, December 2005.
- [341] H Nishimura, F V Pallardo, G A Seidner, S Vannucci, I A Simpson, and M J Birnbaum. Kinetics of GLUT1 and GLUT4 glucose transporters expressed in *Xenopus* oocytes. *J. Biol. Chem.*, 268(12):8514–8520, April 1993.
- [342] S D Lamour, U Straschil, J Saric, and M J Delves. Changes in metabolic phenotypes of *Plasmodium falciparum* in vitro cultures during gametocyte development. *Malar J*, 2014.
- [343] Liao Y Chen. Glycerol inhibits water permeation through *Plasmodium falciparum* aquaglyceroporin. *J Struct Biol.*, 181(1):71–76, January 2013.
- [344] K Moll, H Perlmann, A Scherf, and M Wahlgren. Methods in malaria research, 2008.
- [345] T K Hunt, R Aslam, Z Hussain, and S Beckert. Lactate, with oxygen, incites angiogenesis. *Oxygen Transport to Tissue XXIX*, 2008.
- [346] Ulrike G A Sattler and Wolfgang Mueller-Klieser. The anti-oxidant capacity of tumour glycolysis. *Int J Radiat Biol*, 85(11):963–971, November 2009.
- [347] Eva Gottfried, Leoni A Kunz-Schughart, Stephanie Ebner, Wolfgang Mueller-Klieser, Sabine Hoves, Reinhard Andreesen, Andreas Mackensen, and Marina Kreutz. Tumor-derived lactic acid modulates dendritic cell activation and antigen expression. *Blood*, 107(5):2013–2021, March 2006.
- [348] K Fischer, P Hoffmann, S Voelkl, N Meidenbauer, J Ammer, M Edinger, E Gottfried, S Schwarz, G Rothe, S Hoves, K Renner, B Timischl, A Mackensen, L Kunz-Schughart, R Andreesen, S W Krause, and M Kreutz. Inhibitory effect of tumor cell-derived lactic acid on human T cells. *Blood*, 109(9):3812–3819, May 2007.
- [349] J S Constant, J J Feng, D D Zabel, H Yuan, D Y Suh, H Scheuenstuhl, T K Hunt, and M Z Hussain. Lactate elicits vascular endothelial growth factor

from macrophages: a possible alternative to hypoxia. *Wound Repair Regen*, 8(5):353–360, September 2000.

- [350] Frédérique Végran, Romain Boidot, Carine Michiels, Pierre Sonveaux, and Olivier Feron. Lactate Influx through the Endothelial Cell Monocarboxylate Transporter MCT1 Supports an NF- κ B/IL-8 Pathway that Drives Tumor Angiogenesis. *Cancer Res*, 71(7):2550–2560, April 2011.
- [351] J P Daily, D Scandfeld, N Pochet, K Le Roch, D Plouffe, M Kamal, O Sarr, S Mboup, O Ndir, D Wypij, K Levasseur, E Thomas, P Tamayo, C Dong, Y Zhou, E S Lander, D Ndiaye, D Wirth, E A Winzeler, J P Mesirov, and A Regev. Distinct physiological states of *Plasmodium falciparum* in malaria-infected patients. *Nature*, 450(7172):1091–1095, December 2007.
- [352] Laura M Sanz, Benigno Crespo, Cristina De-Cózar, Xavier C Ding, Jose L Llergo, Jeremy N Burrows, Jose F García-Bustos, and Francisco-Javier Gamo. *P. falciparum* In Vitro Killing Rates Allow to Discriminate between Different Antimalarial Mode-of-Action. *PLoS ONE*, 7(2):e30949, February 2012.
- [353] Katrin Dietl, Kathrin Renner, Katja Dettmer, Birgit Timischl, Karin Eberhart, Christoph Dorn, Claus Hellerbrand, Michael Kastenberger, Leoni A Kunz-Schughart, Peter J Oefner, Reinhard Andreesen, Eva Gottfried, and Marina P Kreutz. Lactic acid and acidification inhibit TNF secretion and glycolysis of human monocytes. *J Immunol*, 184(3):1200–1209, February 2010.
- [354] Laura N Cruz, Yang Wu, Henning Ulrich, Alister G Craig, and Celia R S Garcia. Tumor necrosis factor reduces *Plasmodium falciparum* growth and activates calcium signaling in human malaria parasites. *Biochim. Biophys. Acta*, 1860(7):1489–1497, April 2016.
- [355] D Nguyen, A Joshi-Datar, F Lepine, E Bauerle, O Olakanmi, K Beer, G McKay, R Siehnel, J Schafhauser, Y Wang, B E Britigan, and P K Singh. Active Starvation Responses Mediate Antibiotic Tolerance in Biofilms and Nutrient-Limited Bacteria. *Science*, 334(6058):982–986, November 2011.
- [356] Fabrice Lalubin, Aline Deledevant, Olivier Glaizot, and Philippe Christe. Natural malaria infection reduces starvation resistance of nutritionally stressed mosquitoes. *J Anim Ecol*, 83(4):850–857, July 2014.

Appendix A

NMR metabolomics datasets

Note that Height stands for concentration calculated using peak heights and Volume stands for concentration calculated using peak volumes.

Table A.1: Chapter 3- Cellular extracts concentrations (mM)

Metabolite	Height	Volume	Glucose	Glutamine	Cell
Alanine	0.362760491	0.356800261	Glc 1 mM	No Gln	iRBC
Asparagine	0.418537228	0.414242617	Glc 1 mM	No Gln	iRBC
Aspartate	0.168498509	0.158040594	Glc 1 mM	No Gln	iRBC
Creatine	0.360107285	0.349899691	Glc 1 mM	No Gln	iRBC
Glutamate	0.543795012	0.52725382	Glc 1 mM	No Gln	iRBC
Glutamine	0.95403179	0.94088702	Glc 1 mM	No Gln	iRBC
Glycine	0.390639454	0.371889963	Glc 1 mM	No Gln	iRBC
GSH	1.303729028	1.237572361	Glc 1 mM	No Gln	iRBC
Lactate	1.488635168	1.471178347	Glc 1 mM	No Gln	iRBC
MyoInositol	0.155713886	0.165666985	Glc 1 mM	No Gln	iRBC
NAD	0.836609186	0.802803717	Glc 1 mM	No Gln	iRBC
Serine	0.460602308	0.438412854	Glc 1 mM	No Gln	iRBC
Alanine	0.345293278	0.339307439	Glc 1 mM	Gln 0.6 mM	iRBC
Asparagine	0.262470845	0.267276789	Glc 1 mM	Gln 0.6 mM	iRBC
Aspartate	0.152371677	0.152594794	Glc 1 mM	Gln 0.6 mM	iRBC
Creatine	0.263540513	0.282003427	Glc 1 mM	Gln 0.6 mM	iRBC
Glutamate	0.403335613	0.408537869	Glc 1 mM	Gln 0.6 mM	iRBC
Glutamine	0.856568915	0.887536789	Glc 1 mM	Gln 0.6 mM	iRBC
Glycine	0.261853939	0.267064183	Glc 1 mM	Gln 0.6 mM	iRBC
GSH	0.40041367	0.389887548	Glc 1 mM	Gln 0.6 mM	iRBC

Metabolite	Height	Volume	Glucose	Glutamine	Cell
Lactate	1.507339805	1.60100166	Glc 1 mM	Gln 0.6 mM	iRBC
MyoInositol	0.113259378	0.120260364	Glc 1 mM	Gln 0.6 mM	iRBC
NAD	0.655086473	0.668501559	Glc 1 mM	Gln 0.6 mM	iRBC
Serine	0.372482052	0.359715946	Glc 1 mM	Gln 0.6 mM	iRBC
Alanine	0.370863263	0.370521123	Glc 1 mM	Gln 2 mM	iRBC
Asparagine	0.375199626	0.383294963	Glc 1 mM	Gln 2 mM	iRBC
Aspartate	0.22691703	0.227561943	Glc 1 mM	Gln 2 mM	iRBC
Creatine	0.350264263	0.357740338	Glc 1 mM	Gln 2 mM	iRBC
Glutamate	0.627823939	0.619564523	Glc 1 mM	Gln 2 mM	iRBC
Glutamine	1.360598184	1.403889416	Glc 1 mM	Gln 2 mM	iRBC
Glycine	0.416278826	0.426367496	Glc 1 mM	Gln 2 mM	iRBC
GSH	0.601043587	0.609991542	Glc 1 mM	Gln 2 mM	iRBC
Lactate	1.751908956	1.784825801	Glc 1 mM	Gln 2 mM	iRBC
NAD	0.84797229	0.832534681	Glc 1 mM	Gln 2 mM	iRBC
Serine	0.534204501	0.495717476	Glc 1 mM	Gln 2 mM	iRBC
Alanine	0.371585827	0.355371299	Glc 5 mM	No Gln	iRBC
Asparagine	0.344963488	0.32292266	Glc 5 mM	No Gln	iRBC
Aspartate	0.16921249	0.166687207	Glc 5 mM	No Gln	iRBC
Creatine	0.363658391	0.340721871	Glc 5 mM	No Gln	iRBC
Glutamate	0.492983859	0.464685168	Glc 5 mM	No Gln	iRBC
Glutamine	0.945089428	0.926226684	Glc 5 mM	No Gln	iRBC
Glycine	0.296019846	0.26191575	Glc 5 mM	No Gln	iRBC
GSH	0.933093987	0.869374115	Glc 5 mM	No Gln	iRBC
Lactate	2.79110126	2.736291105	Glc 5 mM	No Gln	iRBC
MyoInositol	0.120835571	0.113309949	Glc 5 mM	No Gln	iRBC
NAD	0.841644897	0.797906833	Glc 5 mM	No Gln	iRBC
Serine	0.508469111	0.480250723	Glc 5 mM	No Gln	iRBC
Alanine	0.335227011	0.328622013	Glc 5 mM	Gln 0.6 mM	iRBC
Asparagine	0.296747334	0.319117359	Glc 5 mM	Gln 0.6 mM	iRBC
Aspartate	0.1608343	0.161728239	Glc 5 mM	Gln 0.6 mM	iRBC
Creatine	0.275774851	0.28833586	Glc 5 mM	Gln 0.6 mM	iRBC
Glutamate	0.459519788	0.465623039	Glc 5 mM	Gln 0.6 mM	iRBC
Glutamine	0.807896547	0.84347187	Glc 5 mM	Gln 0.6 mM	iRBC
Glycine	0.324242892	0.333543712	Glc 5 mM	Gln 0.6 mM	iRBC
GSH	0.787080307	0.76789308	Glc 5 mM	Gln 0.6 mM	iRBC
Lactate	3.610922534	3.732468356	Glc 5 mM	Gln 0.6 mM	iRBC

Metabolite	Height	Volume	Glucose	Glutamine	Cell
MyoInositol	0.104641555	0.103473487	Glc 5 mM	Gln 0.6 mM	iRBC
NAD	0.66137638	0.664204994	Glc 5 mM	Gln 0.6 mM	iRBC
Serine	0.435923473	0.434687576	Glc 5 mM	Gln 0.6 mM	iRBC
Alanine	0.331027072	0.318498125	Glc 5 mM	Gln 2 mM	iRBC
Asparagine	0.194019437	0.2084317	Glc 5 mM	Gln 2 mM	iRBC
Aspartate	0.133652741	0.125967053	Glc 5 mM	Gln 2 mM	iRBC
Creatine	0.269872129	0.281007754	Glc 5 mM	Gln 2 mM	iRBC
Glutamate	0.64227702	0.658388267	Glc 5 mM	Gln 2 mM	iRBC
Glutamine	0.98655018	1.035804243	Glc 5 mM	Gln 2 mM	iRBC
Glycine	0.319464986	0.324909418	Glc 5 mM	Gln 2 mM	iRBC
GSH	1.024742314	1.037397791	Glc 5 mM	Gln 2 mM	iRBC
Lactate	2.274415059	2.351798084	Glc 5 mM	Gln 2 mM	iRBC
MyoInositol	0.08961371	0.091492493	Glc 5 mM	Gln 2 mM	iRBC
NAD	0.745236671	0.731335364	Glc 5 mM	Gln 2 mM	iRBC
Serine	0.443046885	0.42877019	Glc 5 mM	Gln 2 mM	iRBC
Alanine	0.330662234	0.303459313	Glc 1 mM	No Gln	RBC
Asparagine	0.895216134	0.795130264	Glc 1 mM	No Gln	RBC
Aspartate	0.384989918	0.364850501	Glc 1 mM	No Gln	RBC
Creatine	1.426743475	1.377074294	Glc 1 mM	No Gln	RBC
Glutamate	6.164863346	5.85312934	Glc 1 mM	No Gln	RBC
Glutamine	1.776433897	1.757538501	Glc 1 mM	No Gln	RBC
Glycine	0.683601163	0.628985475	Glc 1 mM	No Gln	RBC
GSH	2.233752691	2.136266792	Glc 1 mM	No Gln	RBC
Lactate	1.204409137	1.130160213	Glc 1 mM	No Gln	RBC
Alanine	0.150195469	0.157763807	Glc 1 mM	Gln 0.6 mM	RBC
Asparagine	0.331194997	0.348209849	Glc 1 mM	Gln 0.6 mM	RBC
Aspartate	0.159255734	0.166793206	Glc 1 mM	Gln 0.6 mM	RBC
Creatine	0.490525433	0.514535279	Glc 1 mM	Gln 0.6 mM	RBC
Glutamate	2.251474726	2.262497483	Glc 1 mM	Gln 0.6 mM	RBC
Glutamine	0.791568765	0.831641884	Glc 1 mM	Gln 0.6 mM	RBC
Glycine	0.269052373	0.276693689	Glc 1 mM	Gln 0.6 mM	RBC
GSH	0.802561234	0.802595362	Glc 1 mM	Gln 0.6 mM	RBC
Lactate	0.498441331	0.516320543	Glc 1 mM	Gln 0.6 mM	RBC
NAD	0.12048569	0.118225363	Glc 1 mM	Gln 0.6 mM	RBC
Alanine	0.120302474	0.130986269	Glc 1 mM	Gln 2 mM	RBC
Asparagine	0.389174642	0.397086603	Glc 1 mM	Gln 2 mM	RBC

Metabolite	Height	Volume	Glucose	Glutamine	Cell
Aspartate	0.199315343	0.198101313	Glc 1 mM	Gln 2 mM	RBC
Creatine	0.489866701	0.511264577	Glc 1 mM	Gln 2 mM	RBC
Glutamate	2.267321938	2.27319623	Glc 1 mM	Gln 2 mM	RBC
Glutamine	0.918605141	0.964131114	Glc 1 mM	Gln 2 mM	RBC
Glycine	0.295363217	0.31079257	Glc 1 mM	Gln 2 mM	RBC
GSH	0.615808858	0.62406204	Glc 1 mM	Gln 2 mM	RBC
Lactate	0.450898297	0.444403413	Glc 1 mM	Gln 2 mM	RBC
NAD	0.178170003	0.177538997	Glc 1 mM	Gln 2 mM	RBC
Alanine	0.37516297	0.389845252	Glc 5 mM	No Gln	RBC
Asparagine	0.482855462	0.48579948	Glc 5 mM	No Gln	RBC
Aspartate	0.20192549	0.220476547	Glc 5 mM	No Gln	RBC
Creatine	0.761821012	0.792533625	Glc 5 mM	No Gln	RBC
Glutamate	3.381822068	3.364694784	Glc 5 mM	No Gln	RBC
Glutamine	1.166912926	1.217797335	Glc 5 mM	No Gln	RBC
Glycine	0.427948262	0.422942032	Glc 5 mM	No Gln	RBC
GSH	1.122973067	1.132485124	Glc 5 mM	No Gln	RBC
NAD	0.235423625	0.217996204	Glc 5 mM	No Gln	RBC
Alanine	0.723976088	0.682585502	Glc 5 mM	Gln 0.6 mM	RBC
Asparagine	1.304599989	1.298615424	Glc 5 mM	Gln 0.6 mM	RBC
Aspartate	0.514499296	0.496183542	Glc 5 mM	Gln 0.6 mM	RBC
Creatine	1.484735508	1.585578642	Glc 5 mM	Gln 0.6 mM	RBC
Glutamate	7.359251159	7.408578212	Glc 5 mM	Gln 0.6 mM	RBC
Glutamine	2.755583504	2.885137459	Glc 5 mM	Gln 0.6 mM	RBC
Glycine	0.993049888	1.004453664	Glc 5 mM	Gln 0.6 mM	RBC
GSH	2.002649854	2.047070053	Glc 5 mM	Gln 0.6 mM	RBC
NAD	0.440061929	0.460951706	Glc 5 mM	Gln 0.6 mM	RBC
Alanine	0.242860176	0.235693516	Glc 5 mM	Gln 2 mM	RBC
Asparagine	0.478487753	0.488039569	Glc 5 mM	Gln 2 mM	RBC
Aspartate	0.218641527	0.216963915	Glc 5 mM	Gln 2 mM	RBC
Creatine	0.738077518	0.762933331	Glc 5 mM	Gln 2 mM	RBC
Glutamate	3.37184712	3.362528387	Glc 5 mM	Gln 2 mM	RBC
Glutamine	1.482080035	1.530364796	Glc 5 mM	Gln 2 mM	RBC
Glycine	0.428303439	0.428108245	Glc 5 mM	Gln 2 mM	RBC
GSH	0.928207274	0.928847525	Glc 5 mM	Gln 2 mM	RBC
NAD	0.225196887	0.226539261	Glc 5 mM	Gln 2 mM	RBC

Table A.2: Chapter 3- Supernatant concentrations (mM)

Metabolite	Height	Volume	Glucose	Glutamine	Cell
α -D-glucose	0.213726023	0.212159829	Glc 1 mM	No Gln	iRBC
β -D-glucose	0.220535676	0.218689984	Glc 1 mM	No Gln	iRBC
Glycerol	0.132001543	0.133487396	Glc 1 mM	No Gln	iRBC
Lactate	3.369962155	3.491848417	Glc 1 mM	No Gln	iRBC
Alanine	0	0	Glc 1 mM	No Gln	iRBC
Glutamate	0	0	Glc 1 mM	No Gln	iRBC
Glutamine	0	0	Glc 1 mM	No Gln	iRBC
Alanine	0	0	Glc 1 mM	Gln 0.6 mM	iRBC
α -D-glucose	0.323098867	0.330924679	Glc 1 mM	Gln 0.6 mM	iRBC
β -D-glucose	0.336707181	0.34043376	Glc 1 mM	Gln 0.6 mM	iRBC
Glutamate	0.270153685	0.266425812	Glc 1 mM	Gln 0.6 mM	iRBC
Glutamine	0.238512826	0.241025615	Glc 1 mM	Gln 0.6 mM	iRBC
Glycerol	0.160250226	0.157906561	Glc 1 mM	Gln 0.6 mM	iRBC
Lactate	3.997018137	4.135116229	Glc 1 mM	Gln 0.6 mM	iRBC
Alanine	0.048345917	0.053430932	Glc 1 mM	Gln 2 mM	iRBC
α -D-glucose	0.274817288	0.277218772	Glc 1 mM	Gln 2 mM	iRBC
β -D-glucose	0.283642716	0.280584906	Glc 1 mM	Gln 2 mM	iRBC
Glutamate	0.621384808	0.612595926	Glc 1 mM	Gln 2 mM	iRBC
Glutamine	1.096245856	1.111078329	Glc 1 mM	Gln 2 mM	iRBC
Glycerol	0.155891923	0.15086894	Glc 1 mM	Gln 2 mM	iRBC
Lactate	3.343365039	3.411158241	Glc 1 mM	Gln 2 mM	iRBC
α -D-glucose	2.734634521	2.721705491	Glc 5 mM	No Gln	iRBC
β -D-glucose	2.852300952	2.794635706	Glc 5 mM	No Gln	iRBC
Glycerol	0.22032348	0.215723294	Glc 5 mM	No Gln	iRBC
Lactate	5.723345095	5.776401508	Glc 5 mM	No Gln	iRBC
Alanine	0	0	Glc 5 mM	No Gln	iRBC
Glutamate	0	0	Glc 5 mM	No Gln	iRBC
Glutamine	0	0	Glc 5 mM	No Gln	iRBC
Alanine	0.055264902	0.0517223	Glc 5 mM	Gln 0.6 mM	iRBC
α -D-glucose	3.426810962	3.441545393	Glc 5 mM	Gln 0.6 mM	iRBC
β -D-glucose	3.419015079	3.413330857	Glc 5 mM	Gln 0.6 mM	iRBC
Glutamate	0.141768406	0.140462742	Glc 5 mM	Gln 0.6 mM	iRBC
Glutamine	0.441618634	0.450532461	Glc 5 mM	Gln 0.6 mM	iRBC
Glycerol	0.274144041	0.268438929	Glc 5 mM	Gln 0.6 mM	iRBC

Metabolite	Height	Volume	Glucose	Glutamine	Cell
Lactate	7.224674214	7.349521796	Glc 5 mM	Gln 0.6 mM	iRBC
Alanine	0.070909652	0.068054297	Glc 5 mM	Gln 2 mM	iRBC
α -D-glucose	3.156485836	3.119169687	Glc 5 mM	Gln 2 mM	iRBC
β -D-glucose	2.968978684	2.950823792	Glc 5 mM	Gln 2 mM	iRBC
Glutamate	0.307012201	0.299583375	Glc 5 mM	Gln 2 mM	iRBC
Glutamine	1.113986692	1.117849714	Glc 5 mM	Gln 2 mM	iRBC
Glycerol	0.222083773	0.225881559	Glc 5 mM	Gln 2 mM	iRBC
Lactate	5.462534849	5.512739964	Glc 5 mM	Gln 2 mM	iRBC
α -D-glucose	1.132508497	1.153144034	Glc 1 mM	No Gln	RBC
β -D-glucose	1.158848672	1.150573044	Glc 1 mM	No Gln	RBC
Lactate	0.426616002	0.438985596	Glc 1 mM	No Gln	RBC
α -D-glucose	1.320003436	1.332137423	Glc 1 mM	Gln 0.6 mM	RBC
β -D-glucose	1.376772747	1.348216831	Glc 1 mM	Gln 0.6 mM	RBC
Glutamine	0.429235951	0.43764722	Glc 1 mM	Gln 0.6 mM	RBC
α -D-glucose	1.450753478	1.478840503	Glc 1 mM	Gln 2 mM	RBC
β -D-glucose	1.506528158	1.483588781	Glc 1 mM	Gln 2 mM	RBC
Glutamine	1.842789595	1.858971325	Glc 1 mM	Gln 2 mM	RBC
Lactate	0.543577761	0.551545557	Glc 1 mM	Gln 2 mM	RBC
α -D-glucose	5.086010803	5.136992897	Glc 5 mM	No Gln	RBC
β -D-glucose	5.315772214	5.280710161	Glc 5 mM	No Gln	RBC
α -D-glucose	4.974259885	4.937539409	Glc 5 mM	Gln 0.6 mM	RBC
β -D-glucose	4.916035218	4.895726623	Glc 5 mM	Gln 0.6 mM	RBC
Glutamine	0.420512675	0.434211008	Glc 5 mM	Gln 0.6 mM	RBC
Lactate	0.499295252	0.504645647	Glc 5 mM	Gln 0.6 mM	RBC
α -D-glucose	4.866802868	4.865687	Glc 5 mM	Gln 2 mM	RBC
β -D-glucose	4.908559479	4.891009623	Glc 5 mM	Gln 2 mM	RBC
Glutamine	1.76468287	1.819080441	Glc 5 mM	Gln 2 mM	RBC
Lactate	0.557750726	0.563050819	Glc 5 mM	Gln 2 mM	RBC

Table A.3: Chapter 4- Cellular extracts concentrations (mM)

Metabolite	Height	Volume	SEM-Height	SEM-Volume	Sample
Alanine	0.217806108	0.214715321	0.107223089	0.104396294	RBC
Arginine	0.681208931	0.706907344	0.210334112	0.218630653	RBC
Asparagine	0.780721886	0.814920077	0.252495459	0.255597245	RBC
Aspartate	0.373632192	0.453466209	0.104998107	0.141201101	RBC

Metabolite	Height	Volume	SEM-Height	SEM-Volume	Sample
Creatine	1.393723359	1.482044116	0.491990144	0.525318048	RBC
Glutamate	2.781976307	2.836996792	0.849552823	0.88259953	RBC
Glutamine	1.816662325	1.928521662	0.566507712	0.612300021	RBC
Glycine	0.778188672	0.803423827	0.260584752	0.27106188	RBC
GSH	2.32497469	2.390414708	0.829029138	0.869851808	RBC
Isoleucine	0.574040474	0.559352258	0.235430652	0.227233973	RBC
Lactate	1.280133067	1.353346925	0.401342482	0.428848208	RBC
Leucine	0.260180164	0.275160852	0.058350872	0.058540179	RBC
Lysine	0.28206065	0.291672097	0.090939659	0.091699027	RBC
MyoInositol	0.236835933	0.255410763	0.090811319	0.102638132	RBC
NAD	0.155398462	0.14788263	0.033508686	0.028821223	RBC
Serine	0.687489739	0.688728989	0.230699406	0.234080034	RBC
Valine	0.197026621	0.225350765	0.073867741	0.086575633	RBC
Alanine	0.270711891	0.267117083	0.035460579	0.034876751	Ring
Arginine	0.189098824	0.19876824	0.012589465	0.012755544	Ring
Asparagine	0.291517893	0.308884761	0.04031915	0.047340132	Ring
Aspartate	0.117052026	0.127858216	0.017991513	0.019781695	Ring
Creatine	0.320934552	0.332549529	0.041924342	0.051785271	Ring
Glutamate	0.514069376	0.513640572	0.064979838	0.068371536	Ring
Glutamine	0.681204585	0.71327255	0.076077474	0.084139222	Ring
Glycine	0.292342869	0.291212558	0.031787897	0.033093515	Ring
GSH	1.693258711	1.707625522	0.228795548	0.236948225	Ring
Isoleucine	0.212241145	0.207287053	NA	NA	Ring
Lactate	2.358852525	2.415823053	0.337211094	0.375399174	Ring
Leucine	0.250373748	0.255150631	0.022224267	0.025876914	Ring
Lysine	0.156661744	0.165228007	0.004886553	0.010530466	Ring
MyoInositol	0.13023594	0.129593051	0.011406138	0.012276928	Ring
NAD	0.58585508	0.577626303	0.077090533	0.084106181	Ring
Serine	0.376988503	0.383563309	0.022360289	0.02477281	Ring
Valine	0.133345487	0.138957385	0.017584119	0.019488422	Ring
Acetate	0.15193662	0.155429205	0.008930168	0.012744083	Troph
Alanine	0.282166299	0.278426677	0.032575105	0.029443753	Troph
Arginine	0.276294887	0.285637831	0.030442989	0.032262431	Troph
Asparagine	0.389640963	0.405563375	0.039291248	0.0368004	Troph
Aspartate	0.152071547	0.175115552	0.017412838	0.02022783	Troph
Creatine	0.364392483	0.376899517	0.03840798	0.041175477	Troph

Metabolite	Height	Volume	SEM-Height	SEM-Volume	Sample
Glutamate	0.549646799	0.553855304	0.042898938	0.052982357	Troph
Glutamine	1.061143671	1.112284025	0.065197054	0.075391264	Troph
Glycine	0.329689061	0.330824548	0.027431926	0.035777755	Troph
GSH	1.382900149	1.39518288	0.300300898	0.306887764	Troph
Lactate	2.576181125	2.630981816	0.26788472	0.264267747	Troph
Leucine	0.194870913	0.201250568	0.008232339	0.01165858	Troph
Lysine	0.191401636	0.199603766	0.012456839	0.011244983	Troph
MyoInositol	0.130648033	0.133811036	0.013694701	0.016757128	Troph
NAD	0.573069627	0.567638644	0.053742587	0.061323327	Troph
Serine	0.407900664	0.40752387	0.022655192	0.021619263	Troph
Valine	0.139523382	0.149965132	0.012321836	0.015228305	Troph

Table A.4: Chapter 4- Supernatant concentrations (mM)

Metabolite	Height	Volume	SEM-Height	SEM-Volume	Sample
α -D-glucose	10.9498105	9.847271074	0.988973174	0.885090717	RBC
β -D-glucose	10.75202496	9.740038483	0.826320989	0.772358721	RBC
Acetate	0.230980205	0.223171258	NA	NA	RBC
Arginine	1.205860823	1.104451806	0.114599271	0.103289168	RBC
Asparagine	0.392908798	0.380098671	0.04714155	0.04094719	RBC
Aspartate	0.080612799	0.081213534	0.005875523	0.005371953	RBC
Glutamate	0.191829581	0.177742691	0.016180558	0.014569793	RBC
Glutamine	1.881421526	1.736061739	0.164658733	0.155963965	RBC
Glycine	0.119796155	0.104072476	0.015011836	0.014300658	RBC
Isoleucine	0.450655203	0.404002143	0.052391273	0.048978658	RBC
Lactate	0.938600009	0.87341147	0.08369477	0.076817926	RBC
Leucine	0.43357291	0.387923249	0.033377382	0.027275982	RBC
Lysine	0.264511926	0.245691617	0.024298472	0.022901862	RBC
Valine	0.184552785	0.167821028	0.021651974	0.019475284	RBC
α -D-glucose	8.8189787	7.985064193	0.260554882	0.167560336	Ring
β -D-glucose	9.147431621	8.232425985	0.208449787	0.202281905	Ring
Acetate	0.204649722	0.198107416	0.014092364	0.014737669	Ring
Alanine	0.049409684	0.046454607	0.00462479	0.004799625	Ring
Arginine	0.948699754	0.874555963	0.039786394	0.036550397	Ring
Asparagine	0.353778277	0.350505958	0.040934669	0.034221425	Ring
Aspartate	0.080754246	0.083752355	0.000426604	0.000780979	Ring

Metabolite	Height	Volume	SEM-Height	SEM-Volume	Sample
Glutamate	0.240924375	0.222656488	0.016286334	0.013336933	Ring
Glutamine	1.681040735	1.558238109	0.03259349	0.037211339	Ring
Glycerol	0.108068169	0.101979661	0.028095414	0.025695131	Ring
Isoleucine	0.404406438	0.366354795	0.021615266	0.02206039	Ring
Lactate	3.741540786	3.433104134	0.110465901	0.102271855	Ring
Leucine	0.439893052	0.392428108	0.020955303	0.017091047	Ring
Lysine	0.262207247	0.244662569	0.012398669	0.011950206	Ring
MyoInositol	0.214638702	0.200313005	0.006300111	0.007445042	Ring
Valine	0.179027722	0.164434606	0.008052054	0.006068729	Ring
α -D-glucose	10.97036569	10.01755045	0.425710438	0.458582211	t0
β -D-glucose	11.3901946	10.26272079	0.705413202	0.662990553	t0
Acetate	0.253328592	0.240477006	0.023781205	0.025071357	t0
Arginine	1.263139474	1.170321116	0.056162207	0.06264338	t0
Asparagine	0.374074008	0.374612002	0.043975257	0.046124547	t0
Aspartate	0.087211046	0.092671831	0.011085811	0.011627238	t0
Glutamate	0.193689733	0.181364573	0.01083472	0.010542634	t0
Glutamine	1.908585849	1.774684852	0.123124725	0.121398241	t0
Glycine	0.11964601	0.10721265	0.004372903	0.003389012	t0
Isoleucine	0.423294489	0.376940574	0.031614511	0.033964434	t0
Leucine	0.459009468	0.410892541	0.032542936	0.028320952	t0
Lysine	0.26550078	0.248546456	0.011518378	0.011533232	t0
Serine	0.353346307	0.322785266	NA	NA	t0
Valine	0.169059417	0.157312982	0.008681246	0.010029254	t0
α -D-glucose	8.981098232	8.215606249	0.466642575	0.505396284	Troph
β -D-glucose	9.026944756	8.181030435	0.687747077	0.603182909	Troph
Acetate	0.207311417	0.20289156	0.004462608	0.004635105	Troph
Alanine	0.083307176	0.076074269	0.006232922	0.006774985	Troph
Arginine	0.999545054	0.92175137	0.033583545	0.038133232	Troph
Asparagine	0.467727048	0.454081884	0.060079548	0.058883849	Troph
Aspartate	0.099534187	0.101162125	0.005529051	0.008362271	Troph
Glutamate	0.25589465	0.23807648	0.024895202	0.020774242	Troph
Glutamine	1.844136376	1.712076853	0.055096997	0.054618644	Troph
Glycerol	0.222254806	0.208691354	0.026675037	0.023799799	Troph
Glycine	0.141692067	0.125590905	0.009371381	0.009939386	Troph
Isoleucine	0.425943964	0.380581231	0.007624201	0.011397166	Troph
Lactate	5.406729505	4.992643797	NA	NA	Troph

Metabolite	Height	Volume	SEM-Height	SEM-Volume	Sample
Leucine	0.503709378	0.451960859	0.014260332	0.011228155	Troph
Valine	0.211912441	0.193445117	0.00517975	0.006719324	Troph

Table A.6: Chapter 5- Media concentrations (mM)

Metabolite	Height	Volume	SEM-Height	SEM-Volume	Sample
α -D-glucose	4.839006613	4.216799923	0.343596385	0.191051995	RBC
β -D-glucose	4.712497033	4.127481177	0.259270362	0.108586752	RBC
Alanine	0.028324037	0.026754538	0.001070763	0.001042546	RBC
Arginine	0.065168709	0.059423661	0.034881363	0.03087332	RBC
Glutamate	0.108273252	0.099464668	0.014562227	0.013808206	RBC
Glutamine	0.602557674	0.542388705	0.070133312	0.050189076	RBC
Glycine	0.214532976	0.18641189	0.032512084	0.02243112	RBC
Isoleucine	0.105654978	0.089038824	0.016037485	0.016373621	RBC
Lactate	0.782585985	0.711106881	0.054345318	0.032734118	RBC
Leucine	0.200038226	0.17348806	0.026689685	0.016880897	RBC
Lysine	0.283336598	0.257359562	0.024777191	0.016584833	RBC
Methionine	0.038825169	0.030180784	NA	NA	RBC
Valine	0.229158158	0.208998196	0.02034056	0.012082311	RBC
α -D-glucose	5.002640971	4.431776032	0.009741448	0.032403554	t0
β -D-glucose	4.905788734	4.391064477	0.054764854	0.076080228	t0
Arginine	0.028568506	0.026500789	0.0010746	0.001469483	t0
Glutamate	0.09082238	0.085952267	0.013808807	0.011990235	t0
Glutamine	0.571219221	0.520034985	0.022575212	0.016169223	t0
Glycine	0.229259273	0.121014406	0.009194582	0.090238839	t0
Isoleucine	0.11556468	0.09199758	0.016760238	0.017969131	t0
Leucine	0.182970076	0.162711751	0.010507973	0.006596187	t0
Lysine	0.282903322	0.261940459	0.02497148	0.022395458	t0
Methionine	0.025736738	0.021978006	NA	NA	t0
MyoInositol	0.062762141	0.056585008	0.004123463	0.003320934	t0
Serine	0.080993945	0.068472488	0.026836364	0.024845727	t0
Valine	0.209374395	0.189037837	0.013621953	0.011061903	t0
α -D-glucose	4.118880479	3.665845941	0.100678999	0.068486405	Troph
β -D-glucose	4.095153395	3.637638532	0.285590695	0.206962828	Troph
Alanine	0.037822212	0.036065597	0.004849814	0.005207695	Troph
Arginine	0.065186292	0.066058062	0.002012602	0.003254224	Troph

Metabolite	Height	Volume	SEM-Height	SEM-Volume	Sample
Glutamate	0.095776465	0.089605989	0.003402221	0.003777364	Troph
Glutamine	0.549721175	0.498296706	0.015894421	0.011166868	Troph
Glycerol	0.065966237	0.061642038	0.009733616	0.007627296	Troph
Glycine	0.185602009	0.170248869	NA	NA	Troph
Isoleucine	0.104423742	0.084827222	0.007942632	0.004418335	Troph
Lactate	1.289946922	1.169479505	0.033888669	0.025378404	Troph
Leucine	0.202432182	0.17826606	0.007568328	0.004749621	Troph
Lysine	0.274605188	0.249050811	0.00120117	0.002450533	Troph
Methionine	0.023186832	0.018258256	0.000537405	0.001286107	Troph
MyoInositol	0.046290938	0.043910461	0.00273047	0.003824501	Troph
Valine	0.220956293	0.199937605	0.004045939	0.00234794	Troph

Table A.7: Chapter 6- Media concentrations (mM)

Metabolite	Height	Volume	SEM-Height	SEM-Volume	Media	Time[h]
α -D-glucose	4.87112	4.31009	0.12178	0.09075	BL	0
β -D-glucose	4.69374	4.16627	0.15975	0.14925	BL	0
Glutamate	0.09653	0.08950	0.00996	0.00984	BL	0
Glutamine	0.59322	0.53418	0.00260	0.00218	BL	0
Glycine	0.22988	0.14978	0.00534	0.05951	BL	0
Isoleucine	0.11065	0.08793	0.01085	0.01114	BL	0
Leucine	0.19147	0.16805	0.00344	0.00298	BL	0
Lysine	0.29711	0.27149	0.01756	0.01721	BL	0
Methionine	0.02769	0.02366	0.00195	0.00168	BL	0
MyoInositol	0.05597	0.05054	0.00720	0.00634	BL	0
Valine	0.21844	0.19500	0.00744	0.00727	BL	0
α -D-glucose	3.61097	3.23725	0.04133	0.03204	BL	12
β -D-glucose	3.48114	3.13445	0.03626	0.04020	BL	12
Alanine	0.03903	0.03649	0.00164	0.00287	BL	12
Glutamate	0.09228	0.08684	0.00391	0.00419	BL	12
Glutamine	0.56268	0.51623	0.00841	0.00876	BL	12
Glycerol	0.09194	0.08671	0.00891	0.00809	BL	12
Glycine	0.20003	0.17866	0.01432	0.01414	BL	12
Isoleucine	0.10031	0.08433	0.00185	0.00231	BL	12
Lactate	2.98816	2.74105	0.04579	0.03963	BL	12
Leucine	0.19221	0.17364	0.00829	0.00722	BL	12

Metabolite	Height	Volume	SEM-Height	SEM-Volume	Media	Time[h]
Lysine	0.25963	0.24252	0.00089	0.00099	BL	12
Methionine	0.02220	0.01889	0.00149	0.00244	BL	12
MyoInositol	0.03678	0.03200	0.00277	0.00170	BL	12
Valine	0.20786	0.19190	0.01473	0.01286	BL	12
α -D-glucose	4.23669	3.83384	0.10817	0.07917	BL	15
β -D-glucose	4.29758	3.87060	0.04231	0.05068	BL	15
Alanine	0.02651	0.02569	0.00104	0.00085	BL	15
Glutamate	0.08409	0.08011	0.00793	0.00634	BL	15
Glutamine	0.53820	0.49805	0.00548	0.00344	BL	15
Glycerol	0.04687	0.04364	0.00001	0.00200	BL	15
Glycine	0.21087	0.18747	0.00257	0.00351	BL	15
Isoleucine	0.09999	0.08383	0.00815	0.00684	BL	15
Lactate	0.86612	0.79359	0.00306	0.00594	BL	15
Leucine	0.18504	0.16738	0.00354	0.00260	BL	15
Lysine	0.26766	0.24710	0.01500	0.01274	BL	15
Methionine	0.03108	0.02791	0.00188	0.00209	BL	15
MyoInositol	0.05351	0.05150	0.01278	0.01234	BL	15
Valine	0.20748	0.19025	0.00465	0.00220	BL	15
α -D-glucose	4.09123	3.65252	0.16446	0.09940	BL	18
β -D-glucose	4.12210	3.67368	0.15887	0.11770	BL	18
Alanine	0.03639	0.03437	0.00071	0.00004	BL	18
Glutamate	0.09103	0.08465	0.00961	0.00706	BL	18
Glutamine	0.53626	0.48912	0.01300	0.00945	BL	18
Glycerol	0.06537	0.06091	0.00615	0.00585	BL	18
Glycine	0.20121	0.17961	0.00373	0.00728	BL	18
Isoleucine	0.12881	0.11374	0.00698	0.00022	BL	18
Lactate	1.39877	1.27947	0.05386	0.03756	BL	18
Leucine	0.18639	0.16563	0.00844	0.00752	BL	18
Lysine	0.25413	0.23562	0.00230	0.00338	BL	18
Methionine	0.04233	0.03794	0.00300	0.00279	BL	18
MyoInositol	0.04578	0.04072	0.00351	0.00321	BL	18
Valine	0.20809	0.18962	0.01292	0.01070	BL	18
α -D-glucose	3.77888	3.43730	0.14192	0.10282	BL	21
β -D-glucose	3.74776	3.39996	0.07696	0.06286	BL	21
Alanine	0.04406	0.03992	0.00295	0.00307	BL	21
Glutamate	0.08949	0.08707	0.00378	0.00404	BL	21

Metabolite	Height	Volume	SEM-Height	SEM-Volume	Media	Time[h]
Glutamine	0.52271	0.48618	0.00797	0.00853	BL	21
Glycerol	0.08894	0.08334	0.00572	0.00644	BL	21
Glycine	0.20068	0.17902	0.00424	0.00609	BL	21
Isoleucine	0.11313	0.09714	0.00733	0.00322	BL	21
Lactate	2.05316	1.89877	0.01358	0.02187	BL	21
Leucine	0.19399	0.17379	0.00569	0.00661	BL	21
Lysine	0.27206	0.25263	0.00840	0.00868	BL	21
Methionine	0.02238	0.01743	0.00365	0.00388	BL	21
MyoInositol	0.04467	0.04195	0.00858	0.00803	BL	21
Valine	0.21473	0.19549	0.00867	0.00850	BL	21
α -D-glucose	3.56816	3.20479	0.06486	0.04144	BL	24
β -D-glucose	3.53570	3.18285	0.11345	0.09777	BL	24
Alanine	0.05290	0.04873	0.00538	0.00508	BL	24
Glutamate	0.09704	0.09042	0.00701	0.00678	BL	24
Glutamine	0.52568	0.48361	0.00254	0.00271	BL	24
Glycerol	0.10165	0.09279	0.00874	0.00741	BL	24
Glycine	0.20737	0.18415	0.00805	0.00668	BL	24
Isoleucine	0.09544	0.08044	0.01644	0.01073	BL	24
Lactate	2.79866	2.57195	0.05197	0.03486	BL	24
Leucine	0.19788	0.18130	0.00403	0.00157	BL	24
Lysine	0.26946	0.24847	0.00714	0.00777	BL	24
Methionine	0.02732	0.02299	0.00197	0.00318	BL	24
MyoInositol	0.05043	0.04659	0.00954	0.00808	BL	24
Valine	0.22088	0.20480	0.00214	0.00088	BL	24
α -D-glucose	4.11888	3.66585	0.10068	0.06849	BL	27
β -D-glucose	4.09515	3.63764	0.28559	0.20696	BL	27
Alanine	0.03782	0.03607	0.00485	0.00521	BL	27
Glutamate	0.09578	0.08961	0.00340	0.00378	BL	27
Glutamine	0.54972	0.49830	0.01589	0.01117	BL	27
Glycerol	0.06597	0.06164	0.00973	0.00763	BL	27
Glycine	0.18560	0.17025	NA	NA	BL	27
Isoleucine	0.10442	0.08483	0.00794	0.00442	BL	27
Lactate	1.48021	1.33602	0.07004	0.05617	BL	27
Leucine	0.20243	0.17827	0.00757	0.00475	BL	27
Lysine	0.27461	0.24905	0.00120	0.00245	BL	27
Methionine	0.02319	0.01826	0.00054	0.00129	BL	27

Metabolite	Height	Volume	SEM-Height	SEM-Volume	Media	Time[h]
MyoInositol	0.04629	0.04391	0.00273	0.00382	BL	27
Valine	0.22096	0.19994	0.00405	0.00235	BL	27
α -D-glucose	4.31100	3.83404	0.19040	0.12985	BL	3
β -D-glucose	4.32817	3.82105	0.26590	0.18394	BL	3
Alanine	0.03560	0.03451	0.00230	0.00201	BL	3
Glutamate	0.08950	0.08266	0.01367	0.00998	BL	3
Glutamine	0.57005	0.51988	0.01438	0.00819	BL	3
Glycerol	0.07315	0.06775	0.01062	0.00677	BL	3
Glycine	0.20072	0.17642	0.00916	0.00565	BL	3
Isoleucine	0.12131	0.09935	0.00310	0.00977	BL	3
Lactate	0.95707	0.85944	0.00754	0.00835	BL	3
Leucine	0.17984	0.15900	0.01232	0.00769	BL	3
Lysine	0.26440	0.24247	0.01491	0.01024	BL	3
Methionine	0.02042	0.01755	0.00384	0.00421	BL	3
MyoInositol	0.05174	0.04732	0.00952	0.00725	BL	3
Valine	0.20937	0.18786	0.01250	0.00762	BL	3
α -D-glucose	3.74775	3.38621	0.12133	0.10008	BL	30
β -D-glucose	3.86987	3.41431	0.06951	0.05853	BL	30
Alanine	0.06842	0.06167	0.00526	0.00426	BL	30
Glutamate	0.09794	0.09115	0.00537	0.00404	BL	30
Glutamine	0.57729	0.52100	0.00654	0.00401	BL	30
Glycerol	0.11393	0.10234	0.00489	0.00353	BL	30
Glycine	0.21606	0.19027	NA	NA	BL	30
Isoleucine	0.07457	0.06433	0.01209	0.01129	BL	30
Lactate	2.82705	2.54894	0.07666	0.05707	BL	30
Leucine	0.23833	0.20929	0.00175	0.00107	BL	30
Lysine	0.27071	0.24891	0.00273	0.00225	BL	30
Methionine	0.02747	0.02128	0.00318	0.00387	BL	30
MyoInositol	0.06009	0.05405	0.00232	0.00360	BL	30
Valine	0.24919	0.22306	0.00845	0.00774	BL	30
α -D-glucose	3.26423	2.93016	0.11534	0.07781	BL	33
β -D-glucose	3.34289	2.95205	0.12346	0.08224	BL	33
Alanine	0.09587	0.08654	0.00356	0.00226	BL	33
Glutamate	0.10399	0.09645	0.00400	0.00209	BL	33
Glutamine	0.56669	0.51317	0.01347	0.00724	BL	33
Glycerol	0.18309	0.16029	0.01963	0.01550	BL	33

Metabolite	Height	Volume	SEM-Height	SEM-Volume	Media	Time[h]
Glycine	0.24789	0.21632	0.01201	0.00543	BL	33
Isoleucine	0.09559	0.07785	0.00328	0.00103	BL	33
Lactate	4.22406	3.80604	0.20061	0.14379	BL	33
Leucine	0.26544	0.23272	0.01256	0.00877	BL	33
Lysine	0.28254	0.25967	0.00618	0.00623	BL	33
Methionine	0.02437	0.01875	0.00433	0.00280	BL	33
MyoInositol	0.04877	0.04565	0.00341	0.00631	BL	33
Valine	0.26936	0.24213	0.01308	0.00873	BL	33
α -D-glucose	2.77777	2.49199	0.08555	0.07013	BL	36
β -D-glucose	2.70652	2.44071	0.10983	0.10177	BL	36
Alanine	0.12668	0.11572	0.00584	0.00544	BL	36
Glutamate	0.10205	0.09650	0.00732	0.00577	BL	36
Glutamine	0.55846	0.51138	0.00105	0.00355	BL	36
Glycerol	0.22870	0.21060	0.00711	0.00559	BL	36
Glycine	0.23991	0.21169	0.00686	0.00381	BL	36
Isoleucine	0.08526	0.07517	0.00376	0.00380	BL	36
Lactate	5.73525	5.24541	0.25862	0.24034	BL	36
Leucine	0.28202	0.25213	0.00833	0.00868	BL	36
Lysine	0.28002	0.25994	0.00697	0.00492	BL	36
Methionine	0.03193	0.02544	0.00522	0.00507	BL	36
MyoInositol	0.04873	0.04562	0.00776	0.00711	BL	36
Valine	0.28683	0.26276	0.00320	0.00131	BL	36
α -D-glucose	3.86186	3.48176	0.15817	0.16155	BL	39
β -D-glucose	3.91895	3.46246	0.07704	0.07453	BL	39
Alanine	0.06322	0.05737	0.00495	0.00481	BL	39
Glutamate	0.09733	0.09220	0.00756	0.00624	BL	39
Glutamine	0.56406	0.50846	0.01035	0.01048	BL	39
Glycerol	0.10754	0.09741	0.00700	0.00839	BL	39
Glycine	0.21188	0.18452	0.00626	0.00507	BL	39
Isoleucine	0.09909	0.07774	0.02236	0.01640	BL	39
Lactate	2.32727	2.09938	0.06507	0.07145	BL	39
Leucine	0.23027	0.20323	0.00508	0.00661	BL	39
Lysine	0.26784	0.24762	0.00569	0.00780	BL	39
Methionine	0.01776	0.01404	0.00551	0.00402	BL	39
MyoInositol	0.05085	0.04674	0.00477	0.00314	BL	39
Valine	0.24463	0.21923	0.00700	0.00653	BL	39

Metabolite	Height	Volume	SEM-Height	SEM-Volume	Media	Time[h]
α -D-glucose	3.60066	3.20775	0.11754	0.09402	BL	42
β -D-glucose	3.52881	3.14892	0.14494	0.12548	BL	42
Alanine	0.10351	0.09531	NA	NA	BL	42
Glutamate	0.10436	0.09779	0.00715	0.00522	BL	42
Glutamine	0.60178	0.54671	0.02284	0.02312	BL	42
Glycerol	0.17452	0.15698	0.01076	0.00906	BL	42
Glycine	0.24994	0.22136	0.01337	0.01464	BL	42
Isoleucine	0.07345	0.05971	0.00450	0.00702	BL	42
Lactate	4.26931	3.88001	0.23918	0.21469	BL	42
Leucine	0.27158	0.24182	0.01270	0.01226	BL	42
Lysine	0.30378	0.28092	0.00946	0.01089	BL	42
Methionine	0.02485	0.02063	0.00481	0.00484	BL	42
MyoInositol	0.04607	0.04108	0.00406	0.00368	BL	42
Valine	0.27819	0.25031	0.00796	0.00881	BL	42
α -D-glucose	2.73866	2.47809	0.11379	0.08263	BL	45
β -D-glucose	2.68834	2.41605	0.09792	0.08965	BL	45
Alanine	0.12150	0.10660	0.01452	0.01453	BL	45
Glutamate	0.09586	0.09234	0.00358	0.00457	BL	45
Glutamine	0.57644	0.52076	0.00660	0.00628	BL	45
Glycerol	0.22273	0.20035	0.01461	0.01216	BL	45
Glycine	0.24837	0.22147	0.01008	0.00614	BL	45
Isoleucine	0.08844	0.07659	0.03640	0.03169	BL	45
Lactate	5.63240	5.14068	0.18881	0.16334	BL	45
Leucine	0.28654	0.25294	0.00206	0.00208	BL	45
Lysine	0.27661	0.25250	0.01338	0.01283	BL	45
Methionine	0.02162	0.01887	0.00510	0.00469	BL	45
MyoInositol	0.04676	0.04370	0.00564	0.00603	BL	45
Valine	0.28679	0.25846	0.00432	0.00352	BL	45
α -D-glucose	2.18749	1.98445	0.06779	0.06631	BL	48
β -D-glucose	2.19784	1.94112	0.12710	0.09297	BL	48
Alanine	0.16399	0.14237	0.00979	0.00644	BL	48
Glutamate	0.10659	0.09857	0.01048	0.00953	BL	48
Glutamine	0.57805	0.52386	0.01240	0.01156	BL	48
Glycerol	0.30260	0.27038	0.02056	0.01602	BL	48
Glycine	0.27930	0.24420	0.02085	0.01525	BL	48
Isoleucine	0.10043	0.08275	0.02278	0.01897	BL	48

Metabolite	Height	Volume	SEM-Height	SEM-Volume	Media	Time[h]
Lactate	7.83007	7.05082	0.48460	0.37079	BL	48
Leucine	0.33659	0.29306	0.00761	0.00264	BL	48
Lysine	0.28326	0.25705	0.01214	0.00956	BL	48
Methionine	0.02840	0.02458	0.00079	0.00140	BL	48
MyoInositol	0.05195	0.04757	0.00194	0.00271	BL	48
Valine	0.31842	0.28364	0.01008	0.00548	BL	48
α -D-glucose	3.82773	3.46406	0.23047	0.15529	BL	51
β -D-glucose	3.70734	3.34280	0.30080	0.22662	BL	51
Alanine	0.05236	0.04685	0.01185	0.01004	BL	51
Glutamate	0.08761	0.08309	0.00503	0.00580	BL	51
Glutamine	0.54757	0.50252	0.03872	0.03062	BL	51
Glycerol	0.10603	0.09927	0.01135	0.01111	BL	51
Glycine	0.20621	0.18497	0.01093	0.00806	BL	51
Isoleucine	0.09882	0.07937	0.02054	0.01933	BL	51
Lactate	2.57884	2.36710	0.24377	0.19891	BL	51
Leucine	0.22295	0.19848	0.01115	0.00907	BL	51
Lysine	0.27423	0.25738	0.00730	0.00378	BL	51
Methionine	0.02656	0.02180	0.00373	0.00290	BL	51
MyoInositol	0.04335	0.03924	0.00278	0.00388	BL	51
Valine	0.23759	0.21989	0.00716	0.00583	BL	51
α -D-glucose	3.27118	2.91044	0.04616	0.04073	BL	54
β -D-glucose	3.25429	2.88651	0.15184	0.11234	BL	54
Alanine	0.08261	0.07390	0.00853	0.00602	BL	54
Glutamate	0.10351	0.09582	0.00243	0.00012	BL	54
Glutamine	0.54500	0.49644	0.01512	0.01116	BL	54
Glycerol	0.16878	0.15314	0.00157	0.00164	BL	54
Glycine	0.22913	0.20345	0.00789	0.00309	BL	54
Isoleucine	0.09549	0.08159	0.01019	0.00831	BL	54
Lactate	4.18486	3.78705	0.15060	0.10625	BL	54
Leucine	0.23773	0.21210	0.01215	0.00708	BL	54
Lysine	0.27387	0.25151	0.00989	0.00660	BL	54
Methionine	0.02718	0.02326	0.00219	0.00169	BL	54
MyoInositol	0.04270	0.03814	0.00350	0.00319	BL	54
Valine	0.25428	0.23399	0.00978	0.00521	BL	54
α -D-glucose	3.89263	3.53101	0.09893	0.05628	BL	6
β -D-glucose	3.79816	3.42924	0.12162	0.10500	BL	6

Metabolite	Height	Volume	SEM-Height	SEM-Volume	Media	Time[h]
Alanine	0.02943	0.02873	0.00286	0.00329	BL	6
Glutamate	0.08836	0.08300	0.00398	0.00397	BL	6
Glutamine	0.53926	0.49708	0.01349	0.01165	BL	6
Glycerol	0.06976	0.06476	0.00191	0.00260	BL	6
Glycine	0.18412	0.16368	0.01009	0.00691	BL	6
Isoleucine	0.13162	0.11223	0.01770	0.01493	BL	6
Lactate	1.58786	1.45596	0.04463	0.04535	BL	6
Leucine	0.18521	0.16637	0.00550	0.00674	BL	6
Lysine	0.25696	0.23889	0.00601	0.00500	BL	6
Methionine	0.02894	0.02566	0.00357	0.00285	BL	6
MyoInositol	0.04491	0.04152	0.00362	0.00350	BL	6
Valine	0.20884	0.19173	0.00123	0.00297	BL	6
α -D-glucose	3.78051	3.40356	0.08727	0.06106	BL	9
β -D-glucose	3.82024	3.40702	0.06356	0.02657	BL	9
Alanine	0.04263	0.03920	0.00401	0.00499	BL	9
Glutamate	0.10484	0.09917	0.00481	0.00330	BL	9
Glutamine	0.55436	0.50863	0.01281	0.00821	BL	9
Glycerol	0.08176	0.07786	0.00998	0.01123	BL	9
Glycine	0.20703	0.18522	0.00623	0.00437	BL	9
Isoleucine	0.11814	0.09801	0.00963	0.00550	BL	9
Lactate	2.40106	2.17966	0.06711	0.04039	BL	9
Leucine	0.19860	0.17665	0.00743	0.00635	BL	9
Lysine	0.26180	0.24175	0.01040	0.00921	BL	9
Methionine	0.01888	0.01434	0.00218	0.00130	BL	9
MyoInositol	0.03802	0.03604	0.00592	0.00637	BL	9
Valine	0.21091	0.19189	0.01084	0.00876	BL	9
α -D-glucose	11.24389	10.06315	0.15828	0.06105	CM	0
β -D-glucose	11.73191	10.33157	0.32214	0.20654	CM	0
Acetate	0.22269	0.19993	0.00837	0.00896	CM	0
Arginine	1.25314	1.13949	0.01982	0.01657	CM	0
Asparagine	0.39614	0.35979	0.01974	0.01781	CM	0
Aspartate	0.08191	0.08561	0.00391	0.00287	CM	0
Glutamate	0.20449	0.18440	0.00436	0.00265	CM	0
Glutamine	1.88365	1.70664	0.03580	0.02844	CM	0
Glycine	0.12762	0.11376	0.00750	0.00609	CM	0
Isoleucine	0.44668	0.39686	0.00639	0.00571	CM	0

Metabolite	Height	Volume	SEM-Height	SEM-Volume	Media	Time[h]
Leucine	0.46827	0.40765	0.01238	0.00804	CM	0
Lysine	0.26765	0.24440	0.00670	0.00324	CM	0
Methionine	0.09579	0.08390	0.00346	0.00337	CM	0
MyoInositol	0.23912	0.21987	0.00775	0.00707	CM	0
Serine	0.21184	0.18018	0.01338	0.00367	CM	0
Valine	0.17345	0.15470	0.00410	0.00314	CM	0
α -D-glucose	8.74969	7.91501	0.63354	0.53033	CM	12
β -D-glucose	8.96950	7.98069	0.49845	0.41970	CM	12
Acetate	0.18040	0.17129	0.01635	0.01703	CM	12
Alanine	0.05504	0.05078	0.00480	0.00364	CM	12
Arginine	0.95443	0.86813	0.09173	0.07647	CM	12
Asparagine	0.38259	0.35529	0.01484	0.01605	CM	12
Aspartate	0.06990	0.07036	0.00564	0.00673	CM	12
Glutamate	0.20154	0.18600	0.00905	0.00664	CM	12
Glutamine	1.70466	1.55775	0.08758	0.07413	CM	12
Glycerol	0.17370	0.16181	0.00839	0.00734	CM	12
Glycine	0.11368	0.09936	0.01079	0.01000	CM	12
Isoleucine	0.42104	0.37427	0.01260	0.00998	CM	12
Lactate	4.83175	4.40053	0.21765	0.21322	CM	12
Leucine	0.46147	0.40634	0.02166	0.01788	CM	12
Lysine	0.25247	0.23267	0.00703	0.00651	CM	12
Methionine	0.09744	0.08702	0.00958	0.00879	CM	12
MyoInositol	0.23459	0.21849	0.00860	0.00688	CM	12
Serine	0.17073	0.14234	0.01367	0.01615	CM	12
Valine	0.18099	0.16279	0.00811	0.00644	CM	12
α -D-glucose	10.00262	8.95902	0.11380	0.08980	CM	15
β -D-glucose	9.92671	8.91804	0.03453	0.01632	CM	15
Acetate	0.18974	0.18236	0.00863	0.00814	CM	15
Alanine	0.03681	0.03368	0.00126	0.00056	CM	15
Arginine	1.08974	0.99522	0.03276	0.02437	CM	15
Asparagine	0.35924	0.33394	0.01501	0.01276	CM	15
Aspartate	0.08153	0.08493	0.00529	0.00519	CM	15
Glutamate	0.18456	0.16991	0.00400	0.00366	CM	15
Glutamine	1.65586	1.52028	0.02578	0.01259	CM	15
Glycerol	0.09091	0.08638	0.00566	0.00527	CM	15
Glycine	0.11359	0.09908	0.00204	0.00229	CM	15

Metabolite	Height	Volume	SEM-Height	SEM-Volume	Media	Time[h]
Isoleucine	0.41615	0.36868	0.01188	0.00574	CM	15
Lactate	1.80072	1.63894	0.04279	0.03298	CM	15
Leucine	0.44016	0.39287	0.02091	0.01255	CM	15
Lysine	0.24289	0.22423	0.00463	0.00420	CM	15
Methionine	0.09078	0.07900	0.00576	0.00407	CM	15
MyoInositol	0.22416	0.20828	0.01190	0.00932	CM	15
Serine	0.20713	0.15902	0.03309	0.03634	CM	15
Valine	0.16825	0.15507	0.00476	0.00157	CM	15
α -D-glucose	9.10627	8.30106	0.16308	0.11569	CM	18
β -D-glucose	9.15186	8.24328	0.33882	0.24820	CM	18
Acetate	0.17792	0.17122	0.00540	0.00429	CM	18
Alanine	0.06074	0.05553	0.00445	0.00442	CM	18
Arginine	1.02733	0.94201	0.03069	0.02904	CM	18
Asparagine	0.37139	0.35847	0.01492	0.01447	CM	18
Aspartate	0.08014	0.08403	0.01292	0.01245	CM	18
Glutamate	0.19984	0.18359	0.00742	0.00539	CM	18
Glutamine	1.64820	1.50877	0.02572	0.02306	CM	18
Glycerol	0.13478	0.12658	0.00607	0.00449	CM	18
Glycine	0.12860	0.11774	0.00890	0.00836	CM	18
Isoleucine	0.39940	0.35346	0.00960	0.00621	CM	18
Lactate	3.34609	3.06370	0.05384	0.05708	CM	18
Leucine	0.46143	0.40561	0.00547	0.00382	CM	18
Lysine	0.22903	0.21439	0.00707	0.00496	CM	18
Methionine	0.10051	0.08896	0.00242	0.00233	CM	18
MyoInositol	0.22883	0.21047	0.00423	0.00507	CM	18
Serine	0.22508	0.18809	0.03203	0.02704	CM	18
Valine	0.19190	0.17522	0.00447	0.00452	CM	18
α -D-glucose	8.63309	7.63151	0.46750	0.32805	CM	21
β -D-glucose	8.78785	7.73064	0.67131	0.45534	CM	21
Acetate	0.17785	0.16270	0.02513	0.02153	CM	21
Alanine	0.08569	0.07765	0.00140	0.00121	CM	21
Arginine	0.94701	0.86242	0.07757	0.06337	CM	21
Asparagine	0.36295	0.34301	0.05006	0.05241	CM	21
Aspartate	0.08230	0.08139	0.00484	0.00003	CM	21
Glutamate	0.20422	0.18866	0.02065	0.01322	CM	21
Glutamine	1.64621	1.49839	0.13589	0.09614	CM	21

Metabolite	Height	Volume	SEM-Height	SEM-Volume	Media	Time[h]
Glycerol	0.24138	0.21892	0.00437	0.00427	CM	21
Glycine	0.14524	0.12564	0.00706	0.00583	CM	21
Isoleucine	0.37691	0.33275	0.01271	0.00060	CM	21
Lactate	6.12528	5.52311	0.24162	0.13184	CM	21
Leucine	0.49012	0.43672	0.05207	0.03235	CM	21
Lysine	0.25124	0.23228	0.02402	0.01862	CM	21
Methionine	0.08532	0.07188	0.01109	0.00486	CM	21
MyoInositol	0.22983	0.21111	0.01550	0.01069	CM	21
Serine	0.21223	0.15802	0.01555	0.01486	CM	21
Valine	0.20686	0.18608	0.01293	0.00643	CM	21
α -D-glucose	7.45732	6.71146	0.10062	0.00128	CM	24
β -D-glucose	7.59100	6.72482	0.11905	0.08017	CM	24
Acetate	0.16350	0.15623	0.01063	0.01093	CM	24
Alanine	0.13952	0.12521	0.00353	0.00178	CM	24
Arginine	0.88536	0.80577	0.05299	0.04471	CM	24
Asparagine	0.38208	0.36498	0.00306	0.01547	CM	24
Aspartate	0.07365	0.07260	0.00818	0.00866	CM	24
Glutamate	0.20242	0.18508	0.00019	0.00184	CM	24
Glutamine	1.66148	1.51996	0.02743	0.01935	CM	24
Glycerol	0.38660	0.34452	0.02098	0.01753	CM	24
Glycine	0.16405	0.14302	0.00597	0.00405	CM	24
Isoleucine	0.40708	0.35793	0.01397	0.01552	CM	24
Lactate	9.09581	8.24538	0.55429	0.48020	CM	24
Leucine	0.54238	0.47644	0.00831	0.00890	CM	24
Lysine	0.25303	0.23300	0.00420	0.00075	CM	24
Methionine	0.09840	0.08523	0.00418	0.00314	CM	24
MyoInositol	0.21590	0.19924	0.00061	0.00084	CM	24
Serine	0.25741	0.22911	0.02312	0.01034	CM	24
Valine	0.23293	0.21337	0.00302	0.00581	CM	24
α -D-glucose	9.39042	8.35553	0.55813	0.36827	CM	27
β -D-glucose	9.25456	8.21020	0.70573	0.49552	CM	27
Acetate	0.20095	0.18544	0.00579	0.00460	CM	27
Alanine	0.09535	0.08600	0.00602	0.00559	CM	27
Arginine	1.14701	1.03438	0.05399	0.04464	CM	27
Asparagine	0.39112	0.36356	0.03324	0.03707	CM	27
Aspartate	0.08215	0.08116	0.01081	0.01142	CM	27

Metabolite	Height	Volume	SEM-Height	SEM-Volume	Media	Time[h]
Glutamate	0.21426	0.19502	0.01064	0.00762	CM	27
Glutamine	1.75267	1.58970	0.10386	0.08190	CM	27
Glycerol	0.28758	0.25930	0.02138	0.01519	CM	27
Glycine	0.15897	0.14076	0.01063	0.00993	CM	27
Isoleucine	0.47415	0.41397	0.01770	0.01453	CM	27
Lactate	6.03623	5.43407	0.41359	0.31760	CM	27
Leucine	0.52991	0.46192	0.03517	0.02577	CM	27
Lysine	0.26139	0.24006	0.02377	0.01874	CM	27
Methionine	0.09625	0.08525	0.00705	0.00663	CM	27
MyoInositol	0.24996	0.23015	0.00823	0.00749	CM	27
Serine	0.18189	0.14696	0.03916	0.03148	CM	27
Valine	0.22762	0.20324	0.00678	0.00521	CM	27
α -D-glucose	9.64718	8.66491	0.30007	0.25086	CM	3
β -D-glucose	10.13889	8.92258	0.28797	0.24749	CM	3
Acetate	0.17712	0.16680	0.01892	0.01594	CM	3
Alanine	0.03338	0.03273	0.00163	0.00188	CM	3
Arginine	1.08089	0.97828	0.04591	0.04180	CM	3
Asparagine	0.34833	0.33339	0.01125	0.00760	CM	3
Aspartate	0.07089	0.07010	0.00678	0.00726	CM	3
Glutamate	0.18583	0.16816	0.00164	0.00186	CM	3
Glutamine	1.64469	1.49556	0.07867	0.06974	CM	3
Glycerol	0.07761	0.07236	0.00714	0.00745	CM	3
Glycine	0.11446	0.09833	0.00462	0.00479	CM	3
Isoleucine	0.44530	0.38913	0.01085	0.01073	CM	3
Lactate	1.32716	1.19281	0.02868	0.02818	CM	3
Leucine	0.44073	0.38309	0.00894	0.00881	CM	3
Lysine	0.23774	0.21379	0.01479	0.01324	CM	3
Methionine	0.09522	0.08017	0.00786	0.00692	CM	3
MyoInositol	0.22843	0.21043	0.00436	0.00321	CM	3
Serine	0.17517	0.10999	0.03669	0.04779	CM	3
Valine	0.17211	0.15328	0.00213	0.00293	CM	3
α -D-glucose	7.04408	6.36244	0.15457	0.08639	CM	30
β -D-glucose	6.97437	6.24914	0.13145	0.10714	CM	30
Acetate	0.18066	0.16854	0.00583	0.00375	CM	30
Alanine	0.17405	0.15173	0.00732	0.00672	CM	30
Arginine	1.00227	0.91281	0.02432	0.01712	CM	30

Metabolite	Height	Volume	SEM-Height	SEM-Volume	Media	Time[h]
Asparagine	0.40967	0.38906	0.01235	0.00836	CM	30
Aspartate	0.07608	0.07422	0.00503	0.00424	CM	30
Glutamate	0.21821	0.19854	0.00871	0.00785	CM	30
Glutamine	1.66311	1.52235	0.03304	0.03402	CM	30
Glycerol	0.47227	0.42744	0.03330	0.02909	CM	30
Glycine	0.17019	0.15096	0.01666	0.01504	CM	30
Isoleucine	0.42504	0.37728	0.01384	0.01281	CM	30
Lactate	10.88257	9.90727	0.45237	0.43872	CM	30
Leucine	0.56408	0.49781	0.02141	0.01819	CM	30
Lysine	0.26713	0.24452	0.01120	0.01226	CM	30
Methionine	0.09947	0.08682	0.00271	0.00259	CM	30
MyoInositol	0.23281	0.21373	0.01000	0.00899	CM	30
Serine	0.23152	0.21403	0.02790	0.02717	CM	30
Valine	0.26174	0.23679	0.00345	0.00419	CM	30
α -D-glucose	4.57977	4.20535	0.31086	0.21235	CM	33
β -D-glucose	4.62638	4.18973	0.23812	0.17147	CM	33
Acetate	0.16477	0.15692	0.01122	0.01070	CM	33
Alanine	0.22729	0.20467	0.00812	0.00557	CM	33
Arginine	0.82094	0.76209	0.06111	0.04958	CM	33
Asparagine	0.38407	0.38077	0.00895	0.00449	CM	33
Aspartate	0.06745	0.06883	0.00655	0.00927	CM	33
Glutamate	0.22032	0.20407	0.00797	0.00357	CM	33
Glutamine	1.48271	1.38681	0.03973	0.01410	CM	33
Glycerol	0.65542	0.59533	0.01780	0.02000	CM	33
Glycine	0.17918	0.16156	0.00650	0.00561	CM	33
Isoleucine	0.37056	0.33656	0.01619	0.00674	CM	33
Lactate	15.43335	14.24994	0.48505	0.27627	CM	33
Leucine	0.56917	0.51332	0.00685	0.00544	CM	33
Lysine	0.24928	0.23340	0.00514	0.00315	CM	33
Methionine	0.08246	0.07444	0.00407	0.00348	CM	33
MyoInositol	0.20275	0.19126	0.00324	0.00491	CM	33
Serine	0.27123	0.24690	0.01664	0.01785	CM	33
Valine	0.28555	0.26255	0.00686	0.00417	CM	33
α -D-glucose	2.65735	2.43643	0.20389	0.19647	CM	36
β -D-glucose	2.58172	2.37797	0.21948	0.21661	CM	36
Acetate	0.15375	0.15196	0.00472	0.00546	CM	36

Metabolite	Height	Volume	SEM-Height	SEM-Volume	Media	Time[h]
Alanine	0.27549	0.24937	0.00931	0.00797	CM	36
Arginine	0.67602	0.63239	0.04660	0.04824	CM	36
Asparagine	0.35173	0.35634	0.02292	0.02037	CM	36
Aspartate	0.06061	0.06312	0.00485	0.00387	CM	36
Glutamate	0.19924	0.18613	0.00548	0.00360	CM	36
Glutamine	1.35604	1.28467	0.02734	0.01385	CM	36
Glycerol	0.83501	0.76404	0.05518	0.04884	CM	36
Glycine	0.18360	0.16543	0.01137	0.00871	CM	36
Isoleucine	0.34844	0.32079	0.01085	0.00888	CM	36
Lactate	18.91782	17.68511	0.56125	0.42728	CM	36
Leucine	0.56891	0.51511	0.02256	0.01298	CM	36
Lysine	0.23868	0.22634	0.00756	0.00783	CM	36
Methionine	0.06975	0.06169	0.00059	0.00129	CM	36
MyoInositol	0.18829	0.17835	0.00773	0.00533	CM	36
Serine	0.29648	0.27351	0.01498	0.01248	CM	36
Valine	0.29747	0.27654	0.01268	0.01062	CM	36
α -D-glucose	7.79951	7.03557	0.31243	0.16162	CM	39
β -D-glucose	7.77320	6.98277	0.14289	0.08758	CM	39
Acetate	0.19838	0.18325	0.01069	0.00734	CM	39
Alanine	0.11704	0.10553	0.00427	0.00385	CM	39
Arginine	1.05618	0.96456	0.02275	0.01225	CM	39
Asparagine	0.35186	0.35386	0.00950	0.01306	CM	39
Aspartate	0.07974	0.08064	0.00913	0.00966	CM	39
Glutamate	0.21060	0.19579	0.00596	0.00618	CM	39
Glutamine	1.70930	1.57208	0.04702	0.03495	CM	39
Glycerol	0.34390	0.32005	0.00946	0.00810	CM	39
Glycine	0.13507	0.12141	0.00684	0.00753	CM	39
Isoleucine	0.40058	0.35869	0.02616	0.01993	CM	39
Lactate	8.17617	7.47640	0.51294	0.42213	CM	39
Leucine	0.49751	0.44514	0.00250	0.00028	CM	39
Lysine	0.25061	0.23029	0.00065	0.00311	CM	39
Methionine	0.09073	0.07857	0.00255	0.00207	CM	39
MyoInositol	0.22171	0.20835	0.00353	0.00234	CM	39
Serine	0.20937	0.19200	0.02605	0.02293	CM	39
Valine	0.21516	0.19534	0.00445	0.00387	CM	39
α -D-glucose	5.54476	5.05521	0.37221	0.30176	CM	42

Metabolite	Height	Volume	SEM-Height	SEM-Volume	Media	Time[h]
β -D-glucose	5.48432	5.02130	0.46731	0.38475	CM	42
Acetate	0.18458	0.17849	0.00981	0.01429	CM	42
Alanine	0.15125	0.13781	0.01089	0.00836	CM	42
Arginine	0.88134	0.82230	0.06032	0.05148	CM	42
Asparagine	0.37043	0.36605	0.01655	0.01630	CM	42
Aspartate	0.07501	0.07767	0.00924	0.00901	CM	42
Glutamate	0.21466	0.20026	0.00537	0.00488	CM	42
Glutamine	1.50500	1.41735	0.08133	0.06822	CM	42
Glycerol	0.50378	0.46630	0.01732	0.01458	CM	42
Glycine	0.15385	0.13984	0.01109	0.01015	CM	42
Isoleucine	0.38457	0.34932	0.03007	0.02682	CM	42
Lactate	12.59340	11.73159	0.52420	0.40850	CM	42
Leucine	0.50161	0.45488	0.01830	0.01587	CM	42
Lysine	0.23362	0.22126	0.01666	0.01604	CM	42
Methionine	0.07466	0.06667	0.00317	0.00298	CM	42
MyoInositol	0.20954	0.20019	0.01147	0.00921	CM	42
Serine	0.23277	0.20800	0.01462	0.01081	CM	42
Valine	0.22870	0.21376	0.00888	0.00825	CM	42
α -D-glucose	3.78817	3.45726	0.21951	0.14137	CM	45
β -D-glucose	3.89997	3.52084	0.26351	0.19923	CM	45
Acetate	0.16225	0.15029	0.00152	0.00094	CM	45
Alanine	0.18541	0.16743	0.00987	0.00961	CM	45
Arginine	0.76970	0.71688	0.04575	0.03634	CM	45
Asparagine	0.35290	0.36294	0.00748	0.01095	CM	45
Aspartate	0.07227	0.07391	0.00415	0.00241	CM	45
Glutamate	0.21268	0.19698	0.00827	0.00557	CM	45
Glutamine	1.52817	1.42834	0.04478	0.03696	CM	45
Glycerol	0.74463	0.67441	0.04328	0.04010	CM	45
Glycine	0.16844	0.15130	0.00283	0.00112	CM	45
Isoleucine	0.37319	0.33873	0.00511	0.00553	CM	45
Lactate	18.02106	16.64666	0.77234	0.68926	CM	45
Leucine	0.54396	0.48660	0.01709	0.01365	CM	45
Lysine	0.25546	0.23781	0.00495	0.00186	CM	45
Methionine	0.07224	0.06321	0.00324	0.00255	CM	45
MyoInositol	0.20403	0.19405	0.00780	0.00702	CM	45
Serine	0.29057	0.26429	0.01389	0.01252	CM	45

Metabolite	Height	Volume	SEM-Height	SEM-Volume	Media	Time[h]
Valine	0.24611	0.23303	0.00906	0.00794	CM	45
α -D-glucose	2.25221	2.06652	0.25376	0.23796	CM	48
β -D-glucose	2.20516	2.03390	0.29941	0.28048	CM	48
Acetate	0.12897	0.12188	0.01853	0.01611	CM	48
Alanine	0.20798	0.18953	0.00801	0.00590	CM	48
Arginine	0.64011	0.60138	0.05566	0.05486	CM	48
Asparagine	0.38626	0.38966	0.00815	0.00987	CM	48
Aspartate	0.07289	0.07772	0.00173	0.00142	CM	48
Glutamate	0.22055	0.20930	0.01032	0.01193	CM	48
Glutamine	1.44848	1.37179	0.03649	0.04346	CM	48
Glycerol	0.89867	0.83372	0.00912	0.01092	CM	48
Glycine	0.16650	0.15029	0.00558	0.00188	CM	48
Isoleucine	0.35576	0.33309	0.00801	0.00851	CM	48
Lactate	21.64304	20.27124	0.35231	0.40604	CM	48
Leucine	0.53173	0.48487	0.01532	0.01663	CM	48
Lysine	0.24950	0.23671	0.00612	0.00707	CM	48
Methionine	0.06126	0.05468	0.00543	0.00451	CM	48
MyoInositol	0.19333	0.18244	0.00144	0.00307	CM	48
Serine	0.30903	0.28842	0.00405	0.00479	CM	48
Valine	0.25059	0.23482	0.00709	0.00712	CM	48
α -D-glucose	7.29914	6.63518	0.49969	0.34154	CM	51
β -D-glucose	7.06350	6.28017	0.45409	0.28490	CM	51
Acetate	0.19339	0.17212	0.01810	0.01160	CM	51
Alanine	0.05412	0.04828	0.00639	0.00680	CM	51
Arginine	0.95745	0.87287	0.04576	0.02518	CM	51
Asparagine	0.33422	0.31341	0.00621	0.00469	CM	51
Aspartate	0.08669	0.08977	0.00794	0.00490	CM	51
Glutamate	0.19669	0.18220	0.00615	0.00172	CM	51
Glutamine	1.56120	1.42938	0.05060	0.01927	CM	51
Glycerol	0.22311	0.20506	0.02704	0.03008	CM	51
Glycine	0.12158	0.10682	0.00196	0.00204	CM	51
Isoleucine	0.40033	0.35710	0.00674	0.00984	CM	51
Lactate	5.36452	4.90108	0.77037	0.77394	CM	51
Leucine	0.44222	0.39257	0.02246	0.01216	CM	51
Lysine	0.23272	0.21644	0.00854	0.01066	CM	51
Methionine	0.08740	0.07383	0.00307	0.00025	CM	51

Metabolite	Height	Volume	SEM-Height	SEM-Volume	Media	Time[h]
MyoInositol	0.22418	0.20478	0.02351	0.01411	CM	51
Serine	0.10049	0.07999	0.01086	0.01088	CM	51
Valine	0.18204	0.16567	0.00149	0.00441	CM	51
α -D-glucose	6.41549	5.74084	0.24195	0.25193	CM	54
β -D-glucose	6.22139	5.56693	0.29161	0.28358	CM	54
Acetate	0.17578	0.16597	0.01025	0.00874	CM	54
Alanine	0.07198	0.06584	0.00466	0.00403	CM	54
Arginine	0.84320	0.77415	0.02199	0.01563	CM	54
Asparagine	0.37599	0.36260	0.00630	0.00048	CM	54
Aspartate	0.07212	0.07436	0.00511	0.00511	CM	54
Glutamate	0.19479	0.18127	0.00228	0.00373	CM	54
Glutamine	1.52197	1.40428	0.02084	0.01317	CM	54
Glycerol	0.31511	0.28415	0.04145	0.03564	CM	54
Glycine	0.13066	0.11817	0.00512	0.00606	CM	54
Isoleucine	0.38615	0.34772	0.01598	0.01220	CM	54
Lactate	7.93296	7.23213	0.86583	0.75947	CM	54
Leucine	0.43139	0.38866	0.00550	0.00249	CM	54
Lysine	0.23863	0.22239	0.00473	0.00306	CM	54
Methionine	0.07488	0.06486	0.00412	0.00355	CM	54
MyoInositol	0.20778	0.19500	0.00485	0.00397	CM	54
Serine	0.12838	0.11435	0.01845	0.01415	CM	54
Valine	0.18093	0.16656	0.00845	0.00441	CM	54
α -D-glucose	9.56683	8.50652	0.38881	0.33892	CM	6
β -D-glucose	9.86094	8.68894	0.26840	0.27751	CM	6
Acetate	0.19701	0.18889	0.01764	0.01834	CM	6
Alanine	0.03052	0.02733	0.00044	0.00070	CM	6
Arginine	1.03103	0.93653	0.06482	0.05833	CM	6
Asparagine	0.32640	0.32005	0.01161	0.00784	CM	6
Aspartate	0.07383	0.07533	0.00527	0.00562	CM	6
Glutamate	0.19857	0.18126	0.00366	0.00283	CM	6
Glutamine	1.65228	1.50282	0.05187	0.05568	CM	6
Glycerol	0.08891	0.08140	0.00853	0.00732	CM	6
Glycine	0.11362	0.09863	0.00969	0.00772	CM	6
Isoleucine	0.42220	0.36869	0.00700	0.00407	CM	6
Lactate	2.46362	2.22567	0.11932	0.09517	CM	6
Leucine	0.43410	0.38186	0.00897	0.01179	CM	6

Metabolite	Height	Volume	SEM-Height	SEM-Volume	Media	Time[h]
Lysine	0.23829	0.21810	0.02073	0.01959	CM	6
Methionine	0.08764	0.07567	0.00653	0.00592	CM	6
MyoInositol	0.23864	0.21837	0.00292	0.00222	CM	6
Serine	0.14926	0.10825	0.02446	0.01348	CM	6
Valine	0.17159	0.15585	0.00479	0.00438	CM	6
α -D-glucose	9.04964	8.24361	0.45604	0.37494	CM	9
β -D-glucose	9.16366	8.18619	0.38076	0.35964	CM	9
Acetate	0.16424	0.16060	0.01208	0.01189	CM	9
Alanine	0.03974	0.03572	0.00549	0.00575	CM	9
Arginine	0.99185	0.90163	0.06969	0.06387	CM	9
Asparagine	0.35917	0.33409	0.03347	0.03455	CM	9
Aspartate	0.07532	0.07574	0.00335	0.00079	CM	9
Glutamate	0.18489	0.17157	0.01132	0.01021	CM	9
Glutamine	1.62405	1.48686	0.05701	0.05688	CM	9
Glycerol	0.11755	0.11182	0.00878	0.00820	CM	9
Glycine	0.12264	0.10882	0.00605	0.00450	CM	9
Isoleucine	0.44683	0.39323	0.03066	0.02476	CM	9
Lactate	3.49833	3.18605	0.10655	0.09414	CM	9
Leucine	0.43378	0.38100	0.01710	0.01545	CM	9
Lysine	0.24244	0.22249	0.00937	0.00799	CM	9
Methionine	0.08904	0.07686	0.00585	0.00676	CM	9
MyoInositol	0.22588	0.21209	0.00420	0.00295	CM	9
Serine	0.16977	0.13893	0.00492	0.01177	CM	9
Valine	0.17116	0.15412	0.00134	0.00079	CM	9
α -D-glucose	1.92083	1.72751	0.06642	0.05811	LG	0
β -D-glucose	1.85165	1.64118	0.05766	0.05041	LG	0
Glutamate	0.09272	0.08793	0.00548	0.00492	LG	0
Glutamine	0.59699	0.54786	0.01200	0.01119	LG	0
Glycine	0.21677	0.19129	0.00978	0.00870	LG	0
Isoleucine	0.09558	0.07815	0.00354	0.00265	LG	0
Leucine	0.20345	0.17980	0.00968	0.00924	LG	0
Lysine	0.30061	0.27907	0.00683	0.00663	LG	0
Methionine	0.03314	0.02883	0.00401	0.00445	LG	0
MyoInositol	0.05400	0.04829	0.00045	0.00109	LG	0
Valine	0.22567	0.20590	0.00866	0.00646	LG	0
α -D-glucose	0.71618	0.64927	0.02688	0.02040	LG	12

Metabolite	Height	Volume	SEM-Height	SEM-Volume	Media	Time[h]
β -D-glucose	0.70858	0.64422	0.01922	0.01758	LG	12
Alanine	0.04297	0.03931	0.00476	0.00301	LG	12
Glutamate	0.08107	0.07654	0.00645	0.00605	LG	12
Glutamine	0.51232	0.47590	0.00626	0.00410	LG	12
Glycerol	0.08982	0.08086	0.00979	0.00493	LG	12
Glycine	0.19131	0.16761	0.00679	0.00644	LG	12
Isoleucine	0.09633	0.08275	0.01178	0.01017	LG	12
Lactate	2.71346	2.50494	0.09880	0.08468	LG	12
Leucine	0.18961	0.17361	0.00780	0.00840	LG	12
Lysine	0.26401	0.24699	0.00898	0.00708	LG	12
Methionine	0.02257	0.02092	0.00042	0.00076	LG	12
MyoInositol	0.03385	0.02928	0.00113	0.00138	LG	12
Valine	0.20218	0.18680	0.00466	0.00432	LG	12
α -D-glucose	1.52835	1.34498	0.05670	0.03296	LG	15
β -D-glucose	1.51780	1.32984	0.05365	0.02958	LG	15
Alanine	0.02411	0.02202	0.00275	0.00271	LG	15
Glutamate	0.10326	0.09542	0.00406	0.00240	LG	15
Glutamine	0.56992	0.51728	0.01456	0.00735	LG	15
Glycerol	0.03907	0.03335	0.00385	0.00551	LG	15
Glycine	0.20478	0.17627	0.01281	0.00867	LG	15
Isoleucine	0.13286	0.11323	0.01933	0.01867	LG	15
Lactate	0.80204	0.72076	0.03496	0.02329	LG	15
Leucine	0.19363	0.17006	0.00862	0.00479	LG	15
Lysine	0.29203	0.26542	0.01554	0.01027	LG	15
Methionine	0.02619	0.01882	0.00460	0.00592	LG	15
MyoInositol	0.03999	0.03573	0.00465	0.00318	LG	15
Valine	0.22581	0.20309	0.00439	0.00360	LG	15
α -D-glucose	1.31129	1.17018	0.06159	0.04107	LG	18
β -D-glucose	1.31764	1.15666	0.05592	0.03119	LG	18
Alanine	0.03158	0.02964	0.00042	0.00141	LG	18
Glutamate	0.09853	0.08979	0.00428	0.00465	LG	18
Glutamine	0.55488	0.49632	0.00850	0.01133	LG	18
Glycerol	0.04679	0.04364	0.00105	0.00173	LG	18
Glycine	0.21168	0.18858	0.00741	0.00633	LG	18
Isoleucine	0.09790	0.08081	0.01476	0.01516	LG	18
Lactate	1.25546	1.13679	0.04003	0.02557	LG	18

Metabolite	Height	Volume	SEM-Height	SEM-Volume	Media	Time[h]
Leucine	0.19209	0.16857	0.01008	0.00670	LG	18
Lysine	0.28745	0.26172	0.01001	0.00615	LG	18
Methionine	0.02876	0.02388	0.00158	0.00146	LG	18
MyoInositol	0.03788	0.03540	0.00462	0.00386	LG	18
Valine	0.21443	0.19436	0.00266	0.00068	LG	18
α -D-glucose	1.08183	0.98159	0.03579	0.01884	LG	21
β -D-glucose	1.11294	0.97912	0.03559	0.02111	LG	21
Alanine	0.02893	0.02675	0.00085	0.00164	LG	21
Glutamate	0.08715	0.08518	0.00379	0.00290	LG	21
Glutamine	0.53437	0.48311	0.02055	0.01329	LG	21
Glycerol	0.05908	0.05177	0.00254	0.00280	LG	21
Glycine	0.20039	0.17540	0.00318	0.00199	LG	21
Isoleucine	0.09863	0.08068	NA	NA	LG	21
Lactate	1.71577	1.55491	0.07770	0.05393	LG	21
Leucine	0.19519	0.17066	0.00826	0.00741	LG	21
Lysine	0.26669	0.24340	0.00601	0.00462	LG	21
Methionine	0.02236	0.01835	0.00046	0.00118	LG	21
MyoInositol	0.03185	0.02772	0.00445	0.00361	LG	21
Valine	0.21207	0.19155	0.01619	0.01138	LG	21
α -D-glucose	0.97333	0.88432	0.01425	0.02189	LG	24
β -D-glucose	0.91733	0.81616	0.05226	0.04263	LG	24
Alanine	0.04071	0.03866	0.00372	0.00316	LG	24
Glutamate	0.08100	0.07711	0.00958	0.00660	LG	24
Glutamine	0.51756	0.47414	0.01697	0.01339	LG	24
Glycerol	0.05785	0.05432	0.00682	0.00609	LG	24
Glycine	0.19891	0.17759	0.01187	0.00777	LG	24
Isoleucine	0.11214	0.09380	0.00461	0.00496	LG	24
Lactate	2.25111	2.05641	0.03570	0.01841	LG	24
Leucine	0.19115	0.16891	0.00944	0.00648	LG	24
Lysine	0.28745	0.26399	0.00824	0.00720	LG	24
Methionine	0.01693	0.01444	0.00055	0.00137	LG	24
MyoInositol	0.03596	0.03236	0.00472	0.00451	LG	24
Valine	0.20700	0.18856	0.00261	0.00150	LG	24
α -D-glucose	1.50975	1.33295	0.04556	0.03463	LG	27
β -D-glucose	1.45338	1.28230	0.04825	0.04311	LG	27
Alanine	0.03326	0.03002	0.00297	0.00254	LG	27

Metabolite	Height	Volume	SEM-Height	SEM-Volume	Media	Time[h]
Glutamate	0.09709	0.08865	0.01517	0.01287	LG	27
Glutamine	0.58820	0.53297	0.01816	0.01772	LG	27
Glycerol	0.04337	0.03816	0.01028	0.01070	LG	27
Glycine	0.22010	0.19261	0.00772	0.00279	LG	27
Isoleucine	0.08181	0.06711	0.01974	0.01525	LG	27
Lactate	1.17064	1.05301	0.04359	0.04028	LG	27
Leucine	0.21080	0.18369	0.00662	0.00741	LG	27
Lysine	0.30095	0.27500	0.01247	0.01089	LG	27
Methionine	0.03050	0.02693	0.00371	0.00276	LG	27
MyoInositol	0.03590	0.03157	0.00433	0.00369	LG	27
Valine	0.23211	0.20917	0.00530	0.00490	LG	27
α -D-glucose	1.40157	1.24139	0.10063	0.08200	LG	3
β -D-glucose	1.42083	1.25237	0.06444	0.06077	LG	3
Alanine	0.02326	0.02288	0.00614	0.00704	LG	3
Glutamate	0.08448	0.07811	0.00717	0.00603	LG	3
Glutamine	0.57087	0.51699	0.04693	0.04184	LG	3
Glycerol	0.04721	0.04260	0.00578	0.00573	LG	3
Glycine	0.20510	0.18015	0.01422	0.01425	LG	3
Isoleucine	0.09404	0.07991	0.00968	0.00699	LG	3
Lactate	0.93848	0.84946	0.05972	0.05606	LG	3
Leucine	0.19477	0.17109	0.01120	0.01015	LG	3
Lysine	0.26929	0.24710	0.01079	0.01069	LG	3
Methionine	0.02759	0.02274	0.00524	0.00440	LG	3
MyoInositol	0.03954	0.03533	0.00170	0.00138	LG	3
Valine	0.21380	0.19393	0.01747	0.01500	LG	3
α -D-glucose	1.16353	1.01269	0.02769	0.01906	LG	30
β -D-glucose	1.12348	0.98839	0.03227	0.01589	LG	30
Alanine	0.04446	0.04136	0.00356	0.00482	LG	30
Glutamate	0.10527	0.09807	0.00255	0.00216	LG	30
Glutamine	0.54702	0.49468	0.01959	0.01550	LG	30
Glycerol	0.08120	0.07226	0.00998	0.00363	LG	30
Glycine	0.20526	0.17853	0.00631	0.00654	LG	30
Isoleucine	0.08970	0.07335	0.00291	0.00036	LG	30
Lactate	1.83489	1.64887	0.06250	0.03873	LG	30
Leucine	0.20987	0.18543	0.00959	0.00516	LG	30
Lysine	0.29195	0.26735	0.00381	0.00181	LG	30

Metabolite	Height	Volume	SEM-Height	SEM-Volume	Media	Time[h]
Methionine	0.03890	0.03238	0.01027	0.00887	LG	30
MyoInositol	0.03010	0.02637	0.00318	0.00218	LG	30
Valine	0.23703	0.21222	0.00602	0.00230	LG	30
α -D-glucose	0.84319	0.74946	0.07950	0.07501	LG	33
β -D-glucose	0.82991	0.74983	0.04923	0.04202	LG	33
Alanine	0.07165	0.06487	0.00314	0.00292	LG	33
Glutamate	0.10222	0.09622	0.00354	0.00247	LG	33
Glutamine	0.55346	0.51141	0.03981	0.02935	LG	33
Glycerol	0.09897	0.08815	0.01542	0.01303	LG	33
Glycine	0.21189	0.19677	0.02224	0.01771	LG	33
Isoleucine	0.12471	0.10727	0.01597	0.01514	LG	33
Lactate	2.85317	2.63325	0.18327	0.13436	LG	33
Leucine	0.22452	0.20015	0.01884	0.01675	LG	33
Lysine	0.28034	0.26355	0.01506	0.01177	LG	33
Methionine	0.02692	0.02140	0.00094	0.00146	LG	33
MyoInositol	0.04032	0.03697	0.00362	0.00441	LG	33
Valine	0.23793	0.21965	0.01654	0.01209	LG	33
α -D-glucose	0.55686	0.49371	0.00929	0.01502	LG	36
β -D-glucose	0.52596	0.46763	0.01434	0.01552	LG	36
Alanine	0.09112	0.08196	0.00570	0.00360	LG	36
Glutamate	0.10505	0.09855	0.00946	0.01036	LG	36
Glutamine	0.55110	0.49895	0.01417	0.01424	LG	36
Glycerol	0.14683	0.13017	0.00515	0.00670	LG	36
Glycine	0.22165	0.19440	0.01863	0.01641	LG	36
Isoleucine	0.10895	0.09018	0.00828	0.00923	LG	36
Lactate	3.76809	3.41769	0.17727	0.14264	LG	36
Leucine	0.25489	0.22420	0.00351	0.00050	LG	36
Lysine	0.28402	0.25921	0.00636	0.00799	LG	36
Methionine	0.02631	0.02229	0.00678	0.00500	LG	36
MyoInositol	0.03723	0.03358	0.00478	0.00563	LG	36
Valine	0.26212	0.23539	0.01105	0.01035	LG	36
α -D-glucose	1.24162	1.09740	0.02416	0.00773	LG	39
β -D-glucose	1.20482	1.07565	0.04992	0.02776	LG	39
Alanine	0.04122	0.03926	0.00133	0.00125	LG	39
Glutamate	0.08058	0.07740	0.00631	0.00432	LG	39
Glutamine	0.57967	0.52685	0.01149	0.00300	LG	39

Metabolite	Height	Volume	SEM-Height	SEM-Volume	Media	Time[h]
Glycerol	0.06420	0.05774	0.00784	0.00572	LG	39
Glycine	0.19797	0.17661	0.00885	0.00356	LG	39
Isoleucine	0.09304	0.07776	0.01551	0.01436	LG	39
Lactate	1.54579	1.40096	0.06210	0.03511	LG	39
Leucine	0.21152	0.18862	0.00709	0.00275	LG	39
Lysine	0.27417	0.25343	0.01829	0.01332	LG	39
Methionine	0.02653	0.02412	0.00134	0.00123	LG	39
MyoInositol	0.04037	0.03692	0.00090	0.00013	LG	39
Valine	0.23241	0.21008	0.00975	0.00563	LG	39
α -D-glucose	0.89448	0.80583	0.00436	0.01014	LG	42
β -D-glucose	0.82821	0.74605	0.02207	0.01528	LG	42
Alanine	0.06230	0.05931	0.00662	0.00655	LG	42
Glutamate	0.09847	0.09305	0.01132	0.00913	LG	42
Glutamine	0.56443	0.52109	0.00735	0.00572	LG	42
Glycerol	0.09968	0.09182	0.00412	0.00287	LG	42
Glycine	0.22780	0.20616	0.00684	0.00266	LG	42
Isoleucine	0.11916	0.10355	NA	NA	LG	42
Lactate	2.56041	2.35341	0.02715	0.02574	LG	42
Leucine	0.21479	0.19540	0.00188	0.00303	LG	42
Lysine	0.27176	0.25227	0.00282	0.00327	LG	42
Methionine	0.02897	0.02513	0.00231	0.00363	LG	42
MyoInositol	0.03581	0.03320	0.00457	0.00510	LG	42
Valine	0.24359	0.22566	0.00281	0.00180	LG	42
α -D-glucose	0.52841	0.47240	0.03296	0.02566	LG	45
β -D-glucose	0.49255	0.44234	0.01870	0.01470	LG	45
Alanine	0.09000	0.08095	0.00318	0.00340	LG	45
Glutamate	0.09221	0.08763	0.00230	0.00085	LG	45
Glutamine	0.55574	0.50588	0.02560	0.02144	LG	45
Glycerol	0.14669	0.13192	0.02132	0.01680	LG	45
Glycine	0.20640	0.18475	0.00995	0.00768	LG	45
Isoleucine	0.09248	0.07276	0.00589	0.00422	LG	45
Lactate	3.64068	3.31835	0.24625	0.20557	LG	45
Leucine	0.24837	0.21992	0.01290	0.00977	LG	45
Lysine	0.27855	0.25490	0.01292	0.01004	LG	45
Methionine	0.01910	0.01427	0.00014	0.00085	LG	45
MyoInositol	0.03507	0.03176	0.00687	0.00636	LG	45

Metabolite	Height	Volume	SEM-Height	SEM-Volume	Media	Time[h]
Valine	0.25300	0.22904	0.01694	0.01540	LG	45
α -D-glucose	0.24306	0.21734	0.02374	0.02461	LG	48
β -D-glucose	0.26281	0.23844	0.00891	0.00787	LG	48
Alanine	0.10844	0.09801	0.00291	0.00455	LG	48
Glutamate	0.10928	0.10183	0.00390	0.00356	LG	48
Glutamine	0.54051	0.49893	0.01486	0.01117	LG	48
Glycerol	0.17619	0.15905	0.01346	0.01050	LG	48
Glycine	0.22175	0.20104	0.01220	0.00976	LG	48
Isoleucine	0.08482	0.07306	0.00168	0.00236	LG	48
Lactate	4.39557	4.05320	0.03217	0.02223	LG	48
Leucine	0.26509	0.24015	0.00456	0.00568	LG	48
Lysine	0.28629	0.26679	0.00533	0.00388	LG	48
Methionine	0.02622	0.02290	0.00326	0.00312	LG	48
MyoInositol	0.03210	0.02886	0.00307	0.00277	LG	48
Valine	0.27075	0.24969	0.00441	0.00385	LG	48
α -D-glucose	1.25109	1.10715	0.05809	0.04922	LG	51
β -D-glucose	1.23221	1.07829	0.03473	0.03659	LG	51
Alanine	0.05089	0.04571	0.00145	0.00145	LG	51
Glutamate	0.10693	0.10027	0.00116	0.00061	LG	51
Glutamine	0.58556	0.52483	0.01224	0.01339	LG	51
Glycerol	0.07897	0.06934	0.00159	0.00124	LG	51
Glycine	0.22205	0.19328	0.00932	0.00693	LG	51
Isoleucine	0.12265	0.10257	0.01654	0.01351	LG	51
Lactate	1.72586	1.54587	0.01792	0.02266	LG	51
Leucine	0.22447	0.19485	0.00783	0.00756	LG	51
Lysine	0.28347	0.25885	0.00117	0.00067	LG	51
Methionine	0.03170	0.02856	0.00568	0.00590	LG	51
MyoInositol	0.02916	0.02657	0.00687	0.00571	LG	51
Valine	0.24173	0.21605	0.00300	0.00307	LG	51
α -D-glucose	0.85418	0.76476	0.00468	0.00249	LG	54
β -D-glucose	0.81848	0.74396	0.02233	0.01973	LG	54
Alanine	0.06136	0.05779	0.00279	0.00281	LG	54
Glutamate	0.09781	0.09386	0.01205	0.01073	LG	54
Glutamine	0.51367	0.47686	0.00931	0.00701	LG	54
Glycerol	0.09579	0.08742	0.00249	0.00293	LG	54
Glycine	0.20871	0.18943	0.00720	0.00881	LG	54

Metabolite	Height	Volume	SEM-Height	SEM-Volume	Media	Time[h]
Isoleucine	0.13011	0.11070	0.00088	0.00212	LG	54
Lactate	2.53311	2.33564	0.02317	0.02221	LG	54
Leucine	0.20698	0.19282	0.00089	0.00062	LG	54
Lysine	0.27736	0.25940	0.00428	0.00473	LG	54
Methionine	0.02055	0.01746	0.00082	0.00061	LG	54
MyoInositol	0.04114	0.03738	0.00255	0.00189	LG	54
Valine	0.22136	0.20735	0.00505	0.00386	LG	54
α -D-glucose	1.18283	1.05392	0.05352	0.04175	LG	6
β -D-glucose	1.12233	1.01141	0.07300	0.06242	LG	6
Alanine	0.02967	0.02912	0.00543	0.00557	LG	6
Glutamate	0.09062	0.08559	0.00570	0.00571	LG	6
Glutamine	0.54267	0.50309	0.02516	0.02193	LG	6
Glycerol	0.06968	0.06214	0.01742	0.01503	LG	6
Glycine	0.20203	0.17855	0.00958	0.00847	LG	6
Isoleucine	0.08598	0.07823	0.01719	0.01413	LG	6
Lactate	1.57890	1.45214	0.08695	0.07686	LG	6
Leucine	0.18496	0.16822	0.01206	0.00823	LG	6
Lysine	0.27076	0.25040	0.00967	0.00910	LG	6
Methionine	0.02074	0.01724	0.00474	0.00277	LG	6
MyoInositol	0.03302	0.03088	0.00603	0.00628	LG	6
Valine	0.21258	0.19777	0.00823	0.00555	LG	6
α -D-glucose	0.93120	0.84107	0.05323	0.04813	LG	9
β -D-glucose	0.91124	0.82362	0.02795	0.02500	LG	9
Alanine	0.03829	0.03562	0.00209	0.00194	LG	9
Glutamate	0.07824	0.07595	0.01006	0.00978	LG	9
Glutamine	0.51796	0.47958	0.02610	0.02222	LG	9
Glycerol	0.05940	0.05223	0.00861	0.00701	LG	9
Glycine	0.18977	0.16987	0.00841	0.00792	LG	9
Isoleucine	0.10852	0.09231	0.01178	0.01155	LG	9
Lactate	2.17804	2.00386	0.12705	0.11208	LG	9
Leucine	0.18374	0.16680	0.00605	0.00566	LG	9
Lysine	0.26682	0.24946	0.01469	0.01371	LG	9
Methionine	0.02533	0.02427	NA	NA	LG	9
MyoInositol	0.03936	0.03576	0.00196	0.00262	LG	9
Valine	0.21015	0.19288	0.00584	0.00593	LG	9

Table A.5: Cellular extracts fold change with respect to RBC comparison.

Metabolite	FC-Rings-A	FC-Troph-A	Trend-A	FC-Rings-B	FC-Troph-B	Trend-B
Alanine	2.407	2.509	increase	1.783	4.082	increase
Arginine	0.399	0.582	increase	0.875	1.358	increase
Asparagine	0.546	0.729	increase	0.915	0.899	decrease
Aspartate	0.431	0.559	increase	0.703	0.819	increase
Creatine	0.355	0.403	increase	-	-	-
Glutamate	0.263	0.281	increase	0.559	0.727	increase
Glutamine	0.539	0.839	increase	0.878	1.206	increase
Glycine	0.559	0.631	increase	-	-	-
GSH	1.122	0.917	decrease	0.975	0.927	decrease
Isoleucine*	0.627	0	decrease	0.926	0.498	decrease
Lactate	2.666	2.912	increase	1.931	14.457	increase
Leucine	1.236	0.962	decrease	-	-	-
Lysine	0.82	1.001	increase	1.099	2.006	increase
MyoInositol	0.889	0.892	increase	0.746	1.56	increase
NAD	3.77	3.688	decrease	3.436	4.454	increase
Serine	0.815	0.882	increase	0.901	1.118	increase
Valine	1.083	1.133	increase	0.951	1.675	increase

FC=Fold Change with respect to RBC; A=*In-house* results; B= Olszewski *et al.* results; *Isoleucine and Leucine cannot be distinguished in MS thus a pooled measurement is reported in B.

Appendix B

Publication

The proliferating cell hypothesis: a metabolic framework for *Plasmodium* growth and development[☆]

J. Enrique Salcedo-Sora^{1*}, Eva Caamano-Gutierrez^{1,2}, Stephen A. Ward¹, and Giancarlo A. Biagini¹

¹ Liverpool School of Tropical Medicine, Pembroke Place, Liverpool, L3 5QA, UK

² Warwick Systems Biology Centre, Senate House, University of Warwick, Coventry, CV4 7AL, UK

Open access under CC BY license.

We hypothesise that intraerythrocytic malaria parasite metabolism is not merely fulfilling the need for ATP generation, but is evolved to support rapid proliferation, similar to that seen in other rapidly proliferating cells such as cancer cells. Deregulated glycolytic activity coupled with impaired mitochondrial metabolism is a metabolic strategy to generate glycolytic intermediates essential for rapid biomass generation for schizogony. Further, we discuss the possibility that *Plasmodium* metabolism is not only a functional consequence of the 'hard-wired' genome and argue that metabolism may also have a causal role in triggering the cascade of events that leads to developmental stage transitions. This hypothesis offers a framework to rationalise the observations of aerobic glycolysis, atypical mitochondrial metabolism, and metabolic switching in nonproliferating stages.

Aerobic glycolysis drives proliferation in single-minded eukaryotes

Rapidly proliferating eukaryotes have perfected metabolic modes that efficiently convert glucose and specific amino acids into biomass (see [Glossary](#)) and energy at the required pace. The past decade has brought a change in the accepted paradigm on accelerated cell multiplication. Streamlined metabolic networks and the capacity to support anabolic reactions in a rapidly responsive manner via aerobic fermentative glycolysis and glutaminolysis, instead of pursuing thorough oxidation of the glycolytic carbons via cellular respiration, seems to be a precondition for rather than a consequence of effective proliferative signalling [1]. The corollary of this paradigm points to respiration in nonproliferating cells as the prevalent metabolic mode to generate the energy needed to perform their roles as differentiated cells.

Corresponding author: Biagini, G.A. (Biagini@liv.ac.uk).

Keywords: Warburg effect; glycolysis; malaria; epigenetics; gametocytes; dormancy.

*Current address: School of Health Sciences, Liverpool Hope University, Liverpool, L16 9JD, UK.

1471-4922

© 2014 The Authors. Published by Elsevier Ltd. All rights reserved. <http://dx.doi.org/10.1016/j.pt.2014.02.001>

[☆]This is an open-access article distributed under the terms of the Creative Commons Attribution License, which permits unrestricted use, distribution and reproduction in any medium, provided the original author and source are credited.

Current concept of the Warburg effect

Although originally ascribed to anaerobic metabolism, the preference for fermentative glycolysis even under aerobic conditions was accepted long ago as a feature in cancer cells and is known as the Warburg effect [2]. Similarly, *Saccharomyces cerevisiae* favour fermentation over respiration when glucose is available even under oxygen abun-

Glossary

Aerobic glycolysis: predominant fermentation of glucose even under oxygen pressures considered to be aerobic. Fractions of glycolytic intermediates that are not fermented are redirected and are seemingly sufficient to sustain biosynthetic pathways such as the pentose phosphate pathway, shikimate pathway, and lipid biosynthesis.

Agouti viable yellow mouse model: heterozygous mice for the Agouti yellow allele have yellow coats and have a predisposition towards obesity. Mice that are homozygous for the Agouti yellow allele have the lethal gene. Mice that are homozygous for the non-agouti allele and non-agouti yellow allele have non-agouti coat colour such as black. In this model, coat colour variation is correlated to epigenetic marks established early in development, and is used extensively to investigate the impacts of nutritional and environmental influences on the (foetal) epigenome.

Anabolic reactions: relating to the synthesis of complex molecules in living organisms.

Anaerobic metabolism: relating to metabolism that occurs in the absence of free oxygen, often via substrate level phosphorylation and/or alternative terminal acceptors.

Anaplerosis: the process of replenishment of depleted metabolic cycle or pathway intermediates. Most commonly referring to the TCA cycle, this concept is also used to describe glycolysis and glutaminolysis generated substrates for macromolecular biosynthesis or anabolism.

Biomass: the total quantity or weight of organisms in a given area or volume. The measurement of biomass production is important when studying metabolic reactions that are required for growth.

Dormancy and reversible cell cycle arrest: cell quiescence, hibernation, dormancy, or reversible cell cycle arrest are denominations of a common and important physiological response in free-living microorganisms to control cell size and growth that grants protection against environmental insults including poor nutrient and micronutrient levels.

Fermentative glycolysis: breaking of glucose into different possible final products from the reduction of pyruvate as common intermediate. The better-known products are lactate in mammalian cells and ethanol in yeast. Replenishment of NAD⁺ is a crucial consequence of fermentation.

Glutaminolysis: alternative source of biomass and electrons due to the relative abundance of glutamine in human plasma. After deamination of this amino acid, glutamate feeds part of the TCA cycle. Intermediates such as malate and oxaloacetate can transit to the cytoplasm from mitochondria and be decarboxylated to replenish glycolytic pyruvate with the production of NADPH.

One-carbon mitochondrial metabolism: exchange of one carbon molecules at different levels of oxidation between folate intermediates catalysed by enzyme complexes loosely attached to the inner mitochondrial membrane. The glycine cleavage system (GCV), serine hydroxymethyltransferase (SHMT), and 5,10-methylenetetrahydrofolate dehydrogenase multienzyme complex (MTHFD) are their main components.

Box 1. Metabolic rewiring for rapid parasite proliferation: glycolysis

Glucose entry into the parasite occurs via the hexose transporter PfHT1, which has a K_m of ~0.5 mM. Compared with the ~5 mM blood glucose concentration, this allows for a constant rate of transport [36]. Commitment to glycolysis is then controlled via the highly regulated phosphofructokinase (PFK) that is allosterically inhibited by high levels of ATP. In cancer cells, PFK is overexpressed, and the predominant isoforms of this enzyme possess allosteric alterations that reduce the degree of product inhibition by ATP and citrate whilst being more highly activated by lower concentrations of fructose 2,6-bisphosphate (F26bP) [37–39]. In *P. falciparum* PFK, deregulation is also observed with the enzyme being insensitive to PEP, citrate, and F26bP and only exhibiting allosteric behaviour for ATP and ADP, although at elevated concentrations (>1.0 mM for ATP and >0.1 mM for ADP) [40]. The final irreversible step in glycolysis involves pyruvate kinase (PK), generating pyruvate and ATP. This is a critical step in the control of biosynthetic intermediates for proliferation, and the enzyme is activated by fructose 1,6-bisphosphate and inhibited by both ATP and alanine. There are two isoforms in mammals, M1 and M2. M1 is found in adult tissue and is largely unregulated by fructose 1,6-bisphosphate and ATP, whereas the M2 isoform predominates in proliferating cells including cancer cells and is less active and more tightly regulated [41]. Tight regulation of PK is hypothesised to aid the control of flow of carbons between biosynthesis and lactate production in proliferating cells. Indeed, cancer cells engineered to express the M1 isoform produce more lactate [42,43]. *P. falciparum* PK is not activated by fructose 1,6-bisphosphate but is markedly inhibited by both ATP and citrate, akin to M2 mammalian isoforms [44].

dance (Crabtree effect) [3]. In its original form, the Warburg effect also stated that the oxidation of glucose in mitochondria was ablated. However, more recent evidence points to functional mitochondrial oxidative phosphorylation in some cancer cell lines [3,4]. Under this modern version of the Warburg effect, rapidly proliferating, non-cancerous cells have also been found to undergo aerobic glycolysis/fermentation [5–7].

The advantage provided to rapidly proliferating cells by increased glycolysis is attributed to the capacity of glucose to support biomass generation by redirection of glycolytic intermediates into anabolic reactions while at the same time sustaining a predominant (over 90%) fermentation flux to lactate [3,5,7,8] (Figure 1, Boxes 1 and 2). The latter is necessary for the regeneration of NAD⁺, an essential cofactor of glycolysis itself, but more importantly and less intuitively, to allow the cells to gauge their metabolic status. Thus, only when high levels of fermentative glycolysis are possible does the cell enter high rates of proliferation assisted by the anabolic capacity of glycolysis.

Aerobic glycolysis during the *in vitro* cell cycle of *Plasmodium falciparum*

The intraerythrocytic cycle of human *falciparum* malaria takes the parasites through successive rounds of mitosis every 48 h. Following erythrocyte invasion by a merozoite, but sometimes following multiple invasions, the parasite develops into a ring-shaped form in the first 24 h, and by approximately 30 h, the parasite very rapidly expands to occupy most of the space available within the erythrocyte plasma membrane, resulting in a major increase in biomass. From approximately 40 h, the vastly enlarged nucleus goes through several asynchronous and multiple segmentations that *in vitro* produce a number (small double figures) of

Box 2. Metabolic rewiring for rapid parasite proliferation: TCA and respiration

Pyruvate is a critical metabolic mode for entry into fermentation or the TCA cycle. For fermentation, pyruvate must remain in the cytosol, whereas for entry into the TCA cycle, pyruvate must enter mitochondria in order to be converted to acetyl-CoA. In proliferating cells, where described aerobic glycolysis is required for the generation of biosynthetic intermediates, cells have evolved mechanisms which either: (i) restrict the transport of pyruvate into mitochondria [45]; (ii) inhibit pyruvate dehydrogenase (PDH) activity [46]; or (iii) increase the activity of lactate dehydrogenase [47]. There is no information concerning pyruvate transport into the mitochondrion of *P. falciparum*; however, the parasite does contain PDH, but this is localised to the apicoplast and does not appear to contribute to the acetyl-CoA pool [48]. A mitochondrially localised complex, termed branch chain ketoacid dehydrogenase (BCKDH), with PDH-like activity, has been hypothesised to contribute acetyl-CoA to the TCA, this notwithstanding; however, labelling experiments indicate that the rate of acetyl-CoA production is significantly slower compared with the labelling of glycolytic intermediates [48]. Lactate production in *P. falciparum* is extensive and in line with other key parasite glycolytic enzymes, and lactate dehydrogenase activity is deregulated, exhibiting only weak inhibition by pyruvate or by the pyruvate/NAD⁺ complex [49,50].

Defects of electron transport chain components also appear to be a feature in cancer cells. These include defects at the level of succinate dehydrogenase (SDH), inhibition of ATP synthase, and downregulation of complex I (NADH:dehydrogenase), III (*bc₁* complex), and IV (cytochrome *c* oxidase) [51–53]. *P. falciparum* also possess atypical mitochondrial function, whereby mitochondria have low O₂ consumption and are not actively synthesizing ATP (respiratory state 4) [54]. Several adaptive features, including the absence of a transmembrane proton pumping complex I, enable proton-uncoupled oxidation of NADH, thereby reducing proton ‘back-pressure’ in the absence of extensive ATP synthesis. This in turn reduces mitochondrial superoxide generation and potential DNA damage and, importantly for glycolysis, still allows deregulated oxidation of cytosolic NADH [54]. The reported essentiality of complex V (ATP synthase [55]) is consistent with the need of a small H⁺ leak in order to maintain transmembrane H⁺ pumping by complexes III and IV [54].

next-generation merozoites [9]. Cytokinesis occurs near the end of the cycle before the new daughter cells (merozoites) emerge as free-living forms for seconds to minutes in the search for a new erythrocyte [9]. A fraction, usually less than 1% but dependent on the prevailing environment, of the newly generated intraerythrocytic parasites are programmed to differentiate as gametocytes, the sexual nondividing forms that in the natural environment continue the malaria cycle in the mosquito vector [10].

Malaria parasites committed to proliferation in the intraerythrocytic cycle are fermentative organisms [11–13] (Figure 1, Boxes 1 and 2) with an anabolic central carbon metabolism that can feed all major biomass generating pathways [14]. When directed to differentiation into gametocytes, however, these nonproliferative cells seem to follow the respiration of glucose in a manner more in line with the biology of eukaryotes in stationary phase via the canonical glucose-driven, mitochondrial tricarboxylic acid (TCA) cycle. Current evidence appears to substantiate this dichotomy of fermentation when in proliferation mode versus respiration when committed to sexual differentiation [15].

In proliferating asexual parasites, glutaminolysis feeds part of the TCA cycle through the five-carbon α -ketoglutarate. The four-carbon malate and oxaloacetate are

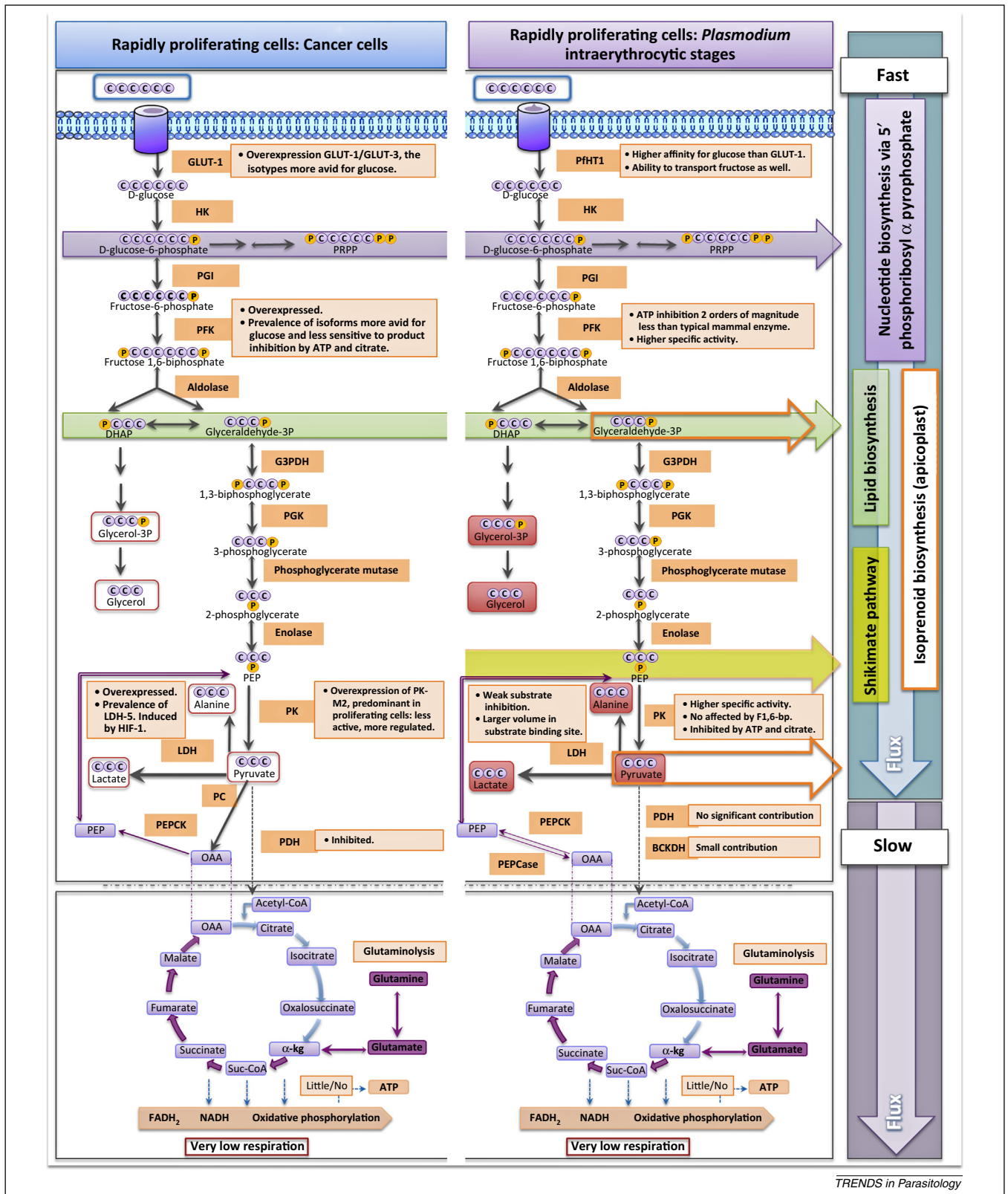


Figure 1. Proliferating cell hypothesis: similarities between cancer cells and *Plasmodium falciparum*. Principle end products of glucose consumption (lactate, alanine, pyruvate, glycerol-3-phosphate, and glycerol, shown in red boxes) are similar in both cancer cells [3] and asexual intraerythrocytic malaria parasites [12]. A high glycolytic flux maintains rate-limiting glycolytic intermediates to support nucleotide (via glucose-6-phosphate to 5-phosphoribosyl- α -pyrophosphate) and lipid biosynthesis (via dihydroxyacetone phosphate to glycerol-3-phosphate). Metabolic modifications (Boxes 1 and 2) allow aerobic glycolysis/fermentation to proceed rapidly whilst keeping tricarboxylic acid (TCA) flux low. Anapleurotic glutaminolysis follows past part of the TCA cycle through the five-carbon α -ketoglutarate [15]. Subsequent conversion of oxaloacetate to phosphoenolpyruvate (PEP) by phosphoenolpyruvate carboxykinase (PEPCK, EC 4.1.1.49) allows for further synthesis of biosynthetic intermediates (e.g., via shikimate pathway [16] and isoprenoid biosynthesis [17]). Abbreviations: GLUT-1, glucose transporter 1; PfHT1, *Plasmodium falciparum* hexose transporter 1; HK, hexokinase (EC 2.7.1.1); PGI, phosphoglucose isomerase (EC 5.3.1.9); PFK, phosphofructokinase (EC 2.7.1.11); G3PDH, glyceraldehyde 3 phosphate dehydrogenase (EC

transported to the cytoplasm. Here phosphoenolpyruvate (PEP) can be synthesised from oxaloacetate by the activity of phosphoenolpyruvate carboxykinase (PEPCK) for onward biosynthetic reactions (e.g., shikimate pathway [16] and isoprenoid biosynthesis [17]) (Figure 1). In non-proliferating gametocytes whereby a more canonical glucose TCA cycle is present, less glucose is catabolised by fermentation to lactate, and minimal glutamine is catabolised by glutaminolysis [15].

The paradigm of the rapidly proliferating eukaryote can then be applied to profile the dividing intraerythrocytic *P. falciparum* as an organism that in the presence of abundant glucose and glutamine, such as the levels available in human plasma, generates the required biomass by aerobic glycolysis/fermentation and glutaminolysis (Figure 1, Boxes 1–3). The rest of the macromolecular biomass is salvaged from the purine precursors, amino acids, and lipids or fatty acids of the human host. Under these conditions, a low flux glycolytic TCA cycle and a modified electron transport chain provides a further selective advantage (Boxes 1 and 2).

Are there metabolic regulatory switches controlling life cycle commitment in *Plasmodium*?

The established dogma states that *Plasmodium* metabolism is simply a functional consequence of the 'hard-wired' genome-wide, just-in-time regulation of expression [18,19]. However, there is increasing evidence in biology to support the notion that metabolism, in response to the environment/diet, can be causal, promoting the switch of cellular phenotypes. Examples in nature range from post-translational modifications (PTMs) of histones by constituents of royal jelly (fatty acids) causing larvae to become queens instead of worker bees [20], to PTMs of histones in the Agouti viable yellow mouse model, whereby different maternal methyl-donor supplementation (e.g., with folic acid, vitamin B12, or betaine) results in different offspring ranging from obese hyperinsulinaemic yellow to leaner nonhyperinsulinaemic pseudoagouti phenotypes [21].

The malaria parasite controls vital virulence processes such as host cell invasion and cytoadherence, at least in part, by epigenetic mechanisms [22]. With this in mind, and given that *in vitro* and *in vivo* nutrient/stress conditions have been linked with life cycle commitment in *Plasmodium* [23–25], it is not inconceivable that parasite metabolism may promote changes in phenotype via one or more of the many metabolites that are known to influence epigenetic gene regulation in other cell types.

In cancer cells and yeast, for example, nutrient availability and metabolic status, including the yeast metabolic cycle (YMC) fluctuating from oxidative phosphorylation and fermentation, is coupled to the control of gene expression via key metabolites such as NAD⁺, acetyl Co-A, FAD, and folates [26–28].

The influence of metabolism on parasite epigenetics is certainly an exciting area for future research, and some

Box 3. Growing fast while fermenting furiously: crunching the numbers

Aerobic glycolysis is able to provide the required biosynthetic intermediates for building biomass, explaining why *Plasmodium* and other proliferating organisms and cell types adopt increased glucose metabolism during rapid growth and multiplication. By way of illustration, the capacity of *Plasmodium* to synthesise some of the required DNA precursors relates to the *de novo* synthesis of the pyrimidine deoxythymidine triphosphate (dTTP). The *de novo* synthesis of dTTP requires folate 5,10-methylene tetrahydrofolate (5,10-myTHF). In its final polyglutamated form, with five glutamic residues as found in an average eukaryote, 5,10-myTHF is a structure of 40 carbons and 11 nitrogens that requires two NADPHs and ten ATPs for its biosynthesis from GTP, D-erythrose-4-phosphate (E4P) and PEP (shikimate pathway [16]). Only two molecules of glucose are needed to contribute seven carbons and the two NADPHs (pentose phosphate pathway). The rest of the carbon count originates from five glutamates and a serine or glycine. The nitrogen sources are GTP (six nitrogens) and glutamate (five nitrogens) from glutaminolysis. Thus, the synthesis of 5,10-myTHF from glucose and GTP can be abbreviated as: 2 glucose (carbon) + 1 GTP + 5 glutamate + 5 glucose (ATP) + 1 serine/glycine → 1 (5,10-myTHF) + 5 ADP + glycine/(CO₂ + NH₃). Malaria parasites salvage precursors for the synthesis of purines such as GTP from the host as well as amino acids from plasma and the digestion of the haemoglobin of the host. Then, for every 100 molecules of glucose, if 90% are used to sustain a high fermentative glycolytic flux, where the needed ATP originates in abundance, ten molecules of glucose can be used to build up to five molecules of 5,10-myTHF. Human plasma contains a strictly regulated level of glucose to ~5 mM, the equivalent of 3 × 10¹⁵ molecules of glucose per microlitre. That would be enough to build up to 7.5 × 10¹⁴ molecules of 5,10-myTHF per microlitre, the equivalent to 625 to 62.5 times what is needed to support an expected intracellular folate concentration in *P. falciparum* of approximately 2–20 μM.

evidence, although circumstantial, exists to link nutrient levels to parasite development. Environmental stress has been consistently correlated with enhanced gametocyte production both *in vitro* and *in vivo*. The methodology applied to enrich *in vitro* cultures of *P. falciparum* with sexual forms has the common denominator of nutrient deprivation: low haematocrit, haemoglobin depletion, lysed erythrocytes, and recycling of spent media, among others [23,29]. Antimalarials that act as antimetabolites such as antifolates have long been known to increase gametocyte production *in vivo* [24]. *In vivo* transcriptional profiles of *P. falciparum* blood stages show that a proportion of the parasite population appears to be in states similar to what is known as either a starvation response or environmental stress in yeast [25]. Therefore, natural variability of substrate levels in the human host, perhaps not surprisingly, seems to be a selective force for life cycle commitment pathways in field populations of *Plasmodium*. Unfortunately, cellular metabolism of malaria parasites under variable nutrient availability has been poorly investigated, a situation not helped by the routine use of highly enriched media normally used for the *in vitro* culture of *P. falciparum* [30].

The decision of a parasite to commit to a sexual lineage is believed to take place in the first 20 h (the 'ring' stage) of the preceding erythrocytic cycle [29]. Interestingly, the

1.2.1.12); PGK, phosphoglycerate kinase (EC 2.7.2.3); PK, pyruvate kinase (EC 2.7.1.40); LDH, lactate dehydrogenase (EC 1.1.1.27); PEPCase, phosphoenolpyruvate carboxylase (EC 4.1.1.31); PC, pyruvate carboxylase (EC 6.4.1.1); PDH, pyruvate dehydrogenase (EC 1.2.4.1); BCKDH, branched chain ketoacid dehydrogenase (EC 1.2.4.4); Suc-CoA, succinyl-CoA.

Box 4. Outstanding questions

- As described here, our hypothesis is that metabolism in the malaria parasite is highly evolved to promote rapid proliferation, in a similar manner to that seen in other rapidly proliferating cells, for example, cancer cells, activated lymphocytes, and yeast.
- The major 'step change' for future research questions will be to determine if metabolism can be causal. This will necessitate a deeper understanding of the metabolic nodes and checkpoints used by the parasite during growth and in response to its environment in its various hosts.

early ring stages of *P. falciparum* have less compact histone cores (nucleosomes) than in later stages [9], and usually this 'open' conformation is reflective of, and conducive to, transcriptional regulation. As in other organisms and cell types it is therefore possible that in *Plasmodium* there exists a metabolic component that controls, via an epigenetic mechanism, the commitment to replicate or to differentiate.

A further, metabolically controlled, decision-making option open to the parasite in the early hours of intracellular parasite life is the possibility of reversible cell cycle arrest. As part of their parasitic lifestyle, *P. falciparum* become dependent on the extracellular supply of isoleucine due to an absence of this amino acid in human haemoglobin. Media that lacks isoleucine induce reversible cell cycle arrest with parasites not progressing beyond the first half, the ring stage, of their asexual intraerythrocytic life cycle unless the missing nutrient is provided [31]. In malaria, the phenomenon of reversible cell cycle arrest is poorly understood. Nonetheless, there is a new interest in studying malaria dormancy in the intraerythrocytic stages of the parasite life cycle due to the potential role of reversible cell cycle arrest in the slow clearance and/or ring stage survival (RSA_{0-3h}) phenotypes seen in clinical failures with artemisinins [32–35].

Concluding remarks

Glucose and glutamine contribute to malaria parasite biomass for the biosynthesis of nucleotides and lipids via aerobic glycolysis/fermentation and glutaminolysis. Together with salvaged amino acids, fatty acids, and purines, these are the main biochemical resources used to assemble the macromolecular structure of the plasmodial cell. However, there are two further options available: (i) differentiation into a sexual lineage as gametocytes and (ii) cell cycle arrest. The first half of the intraerythrocytic cycle of *P. falciparum*, particularly within the initial 10 h, seems to be the stage at which quorum sensing and decision making is most relevant. As seen with other organisms and cell types, we have discussed the possibility that this occurs via nutrient/metabolite-dependent epigenetic mechanisms. Deconvolution of these regulatory processes offers a new and exciting chapter in our understanding of *Plasmodium* biology (Box 4).

Acknowledgements

This work was supported by grants from the Medical Research Council (MRC) and the Wellcome Trust. E.C.G. is supported by a Warwick University–Liverpool School of Tropical Medicine PhD studentship.

References

- 1 Hanahan, D. and Weinberg, R.A. (2011) Hallmarks of cancer: the next generation. *Cell* 144, 646–674
- 2 Warburg, O. (1956) On the origin of cancer cells. *Science* 123, 309–314
- 3 Lunt, S.Y. and Vander Heiden, M.G. (2011) Aerobic glycolysis: meeting the metabolic requirements of cell proliferation. *Annu. Rev. Cell Dev. Biol.* 27, 441–464
- 4 Chang, C.H. *et al.* (2013) Post-transcriptional control of T cell effector function by aerobic glycolysis. *Cell* 153, 1239–1251
- 5 Gerriets, V.A. and Rathmell, J.C. (2012) Metabolic pathways in T cell fate and function. *Trends Immunol.* 33, 168–173
- 6 De Bock, K. *et al.* (2013) Role of PFKFB3-driven glycolysis in vessel sprouting. *Cell* 154, 651–663
- 7 Vander Heiden, M.G. *et al.* (2009) Understanding the Warburg effect: the metabolic requirements of cell proliferation. *Science* 324, 1029–1033
- 8 Schulze, A. and Harris, A.L. (2012) How cancer metabolism is tuned for proliferation and vulnerable to disruption. *Nature* 491, 364–373
- 9 Hoeijmakers, W.A. *et al.* (2012) *Plasmodium falciparum* centromeres display a unique epigenetic makeup and cluster prior to and during schizogony. *Cell. Microbiol.* 14, 1391–1401
- 10 Alano, P. (2007) *Plasmodium falciparum* gametocytes: still many secrets of a hidden life. *Mol. Microbiol.* 66, 291–302
- 11 Sherman, I.W. (1979) Biochemistry of *Plasmodium* (malaria parasites). *Microbiol. Rev.* 43, 453–495
- 12 Lian, L.Y. *et al.* (2009) Glycerol: an unexpected major metabolite of energy metabolism by the human malaria parasite. *Malar. J.* 8, 38
- 13 Bryant, C. *et al.* (1964) The incorporation of radioactivity from (14c)glucose into the soluble metabolic intermediates of malaria parasites. *Am. J. Trop. Med. Hyg.* 13, 515–519
- 14 Sana, T.R. *et al.* (2013) Global mass spectrometry based metabolomics profiling of erythrocytes infected with *Plasmodium falciparum*. *PLoS ONE* 8, e60840
- 15 Macrae, J.I. *et al.* (2013) Mitochondrial metabolism of sexual and asexual blood stages of the malaria parasite *Plasmodium falciparum*. *BMC Biol.* 11, 67
- 16 Salcedo-Sora, J.E. and Ward, S.A. (2013) The folate metabolic network of *Falciparum* malaria. *Mol. Biochem. Parasitol.* 188, 51–62
- 17 Yeh, E. and DeRisi, J.L. (2011) Chemical rescue of malaria parasites lacking an apicoplast defines organelle function in blood-stage *Plasmodium falciparum*. *PLoS Biol.* 9, e1001138
- 18 Bozdech, Z. *et al.* (2003) The transcriptome of the intraerythrocytic developmental cycle of *Plasmodium falciparum*. *PLoS Biol.* 1, E5
- 19 Le Roch, K.G. *et al.* (2003) Discovery of gene function by expression profiling of the malaria parasite life cycle. *Science* 301, 1503–1508
- 20 Dickman, M.J. *et al.* (2013) Extensive histone post-translational modification in honey bees. *Insect Biochem. Mol. Biol.* 43, 125–137
- 21 Wolff, G.L. *et al.* (1998) Maternal epigenetics and methyl supplements affect agouti gene expression in Avy/a mice. *FASEB J.* 12, 949–957
- 22 Merrick, C.J. and Duraisingh, M.T. (2010) Epigenetics in *Plasmodium*: what do we really know? *Eukaryot. Cell* 9, 1150–1158
- 23 Lucantoni, L. and Avery, V. (2012) Whole-cell in vitro screening for gametocytocidal compounds. *Future Med. Chem.* 4, 2337–2360
- 24 Sowunmi, A. *et al.* (2005) Effects of antifolates – co-trimoxazole and pyrimethamine-sulfadoxine – on gametocytes in children with acute, symptomatic, uncomplicated, *Plasmodium falciparum* malaria. *Mem. Inst. Oswaldo Cruz* 100, 451–455
- 25 Daily, J.P. *et al.* (2007) Distinct physiological states of *Plasmodium falciparum* in malaria-infected patients. *Nature* 450, 1091–1095
- 26 Lu, C. and Thompson, C.B. (2012) Metabolic regulation of epigenetics. *Cell Metab.* 16, 9–17
- 27 Teperino, R. *et al.* (2010) Histone methyl transferases and demethylases; can they link metabolism and transcription? *Cell Metab.* 12, 321–327
- 28 Tu, B.P. *et al.* (2005) Logic of the yeast metabolic cycle: temporal compartmentalization of cellular processes. *Science* 310, 1152–1158
- 29 Baker, D.A. (2010) Malaria gametocytogenesis. *Mol. Biochem. Parasitol.* 172, 57–65
- 30 LeRoux, M. *et al.* (2009) *Plasmodium falciparum* biology: analysis of in vitro versus in vivo growth conditions. *Trends Parasitol.* 25, 474–481
- 31 Babbitt, S.E. *et al.* (2012) *Plasmodium falciparum* responds to amino acid starvation by entering into a hibernatory state. *Proc. Natl. Acad. Sci. U.S.A.* 109, E3278–E3287

- 32 Cheeseman, I.H. *et al.* (2012) A major genome region underlying artemisinin resistance in malaria. *Science* 336, 79–82
- 33 Takala-Harrison, S. *et al.* (2013) Genetic loci associated with delayed clearance of *Plasmodium falciparum* following artemisinin treatment in Southeast Asia. *Proc. Natl. Acad. Sci. U.S.A.* 110, 240–245
- 34 Witkowski, B. *et al.* (2013) Novel phenotypic assays for the detection of artemisinin-resistant *Plasmodium falciparum* malaria in Cambodia: in-vitro and ex-vivo drug-response studies. *Lancet Infect. Dis.* 13, 1043–1049
- 35 Witkowski, B. *et al.* (2013) Reduced artemisinin susceptibility of *Plasmodium falciparum* ring stages in western Cambodia. *Antimicrob. Agents Chemother.* 57, 914–923
- 36 Woodrow, C.J. *et al.* (1999) Intraerythrocytic *Plasmodium falciparum* expresses a high affinity facilitative hexose transporter. *J. Biol. Chem.* 274, 7272–7277
- 37 Vora, S. *et al.* (1985) Characterization of the enzymatic lesion in inherited phosphofructokinase deficiency in the dog: an animal analogue of human glycogen storage disease type VII. *Proc. Natl. Acad. Sci. U.S.A.* 82, 8109–8113
- 38 Vora, S. *et al.* (1985) Alterations in the activity and isozymic profile of human phosphofructokinase during malignant transformation in vivo and in vitro: transformation- and progression-linked discriminants of malignancy. *Cancer Res.* 45, 2993–3001
- 39 Staal, G.E. *et al.* (1987) Subunit composition, regulatory properties, and phosphorylation of phosphofructokinase from human gliomas. *Cancer Res.* 47, 5047–5051
- 40 Mony, B.M. *et al.* (2009) Plant-like phosphofructokinase from *Plasmodium falciparum* belongs to a novel class of ATP-dependent enzymes. *Int. J. Parasitol.* 39, 1441–1453
- 41 Mazurek, S. (2011) Pyruvate kinase type M2: a key regulator of the metabolic budget system in tumor cells. *Int. J. Biochem. Cell Biol.* 43, 969–980
- 42 Atsumi, T. *et al.* (2002) High expression of inducible 6-phosphofructo-2-kinase/fructose-2,6-bisphosphatase (iPFK-2; PFKFB3) in human cancers. *Cancer Res.* 62, 5881–5887
- 43 Christofk, H.R. *et al.* (2008) The M2 splice isoform of pyruvate kinase is important for cancer metabolism and tumour growth. *Nature* 452, 230–233
- 44 Chan, M. and Sim, T.S. (2005) Functional analysis, overexpression, and kinetic characterization of pyruvate kinase from *Plasmodium falciparum*. *Biochem. Biophys. Res. Commun.* 326, 188–196
- 45 Paradies, G. *et al.* (1983) Transport of pyruvate in mitochondria from different tumor cells. *Cancer Res.* 43, 5068–5071
- 46 Kim, J.W. *et al.* (2006) HIF-1-mediated expression of pyruvate dehydrogenase kinase: a metabolic switch required for cellular adaptation to hypoxia. *Cell Metab.* 3, 177–185
- 47 Goldman, R.D. *et al.* (1964) Lactic dehydrogenase in human neoplastic tissues. *Cancer Res.* 24, 389–399
- 48 Cobbold, S.A. *et al.* (2013) Kinetic flux profiling elucidates two independent acetyl-CoA biosynthetic pathways in *Plasmodium falciparum*. *J. Biol. Chem.* 288, 36338–36350
- 49 Bzik, D.J. *et al.* (1993) Expression of *Plasmodium falciparum* lactate dehydrogenase in *Escherichia coli*. *Mol. Biochem. Parasitol.* 59, 155–166
- 50 Dunn, C.R. *et al.* (1996) The structure of lactate dehydrogenase from *Plasmodium falciparum* reveals a new target for anti-malarial design [letter]. *Nat. Struct. Biol.* 3, 912–915
- 51 Gottlieb, E. and Tomlinson, I.P. (2005) Mitochondrial tumour suppressors: a genetic and biochemical update. *Nat. Rev. Cancer* 5, 857–866
- 52 Cuezva, J.M. *et al.* (2007) A message emerging from development: the repression of mitochondrial β -F1-ATPase expression in cancer. *J. Bioenerg. Biomembr.* 39, 259–265
- 53 Sun, A.S. and Cederbaum, A.I. (1980) Oxidoreductase activities in normal rat liver, tumor-bearing rat liver, and hepatoma HC-252. *Cancer Res.* 40, 4677–4681
- 54 Fisher, N. *et al.* (2007) The malaria parasite type II NADH:quinone oxidoreductase: an alternative enzyme for an alternative lifestyle. *Trends Parasitol.* 23, 305–310
- 55 Balabaskaran Nina, P. *et al.* (2011) ATP synthase complex of *Plasmodium falciparum*: dimeric assembly in mitochondrial membranes and resistance to genetic disruption. *J. Biol. Chem.* 286, 41312–41322

Appendix C

Curriculum Vitae

Eva Caamaño-Gutiérrez

e.caamano@warwick.ac.uk

tel:+44(0)7572306788

Work Experience

- Feb 2016 - Present **Early Career Fellow**, Warwick Antimicrobial Interdisciplinary Centre, UK.
Core skills: Cell cultures in Biosafety Level 2. Carbohydrate microarrays. Gold nanoparticle functionalisation. Development of pathogen detection methods in biofluids. Data analysis.
- Jul 2010 - Aug 2011 **Research Assistant**, Life Sciences Department, The University of Warwick, UK.
Core skills: DNA and RNA extraction. PCR genotyping. Cloning. Genetic transformation. Confocal microscopy. Plant crops: glasshouse and control environment chambers. Student mentoring.
- Jul-Sep 2009 **Summer Internship**, Genetics Unit, Molecular Biology Department, University of Leon, Spain.
Working on analysis of SSR markers in *Lens culinaris*.
Core skills: DNA extraction. PCR and electrophoresis.
- Jul 2007-Sep 2008 **Volunteer Researcher**, Genomics and Proteomics Institute, University of Leon, Spain. Working on genotyping of an apple tree collection through self-incompatibility alleles.

Publications

Salcedo-Sora, J. E., **Caamaño-Gutiérrez E.**, Ward, S. A., Biagini, G. A. The proliferating cell hypothesis: a metabolic framework for *Plasmodium* growth and development. *Trends Parasitol.* **30**, 170–175 (2014).

(In preparation:) Gant, M.S., Phelan, M.M, **Caamaño-Gutiérrez, E.**, Grosman, R., Madine, J. Using an NMR metabolomics approach to investigate the pathogenicity of amyloid-beta and alpha-synuclein.

(In preparation:) **Caamaño-Gutiérrez, E.**, Otten, L., Panchana, M., Saif, A. Biagini, B., Gibson, M. The sweet tooth of *Plasmodium falciparum*: a key for artemisinin resistance classification.

Acknowledgements: (1) Costa, L. M. *et al.* Central Cell-Derived Peptides Regulate Early Embryo Patterning in Flowering Plants. *Science* **344**, 168–172 (2014). (2) Costa, L. M. *et al.* Maternal control of nutrient allocation in plant seeds by genomic imprinting. *Curr. Biol.* **22**, 160–165 (2012).

Education

- 2012-2016 **PhD in Systems Biology**. The University of Warwick & Liverpool School of Tropical Medicine (LSTM), UK.
Thesis: “Investigating metabolic control in *Plasmodium falciparum*.”
Core skills: R programming. Metabolomics method development, sample preparation and data analysis. NMR spectroscopy. Microscopy: bright field and confocal, including Operetta. IC₅₀s. Cell cultures in Biosafety Level 2. Student mentoring. Teaching.
- 2012-2016 Certificate in **Transferable skills**. The University of Warwick, UK. Core modules: (1) **Team Working in a Research environment**, (2) **Science Communication to different audiences**. Follow up project: “Analytics day (A-level)”. NMR Centre. University of Liverpool (UoL). (3) **Decision Making and Leadership**, (4) **Doctoral Skills 1-3** including teaching and paper writing.
- Sep 2011- Sep 2012 **MSc in Systems Biology**. (Merit) The University of Warwick, UK
Theoretical project (71%): “The role of iron and zinc in retinal physiology and disease. Development of a metabolic model.”
Core skills: Deterministic modeling. Parameter value systematic review. Matlab.
Experimental project (72%): “Analysing the role of pathogen effector targets in the plant immune system.”
Core skills: *In vitro* and *ex vitro* culturing. Pathogen infection analysis. Primer design. PCR analysis.
- 2005-2010 **BSc in Biotechnology (72%)** University of Leon, Spain

Conferences and Presentations

- 30 Oct 2015 Metabolomics workshop. NMR Centre University of Liverpool. **Oral communication: An introduction to univariate and multivariate analysis in metabolomics.**
- 28 Jun-2 Jul 2015 11th International Conference of the Metabolomics Society. San Francisco. USA. **Poster presentation.** Blogger for the Biochemical Society.
- 19 Mar-4 Jun 2015 An introduction to R. **Volunteer co-organiser and lecturer.** LSTM.
- 24 Apr 2015 PGR meeting. Liverpool. **Oral communication.**
- 16-18 Apr 2015 British Society for Parasitology spring meeting. Liverpool. **Poster presentation and organisation volunteer.**
- 23 Oct 2014 Science communication project *Analytics day* (A-level). NMR Centre. UoL. **Co-organiser.**
- 1-3 Sep 2014 Collaborative Computer Project for NMR national conference, Scarborough, UK. **Poster presentation.**
- 19-21 Mar 2014 Systems Biology DTC Annual Conference, Stratford Upon Avon, UK. **Poster presentation.**
- 14 Apr 2014 PGR meeting. Liverpool. **Poster presentation**
- 12-14 Jun 2013 Systems Biology DTC Annual Conference, Stratford Upon Avon, UK. **Poster presentation.**
- 16-17 May 2013 ID² conference, UCL, London, UK. **Poster presentation.**
- 11-14 Jun 2012 Systems Biology DTC Annual Conference, York, UK. **Poster presentation.**
- 9-12 Jul 2008 Member of the organising committee of the III university conference of biotechnology. Head of the committee on tourism and activities.

Awards

- Feb 2016 Early Career Fellowship, The University of Warwick.
- July 2015 Spanish Researchers in the United Kingdom Travel Grant.
- May 2015 Biochemical Society Travel Grant.
- 2011 Fully funded MSc and PhD. University of Warwick Scholarship.
- Jun-Sep 2010 Erasmus Practice Scholarship Award. University of Leon.
- 3-7 August 2009 Course: The transgenics in our life, diet and agriculture. UIMP. Funded.

Courses

- 26 November 2014 Good Clinical Practice. LSTM.
- 7 November 2013 A beginners guide to qPCR. Primer Design. Organiser and attendee.
- 2013 Computing for data analysis. John Hopkins University. Online.
- 2013 Statistics One. Princeton University. Online.
- 12 March 2013 Delivering effective presentations. UoW.

Computer Skills

- Statistics, calculus: R, SPSS, basics of Matlab and Mathematica.
- Image analysis: ImageJ, Harmony, GIMP.
- Metabolomics: CCPN project, Topspin, AMIX, Chenomx, MetaboAnalyst, rNMR.
- Databases: KEGG, HMDB, MMCD, PlasmoDB, BMRB, BioCyc.
- Other: \LaTeX , Microsoft Office, NCBI tools, Origin.
- Operating Systems: Mac OS X, Windows, Linux.

Management and organisation skills

- Mar 15-Apr 15 Co-organiser and instructor of the course "An introduction to R" at LSTM.
- Mar 13-Apr 14 Student representative at LSTM. Member of the Board of Studies.
- Jul 09-Sep 10 Treasurer of the Spanish Federation of Biotechnologists (FEBiotec).
- Nov 06-Oct 08 Founding member and part of the Directive of the Association of Biotechnologists of Leon (ABLE).
- Oct 08-Sep 10 Student representative and member of the Biology Faculty Board.
- Memberships** Metabolomics society; Biochemical society; British Society For Parasitology; Society of Spanish researchers in the United Kingdom.